UNIVERSITY OF OXFORD

MEDICAL SCIENCES DIVISION

Degree of

DOCTOR of MEDICINE (D.M.)



Connecting the pathways of retinal ganglion cell survival and death in glaucoma: new tools to diagnose, repair and regenerate

Tasneem Khatib

Lady Margaret Hall, University of Oxford

Supervisor: Professor Keith R. Martin

Oxford Academic Advisor: Professor Neville Osborne

Submission: Hilary Term 2021

Thesis title:

Connecting the pathways of retinal ganglion cell survival and death in glaucoma: new tools to diagnose, repair and regenerate

Degree:

Doctor of Medicine (DM)

Term of submission:

Hilary 2021

ABSTRACT

A recent analysis of blindness and vision impairment trends over the past 30 years by the Vision Loss Expert Group for the Global Burden of Disease Study revealed that glaucoma remains the leading cause of irreversible blindness worldwide in an ageing population. The mechanisms underlying retinal ganglion cell degeneration in glaucoma are not fully understood. This thesis examines two key features of glaucomatous neurodegeneration, namely impairment of optic nerve axonal transport and dysregulation of aqueous outflow.

First we demonstrate the continued need to develop new diagnostic and therapeutic approaches for glaucoma by assessing rates of glaucoma progression in the local Cambridge population. We show there is still a clear rate of progression despite tertiary level access to the best treatments currently available.

We describe a new non-invasive tool to assess and quantify the dysregulation of aqueous outflow. Despite being a key therapeutic target in current clinical practice, our understanding of this system is derived largely from post-mortem studies, indirect estimates or, more recently, invasive techniques that alter the physiology of aqueous outflow and are limited in the

information they provide. There are currently no non-invasive techniques available that directly visualise detailed aqueous outflow *in vivo*. We use a non-invasive imaging modality developed to image the anterior microcirculation of the human eye – haemoglobin video imaging – to examine aqueous outflow into the episcleral venous circulation in detail, and to observe and quantify alterations in aqueous outflow following treatments that aim to selectively target this pathway.

We then evaluate a combined receptor-ligand gene therapy construct which overexpresses brain derived neurotrophic factor and its receptor tropomyosin kinase B on optic nerve axonal transport and retinal ganglion cell function. We use a rat glaucoma model and a humanised tauopathy model of reduced axonal transport and showed combined overexpression is more effective in stimulating axonal transport than either receptor administration or ligand administration alone. We also demonstrate functional recovery in the glaucoma model. Furthermore, we offer promising evidence there may be an improvement in short term memory loss in the tauopathy model, suggesting that this strategy to target intrinsic mechanisms to improve neuronal function and facilitate repair may be relevant to multiple neurodegenerative diseases.

We then assess whether manipulating the degenerative process could also be associated with optic nerve regeneration in experimental glaucoma. We demonstrate for the first time the glaucomatous optic nerve also has the potential to regenerate using strategies previously only used after traumatic injury.

ACKNOWLEDGEMENTS

This thesis is the product of my own research except where specifically indicated below. All sources have been acknowledged and accurately reported. It was completed under the supervision of Professor Keith Martin. Professor Neville Osborne is my Oxford Academic Advisor. All experimental work was conducted at the Centre for Brain Repair, University of Cambridge and in the Glaucoma Clinic, Cambridge University Hospitals NHS Trust.

I am extremely grateful to Professor Keith Martin for providing me with this opportunity and for his guidance and mentorship throughout, both in Cambridge and from Melbourne – no problem was ever too small. I can't thank you enough for your patience, support through the failures as well the successes and belief in me, and for your encouragement to pursue my ideas. Thank you also to Professor Neville Osborne who has been there since the beginning of my journey in retinal ganglion cell biology while at Oxford and for supporting me again through the DM.

Particular mention and thanks to Dr Andy Osborne, for all the training in the lab, lending a listening ear for my ideas and for the encouragement to keep going. Thank you also for reminding me of my passion for the work when it all got a bit much! To my colleagues in the lab and the clinic, both those who are co-authors on the various papers from this thesis and those who are not - it has been a real privilege to have met and worked with so many passionate, talented and inspiring scientists and researchers, many of whom will remain lifelong friends.

Astellas Pharmaceuticals have been fantastic industry collaborators, have encouraged freedom of scientific thought and given importance to ensuring appropriate credit is given for any work performed. I have appreciated the support from them to complete the experiments for my thesis despite the sale and acquisition of the gene therapy construct that was central

to the work. It has been a real learning experience to be part of the development of a translational therapy from the pre-clinical to clinical stages.

Most of all, thank you to my family and friends. I am truly grateful for the unconditional support you have shown me and for reminding me of the importance of balance and perspective.

I have grown both personally and professionally during the course of my DM studies and achieved things that I did not think would ever be possible. It has also been a privilege to be able to contribute to the scientific body of knowledge and step closer towards understanding and treating intractable glaucoma. I hope that I will be able to give future generations the same chance and provide the same opportunities that I have been fortunate enough to experience.

Table of Contents

TITLE PAGE **1**

ABSTRACT **2**

ACKNOWLEDGEMENTS **4**

LIST OF FIGURES AND TABLES **11**

VIDEO CLIP LEGENDS **14**

LIST OF PUBLICATIONS ARISING FROM THIS THESIS **15**

LIST OF PRESENTATIONS ARISING FROM THIS THESIS **16**

LIST OF PUBLICATIONS PRIOR TO THESIS SUBMISSION **18**

CHAPTER 1: INTRODUCTION **21**

1.1 PRIMARY OPEN ANGLE GLAUCOMA 22

1.2 UNMET CLINICAL NEED 24

1.3 ASSESSING AQUEOUS OUTFLOW 25

1.4 NEUROPROTECTION STRATEGIES 28

1.4.1 Brimonidine 28

1.4.2 Cell therapy 30

1.4.3 Neurotrophins 33

1.4.4 Memantine 35

1.4.5 Nicotinamide 36

1.5 GENE THERAPY 39

CHAPTER 2: MATERIALS AND METHODS **43**

2.1 METHODS FOR CHAPTER 3 43

2.2 METHODS FOR CHAPTER 4 43

2.2.1 Imaging aqueous veins 44
2.2.2 Image processing 44
2.2.3 Aqueous column cross-sectional area following SLT 45
2.2.4 Quantifying flow rate 45
2.3 METHODS FOR CHAPTER 5 46
2.3.1 Vector production 46
2.3.2 Animals 47
2.3.3 Intravitreal vector injection 48
2.3.4 Rat Laser Induced Ocular Hypertension 49
2.3.5 Electroretinography 49
2.3.6 Spontaneous object recognition task 50
2.3.7 Perirhinal cortex AAV5 injections 50
2.3.8 Western blots 51
2.3.9 Measuring anterograde axonal transport 51
2.3.10 Immunohistochemistry 53
2.3.11 I-TASSER molecular modelling of TrkB receptor 55
2.3.12 Statistical analysis 55
2.4 METHODS FOR CHAPTER 5 58
2.4.1 Animals 58
2.4.2 Intravitreal vector injection 58
2.4.3 Induction of ocular hypertension 58
2.4.4 Measuring anterograde axonal transport 59
2.4.5 Immunohistochemistry 60
CHAPTER 3: PROGRESSIVE AND IRREVERSIBLY BLINDING: THE CLINICAL NEED FOR NEW GLAUCOMA TOOLS 63
3.1 INTRODUCTION 63
3.1.1 Visual loss in glaucoma 63

3.1.2 Classification of glaucomatous disease progression 64
3.1.3 Glaucoma progression despite 'normal' IOP – normal tension glaucoma 64
3.1.4 Patients at highest risk for glaucomatous progression 65
3.1.5 Capacity for glaucoma services 66
3.1.6 Increased referral rates 66
3.1.7 Shared care models 67
3.2 AIM 67
3.2.1 The Cambridge Community Optometrist Glaucoma Scheme (COGS) 67
3.2.2 Risk stratification 67
3.2.3 Community assessment 69
3.3 RESULTS 70
3.4 DISCUSSION 76
3.5 ACKNOWLEDGEMENTS FOR CHAPTER 3 80

CHAPTER 4: DEVELOPING A NEW DIAGNOSTIC TOOL FOR GLAUCOMA: HAEMOGLOBIN VIDEO IMAGING 81

4.1 INTRODUCTION 81
4.2 RESULTS 83
4.3 DISCUSSION 90
4.4 FUTURE DIRECTIONS 91
4.5 ACKNOWLEDGEMENTS FOR CHAPTER 4 92

CHAPTER 5: GENE THERAPY AS A THERAPEUTIC TOOL FOR PRIMARY OPEN ANGLE GLAUCOMA 94

5.1 INTRODUCTION 94
5.2 AIM 96
5.3 RESULTS 96
5.3.1 2A linker region does not interfere with TrkB receptor activation segment 96

5.3.2 Transduction efficiency of the rodent retina 99
5.3.3 Combined replacement is more effective than receptor or ligand replacement alone 104
5.3.4 Intervention is effective after the onset of pathology in a humanised tauopathy model 106
5.3.5 AAV2 TrkB-2A-mBDNF enhances axonal transport in experimental glaucoma with functional recovery 108
5.3.6 Translating from the visual pathway to memory: AAV5 TrkB-2A-mBDNF improves short term memory loss in a humanised dementia model. 115
5.4 DISCUSSION 117
5.5 FUTURE DIRECTIONS: PRELIMINARY WORK 122
5.6 ACKNOWLEDGEMENTS FOR CHAPTER 5 127

CHAPTER 6: OPTIC NERVE REGENERATION IN EXPERIMENTAL GLAUCOMA..... 129

6.1 INTRODUCTION 129
6.1.1 Mature retinal ganglion cells neurons lose ability to grow 129
6.1.2 Approaches to regenerate the optic nerve 129
6.1.3 Phosphatase and tensin homolog and the PI3 kinase pathway 130
6.2 AIM 130
6.3 RESULTS 131
6.4 DISCUSSION 139
6.5 ACKNOWLEDGEMENTS FOR CHAPTER 6 140

CHAPTER 7: DISCUSSION..... 142

7.1 NON-INVASIVE IMAGING..... 142
7.2 PRECLINICAL TO CLINICAL TRANSLATION 142
7.3 OPTIMISING CLINICAL ENDPOINTS..... 144

7.4 COMPARTMENTALISED DEGENERATION 146

7.5 FUNCTIONAL RECOVERY 148

7.6 A NEW ERA OF TRANSLATIONAL MEDICINE: LESSONS LEARNED FROM OTHER GENE THERAPY TRIALS 148

7.7 TOWARDS PRECISION MEDICINE 154

APPENDIX 1: MATLAB CODE FOR HVI IMAGE REGISTRATION 156

APPENDIX 2: PYTHON CODE FOR SEMI-AUTOMATED AXON TRANSPORT QUANTIFICATION 158

APPENDIX 3: MANUAL VALIDATION OF RETINAL GANGLION CELL QUANTIFICATION AND GREEN FLUORESCENT PROTEIN COLOCALISATION 165

LIST OF FIGURES AND TABLES

LIST OF FIGURES

CHAPTER 1

FIGURE 1-1: GLOBAL PREVALENCE OF PRIMARY OPEN-ANGLE GLAUCOMA

FIGURE 1-2: RETINAL GANGLION CELL INJURY AND RESPONSE IN GLAUCOMA

FIGURE 1-3: RELATIONSHIP BETWEEN VISUAL FIELD INDEX AND RETINAL GANGLION CELLS

FIGURE 1-4: AGE-SPECIFIC PREVALENCE RATES OF DISTANCE BLINDNESS AND MSVI

FIGURE 1-5: AQUEOUS HUMOUR PRODUCTION AND FLOW

FIGURE 1-6: NEOPRENE CAST OF SCHLEMM'S CANAL

FIGURE 1-7. STRUCTURAL RECONSTRUCTION OF THE AQUEOUS OUTFLOW SYSTEM

FIGURE 1-8: BRIMONIDINE ASSOCIATED ANTERIOR UVEITIS.

FIGURE 1-9: MOLECULAR MECHANISMS INDUCING REACTIVE GLIOSIS

FIGURE 1-10: HAEMORRHAGIC RETINOPATHY AND TRACTIONAL RETINAL DETACHMENT

FIGURE 1-11: SCHEMATIC ILLUSTRATING ENCAPSULATED CNTF IN VITREOUS.

FIGURE 1-12: RECOMBINANT HUMAN NERVE GROWTH FACTOR TO TREAT NEUROTROPHIC KERATITIS.

FIGURE 1-13: MECHANISM OF ACTION OF NICOTINAMIDE.

FIGURE 1-14: MYOCILIN AND PRIMARY OPEN ANGLE GLAUCOMA.

FIGURE 1-15: ROLE OF THE ANGIOPOIETIN/TIE2 PATHWAY IN MAINTENANCE OF SCHLEMMS CANAL.

CHAPTER 2

FIGURE 2-1: P301S MUTATION WITH DISRUPTION TO AXONAL INTEGRITY.

FIGURE 2-2: EXPERIMENTAL TIMELINES.

CHAPTER 3

FIGURE 3-1: THE EFFECT ON VISUAL DISABILITY OF PATIENTS WITH GLAUCOMA.

FIGURE 3-2: VISUAL FIELD LOSS AND MD PROGRESSION RATE.

FIGURE 3-3: LOSS OF SIGHT YEAR ANALYSIS.

CHAPTER 4

FIGURE 4-1: AQUEOUS VEIN CAPTURED USING CONVENTIONAL TECHNIQUES AND HAEMOGLOBIN VIDEO IMAGING.

FIGURE 4-2: EXAMPLES OF AQUEOUS VEINS OBTAINED USING HAEMOGLOBIN VIDEO IMAGING.

FIGURE 4-3: DISPLACEMENT OF AQUEOUS FOLLOWING DIGITAL PRESSURE ON THE INFERIOR GLOBE.

FIGURE 4-4: COMPRESSION OF AN AQUEOUS VEIN.

FIGURE 4-5: INTENSITY PROFILE OF TRANSMITTED LIGHT IN AN AQUEOUS VEIN

FIGURE 4-6: AQUEOUS COLUMN CROSS SECTIONAL AREA AS A TOOL FOR QUANTIFYING AQUEOUS OUTFLOW.

FIGURE 4-7: FLOW RATE USING AUTOCORRELATION ANALYSIS BEFORE AND AFTER SLT.

CHAPTER 5

FIGURE 5-1 BDNF MEDIATED AUTOCRINE SELF-AMPLIFYING POSITIVE FEEDBACK MECHANISM TO STIMULATE ANTEROGRADE AXONAL TRANSPORT.

FIGURE 5-2: DEVELOPMENT OF THE TRKB-2A-MBDNF CONSTRUCT.

FIGURE 5-3: SIMULTANEOUS ADMINISTRATION OF A LIGAND AND ITS RECEPTOR BY A SINGLE SELF-CLEAVING 2A PEPTIDE-BASED GENE THERAPY VECTOR UNDER THE CONTROL OF ONE PROMOTER.

FIGURE 5-4: RETINAL GANGLION CELL TRANSDUCTION INCREASES WITH VIRAL TITRE.

FIGURE 5-5: MOUSE RETINAL GANGLION CELL TRANSDUCTION RATE INCREASED WITH VIRAL TITRE.

FIGURE 5-6: GREEN FLUORESCENT PROTEIN INTENSITY INCREASES WITH VIRAL TITRE.

FIGURE 5-7: THE SPATIAL PATTERN OF GREEN FLUORESCENT PROTEIN EXPRESSION.

FIGURE 5-8: GREEN FLUORESCENT PROTEIN EXPRESSION IN RETINAL CELLS.

FIGURE 5-9: INCREASED EXPRESSION OF TRKB AND BDNF FOLLOWING AAV2 TRKB-2A-MBDNF ADMINISTRATION IN THE RODENT RETINA.

FIGURE 5-10: COMBINED LIGAND RECEPTOR REPLACEMENT MORE EFFECTIVE THAN LIGAND OR RECEPTOR ALONE

FIGURE 5-11: INTERVENTION IS EFFECTIVE AFTER THE ONSET OF PATHOLOGY IN A HUMANISED TAUOPATHY MODEL.

FIGURE 5-12: INTRAOCULAR PRESSURE PROFILE

FIGURE 5-13: FUNCTIONAL DEFICITS PRECEDE TRANSPORT DEFICITS AND ARE RESTORED WITH AAV2 TRKB-2A-MBDNF.

FIGURE 5-13: REDUCTION IN OPTIC NERVE AXONAL TRANSPORT OR RETINAL GANGLION CELL FUNCTION IS NOT ASSOCIATED WITH RETINAL GANGLION CELL SOMA LOSS.

FIGURE 5-14 AAV2 TRKB-2A-MBDNF ENHANCES ANTEROGRADE OPTIC NERVE AXONAL TRANSPORT IN EXPERIMENTAL GLAUCOMA.

FIGURE 5-15: ANTEROGRADE TRANSPORT OF CTB IN THE SUPERIOR COLLICULUS.

FIGURE 5-16: REDUCTION IN OPTIC NERVE AXONAL TRANSPORT OR RGC FUNCTION IS NOT ASSOCIATED WITH RGC SOMA LOSS.

FIGURE 5-17: COLOCALISATION OF RETINAL GANGLION CELL MARKERS.

FIGURE 5-18: AAV5 TRKB-2A-MBDNF IMPROVES SHORT TERM MEMORY IN A HUMANISED TAUOPATHY MODEL OF DEMENTIA.

FIGURE 5-19: CHANGES IN RETINAL TAU FOLLOWING LASER INDUCED OCULAR HYPERTENSION.

FIGURE 5-20: REGULATION OF RETINAL TAU HYPERPHOSPHORYLATION FOLLOWING LASER INDUCED OCULAR HYPERTENSION.

FIGURE 5-21: RETINAL TAU IN THE OPTIC NERVE OF P301S MICE HOMOZYGOUS FOR HUMAN MUTANT TAU FOLLOWING ADMINISTRATION OF AAV2 TRKB-2A-BDNF.

CHAPTER 6

FIGURE 6-1: VALIDATION OF PTEN DELETION.

FIGURE 6-2: VALIDATION OF THE INTRACAMERAL GEL MODEL OF INTRAOCULAR PRESSURE ELEVATION.

FIGURE 6-3: EFFECTS OF PTEN DELETION ON ANTEROGRADE OPTIC NERVE AXONAL TRANSPORT AND OPTIC NERVE REGENERATION IN EXPERIMENTAL GLAUCOMA.

FIGURE 6-4: GAP43 LEVELS IN THE RETINAL GANGLION CELL BODIES AND SYNAPSES.

FIGURE 6-5: PHOSPHO-S6 (PS6) RIBOSOMAL PROTEIN LEVELS IN THE RETINAL GANGLION CELL LAYER

APPENDIX 3

FIGURE 1: MANUAL VALIDATION OF THE ITCN PLUGIN FOR FIJI

FIGURE 2: MANUAL VALIDATION OF THE GFP/Brn3a COLOCALISATION USING VOLOCITY

LIST OF TABLES

TABLE 3-1: GLAUCOMATOUS VISUAL FIELD LOSS AS DEFINED BY HODAPP-PARISH-ANDERSON CLASSIFICATION.

TABLE 3-2: THE CAMBRIDGE COMMUNITY OPTOMETRY GLAUCOMA SCHEME (COGS)

TABLE 3-3: SUMMARY STATISTICS

TABLE 3-4: DISTRIBUTION OF MD PROGRESSION RATES.

VIDEO CLIP LEGENDS

Viewing order as in the text and in ascending order as numbered.

Video clip 1: unstabilised.mpg: Captured images of an aqueous vein as played back prior to stabilisation.

Video clip 2: stablised.mpg: Images as in video clip 1 following stabilisation using Image J 'Image Stabilizer plugin'.

Video clip 3: aqueous vein examples.mpg: separate recordings of individual aqueous veins using haemoglobin video imaging.

Video clip 4: pulsatile.mpg: Pulsatile nature of aqueous flow captured using haemoglobin video imaging. 3 separate examples of displacement of aqueous following digital pressure on the globe away from the vessels of interest. Aqueous is redirected into an episcleral blood filled vessel following digital pressure on the globe with immediate resumption of usual aqueous and blood flow following release of pressure. A final example demonstrates compression of an aqueous vein using a 10/0 vicryl loop redirects aqueous to a nearby episcleral blood vessel. Aqueous flow resumes once the manoeuvre is complete.

Video clip 5: pre and post intervention.mpg: Imaging of individual aqueous veins in 4

glaucoma patients before and after intervention.

LIST OF PUBLICATIONS ARISING FROM THIS THESIS

Khatib TZ, Osborne A, Ali Z, Jia J, Manyakin I, Watt R, Widdowson P, Martin KR Receptor-ligand supplementation through a self-cleaving 2A peptide-based gene therapy promotes CNS axonal transport with functional recovery *Science Advances.* 2021 Mar 31;7(14):eabd2590.

Khatib TZ, Meyer PAR, Lusthaus J, Manyakin I, Mushtaq Y, Martin KR. Hemoglobin Video Imaging Provides Novel In Vivo High-Resolution Imaging and Quantification of Human Aqueous Outflow in Patients with Glaucoma. *Ophthalmol Glaucoma.* 2019 Sep-Oct;2(5):327-335.

Mushtaq Y, Panchasara B, Nassehzadehtabriz N, Lim HK, Mushtaq M, Kean J, Farrell S, Bourne RA, Shahid H, **Khatib TZ*,** Martin KR* Evaluating multidisciplinary glaucoma care: visual field progression and loss of sight year analysis in the community vs hospital setting *Eye (Lond).* 2021 Mar 21:1–9.

Khatib TZ, Martin KR. Neuroprotection in Glaucoma: Towards Clinical Trials and Precision Medicine. *Curr Eye Res.* 2020 Mar;45(3):327-338.

Nieuwenhuis B, Barber AC, Evans RS, Pearson CS, Fuchs J, MacQueen AR, van Erp S, Haenzi B, Hulshof LA, Osborne A, Conceicao R, **Khatib TZ**, Deshpande SS, Cave J, Ffrench-Constant C, Smith PD, Okkenhaug K, Eickholt BJ, Martin KR, Fawcett JW, Eva R PI 3-kinase delta enhances axonal PIP3 to support axon regeneration in the adult CNS *EMBO Mol Med* 2020 12:e11674

Osborne A, **Khatib TZ**, Songra L, Barber AC, Hall K, Kong GYX, Widdowson PS, Martin KR. Neuroprotection of retinal ganglion cells by a novel gene therapy construct that achieves sustained enhancement of brain-derived neurotrophic factor/tropomyosin-related kinase receptor-B signaling. *Cell Death Dis*. 2018 Sep 26;9(10):1007.

Lusthaus JA, **Khatib TZ**, Meyer PAR, McCluskey P, Martin KR. Aqueous outflow imaging techniques and what they tell us about intraocular pressure regulation. *Eye* (Lond). 2020 Aug 21.

Khatib TZ, Martin KR. Protecting retinal ganglion cells. *Eye* (Lond). 2017 Feb;31(2):218-224.

Lusthaus JA, Meyer PA, **Khatib TZ**, Martin KR The effects of trabecular bypass surgery on conventional aqueous outflow, visualized by Hemoglobin Video Imaging *Journal of Glaucoma* 2020 Aug 29 (8): 656-665

Khatib TZ, Whitehead M, Osborne A, Evans R, Ching J, Ali Z, Martin KR Phosphatase and tensin homolog (PTEN) knockdown promotes anterograde axonal transport and stimulates optic nerve regeneration in experimental glaucoma (Manuscript in preparation)

LIST OF PRESENTATIONS ARISING FROM THIS THESIS

American Academy of Ophthalmology Annual Meeting **Tasneem Z. Khatib**, Paul AR Meyer, Jed Lusthaus, Ilya Manyakin, Yusuf Mushtaq, Keith R Martin (2019) Haemoglobin Video Imaging provides novel in vivo high-resolution imaging and quantification of human aqueous outflow in glaucoma patients **Awarded Best Paper in Session

Association for Research in Vision and Ophthalmology Annual Meeting **Tasneem Khatib**, Paul AR Meyer, Jed Lusthaus, Ilya Manyakin, Yusuf Mushtaq, Keith R Martin; Non-invasive *in vivo* imaging and quantification of human aqueous outflow. *Invest. Ophthalmol. Vis. Sci.* 2019;60(9):5606.

World Glaucoma Congress Optic nerve regeneration following glaucomatous injury in aged mice. **Tasneem Khatib**, Andrew Osborne, Michael Whitehead, Zara Ali, Jared Ching, Rachel Evans, Raquel Conceicao, Keith Martin (2019) Optic nerve regeneration following glaucomatous injury in aged mice.

Association for Research in Vision and Ophthalmology Annual Meeting **Tasneem Khatib**, Andrew Osborne, Peter S Widdowson, Keith R Martin; Tau dysfunction in glaucoma: modulation of optic nerve axonal transport via gene therapy. *Invest. Ophthalmol. Vis. Sci.* 2018;59(9):3716. **Awarded Outstanding Members-in Training Poster Award for Glaucoma Section

Association for Research in Vision and Ophthalmology Annual Meeting Peter S Widdowson, Andrew Osborne, **Tasneem Khatib**, Katie Hall, Keith R Martin; QTA020V, a novel rAAV2 vector, reduces retinal ganglion cell body and axon loss in rats with laser-induced intraocular pressure elevation. *Invest. Ophthalmol. Vis. Sci.* 2018;59(9):6132.

Association for Research in Vision and Ophthalmology Annual Meeting Keith R Martin, Andrew Osborne, **Tasneem Khatib**, Amanda Barber, George Kong, Peter S Widdowson; QTA020V, a novel rAAV2 vector, delays retinal ganglion cell loss following optic nerve crush in the mouse. *Invest. Ophthalmol. Vis. Sci.* 2017;58(8):2954.

Association for Research in Vision and Ophthalmology Annual Meeting **Tasneem Z Khatib**, Paul AR Meyer, Jed Lusthaus, Keith R Martin; *In vivo* imaging of human aqueous outflow and calculation of aqueous column diameter. *Invest. Ophthalmol. Vis. Sci.* 2017;58(8):2097.

European Vision and Eye Research Annual Meeting **Tasneem Khatib**, Andrew Osborne, Peter Widdowson, Keith Martin. (2016), Quantification of green fluorescent protein expression in mouse retinal ganglion cells following intravitreal injection of recombinant adeno-associated virus. Acta Ophthalmol, 94. **Awarded Glaucoma Section Prize

Oxford Ophthalmological Congress **Tasneem Khatib**, Andrew Osborne, Zara Ali, Peter Widdowson, Keith Martin (2018) AAV2 BDNF TrkB gene therapy restores optic nerve axonal transport and retinal ganglion cell function in experimental glaucoma.

Obergugl Optic Nerve Meeting **Tasneem Khatib**, Andrew Osborne, Zara Ali, Wanyi Jia, Ilya Manyakin Peter Widdowson, Keith Martin (2018) Axon transport and regeneration following glaucomatous injury.

University of Cambridge Clinical Neurosciences Away Day **Tasneem Khatib**, Andrew Osborne, Peter Widdowson, Keith Martin (2017) *Tau dysfunction in glaucoma: modulation of optic nerve axonal transport via gene therapy.*

LIST OF PUBLICATIONS PRIOR TO THESIS SUBMISSION

Whitehead M, Osborne A, **Khatib TZ**, Watt R, Yu-Wai-Man P, Martin KR Neutralising antibody responses to intravitreally delivered AAV2 and exosome-associated AAV2 vectors are associated with a failure of repeated gene transfer following vector readministration in the ipsilateral eye *Manuscript in preparation*

Scollo P, Pujari R, Somner J, Pesudovs K, Shah P, Rajani S, Dufour L, Pujari R, Hassan A, Hanspal I, **Khatib TZ**, Tapply I, Bourne RRA; Developing a Patient-Reported Outcome and Experience Measure for Glaucoma. *Manuscript in preparation*

Nicolaou S, **Khatib TZ**, Lin Z, Sheth T, Ogbonna G, Hamidovic L, Zaheer A, Dimitriou C
A retrospective review of XEN implant surgery in glaucoma patients; efficacy, safety and the effect of combined cataract surgery *Manuscript in preparation*

Jia W, **Khatib TZ**, Martin KR, Karadottir R Neuronal Activity-Dependent Myelin Plasticity during Adulthood *Work still in progress*

Hamza M, **Khatib TZ**, Nicolaou S, Fajardos A, Mukherjee Clinical Results Of An Extended Ab Interno Trabeculotomy Using KDB And Indirect Gonioscopy In Open Angle And Angle Closure Glaucoma *Journal of MAR Ophthalmology* 2021 Mar 2 (2)

Khatib T, Martin K Comment on 'Stage-specific differentiation of iPSCs toward retinal ganglion cell lineage, Deng F, Chen M, Liu Y, Hu H, Xiong Y, Xu C, Liu Y, Li K, Zhuang J, Ge J, Molecular Vision 2016; 22: 536-547' *International Glaucoma Review The Journal of the World Glaucoma Association* 2017;18 (1):44-45

Skalicky S, McAlinden C, **Khatib T**, Anthony LM, Sing SY, Martin KR, Goldberg I, McCluskey P Activity Limitation in Glaucoma: Objective Assessment by the Cambridge Visual Function Test *Invest Ophthalmol Vis Sci.* 2016 Nov 1;57(14):6158-6166

Khatib T, Hughes PW, Burton BJL Unilateral choroidal granulomas complicated by choroidal neovascular membrane treated successfully with intravitreal triamcinolone in a patient with sarcoidosis *BMJ Case Rep* 2014 Aug 28;2014

Khatib T, Singh AD, Dua HS Looking back at Orpheus *Br J Ophthalmol* 2012;96:489

Faraj LA, Hashmani K, **Khatib T**, Al-Aqaba M, Dua HS The changing face of corneal graft rejection *Br J Ophthalmol* 2012;96:8 1049-1050

Khatib T, Singh AD, Dua HS The Graeae sisters: one eye for three *Br J Ophthalmol* 2012;96:161

Khatib T, Singh AD, Dua HS One-eyed Odin: an eye for wisdom *Br J Ophthalmol* 2011;95: 1651

Said DG, Otri M, Miri A, Kailasanathan A, **Khatib T**, Dua HS The challenge of fungal keratitis *Br J Ophthalmol* 2011;95:1623-162

Khatib T, Dua A, Singh AD, Dua HS Oedipus: repenting eyes *Br J Ophthalmol* 2011;95:1371

Khatib T, Dua A, Singh AD, Dua HS Peacock-eyed: hundred eyes on a peacock's tail *Br J Ophthalmol* 2011;95:1105

CHAPTER 1

INTRODUCTION

Vision researchers have been at the forefront of translational medicine and therapeutics at least in part due to the accessibility of ocular structures, the relative immune privilege of the ocular environment, well defined objective and subjective endpoints and sophisticated imaging modalities that harness the optical clarity of ocular media, permitting real-time submicron resolution of ocular structures and direct visualisation of the central nervous system. Despite these significant advances, primary open angle glaucoma (POAG) remains the leading cause of irreversible blindness worldwide (Steinmetz et al., 2021), where traditional intraocular pressure (IOP)-lowering therapies are often not sufficient to prevent progression to blindness even for patients with access to high quality healthcare.



Figure 1-1: Global prevalence of primary open-angle glaucoma. Taken from (Weinreb et al., 2016)

1.1 PRIMARY OPEN ANGLE GLAUCOMA

Adult-onset POAG is associated with optic nerve head damage, retinal ganglion cell (RGC) death, axonal degeneration and progressive visual loss [Figure 1-2]. There are multiple underlying genetic and environmental factors that contribute to the development of POAG, but how these interact to determine the disease course in each individual with glaucoma remains incompletely understood.

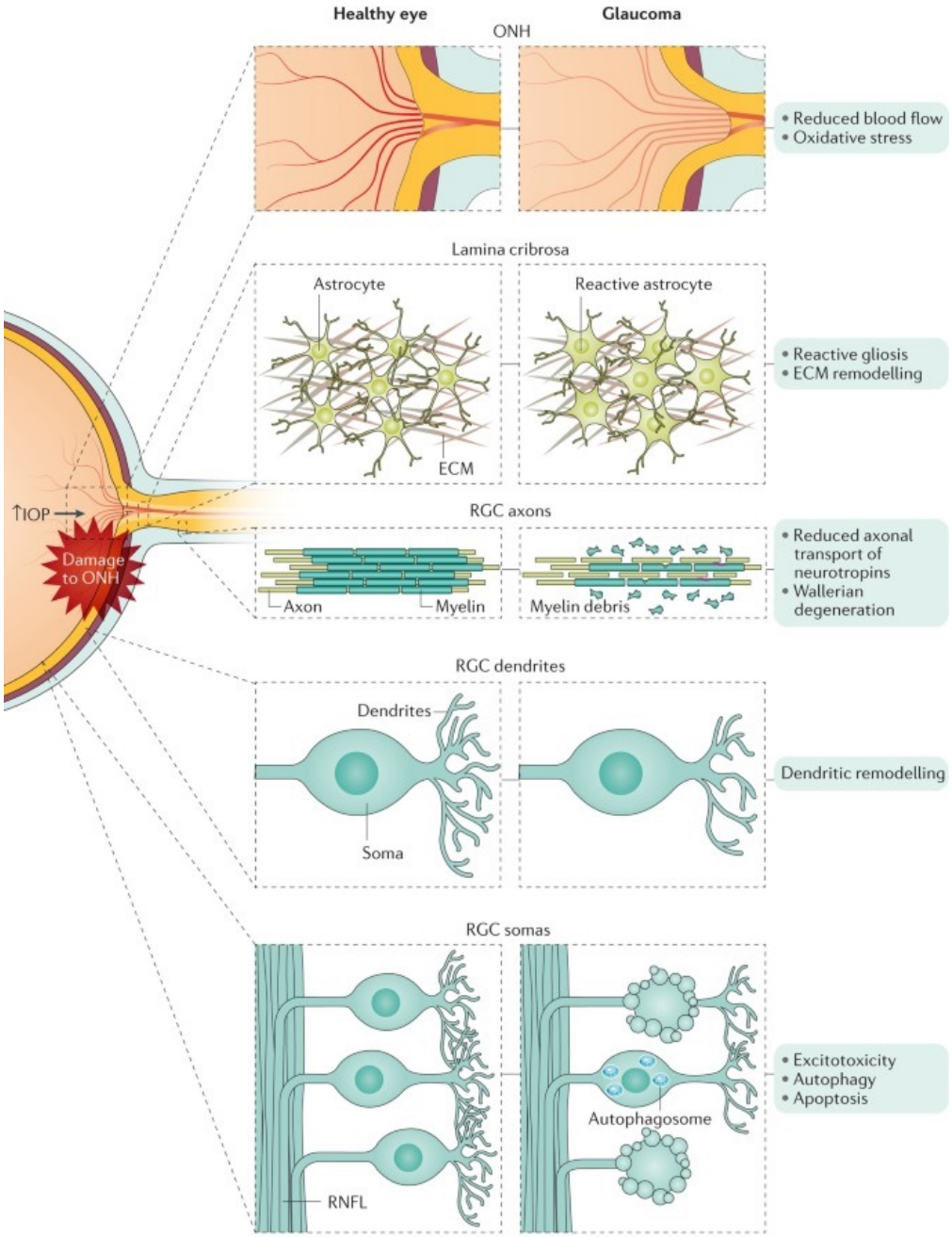


Figure 1-2: Retinal ganglion cell injury and response in glaucoma. Taken from (Weinreb et al., 2016)

Individuals with early to moderate chronic glaucoma are mostly asymptomatic and unaware of any damage to their field of vision. Our current tests do not provide a statistically significant estimate of ganglion cell loss until a substantial proportion have been lost (Harwerth et al., 1999; Harwerth & Quigley, 2006; Kerrigan–Baumrind et al., 2000; Marvasti et al., 2013).

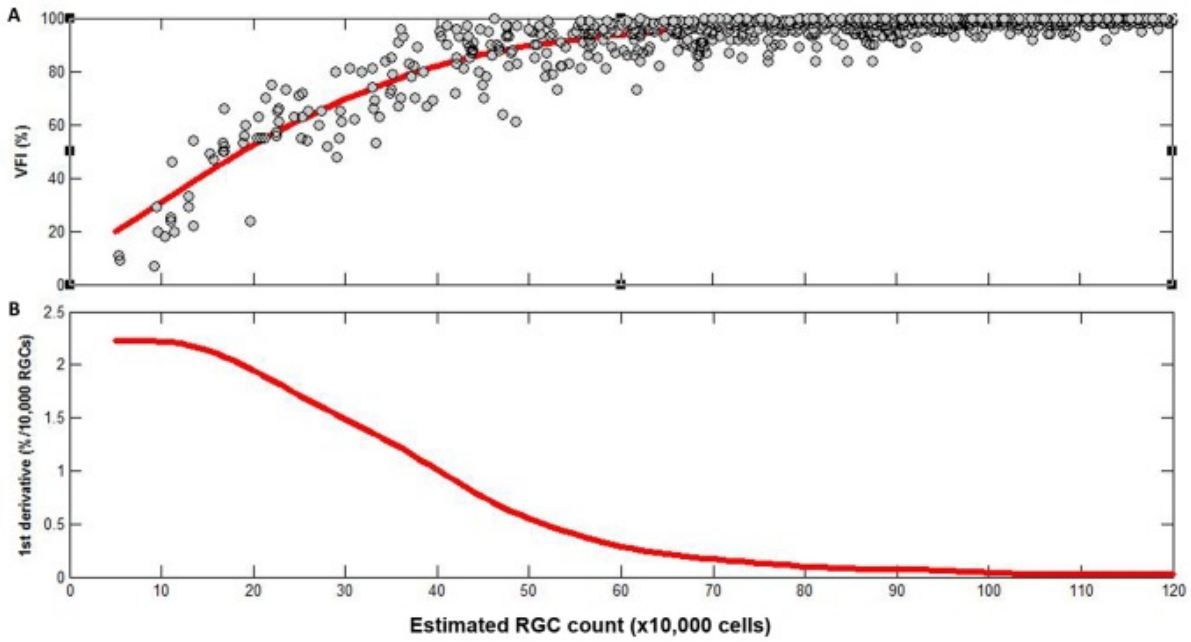


Figure 1-3: Relationship between visual field index (VFI) and retinal ganglion cells (RGC). Taken from (Marvasti et al., 2013)

Early detection and effective treatment by healthcare professionals are thus key elements in avoiding permanent blindness.

Screening for glaucoma is usually performed as part of a standard eye examination performed by optometrists or ophthalmologists who examine for changes in the visual field, optic disc appearance and IOP. Once diagnosed, affected individuals require lifelong monitoring for disease control and to detect possible progression of visual damage. Minimisation of ongoing damage is paramount to maintenance of a sighted lifetime and to lower the impact on disease management costs.

The mainstay of current treatment is to lower the IOP which has been established as the strongest modifiable risk factor associated with disease progression (Friedman et al., 2004; Leske et al., 2007). IOP can be lowered medically, using laser therapy or by surgical intervention but remains the only treatment strategy across all POAG populations regardless of the underlying pathophysiology.

1.2 UNMET CLINICAL NEED

Recent clinical trials (Garway-Heath et al., 2015) have shown that IOP lowering with topical anti-hypertensives such as the prostaglandin analogue Latanoprost in the United Kingdom Glaucoma Treatment Study ((UKGTS) trial registration number ISRCTN96423140) can effectively reduce the rate of POAG progression. However, the clinical need to develop additional strategies remains, as a proportion of patients may continue to worsen despite IOP lowering treatment. Even in populations with good access to glaucoma care, an estimated one in eight patients will still eventually become blind in at least one eye due to glaucoma progression over 20 years (Malihi et al., 2014).

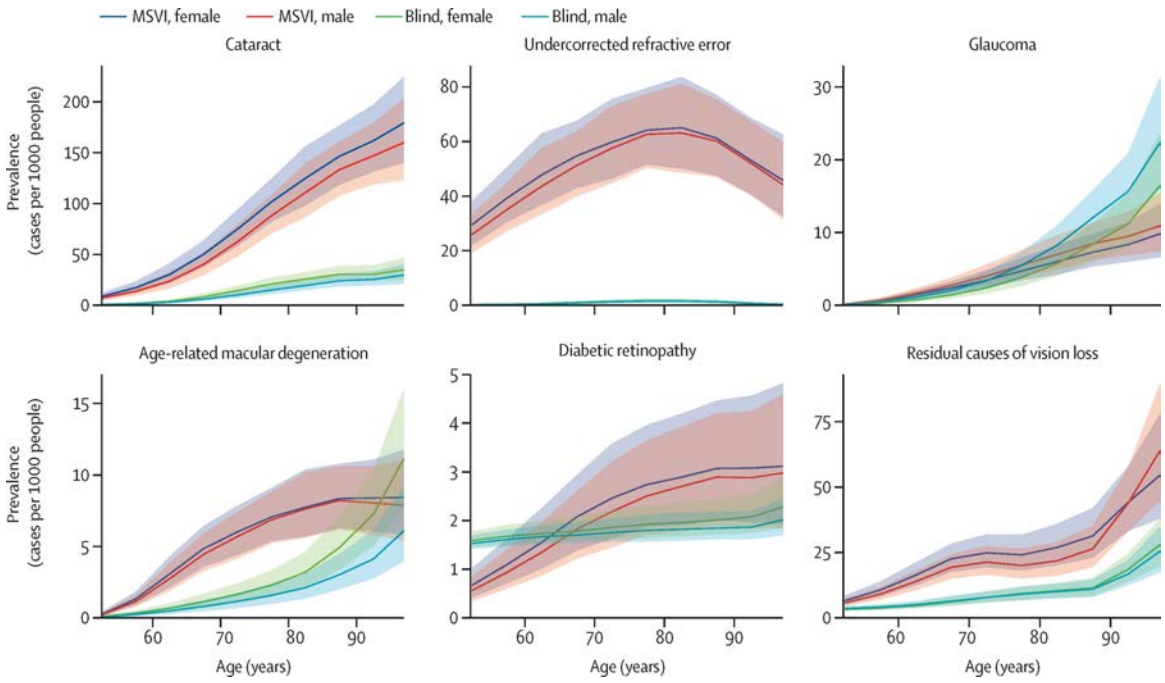


Figure 1-4: Age-specific prevalence rates of distance blindness and MSVI by cause and sex in adults aged 50 years and older in 2020. Solid lines show sex-specific prevalence estimates,

with shaded areas indicating 95% uncertainty intervals. MSVI=moderate to severe vision impairment. Taken from (Steinmetz et al., 2021)

Of 2208 patients under UK hospital glaucoma care and receiving regular follow up and full conventional treatment to lower IOP followed for mean of 6.7 years, 21.2% progressed at greater than 0.5 dB/year, 10.7% progressed at more than 1.0 dB/year and 2.1% progressed at more than 2.0 dB/year in their better eye. If these results were extrapolated to England and Wales, with a glaucoma population of >500,000 diagnosed patients under conventional care, one would predict approximately 10% of treated glaucoma patients (50,000) are progressing at >1dB/year. Approximately 15% (J. Landers et al., 2012)-46%(Parc et al., 2001) of patients who underwent maximal medical and surgical intervention continued to progress to blindness at up to 20 years follow up despite low IOPs. Chapter 3 further discusses the continued need to develop new diagnostic and therapeutic approaches for glaucoma by assessing rates of glaucoma progression in the local Cambridge population.

1.3 ASSESSING AQUEOUS OUTFLOW

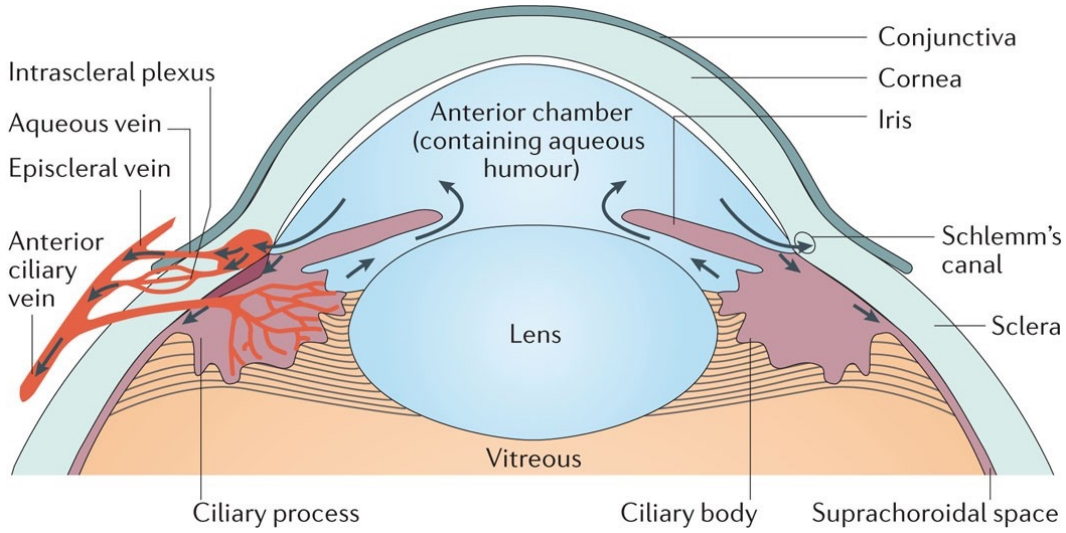


Figure 1-5: Aqueous humour production and flow. Taken from (Weinreb et al., 2016)

Aqueous is produced by the ciliary body and drains through the conventional route through the trabecular meshwork [Figure 1-5] into the episcleral venous circulation or via the uveoscleral route.

All current conventional glaucoma therapies target aqueous outflow. However, non-invasive, detailed measurement of the dynamics of human aqueous outflow is difficult to achieve with currently available clinical tools. Our knowledge of the anatomy and physiology of aqueous outflow is based on studies in ex vivo tissue (Ashton, 1952; Ashton & Smith, 1953) and in vivo techniques that are static (Kagemann et al., 2011a) or invasive or involve a degree of manipulation of physiologic parameters (Huang, Camp, et al., 2017). The widely used fluorescein disappearance test is at best an indirect estimate of aqueous outflow, and the outflow pathway cannot be visualised using this technique.

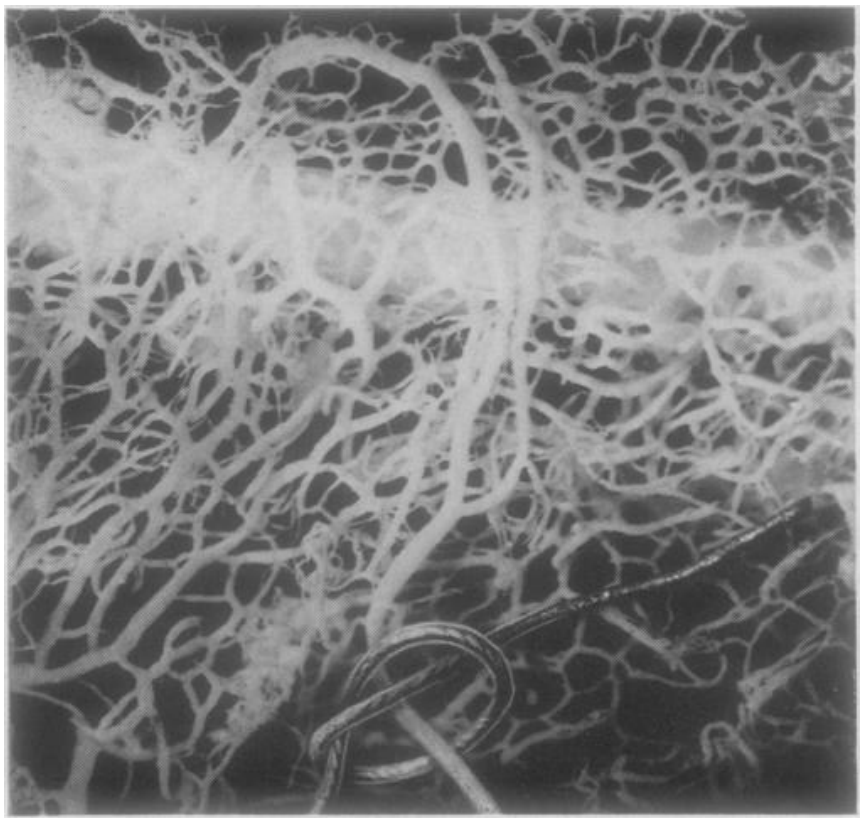


Figure 1-6: Neoprene cast of Schlemm's canal and limbal vessels showing sector containing marked aqueous vein. Taken from (Ashton, 1952)

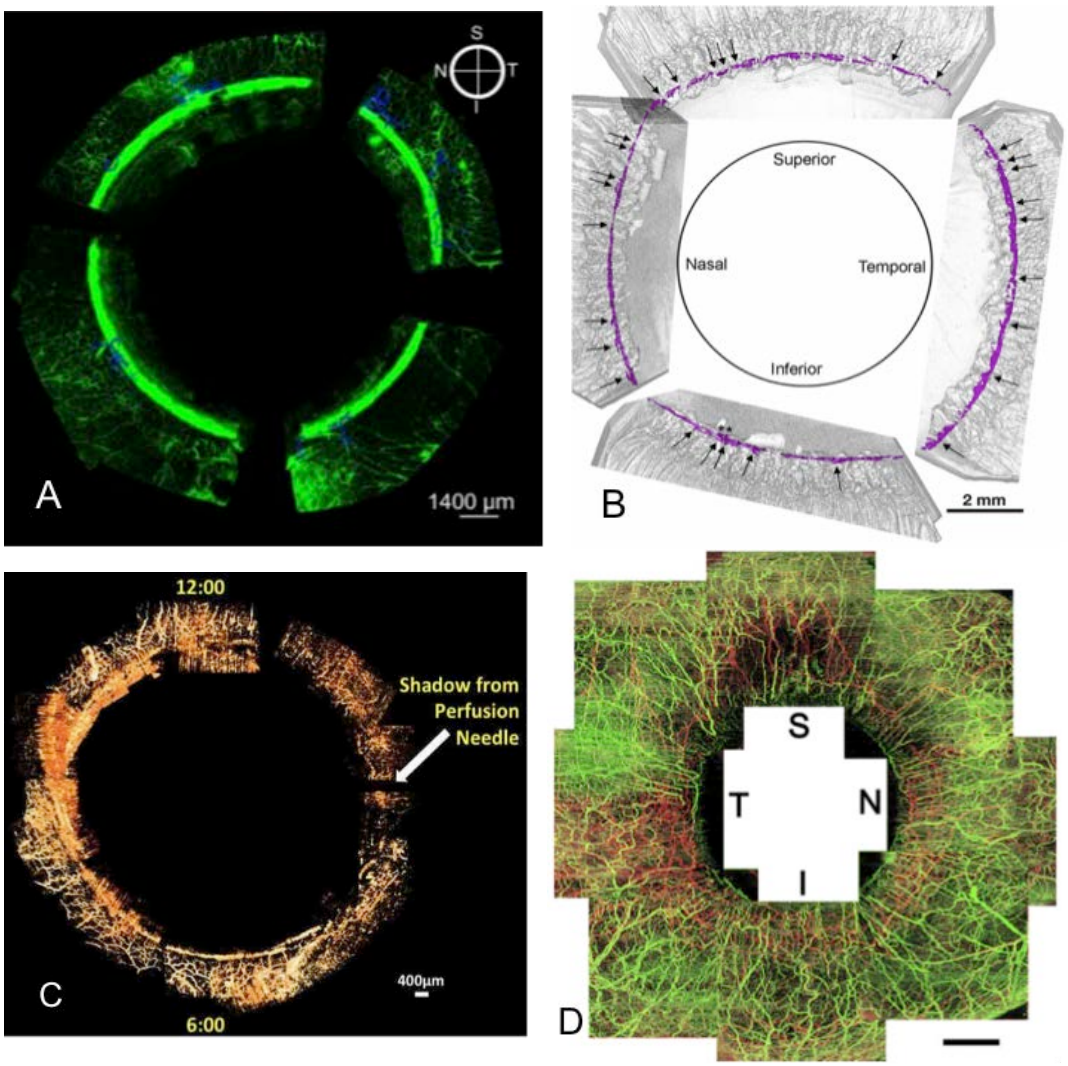


Figure 1-7. Structural reconstruction of the aqueous outflow system A: Ribbon-scanning confocal microscopy with collector channels depicted in blue. Taken from (Loewen et al., 2020) B: 3D micro-CT reconstruction demonstrating Schlemm's canal, Black arrows represent sites of collector channels Taken from (Hann et al., 2011) C: Virtual casting reconstruction of collector channels imaged with SD-OCT Taken from (Kagemann et al., 2011b) D: OCT-A reconstructed image of merged superficial (green) and deep (red) vascular networks. Note that aqueous veins are not seen. Taken from (Akagi et al., 2018). Adapted from (Lusthaus et al., 2021).

Chapter 3 discusses a technique to visualise and quantify aqueous veins noninvasively using haemoglobin video imaging (HVI). This uses the haemoglobin absorption spectrum to enhance the contrast between red blood cells and their surroundings. The effect of laser

trabeculoplasty on aqueous outflow in glaucoma patients is discussed and as well as how HVI may be used to refine surgical technique and tailor it to the anatomy of an individual's aqueous vein distribution with a move towards offering personalised and targeted treatment.

1.4 NEUROPROTECTION STRATEGIES

Alternatives to IOP-lowering approaches for POAG have focused on neuroprotection. Neuroprotection strategies typically either exploit signalling pathways to stimulate cell survival or inhibit cell death pathways as a way to boost the cells ability to withstand a pathological insult. A large number of studies have demonstrated effective neuroprotection for glaucoma in animal models (Cheung et al., 2002; Geyer et al., 1995; Gregory-Ksander et al., 2016; Howell et al., 2014; S.-Y. Kim et al., 1998; K. R. G. Martin et al., 2003; Mozaffarieh et al., 2016; Rosenthal & Fromm, 2011; Russo et al., 2008; Vorwerk et al., 1996). However, demonstrating that agents which have achieved neuroprotection in animal models of glaucoma have translational potential in human POAG clinical trials has presented several major challenges to date.

1.4.1 Brimonidine

Laboratory studies have demonstrated that systemic administration of brimonidine provides retinal ganglion cell neuroprotection in animal glaucoma models independent of its effect on IOP (Hernández et al., 2008; Woldemussie et al., 2001). This neuroprotective effect has been postulated to be mediated via a variety of mechanisms including brain derived neurotrophic factor (BDNF) (H. Gao et al., 2002) and basic fibroblast growth factor upregulation, nitric oxide synthase 3 metabolism and retinal vasomodulation (Feke et al., 2014), the activation of cell survival signalling pathways and prevention of apoptosis and $\alpha 2$ modulation of *N*-methyl-*D*-aspartate (NMDA) receptor function (Dong et al., 2008; Wheeler et al., n.d.). Brimonidine administered topically twice a day for 2 weeks prior to elective pars plana vitrectomy achieved 2nM in the vitreous (Kent et al., 2001) which was at a sufficient concentration for neuroprotection in the preclinical studies (Burke & Schwartz, 1996).

Brimonidine monotherapy lowered the incidence of visual field progression compared to timolol treated patients (9% vs 39%) in the Low Pressure Glaucoma Study Group (ClinicalTrials.gov identifier NCT00317577) over a period of 30 months in patients who were able to tolerate the treatment (Krupin et al., 2011). However, in this trial, the progression rate in the timolol cohort was worse than control untreated group of other trials such as the Collaborative Normal Tension Glaucoma Study ("Comparison of Glaucomatous Progression between Untreated Patients with Normal-Tension Glaucoma and Patients with Therapeutically Reduced Intraocular Pressures. Collaborative Normal-Tension Glaucoma Study Group," 1998). This raises the possibility that the difference reported between the two arms in the Low Pressure Glaucoma Treatment Study was due to timolol enhancing progression rather than brimonidine reducing progression, or a combination of the two. Brimonidine has a greater incidence of topical side effects [Figure 1-8] such as hyperaemia (Clemente-Tomás et al., 2018; Goyal & Raghu Ram, 2000), discomfort and hypersensitivity compared to other topical anti-glaucoma medications and the results reported could have been skewed by a selectively higher dropout rate in the brimonidine arm compared to the timolol arm.

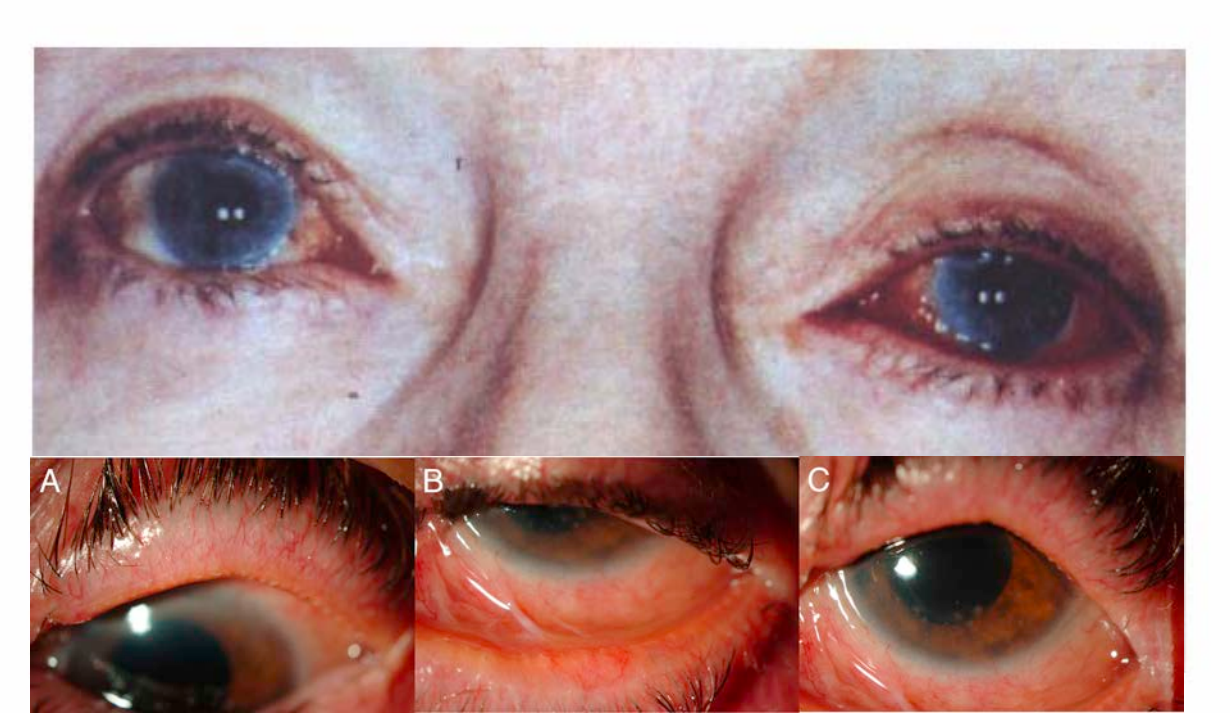


Figure 1-8: Side effects of Brimonidine topical therapy. Upper panel from (Goyal & Raghu Ram, 2000) and lower panel A-C from (Clemente-Tomás et al., 2018)

1.4.2 Cell therapy

Local administration via intravitreal injection to target retinal ganglion cells theoretically minimises unwanted side effects seen with repeated topical application. Single injections into the eye are well tolerated by patients with other chronic eye diseases such as age-related macular degeneration and may have a sustained therapeutic effect.

Intravitreal administration of mesenchymal stromal cells (MSC) has been shown to be strongly neuroprotective in experimental glaucoma (Emre et al., 2015; T. V. Johnson et al., 2010; Yu et al., 2006). Advantages of MSCs compared to other types of cells include the fact that they are easy to obtain from a variety of sources including adult bone marrow, avoid ethical concerns and can be used without immune suppression. An analysis of the protective factors produced by MSCs strongly implicated platelet-derived growth factor (PDGF) and subsequent blockage of PDGF signalling prevents MSC-mediated neuroprotection in animal models(T. V. Johnson et al., 2014). We have also demonstrated a dose dependent protection against apoptosis with PDGF treatment with greater protection from MSCs in human post mortem retinal tissue (A. Osborne, Sanderson, et al., 2018).

However, despite these encouraging results, PDGF and MSCs can induce reactive gliosis in retinal Muller cells and astrocytes [Figure 1-9] with upregulation of intermediate filament proteins and retinal folding (Tassoni et al., 2015).

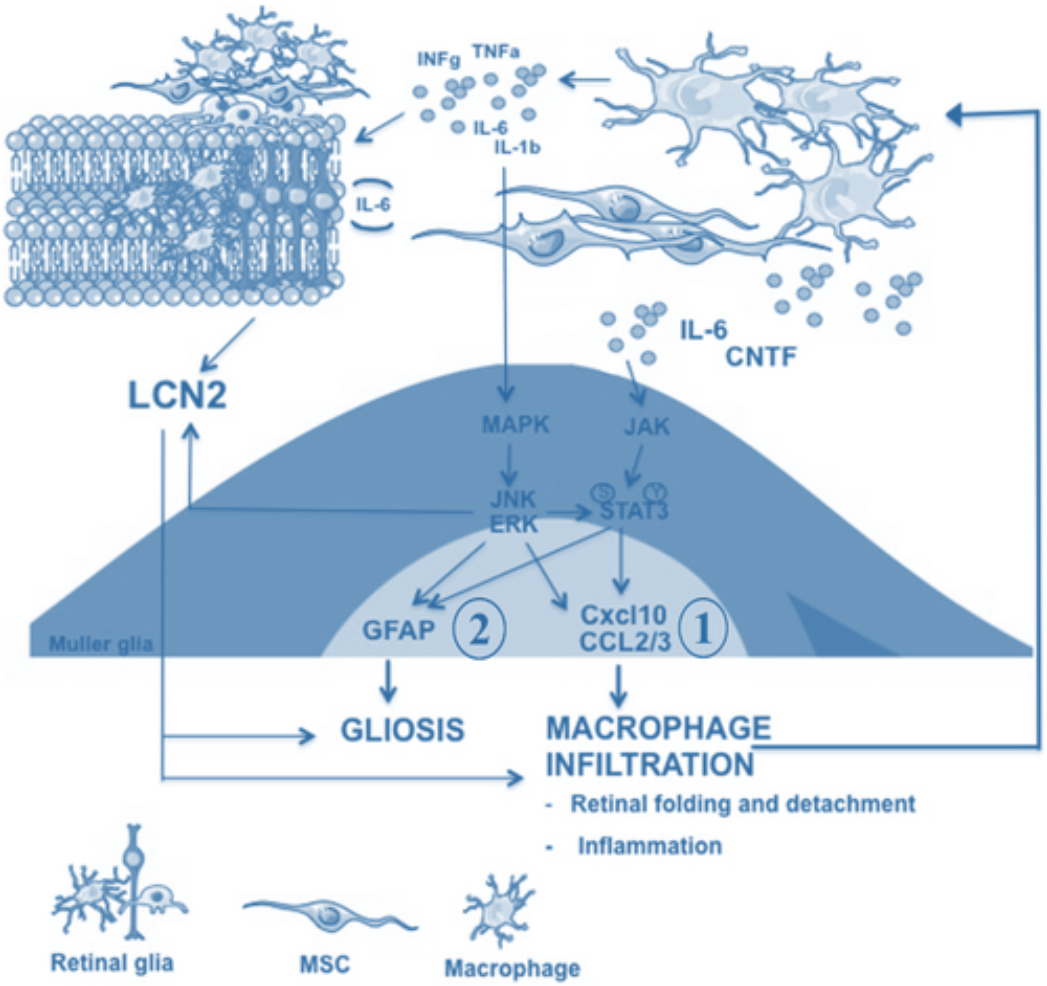


Figure 1-9: Molecular mechanisms inducing reactive gliosis following intravitreal mesenchymal stem cell administration. Adapted from (Tassoni et al., 2015)

There have been similar recent reports of proinflammatory vitreous clumping (Tzameret et al., 2014) of MSCs injected intravitreally as well as thick epiretinal membrane formation following MSC administration in humans (J. Y. Kim et al., 2016). These adverse effects may also be due in part to the inconsistency in MSC isolation and preparation. An attempt to standardise the identification of these cells led to the development of the International Society for Cellular Therapy criteria (Dominici et al., 2006), but problems continue to be reported despite this and may limit the degree to which MSCs can successfully be used to confer neuroprotection to retinal ganglion cells.

There have been significant concerns regarding the unregulated use of stem cells in various centres around the world. Most stem cell treatments for glaucoma administered worldwide are unregulated and currently most registered trials are patient funded, open-label studies. Kuriyan *et al.* reported severe bilateral visual loss in three patients who received intravitreal injections of autologous adipose tissue–derived stem cells for age-related macular degeneration (Kuriyan et al., 2017). Visual loss was related to ocular hypertension, haemorrhagic retinopathy, vitreous haemorrhage, combined traction and rhegmatogenous retinal detachment, or lens dislocation [Figure 1-10]. The pre-injection visual acuity ranged from 20/30 to 20/200 and measured between 20/200 and no light perception one year post injection.

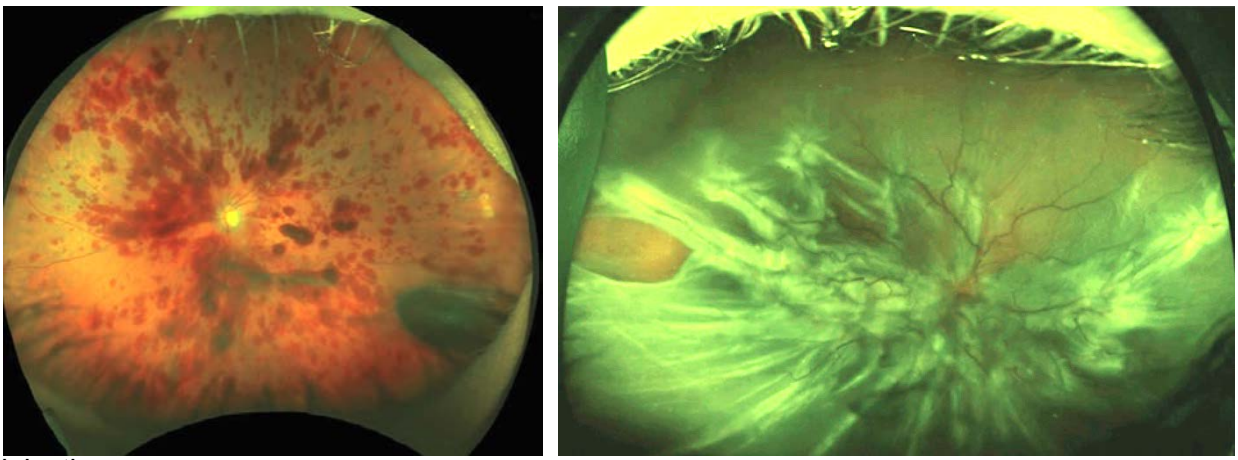


Figure 1-10: Haemorrhagic retinopathy (left) and tractional retinal detachment (right) following intravitreal injection of autologous adipose tissue-derived stem cells. Taken from (Kuriyan et al., 2017)

There are currently at least four registered clinical trials evaluating the use of stem cells in glaucoma. The Intravitreal Mesenchymal Stem Cell Transplantation in Advanced Glaucoma study (NCT02330978) is a Phase 1 safety study in 10 patients who meet the legal definition of bilateral blindness, with intravitreal injection of autologous MSCs administered to the worst-affected eye. Secondary outcome measures include visual acuity, visual fields, optical coherence tomography and electroretinography. Stem Cell Ophthalmology Treatment Study

(NCT01920867) and Stem Cell Ophthalmology Treatment Study II (NCT03011541) are non-randomised, open label efficacy studies evaluating the use of MSCs in multiple eye diseases including glaucoma delivered through either the sub-Tenon's, retrobulbar, intravitreal or intravenous route. The study is patient funded and claims to be associated with a risk of potential complications of 0.0008% to 5% depending on the physician-selected treatment protocol chosen for individual patients. The study website declares that the investigators hope for visual improvement in the vast majority of individuals enrolled, but very little information is provided with regard to outcomes of those already treated. The Effectiveness and Safety of Adipose-Derived Regenerative Cells for Treatment of Glaucomatous Neurodegeneration study (NCT02144103) is an open-label safety and efficacy study in Russia. Stem cells are delivered via the sub-Tenon's route with structural and functional endpoints and is a single-arm study with no control group.

It remains conceivable that stem cells do have the potential to provide a useful treatment strategy for glaucoma, either by a neuroprotective or neuroregenerative mechanism. However, in order to assess such strategies we need randomised, masked, controlled clinical trials and further work on the optimal mode of delivery. Care needs to be taken to prevent the exploitation of vulnerable patients and false promise of success with unproven treatments.

1.4.3 Neurotrophins

Ciliary Neurotrophic Factor

Ciliary neurotrophic factor (CNTF) has been shown to be neuroprotective in experimental glaucoma (Pease et al., 2009). A randomised, sham-controlled, masked Phase II clinical trial by Neurotech Pharmaceuticals is currently underway to assess the effects of encapsulated cell-based delivery of ciliary neurotrophic factor (CNTF) in 54 glaucoma patients using the NT-501 device. Retinal pigment epithelial cells that have been engineered to release CNTF are encased in a semi-permeable membrane which permits the selective and sustained release of CNTF to retinal ganglion cells when implanted intravitreally.

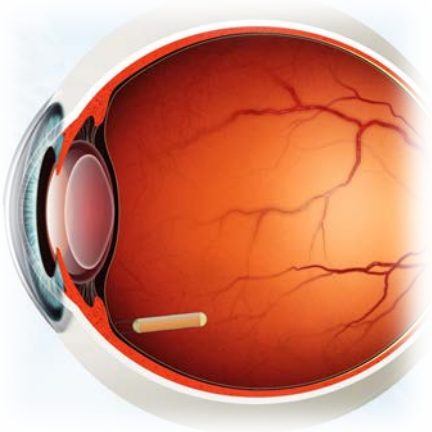


Figure 1-11: schematic illustrating encapsulated CNTF in vitreous. From neurotechusa.com

The NT-501 implant has also been shown to slow the progression of retinal photoreceptor degeneration and stabilise visual function in the patients with macular-telangiectasia type 2 (NCT01949324) (Chew et al., 2019). A Phase III study to further assess the effects of NT-501 in macular-telangiectasia type 2 is currently enrolling across the US, Australia and Europe.

Recombinant human nerve growth factor

Eye drops containing recombinant human nerve growth factor (rhNGF) have received FDA approval to treat neurotrophic keratitis (Lambiase et al., 1998) with encouraging safety and efficacy results in dry eye disease (NCT02101281) with data from further trials to follow (NCT03019627, NCT03035864).

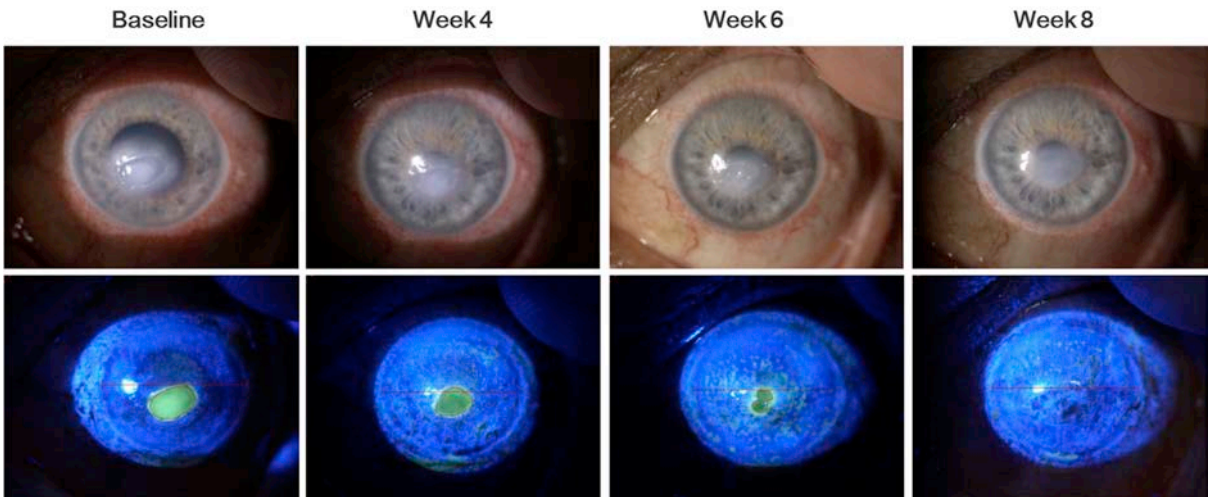


Figure 1-12: Recombinant human nerve growth factor to treat neurotrophic keratitis. Top panel, Photographs of the cornea. Bottom panel, Corneal ulcer epithelial fully healed at week 8 assessed using fluorescein dye under cobalt blue illumination. Taken from (Bonini et al., 2018)

A Phase 1b randomised, double-masked study to assess the safety and tolerability of rhNGF eye drops in progressive POAG patients compared to vehicle has completed recruitment (NCT02855450). Secondary objectives include structural and functional assessments using changes in visual field, ERG and optical coherence tomography of the ganglion cell layer and retinal nerve fibre layer thickness. The investigators also plan functional assessments to determine whether any biological effect persists following discontinuation of the study treatment.

1.4.4 Memantine

Oral administration of existing therapies that have been repurposed for glaucoma is an approach which can help overcome some issues with safety profile and regulatory agency approval meaning that an effective treatment can reach the clinic more quickly. Memantine is a non-competitive NMDA receptor antagonist (Vorwerk et al., 1996) which is used in the

treatment of moderate to severe Alzheimer's disease and showed promising results in a monkey model of glaucoma (Hare et al., 2004). NMDA receptors are widely distributed throughout the central nervous system and are essential for neurotransmission and the healthy function of neuronal cells. However, overstimulation in the presence of excessive glutamate can lead to Ca^{2+} - mediated neurotoxicity. The dysregulation of this cascade has been widely implicated in many chronic neurodegenerative conditions including glaucoma and led to the memantine glaucoma trials, the results of which were anticipated with great interest. However, large scale multicentre, randomised double-masked placebo controlled Phase III clinical trials (NCT00141882, NCT00168350) conducted to test the efficacy of oral memantine for glaucoma, showed there was no evidence of any statistical benefit compared to placebo in reducing visual field progression. The failure to demonstrate statistical significance relative to placebo in trials that took nearly 5 years at an estimated cost of over $100 million highlighted a need for better glaucoma clinical trial design and more effective use of relevant endpoints as required by regulatory agencies.

1.4.5 Nicotinamide (Vitamin B3)

A team from the Centre for Eye Research Australia led by Jonathan Crowston has recently completed a neuroprotection pilot study investigating the short-term effect of taking the nicotinamide adenine dinucleotide (NAD) precursor nicotinamide (Vitamin B3) supplementation on patients with glaucoma(Hui et al., 2020). NAD is an essential co-factor in the redox reactions of the mitochondrial respiratory chain required to maintain sufficient levels of adenosine triphosphate (ATP). The intraocular portion of the retinal ganglion cell axon is unmyelinated and therefore has a particularly high energy requirement. Nicotinamide deficiency and NAD depletion therefore have the potential to disrupt mitochondrial and energy metabolism and ganglion cell function.

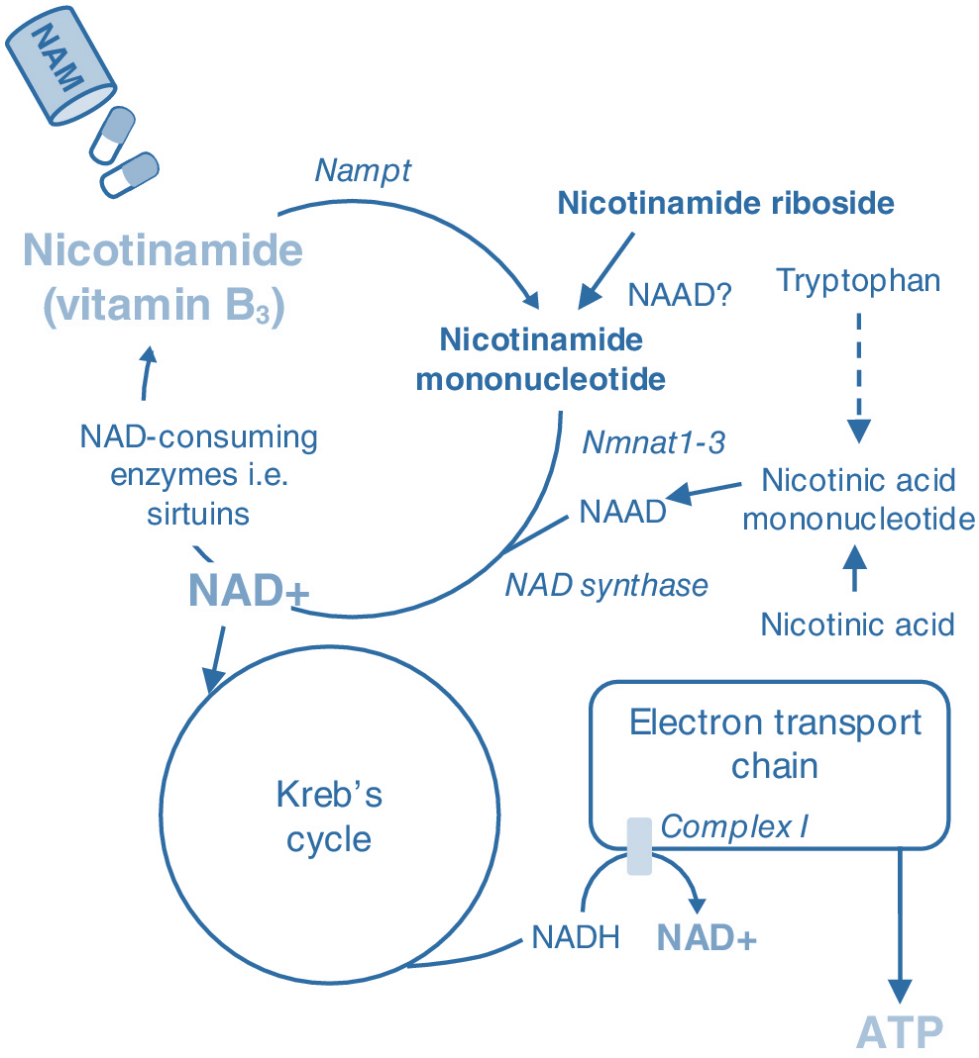


Figure 1-13: Mechanism of action of Nicotinamide (Vitamin B3). Adapted from (Hui et al., 2020)

Recent work (Kouassi Nzoughet et al., 2019) has demonstrated a significantly lower plasma nicotinamide concentration in POAG patients relative to controls which lends support to this hypothesis.

Furthermore, Williams *et al.* demonstrated that nicotinamide supplementation conferred significant neuroprotection both prophylactically and as an intervention in the DBA/2J chronic, age related open angle mouse model of glaucoma which confers a phenotype similar to pigment dispersion syndrome (Williams et al., 2017). Treatment at the highest dose (2000

mg/kg/day) tested reduced the risk of developing glaucoma by 10-fold (equivalent human dose 162.6 mg/kg/day). The authors had also demonstrated an age-dependent reduction in retinal levels of NAD and postulated that this reduction led to mitochondrial dysfunction and rendered aging neurons more susceptible to raised IOP (Williams *et al.*, 2018). They analysed age- and IOP- dependent changes in transcripts of NAD producing enzymes within retinal ganglion cells and showed that nicotinamide treatment prevents these transcriptomic changes. Similar neuroprotective effects were also seen by overexpressing Nmnat1, an enzyme required for NAD production, using a gene therapy approach. The ability to confer neuroprotection by modulating mitochondrial vulnerability builds upon the significant body of work implicating age, metabolic stress and mitochondrial dysfunction in POAG (Williams *et al.*, 2018).

Primary outcomes for the nicotinamide clinical trial include functional changes measured using visual fields and electroretinography and structural outcomes including hyperspectral imaging and OCT. Participants were randomly assigned to take oral nicotinamide or placebo daily for 12 weeks with functional and structural testing at baseline, 6 and 12 weeks post-intervention. A crossover design switched patients without a washout period to take placebo or nicotinamide for another 12 weeks with the same outcome measures repeated at 6 and 12 weeks post-intervention.

The safety and efficacy of oral nicotinamide has already been demonstrated in a Phase III randomised clinical trial (UTN U1111-1131-4069) published in the *New England Journal of Medicine*, where the rate of new non-melanoma skin cancers and actinic keratoses in high-risk patients was reduced following oral supplementation at a dose of 500 mg of nicotinamide twice daily for 12 months compared to placebo (A. C. Chen et al., 2015). The protective effects of nicotinamide in this trial were thought be mediated by minimising the damage from UV radiation. Radiation exposure coupled with a bioenergetic defect from mitochondrial dysfunction has also been implicated in POAG, rendering retinal ganglion cells susceptible to injury (N. N. Osborne et al., 2006).

The promise from the pre-clinical data, other fields and the pilot study together with the use of electroretinography and hyperspectral imaging to provide functional outcomes in a short period of time has the potential to make a significant impact and the results from the larger planned follow up trial to this pilot are anticipated with interest.

1.5 GENE THERAPY

At present, no gene therapy for glaucoma neuroprotection has reached the clinical trial stage. Successes in gene therapy to treat other progressive retinal and optic nerve pathologies that were previously deemed untreatable have been encouraging, not only with regards to prospects for POAG treatment, but for the scientific and medical community as a whole.

Those trials that have progressed the furthest are single gene replacement therapies for a specific genetic defect in people with inherited retinal diseases. The immediate comparison for glaucoma patients is perhaps for those with congenital or juvenile open angle glaucoma who have a specific genetic defect. Dominant mutations in myocilin have been shown to affect trabecular meshwork function and raise the IOP with subsequent development of glaucoma (Kwon et al., 2009).

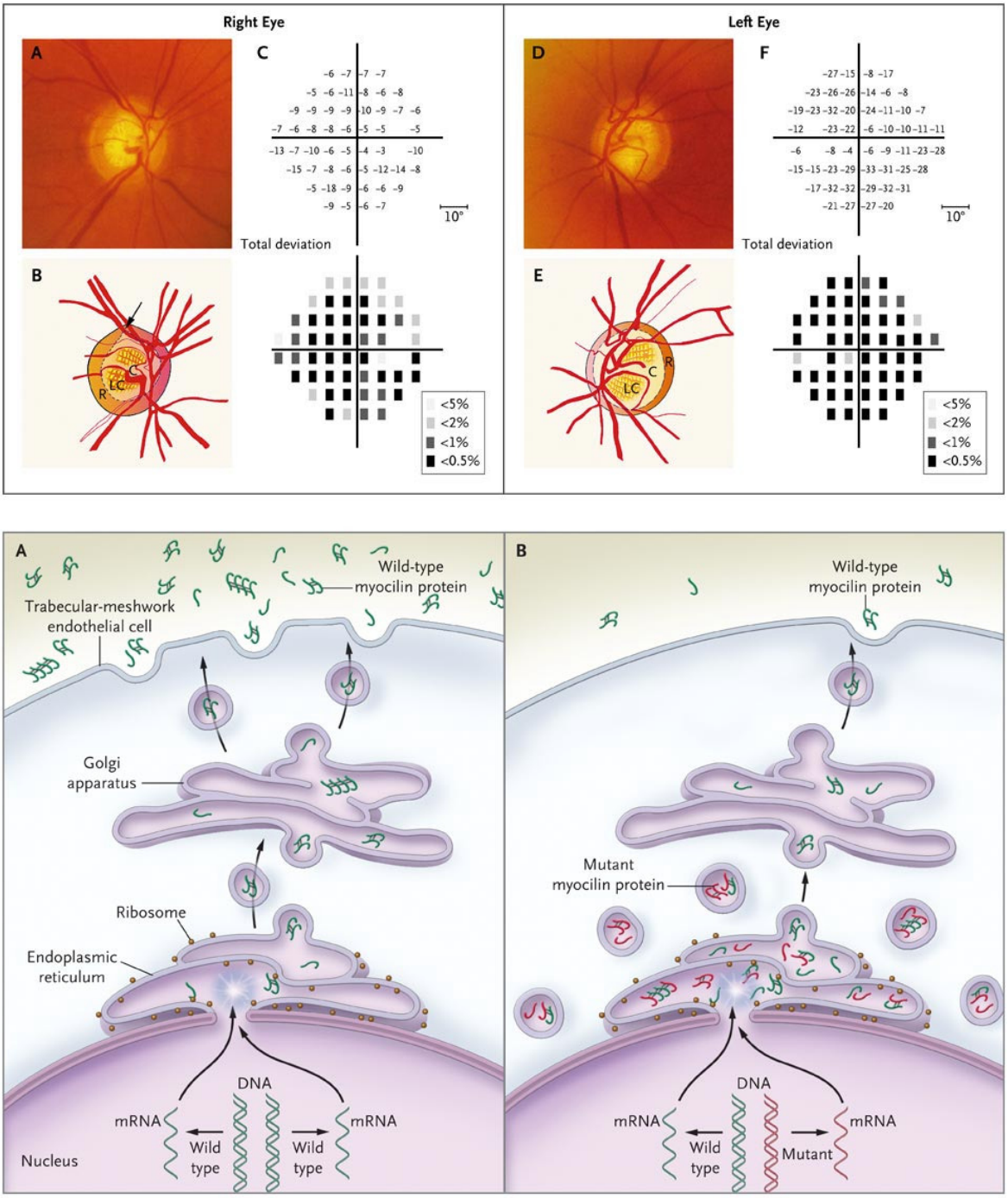


Figure 1-14: Myocilin and POAG. Upper panel showing glaucomatous optic neuropathy and corresponding visual field loss in a patient with a MYOC mutation. Lower panel shows proposed pathways for normal secretion of myocilin into the aqueous humour (lower left) and for secretion reduced by a MYOC mutation (lower right). Taken from (Kwon et al., 2009)

Jain *et al.* disrupted the effects of the mutant myocilin gene using AAV-CRISPR/Cas9 (Ad5-cas9 and Ad5-crMYOC) in a mouse model of myocilin-associated POAG (Jain et al., 2017). They were able to lower the IOP in treated eyes and prevent further glaucomatous damage. The authors also applied these constructs to human explants and demonstrated a reduction in trabecular meshwork myocilin mRNA. More recently, mutations in angiopoietin receptor TEK (tunica interna endothelial cell kinase, also known as Tie2) have been implicated in Schlemm's canal development with congenital glaucoma phenotypes seen in mice that lack functional angiopoietin-TEK signalling (Thomson et al., 2014). Human mutations in TEK with variable expressivity have also recently been identified in a primary congenital glaucoma cohort that do not carry mutations in other known disease-causing genes (Souma *et al.*, 2016) and work is ongoing to assess the effects of TEK augmentation in these patients.

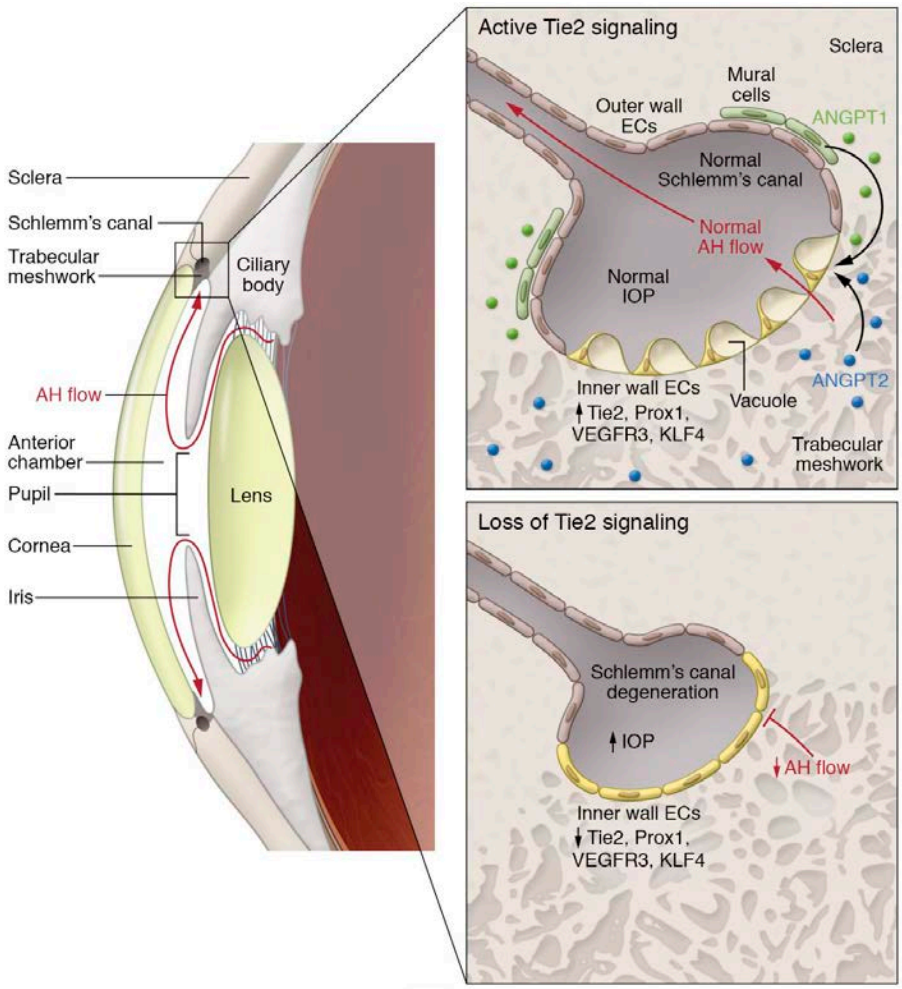


Figure 1-15: Role of the angiopoietin/TIE2 pathway in maintenance of Schlemms canal. Taken from (Bernier-Latmani & Petrova, 2017)

Gene therapy for glaucoma patients who have a specific genetic defect is conceivable, but gene therapy could also be used to deliver protective or regenerative factors in patients with disease not caused by single gene defects (L. Cheng, Sapieha, Kittlerova, et al., 2002; de Lima et al., 2012; Adriana Di Polo et al., 1998; Lim et al., 2016; K. R. Martin et al., 2003; K. K. Park et al., 2008; Pease et al., 2009). This approach has recently been summarised (Rhee & Shih, 2021) and forms the basis of the experimental work outlined in Chapters 5 and 6 to develop approaches to repair and regenerate the optic nerve.

CHAPTER 2

MATERIALS AND METHODS

2.1 METHODS FOR CHAPTER 3

A retrospective comparative cohort review was performed of patients attending the Addenbrooke's Glaucoma Clinic (AGC) or Community Optometrist Glaucoma Scheme (COGS) clinic. All patients had SITA-standard automated perimetry performed with the Humphrey Field Analyzer (HFA, Carl Zeiss Meditec, Dublin, Calif.) using the 24-2 full-threshold programme with a Goldmann size III stimulus and appropriate refractive correction. Patients that had either had one or two eyes with 5 or more SITA-standard 24-2 visual field tests were included in the analysis. All patients from the COGS service since its inception in 2010 to 2019 and a similar cohort from the AGC group were analysed. Data for each eye was processed separately where both eyes were included. The Zeiss Forum software was used to extract the data and calculate the MD progression rate (dB/year) using Guided Progression Analysis. Graphpad Prism software was used for statistical analysis. The D'Agostino-Pearson test was used to evaluate whether the distribution of continuous variables was normal. The descriptive statistics for non-normally distributed variables (number of visual field tests, follow-up, mean deviation rate of progression, loss of sight years) are presented as median (25^{th}-75^{th} percentiles) unless otherwise specified. The Mann-Whitney test was used to compare non-normally distributed independent variables between groups. Loss of sight year (LSY) analysis was performed by estimating the number of years each patient would develop bilateral visual field loss worse than MD of −22 dB in their predicted remaining lifetime as previously described (Bryan & Crabb, 2018).

2.2 METHODS FOR CHAPTER 4

This study was conducted in accordance with the tenets of the Declaration of Helsinki. The Institutional Review Board of Cambridge University Hospitals NHS Foundation Trust and the

Local Research Ethics Committee approved the study (REC reference number: 15/LO/2171) . All subjects gave written informed consent before participation in the study.

2.2.1 Imaging aqueous veins

We performed an observational study on 30 glaucomatous eyes to determine characteristics of aqueous veins using Haemoglobin Video Imaging (HVI). Images were captured using a monochromatic Prosilica GC1380H camera attached to a Zeiss SL130 slit lamp. As described previously (Meyer, 2018) the slit-lamp illumination system is fitted with a band-pass interference filter (steep long and short wavelength cut-off; >50% transmission between 505 and 575 nm) and a hot mirror that stops light with wavelengths beyond 730 nm from reaching the camera. The video camera is mounted on a 50% beam-splitter with a 220 mm focal length C-mount. Images are captured at 30 frames per second, without compression. During the live recording of aqueous veins, images are displayed in real time using bespoke HVI software.

2.2.2 Image processing

Raw image data was exported from the HVI software in .pgm format and processed using Image J. A code to stabilise the images is provided in Appendix 1 and was used for the initial validation experiments. Image sequences were subsequently stabilised using the 'Image J Stabilizer' plugin (Video clips 1 and 2) prior to quantification. As blood-filled episcleral veins join those containing aqueous, the stream of aqueous migrates towards the centre of the vessel, while blood remains at its periphery: the axial zone of low pixel density defines the aqueous stream. Outside the aqueous stream, pixel density was taken to be proportionate to the depth of red cells in the blood column. Transepts of aqueous veins show increasing density from the periphery until the low-density central aqueous column so that the aqueous column diameter is found the distance (δ) between intensity minima. For calculation of the cross-sectional area, we assumed the vessel had a circular section. Measurements were made upstream of a vessel confluence. We assessed the repeatability of measurements by comparing values from 4-10 separate images per eye for 9 individuals. For extended length

sequences to enable detailed observation of aqueous vein characteristics, stabilisation was performed using Adobe After Effects CC (version 15.1.12).

2.2.3 Aqueous column cross-sectional area following selective laser trabeculoplasty

We performed HVI on 8 eyes, immediately before and 10 minutes after selective laser trabeculoplasty (SLT). SLT energy settings were 0.3-1.2 mJ targeting 90-360^{o} of the trabecular meshwork. IOP was measured immediately before and 30 minutes post-procedure. Pilocarpine nitrate 2% (Bausch and Lomb) and apraclonidine 1% (Alcon) eye drops were instilled 30 minutes prior to SLT. The CSA of the aqueous column was calculated and correlated with the degree of IOP reduction observed and the change in mean deviation (MD) using 24-2 Humphrey visual field SITA standard testing pre and post intervention. The mean length of time for MD measurement post intervention was 23 weeks (range 15-30 weeks).

2.2.4 Quantifying flow rate

Aqueous flows as a central stream through a column of venous blood. Therefore, enhancement of aqueous drainage can be expected to increase the flow rate of the surrounding red blood cells and it is this effect that we aimed to exploit.

We used principles derived from photon correlation spectroscopy and laser doppler velocimetry where fluctuations in the recorded intensity signal are examined to estimate parameters such as particle size or velocity. For aqueous flow using successive HVI images, fluctuations in contrast and pixel intensity of red blood cells through an aqueous vein were calculated and used to compare the rate of flow before and after our SLT protocol.

Quantifying flow rate: fluctuation transformation

The sum of the absolute values of pixel-wise differences from successive stabilised HVI frames were taken:

$$d_{ij} = \sum_{t=0}^{N-1} |p_{ij}(t+1) - p_{ij}(t)|$$

where *t* denotes frame number, (i,j) denotes pixel coordinates of the individual pixels and $p_{ij}(t)$ is the pixel intensity in frame t, with N being the total number of recorded frames and d_{ij} being the un-normalised fluctuation value. In order to extract the relative scale of the fluctuations in comparison with the whole image, we then normalise the computed values as follows:

$$n_{ij} = (d_{ij} - \mu)/\sigma$$

where μ, σ are, respectively, the mean and standard deviations of the fluctuations values d_{ij} in the image.

Quantifying flow rate: autocorrelation analysis

The above transformation was used to segment the pixels of interest from the background and compute an "autocorrelation" to quantify the timescale of pixel fluctuations and how fast the pixel values change. Pixels with normalized fluctuation value above a given threshold of 2.5 were selected and the mask applied to all frames in the video.

$$R_{ij}(n) = \frac{\mathbb{E}[\,(p_{ij}(t) - \mu)(p_{ij}(t+n) - \mu)]}{\sigma^2}$$

Where $R_{ij}(n)$ denotes the autocorrelation function value for a pixel at position (i,j) at a frame delay value *t*, μ is the mean pixel value in the segmented image, σ is the standard deviation of the pixel values in the segment. The mean signal was computed by averaging the autocorrelation across all pixels. In order to show invariance we also computed the autocorrelations for the background of the HVI images.

2.3 METHODS FOR CHAPTER 5

2.3.1 Vector production

AAV vectors were manufactured by Vigene Biosciences (9430 Key West Avenue, Suite 105, Rockville, MD 20850, USA). Vector particles were liberated following freeze-thaw of HEK293 cells transduced with plasmid DNA, followed by iodixanol gradient ultracentrifugation, de-salting and were suspended in phosphate-buffered saline (PBS) buffer (Thermo Fisher Scientific). Titres were confirmed by Vigene Biosciences through qPCR using primers recognising the ITR regions. All vectors contained a modified CAG promoter, shortened Woodchuck Hepatitis Virus Posttranscriptional Regulatory Element (WPRE) and simian virus 40 late polyadenylation signal (polyA), as described previously (A. Osborne, Wang, et al., 2018).

2.3.2 Animals

Homozygous mice transgenic for human mutant P301S tau (original colony from M Goedert (Allen et al., 2002)) were used at 1, 3 and 4 months of age. These mice are bred on a C57BL/6 background and the P301S mutation is under the control of the Thy-1 promoter. Filamentous inclusions made of hyperphosphorylated tau are present in the central nervous system of 3- and 5-month old transgenic mice and we have previously described the phenotypic appearance of the retina and optic nerve, expression of human mutant P301S tau in RGCs and the formation of tau inclusions (Gasparini et al., 2011) together with a reduction in optic nerve axonal transport and an increased susceptibility to injury (Bull et al., 2012). Age- and sex-matched C57BL/6 mice (Charles River, UK) were used as controls. Wild-type adult Sprague-Dawley rats were used for the laser induced ocular hypertension model of experimental glaucoma. Animals had unrestricted access to food and water, and were maintained on a 12 h light/dark cycle. All experiments were carried out in accordance with the UK Home Office Regulations for the Care and Use of Laboratory Animals and the UK Animals (Scientific Procedures) Act 1986 and the Association for Research in Vision and Ophthalmology's Statement for the Use of Animals in Ophthalmic and Visual Research. They were approved by the University of Cambridge Animal Ethics Committee (Project Licence 70/8152).

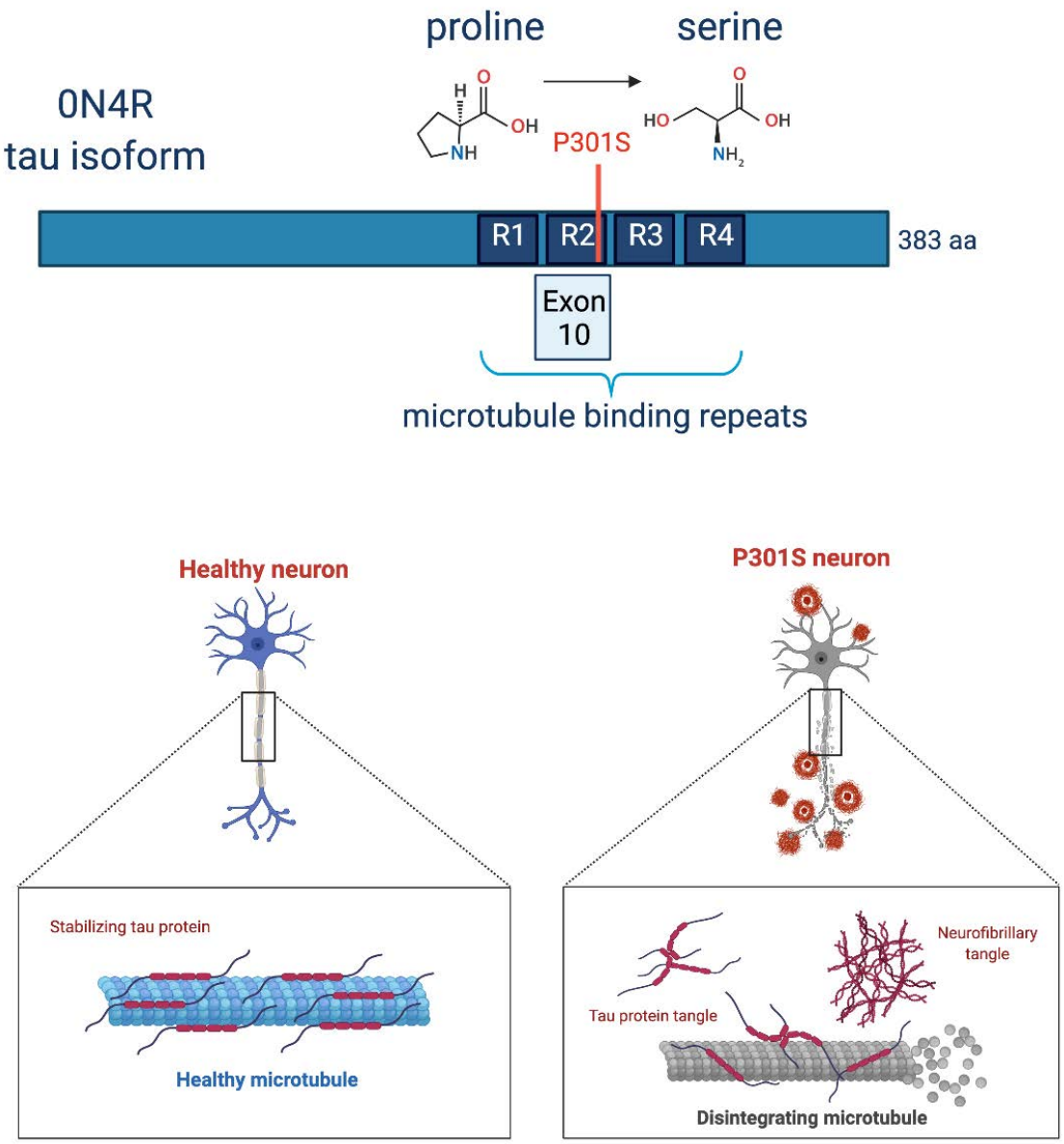


Figure 2-1: P301S mutation with disruption to axonal integrity.

2.3.3 Intravitreal vector injection

Animals were anaesthetised with intraperitoneal injection of ketamine (50mg/kg) and xylazine (10mg/kg) and topical 1% tetracaine eye drops (Bausch&Lomb) prior to injection. Freshly thawed AAV2 vectors were diluted to working stock in sterile PBS and 2µL (mice) or 5µL (rats) of vector injected through the sclera into the vitreous of the eye posterior to the limbus (Syringe: 5µL, #65RN; Needle: ga33, 8mm, pst2. Hamilton Co.). Injections were given slowly over 1 minute to allow diffusion of the vector suspension. All injections for the experimental work were

carried out by the same surgeon and vectors were administered at 1 x 10^{10} GC (genomic copies)/eye. Tissue was collected at the indicated time points following transcardial perfusion with 4% paraformaldehyde (PFA) under terminal anaesthesia. For the viral vector titre optimisation, sixteen adult immunocompetent C57bL/6 mice received intravitreal injections of AAV2-CAG-GFP at 3 different titres: 1 x10^{8}, 1 x 10^{9} or 1 x 10^{10} GC/eye. 2µl of the virus was injected at each concentration. To determine the effect of volume on transduction efficiency, a subset of animals received 1 µl of the highest viral titre. Animals were sacrificed 21 days after injection.

2.3.4 Rat Laser Induced Ocular Hypertension

21 days after intravitreal vector injection, ocular hypertension was induced in rats as previously described (Marina et al., 2010). Rat were placed in front of a slit-lamp and forty to sixty laser pulses (wavelength 532nm, spot size 50µm, power 700mW, duration 600 msec) were directed around the circumference of the trabecular meshwork to impair aqueous drainage. Contralateral fellow eyes served as normotensive controls. IOP was measured bilaterally under anaesthesia on procedure days and whilst awake at subsequent time points using a TonoLab rebound tonometer calibrated for the rat eye (Tiolat Oy). Tonometry was performed within 5 mins of anaesthesia onset and between the hours of 9:00am and 11:00am. Fifteen recordings were taken from each eye at each time point.

2.3.5 Electroretinography (ERG)

Full-field ERGs were recorded simultaneously from both eyes of each animal as described previously (Y. X. Kong et al., 2009). Animals were dark-adapted overnight and ERG recordings were performed under low level, red light illumination. ERG recordings were acquired using an Espion E3 system with full- field Ganzfeld sphere (Diagnosys, Cambridge, UK) as follows: Scotopic threshold response recorded at -4.73 log cd.s.m^{-2} (averaged responses from between 20 recordings with interstimulus interval of 3 seconds). Peak

amplitude between 80-120 msec was taken as the positive scotopic threshold response (pSTR) amplitude.

2.3.6 Spontaneous object recognition task

The spontaneous object recognition task was performed as previously described (Romberg et al., 2013; S. Yang et al., 2015), using a Y-shaped apparatus. Briefly, all mice were habituated in three consecutive daily sessions in the empty Y-maze apparatus for 5 minutes. Each test session consisted of a sample phase and a choice phase. In the sample phase, the animal was placed in the start arm and left to explore the two identical objects, which were placed on the end of two arms for 5 minutes. The choice phase followed after a delay of either 3 hours or 24 hours during which the animal spent in the home cage. The choice phase was procedurally identical to the sample phase, except that one arm contained a novel object, whereas the other arm contained a copy of the repeated object. An unused copy of the repeated object was used in order to avoid olfactory disturbance. Each animal received 2 test sessions for each delay. A different object pair was used for each session for a given animal, and the order of exposure to object pairs as well as the designated sample and novel objects for each pair were counterbalanced within and across groups. The object exploration time was assessed from video recordings of the sample and choice phase. Direct nasal or head contacts only were regarded as an exploratory behaviour. For the choice phase, a discrimination ratio was calculated by dividing the difference in exploration of the novel and familiar objects by the total object exploration time. Therefore, the discrimination ratio varies from 0 (equal exploration for novel and familiar objects) to 1 (exploration of the novel object only). The mean discrimination ratio across two test sessions was calculated for each animal.

2.3.7 Perirhinal cortex AAV5 injections

Six injections into the perirhinal cortex (3 per hemisphere, 0.5 µl with a speed of 0.2 µl/minutes) were performed stereotaxically under isoflurane anaesthesia with a 10 µl Hamilton syringe (Syringe: 10µL, #701RN; Needle: ga33 Hamilton Co.) and a 33 gauge needle at the following

sites (in mm from bregma and the surface of skull): 1. anterior–posterior (AP): − 1.8; lateral (L): ± 4.6; ventral (V): − 4.4, 2. AP: − 2.8; L: ± 4.8; V: − 4.3 and 3. AP: − 3.8; L: ± 4.8; V: − 3.8. The needle remained in place at the injection site for 3 minutes before being slowly withdrawn over 2 minutes.

2.3.8 Western blots

Retinas were excised from the eye cup immediately after death and tissue snap frozen on dry ice prior to lysing using a Lysis-M reagent containing cOmplete Mini Protease Inhibitor (Roche) and phosphatase inhibitors (Thermo Fisher Scientific). Following 20 minutes homogenization, tissue was centrifuged at 13,000 rpm for 10 minutes to isolate the soluble cell extract. Protein concentration was determined using a bicinchoninic acid (BCA) protein assay (Thermo Fisher Scientific) and equal quantities of protein loaded into 10% or 4–12% Bis–Tris gels (NuPAGE Novex, Thermo Fisher Scientific). Membranes were blocked in 5% dried skimmed milk in PBS with 0.2% Tween20 (Sigma-Aldrich) for 60 minutes and then incubated overnight at 4 °C in primary antibody (BDNF N-20, rabbit, 1:200, sc-546, Santa Cruz Biotechnology; TrkB, rabbit, 1:500, ab33655, Abcam; beta-actin, rabbit, 1:1000, 4967, Cell Signaling). Primary antibodies were visualized with HRP conjugated anti-rabbit secondary antibody (1:8000; PI-1000; Vector Laboratories) and signal detection using ECL Prime (GE Healthcare) and an Alliance Western blot imaging system (UVItec Ltd.).

2.3.9 Measuring anterograde axonal transport

Tracing the optic nerve

The vitreous body of the left eye was injected with 2 µl of 0.1% solution of cholera toxin B protein subunit b (CTB) conjugated to Alexa Fluor (AF)-555 in sterile phosphate-buffered saline (PBS) (Thermo Fisher Scientific). CTB binds the GM1 ganglioside receptor on RGCs and is widely used as an axonal tracer and marker of transport because it is selectively taken up by RGCs in the retina (Crish et al., 2010). Following the injection, the needle was held in

place for 1 minute, to prevent reflux. Animals were perfused intracardially with 4% paraformaldehyde (PFA) 24 hours post CTB administration.

Tissue processing

Optic nerves of perfused mice were dissected immediately behind the posterior globe at the optic nerve head and the optic chiasm, and brains were removed. Nerve and brain tissue was post-fixed overnight at 4°C, washed in PBS and cryo-preserved by overnight immersion in 30% sucrose at 4°C. Following embedding in optimal cutting temperature compound (Tissue-Tek, Miles Laboratories), serial 30 µm thickness coronal cryosections of the entire superior colliculus from each animal were obtained and 14 µm-thick longitudinal sections of the optic nerve were cut using a cryostat and mounted onto microscope slides in darkened conditions. Immunohistochemical visualisation of CTB was not required as the fluorophore was directly conjugated to the CTB. Sections were visualised under epifluorescent illumination on a single Leica DMi8 microscope using a 20X objective (optic nerve) and 10X objective (superior colliculus). Contiguous images were captured and tiled using LAS AF software (Leica Inc.) and identical camera settings.

Quantification of anterograde axonal transport of cholera toxin B

We developed a semi-automated tool [Figure 5-10I] to quantify mean CTB fluorescence intensity across the width of each optic nerve, perpendicular to the long axis of the nerve, at 100 µm intervals as previously described (Bull et al., 2012). Images were segmented by applying a normalised box filter to remove high spatial frequency noise followed by binary thresholding. A bespoke graphic user interface permitted manual segmentation if required to optimise the analysis.

Intermediate waypoints with a user-defined spacing (100 µm here) along the proximal-distal longitudinal axis of the optic nerve were generated using

$$P_n = P_0 + n \cdot d \cdot \hat{v}_{\parallel}$$

where P_0 is the start waypoint, *n* is the integer index of the intermediate waypoint, *d* is a user defined inter-waypoint distance and $\hat{v}_{\parallel}$ is the normalised unit vector parallel to the segment defined by the start and end waypoints. Pixel coordinates were produced along the line passing through the intermediate waypoint P_n that is perpendicular to the segment and pixel intensity was normalised to 3 independent measures of background fluorescence. Intensity measures were plotted against distance along the nerve from the optic nerve head and the area under the curve calculated. Ninety- nine percent crossover of axons occurs at the optic chiasm in albino strains (Lund, 1965; Sheridan & Shrout, 1966) and the mean corrected total CTB fluorescence from 6-9 sections of the contralateral superior colliculus were taken to represent distal anterograde transport for vector treated or control groups as previously described (Foxton et al., 2016).

2.3.10 Immunohistochemistry

Wholemounts

Retinal wholemounts were prepared by removal of the anterior segment, lens and vitreous from the globe and dissection of the neurosensory retina from the underlying retinal pigment epithelium. Retinas were flattened and post-fixed for 30 minutes in 4% PFA prior to immunohistochemistry. Wholemounts were washed in 0.5% Triton X-100 in PBS and frozen at -80°C for 10 minutes to permeate the nuclear membrane and improve antibody permeation before blocking in 10% normal donkey serum (NDS), 2% Bovine Serum Albumin (BSA) and 2% Triton X-100 in PBS for 60 minutes. RGCs were labelled with Brn3a (C-20, goat, 1:200, sc-31984, Santa Cruz Biotechnology) TUJ1 (mouse, 1:500, G7121, Promega) and RBPMS (guinea pig, 1:500, 1832, PhosphoSolutions) diluted in blocking solution for 2 hours incubation at room temperature and then at 4°C overnight. Donkey anti-mouse AF488 (1:1000, a32766, Invitrogen), Donkey anti-guinea pig AF555 (1:500, SAB4600297, Sigma) and Donkey anti-

goat AF555 or AF647 (1:500, a32816 or 1:500, a21447 Invitrogen) were used as secondary antibody in 2% PBS-Triton X-100 with a 2 hours incubation period at room temperature followed by three wash steps in PBS. Retinal wholemounts were mounted onto slides with FluorSave reagent (345789, MilliporeSigma). Wholemounts were visualised under epifluorescent illumination on a Leica DMi8 microscope using a 20X objective. RGC counts were measured using Fiji (Schneider et al., 2012) and an image-based tool for counting nuclei (ITCN) plugin as previously described (A. Osborne, Khatib, et al., 2018). Volocity software was used to quantify transduction efficiency by determining the percentage colocation of green fluorescent protein (GFP) expressed in Brn3a positive RGCs. To assess the spatial pattern of expression, 20 – 25 images at 10X magnification were captured for each viral titre and merged to reconstruct the entire wholemount to assess the spatial pattern of expression.

Sections

Globes were post-fixed in 4% PFA overnight at 4°C, washed in PBS and cryo-preserved by overnight immersion in 30% sucrose at 4°C. Following embedding in optimal cutting temperature compound (Tissue-Tek, Miles Laboratories) eyes were then frozen on dry ice and sectioned at 13 µm through the dorsal–ventral/superior–inferior axis of the retina onto Superfrost® Plus slides (VWR), using a Bright OTF 5000 cryostat (Bright Instruments). Sections were simultaneously blocked and permeabilized by incubation in 5% normal goat serum in PBS with 0.3% Triton X-100 and 2% BSA for 60 mins at room temperature. Sections were then incubated in primary antibody, (BDNF N-20, rabbit, 1:200, sc-546, Santa Cruz Biotechnology; TrkB, rabbit, 1:300, ab33655, Abcam; RBPMS, guinea pig, 1:500, 1832, PhosphoSolutions; PKC α, mouse, 1:500, sc-8393, Santa Cruz; Vimentin, chicken, 1:500, ab5733, Millipore; Calretinin, rabbit, 1:500, ab702 Abcam; Calbindin, rabbit, 1:500, ab11426, Abcam; GFP, mouse, 1:500, ab1218, Abcam; GFP, rabbit, 1:500, ab290, Abcam; TUJ1, rabbit, 1:500, ab18207, Abcam; Total tau; 1:1000, A0024, Dako; Phospho-Tau (Ser202, Thr205) AT8, 1:500, MN1020, Invitrogen; Phospho-Tau (Ser96,Thr404) PHF-1, 1:500, kind gift from Maria Spillantini) diluted in blocking solution overnight at 4°C, before incubation with

secondary antibody (goat anti-mouse AF488, 1:1000, a11029, Invitrogen; goat anti-rabbit AF488, 1:1000, a11034, Invitrogen; goat anti-mouse AF555, 1:1000, a21424, Invitrogen; goat anti-chicken AF568, 1:1000, a11041, Invitrogen; goat anti-guinea pig AF555, 1:1000, a21435, Invitrogen; goat anti-rabbit AF555, 1:1000, a21428, Invitrogen; goat anti-rabbit AF647, 1:1000, a32733, Invitrogen; goat anti-mouse AF647, 1:1000, a21235, Invitrogen) diluted in blocking solution for 120 minutes at room temperature. Nuclei were counterstained with DAPI (1:10000, D1306, Invitrogen). Sections were imaged using a Leica DM6000 epifluorescence microscope (Leica Microsystems) and high magnification images achieved using a SP5 confocal microscopy equipped with a 40× lens (Leica Microsystems). RGC counts were measured by counting the mean number of TUJ1 positive cells from 3 separate 350μm length sections of retina per animal. Images were adjusted for intensity to facilitate quantification of cell bodies. Original fluorescence intensities are shown.

2.3.11 I-TASSER molecular modelling of TrkB receptor

I-TASSER (Iterative Threading ASSEmbly Refinement) is an online platform used to predict protein structure and structure-based function (Zhang, 2008, 2009). It first identifies structural templates from the Protein Data Bank by multiple threading approach and generates 3D models for a given sequence. Functional insights can be derived by re-threading the 3D models through the protein function database BioLiP. The conformation of the extended TrkB receptor containing the remaining viral-2A peptide linker was modelled using the online I-TASSER tool.

2.3.12 Statistical analysis

Data was analysed using Student's two-paired t-test or ANOVA followed by Bonferroni-modified t- tests for multiple comparisons; $p<0.05$ was considered significant. All analyses were performed blind with respect to treatment groups. Sample sizes were calculated using a

pilot study and on-line sample size calculator (https://www.stat.ubc.ca/) adopting a two-sided α-level of 0.05 and 80% power.

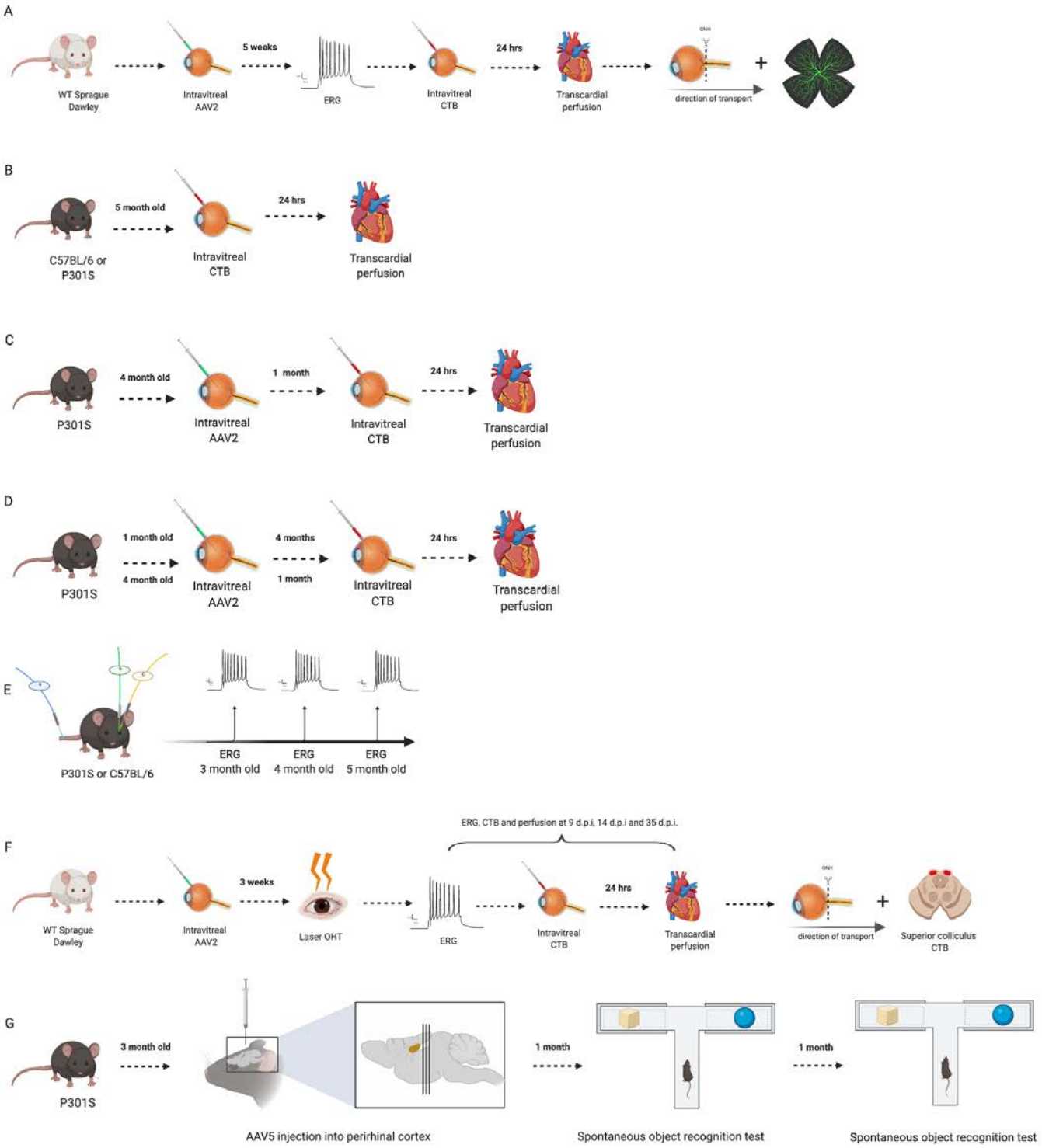


Figure 2-2: Experimental timelines for Chapter 5. A: Timeline for Figure 5-10. B-E: Timelines for Figure 5-11. F: Timelines for Figures 5-12 to 5-16. G: Timeline for Figure 5-17.

2.4 METHODS FOR CHAPTER 6

2.4.1 Animals

All experiments were carried out in accordance with the UK Home Office Regulations for the Care and Use of Laboratory Animals and the UK Animals (Scientific Procedures) Act 1986 and the Association for Research in Vision and Ophthalmology's Statement for the Use of Animals in Ophthalmic and Visual Research. They were approved by the University of Cambridge Animal Ethics Committee (Project Licence 70/8152). Animals had unrestricted access to food and water, and were maintained on a 12 h light/dark cycle. Wild type Balb/cJ (WT - 000651) and conditional PTEN KO mice (PTEN flx/flx - 004597 - C;129S4-Pten^{tm1Hwu}/J) were used for the glaucoma and regeneration experiments and 6-8 week old Cre-reporter strain mice (007908 - B6;129S6-Gt(ROSA)26Sor$^{tm14(CAG-tdTomato)Hze}$/J) were used to validate the AAV2-Cre virus used to induced PTEN deletion. Tissue was collected following transcardial perfusion with 4% paraformaldehyde (PFA) under terminal anaesthesia.

2.4.2 Intravitreal vector injection

Animals were anaesthetised with intraperitoneal injection of ketamine (50mg/kg) and xylazine (10mg/kg) and topical 1% tetracaine eye drops (Bausch&Lomb) prior to injection. Freshly thawed AAV2 vectors were diluted to working stock in sterile PBS and 2µL of vector injected through the sclera into the vitreous of the eye posterior to the limbus (Syringe: 5µL, #65RN; Needle: ga33, 8mm, pst2. Hamilton Co.) Injections were given slowly over 1 min to allow diffusion of the vector suspension. All injections were carried out by the same surgeon and vectors were administered at 1 x 10^{10} GC (genomic copies)/eye.

2.4.3 Induction of ocular hypertension

Ocular hypertension was induced by intracameral injection of crosslinking hydrogel (mixture of vinysulfonated hyaluronic acid and thiolated hyaluronic acid dissolved in PBS) as previously described(K. C. Chan et al., 2019). Contralateral fellow eyes served as normotensive controls.

Intraocular pressure (IOP) was measured bilaterally under anaesthesia on procedure days using a TonoLab rebound tonometer calibrated for the mouse eye (Tiolat Oy). Tonometry was performed within 5 mins of anaesthesia onset and between the hours of 9:00am and 11:00am. Fifteen recordings were taken from each eye at each time point.

2.4.4 Measuring anterograde axonal transport

The vitreous body of the left eye was injected with 2µl of 0.1% solution of cholera toxin B protein subunit b (CTB) conjugated to Alexa Fluor-555 in sterile phosphate-buffered saline (PBS) (Thermo Fisher Scientific). CTB binds the GM1 ganglioside receptor on retinal ganglion cells and is widely used as an axonal tracer and marker of transport because it is selectively taken up by retinal ganglion cells in the retina (Chiasseu et al., 2017). Following the injection, the needle was held in place for 1 minute, to prevent leakage. Animals were perfused intracardially with 4% PFA 24 hours post CTB administration.

Optic nerves of perfused mice were dissected immediately behind the posterior globe at the optic nerve head and were removed. Nerve tissue was post-fixed overnight at 4C, washed in PBS and cryo-preserved by overnight immersion in 30% sucrose at 4C. Following embedding in optimal cutting temperature compound (Tissue-Tek, Miles Laboratories), 12 µm-thick longitudinal sections of the optic nerve were cut using a cryostat and mounted onto microscope slides in darkened conditions. Immunohistochemical visualisation of CTB was not required as the fluorophore was directly conjugated to the CTB. Sections were visualised under epifluorescent illumination on a single Leica DMi8 microscope using a 20X objective (optic nerve). Contiguous images were captured and tiled using LAS AF software (Leica Inc.) and identical camera settings.

We quantified mean CTB fluorescence intensity across the width of each optic nerve, perpendicular to the long axis of the nerve, at 100 µm intervals as previously described(Bull et al., 2012).

2.4.5 Immunohistochemistry

Retinal wholemounts

Retinal wholemounts were prepared by removal of the anterior segment, lens and vitreous from the globe and dissection of the neurosensory retina from the underlying retinal pigment epithelium. Retinas were flattened and post-fixed for 30 minutes in 4% PFA prior to immunohistochemistry. Wholemounts were washed in 0.5% Triton X-100 in PBS and frozen at -80C for 10 minutes to permeate the nuclear membrane and improve antibody permeation before blocking in 10% normal donkey serum (NDS), 2% BSA and 2% Triton X-100 in PBS for 60 minutes. RGCs were labelled with Brn3a (C-20, goat, 1:200, sc-31984; Santa Cruz Biotechnology) and TUJ1 (rabbit, 1:500, ab18207, Abcam) diluted in blocking solution for 2 hours incubation at room temperature and then at 4C overnight. Donkey anti-goat AF555 (1:500, A21432, Invitrogen) and donkey anti-rabbit AF647 (1:500, A32733, Invitrogen) were used as secondary antibody in 2% PBS-Triton X-100 with a 2 hour incubation period at room temperature followed by three wash steps in PBS. Retinal wholemounts were mounted onto slides with FluorSave reagent (345789, MilliporeSigma). Wholemounts were visualised under epifluorescent illumination on a Leica DMi8 microscope using a 20X objective. RGC counts were measured using Fiji(Schneider et al., 2012) and an image-based tool for counting nuclei (ITCN) plugin as previously described (A. Osborne, Khatib, et al., 2018).

Sections

Globes and nerves were post-fixed in 4% PFA overnight at 4°C, washed in PBS and cryo-preserved by overnight immersion in 30% sucrose at 4°C. Following embedding in optimal cutting temperature compound (Tissue-Tek, Miles Laboratories) eyes were then frozen on dry ice and sectioned at 12 µm (dorsal–ventral/superior–inferior axis of the retina and longitudinal sections of the optic nerve) onto Superfrost® Plus slides (VWR). Sections were simultaneously blocked and permeabilized by incubation in 5% normal goat serum in PBS with 0.3% Triton X-100 and 2% BSA for 60 mins at room temperature. Sections were then incubated in primary antibody [phospho-S6 ribosomal protein (Ser235/236) (91B2) (rabbit,

1:200, Cell Signalling 4857S); TUJ1 (rabbit, 1:500, ab18207, Abcam); PTEN (D4.3) XP (rabbit, 1:100, Cell Signalling 9188S)], diluted in blocking solution overnight at 4°C, before incubation with secondary antibody (goat anti-rabbit AF647, 1:1000, a32733, Invitrogen) diluted in blocking solution for 120 minutes at room temperature. Nuclei were counterstained with DAPI (1:10000, D1306, Invitrogen).

GAP-43 was visualized using the IgG fraction of an antibody prepared in sheep(Benowitz et al., 1988) (kind gift from Larry Benowitz) and incubated as previously described(Leon et al., 2000). Briefly, slides were rinsed in TBS (50 mM Tris buffer containing 8.766 g/L NaCl) and then washed with methanol for 10 min. Slides were blocked in TBS containing 10% donkey serum for 1 hr. The GAP-43 antibody was diluted 1:50,000 in a solution of TBS_2T (50 mM Tris buffer, 17.532 g/L NaCl, and 0.1% Tween) containing 5% donkey serum and 2% BSA. Slides were incubated with primary antibody overnight on a rocking platform. Slides were then washed with TBS_2T for 1 hr, with TBS_2T plus 5% donkey serum and 2% BSA for 1 hr, and with TBS_2T for 1 hr, all on a rocking platform. The secondary antibody (donkey anti-sheep AF647, 1:1000, ab150179, Abcam) was diluted 1:1000 in TBS_2T plus 5% donkey serum and 2% BSA. Slides were incubated with the secondary antibody solution for 2 hr, followed by 30 min washes with TBS_2T, TBS_2T, and TBS.

Slides were mounted using FluorSave and glass cover slips, and stored at 4°C in darkness for imaging. Sections were imaged using a Leica DM6000 epifluorescence microscope (Leica Microsystems) and high magnification images achieved using a SP5 confocal microscopy equipped with a 40× lens (Leica Microsystems). RGC counts were measured by counting the mean number of TUJ1 positive cells from 8 separate 350μm length sections of retina per animal. Fluorescence was calculated as corrected total cell fluorescence (CTCF) using an established quantification protocol (A. Osborne, Khatib, et al., 2018). Using the freehand tool in Fiji, the ganglion cell layer (GCL) or boundary between the inner plexiform layer (IPL) and inner nuclear layer (INL) were outlined and the integrated density

measurement taken. Background fluorescence for each image was also obtained. The following calculation was applied to each image quantified: CTCF = integrated density − (area × mean background fluorescence).

CHAPTER 3

PROGRESSIVE AND IRREVERSIBLY BLINDING: *THE CLINICAL NEED FOR NEW GLAUCOMA TOOLS*

3.1 INTRODUCTION

3.1.1 Visual loss in glaucoma

The characterisation of visual loss in glaucoma remains under avid investigation and refinement (Moraes et al., 2017). A number of functional outcome measures have been utilised in the assessment of glaucoma patients including visual field testing (Bayer & Erb, 2002; Beck et al., 1985; C. A. Johnson, 1993, 1995; J. A. Landers et al., 2003), visual acuity (Mayer et al., 2010), contrast sensitivity (Mayer et al., 2010; Mckendrick et al., 2007), electrophysiology (Wilsey & Fortune, 2016), task completion or simulation (Goh et al., 2018; Skalicky et al., 2016) as well as patient reported experience of visual loss (Crabb et al., 2013). At present the most widely used tool both in clinical practice and as a functional endpoint in clinical trials (Canadian Glaucoma Study Group, 2006; "Comparison of Glaucomatous Progression between Untreated Patients with Normal-Tension Glaucoma and Patients with Therapeutically Reduced Intraocular Pressures. Collaborative Normal-Tension Glaucoma Study Group," 1998; "The Advanced Glaucoma Intervention Study (AGIS): 1. Study Design and Methods and Baseline Characteristics of Study Patients," 1994; Gordon et al., 1999; Leske et al., 1999; Musch et al., 1999) to monitor visual loss in glaucoma patients and guide therapeutic decisions is the Humphrey Visual Field SITA-Standard automated perimetry test (Beck et al., 1985). Visual field testing generates a large amount of data and meaningful interpretation can be complex which has led to the development of a number of automated disease progression analysis tools (Antón et al., 2013; Artes et al., 2005, 2014; McNaught et al., 1996; Nouri-Mahdavi et al., 2011; Viswanathan et al., 2003). These broadly use one of two approaches to evaluating the progression of visual field defects have been employed, namely

event-based change analysis which compares a visual field result to a prior visual field or trend-based analysis which looks for the rate of change in the visual field over time.

3.1.2 Classification of glaucomatous disease progression

The Hodapp-Parish-Anderson (Hodapp et al., 1993) classification of visual field loss for the stages of glaucoma uses two criteria: the overall extent of damage using mean deviation (MD) and the number of defective points in the Humphrey pattern deviation probability map of the full-threshold 24-2 SITA-Standard test.

They can be approximated as follows:

Stage	Mean Deviation	Probability level defect	Sensitivity
Early	< -6 dB	<25% of points below 5% <10% of points below 1%	> 15 dB in central
Moderate	-6 < dB < -12	<50% of points below 5% <20% of points below 1%	< 15 dB in central
Severe	-12 < dB < -20	>50% of points below 5% >20% of points below 1%	< 15 dB in central
End-stage	> -20 dB		< 15 dB in central

Table 3-1: Glaucomatous visual field loss as defined by Hodapp-Parish-Anderson classification.

3.1.3 Glaucoma progression despite “normal” IOP – normal tension glaucoma

30-40% or more of glaucoma patients in many populations show ‘normal tension’ in IOP measurements (generally less than 22mmHg) (Kamal & Hitchings, 1998). In Japan, normal tension glaucoma (NTG) accounts for the majority of patients diagnosed with open-angle glaucoma (Cho & Kee, 2014). Although aggressively lowering the IOP by 30% has been

shown to reduce the risk of progression for patients with NTG from 35% to 12 % over 5 years, this still means a large number of people will continue to lose vision despite best available current treatment.

3.1.4 Patients at highest risk for glaucomatous progression

Identifying those at highest risk of disease progression is important as more aggressive treatment of such patients should be considered to prevent visual disability [Figure 3-1]. 566 glaucoma patients from the Advanced Glaucoma Intervention Study (AGIS) and the clinical database from Jules Stein Eye Institute's Glaucoma Division (Los Angeles, USA) were assessed to determine which baseline prognostic factors predicted rapid visual field deterioration in glaucoma (Lee et al., 2014). 222 eyes from 566 glaucoma patients (28.9%) were identified as rapid progressors (greater than 36% field loss/year). The following baseline factors were predictors of faster deterioration and associated with more severe glaucomatous damage: worse MD, larger vertical cup-to-disc ratio and older age. The likelihood of being a rapid progressor was 54% greater in African Americans than in Caucasians.

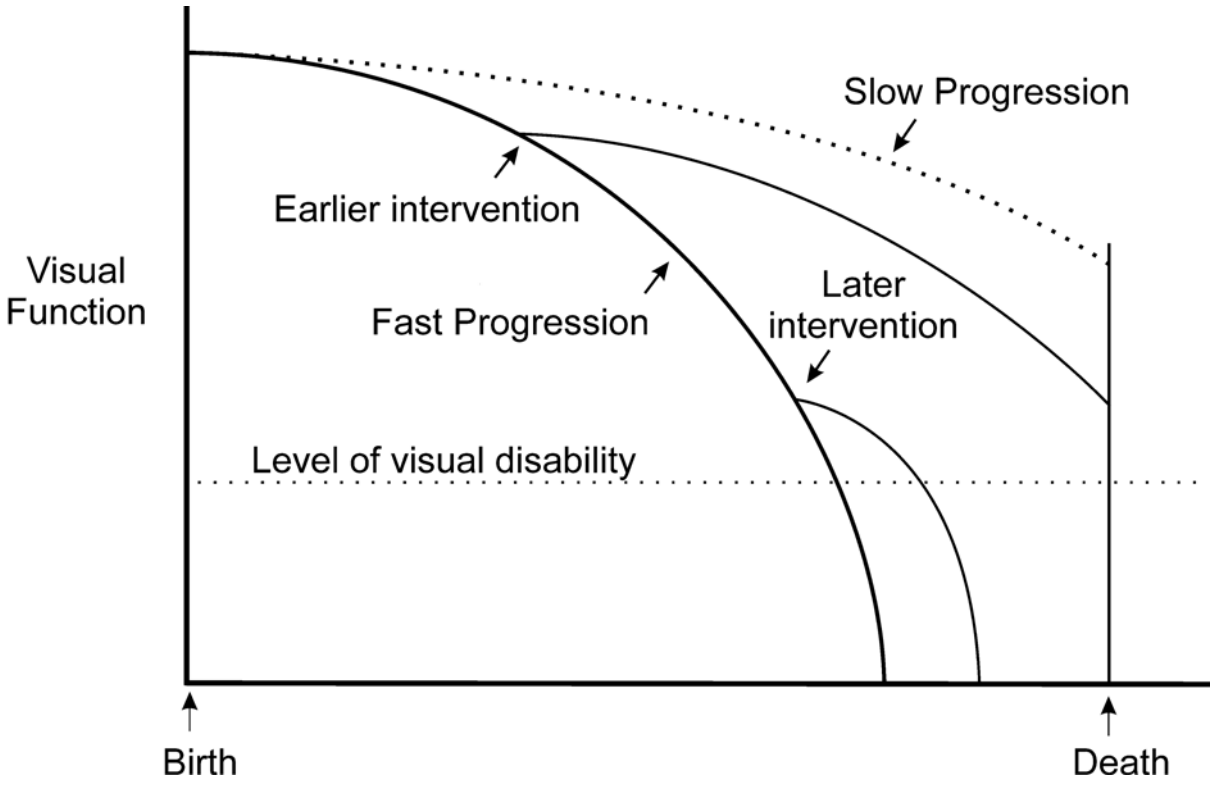


Figure 3-1: The effect on visual disability of patients with glaucoma as a function of rate of progression and time of intervention. Reproduced from Caprioli (Caprioli, 2007)

3.1.5 Capacity for glaucoma services

The lack of capacity in the United Kingdom's hospital eye services (HES) for glaucoma patients has been highlighted in a recent report from the Healthcare Safety Investigation Branch and the award of £3.2 million in compensation by the National Health Service (NHS) to a 34 year old glaucoma patient who went blind due to follow-up delays (*Lack of Timely Monitoring of Patients with Glaucoma. Healthcare Safety Investigation 2019/001. United Kingdom: Healthcare Safety Investigation Branch; 2020.*, n.d.). An estimated 22 people a month suffer severe or permanent loss of sight due to delays in follow-up appointments, and this has also been attributed to insufficient capacity within HES(Foot & MacEwen, 2017). The COVID-19 pandemic has further accelerated the need to manage patients away from HES.

3.1.6 Increased referral rates

Referral rates for glaucoma suspects and ocular hypertensives also increased following the publication of the initial National Institute for Health and Care Excellence (NICE) guidelines for POAG and OHT (Chalk & Smith, 2013). The Royal College of Ophthalmologists (RCOphth) issued national guidance to address the anticipated lack of capacity associated with increased referral rates, recommending that a proportion of glaucoma-related NHS HES attendances were contracted to community-based practitioners (*Royal College of Ophthalmologists (2016). Commissioning Guide: Glaucoma Available at: Https://Www.Rcophth.Ac.Uk/Wp-Content/Uploads/2016/06/Glaucoma-Commissioning-Guide-Long-June-2016-Final.Pdf*, n.d.). Community-based care particularly applied to patients being monitored for OHT and suspected glaucoma to reduce the HES workload; a case mix representing over 30% of HES glaucoma-related visits and over 1 million people in England.

3.1.7 Shared care models

A variety of shared care models have been developed in the UK and overseas which aim to stratify glaucoma patients according to risk of disease progression (Gray et al., 1997, 2000; Keenan et al., 2015; Kotecha et al., 2017; Mandalos et al., 2012; Vernon & Adair, 2010). Often, one goal in such schemes is for hospital-based care to be focused on those at higher risk of disease progression where more aggressive treatment may be required to prevent visual disability (Caprioli, 2007), with lower risk patients managed outside the hospital according to available local expertise and resources. However, there is limited published data on the rate of glaucoma progression in hospital versus community setting for many of these schemes.

3.2 AIM

Our aim was to compare rates of glaucomatous visual field progression and loss of sight years in the Cambridge Community Optometrist Glaucoma Scheme (COGS) and Addenbrooke's Hospital Glaucoma Clinic (AGC).

3.2.1 The Cambridge Community Optometrist Glaucoma Scheme (COGS)

COGS was established in 2010 and initially used for referral refinement(Keenan et al., 2015). All new referrals to AGC were triaged by a glaucoma specialist nurse into high risk and low risk categories. Those deemed low risk (IOP below 30mmHg or a field defect suspicious of glaucoma or an optic disc suspicious of glaucoma) were assessed in COGS. In 2012, the scheme expanded to monitor ocular hypertensive and glaucoma suspect patients (treated and untreated) and in 2015 it was expanded further to allow the monitoring of patients with early primary open angle glaucoma, considered low risk for vision loss. In 2019 the scheme widened the inclusion criteria to include more complex and moderate risk glaucoma cases.

3.2.2 Risk stratification

The current risk stratification guideline used to determine if a patient is suitable for COGS follow-up is outlined in Table 1 below. This guideline is based on an agreed empiric assessment of risk, in conjunction with local stakeholders and clinicians. Changes to the National Institute for Health and Care Excellence guidelines for the diagnosis and management in glaucoma in 2017, including an increased emphasis on optic disc imaging which was not available uniformly in our community clinics, led to a modification of the scheme such that all newly referred patients are now first assessed in AGC with baseline imaging and then referred to the COGS scheme if appropriate.

Risk	Guideline	Clinician
Low	Family history only/no glaucoma OHT < 24mmHg Glaucoma suspect unchanged over 3+ years	Discharge
Low	Stable OHT & Glaucoma suspect - on/off treatment - once baseline imaging completed in HES - includes PDS/PXF POAG (MD <12dB), stable on 2 consecutive occasions. Can include post-trabeculectomy > 24 months - No dense lens opacity - Not on hospital transport or limited mobility Does not require OCT for definitive management	COGS
Low	As for community low risk but requires transport/community not possible due to mobility issues/ if regular OCT required	Virtual hospital clinic
Low	Community returns for consideration of discharge	Consultant
Moderate	Secondary glaucoma or OHT Angle closure patients Stable moderate to advanced glaucoma (MD >12dB), stable on 2 occasions, can include post-trabeculectomy >12 months Only eye any diagnosis	COGS

	- No dense lens opacity - Not on hospital transport or limited mobility Does not require OCT for definitive management	
Moderate	Post-laser or medication change	AGC: Nurse-led
Moderate	Glaucoma progression is suspected Pre and post- cataract assessments in glaucoma patients Post-op trabeculectomy < 12 months but > 2 months	AGC: Doctor or optometrist clinics
High	Unstable advanced glaucoma For consideration of surgery Post-op trabeculectomy/ tube/other (< 2 months)	AGC: Consultant slot

Table 3-2: The Cambridge Community Optometry Glaucoma Scheme (COGS)

3.2.3 Community assessment

Patients are examined according to a local protocol using equipment standardised to AGC. Due to a lack of uniform capacity for ocular coherence tomography (OCT) in community optometry practices participating in COGS during the period reported, OCT was not mandated in the COGS clinical assessment, but was performed in the AGC. Participating optometrists complete training in glaucoma under the supervision of a consultant ophthalmologist. They are also required to complete the College of Optometrists Professional Certificate in Glaucoma (*The College of Optometrists Learning Outcomes for the Professional Certificate in Glaucoma Available at: Https://Www.College-Optometrists.Org/Uploads/Assets/0e49d21f-7691-4e1c-Ad46f8b4ac29268e/Learning-Outcomes-Professional-Certificate-in-Glaucoma.Pdf*, n.d.).

Community optometrists have remote access to hospital electronic records and enter all their results in real time. Findings are summarised using a standardised template. All results are reviewed by a consultant ophthalmologist or hospital optometrist within four weeks of the community glaucoma assessment. An outcome letter is generated by the reviewing clinician

and copies sent to the GP and patient within six weeks of the community glaucoma assessment.

3.3 RESULTS

8465 visual field tests from a total of 854 patients were reviewed. 362 eyes from the AGC group and 210 eyes from the COGS group met the eligibility criteria of 5 or more SITA-standard 24-2 visual field tests. All diagnoses and visual field tests performed were included in the analysis (Table 2).

	Tertiary (AGC)	Community (COGS)
Number of eyes	362	210
Number of patients	188	119
Age, years (mean ± SEM)	74.8 (±0.80)	69.9 (±0.98)
Gender, n (%)		
Male	100 (53.2)	69 (57.9)
Female	88 (46.8)	50 (42.1)
Median number of VF tests	7 (6-10)	6 (5-8)
Median follow up, years	8 (4-11)	5 (4-8)
Baseline severity MD	-2.43 (-5.8 – -0.8)	-2.08 (-4.9 – -0.4)
Diagnosis, n (%)		
Primary open angle glaucoma	194 (53.8)	140 (66.2)
Ocular hypertension	39 (10.9)	24 (11.3)
Primary angle closure glaucoma	24 (6.7)	0
Normal tension glaucoma	44 (12.0)	34 (16.4)
Glaucoma suspect	19 (5.3)	4 (1.9)
Secondary open angle glaucoma	26 (7.2)	4 (1.9)
Neovascular glaucoma	3 (0.8)	2 (0.9)
Uveitic glaucoma	11 (3.1)	3 (1.4)
Juvenile onset glaucoma	1 (0.3)	0

Table 3-3: Summary statistics

The median MD rates highlighted worsening vision over time in both groups (Table 3). However, the rate of deterioration was significantly lower in the COGS patients compared with the AGC group. (-0.1 dB/year vs -0.3 dB/year; p<0.0001).

	Tertiary (AGC)	Community (COGS)
MD progression dB/yr	-0.3 (-0.7 – 0.0)	-0.1 (-0.4 – 0.1)
Range	-6.3 – 1.1	-2.1 – 1.3
-0.5 < x ≤ -0.1	134/362 (37.0%)	141/210 (67.1%)
-1 < x ≤ -0.5	78/362 (21.5%)	27/210 (12.9%)
-2 < x ≤ -1	40/362 (11.0%)	12/210 (5.7%)
-3 < x ≤ -2	7/362 (1.9%)	1/210 (0.5%)
-4 < x ≤ -3	1/362 (0.3%)	0/210 (0%)
x ≤ -4	4/362 (1.1%)	0/210 (0%)

Table 3-4: Distribution of MD progression rates**.** A,C: COGS and AGC MD progression rates Median MD ± 95% CI displayed. B,D: Distribution of MD progression rates

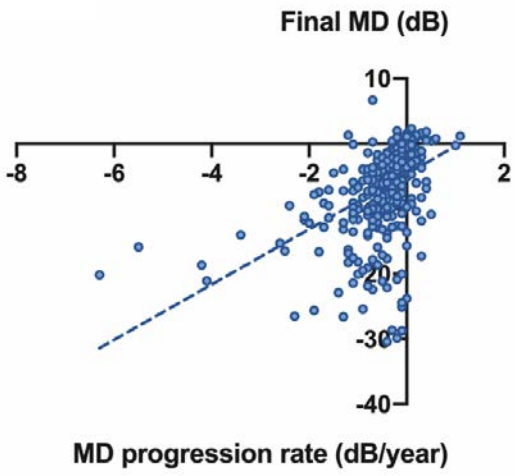
COGS followed up the majority of patients progressing between 0 to 1 dB per year. 14.3% of patients in the AGC were progressing at a rate greater than 1 dB/year compared to 6.2% in the COGS group. Of the 13 patients in the COGS service that were progressing at greater than 1 dB/year, 11 (87%) had additional non-glaucoma diagnoses that would also affect the

visual field. There were no patients in the COGS group deteriorating at rates greater than 3 dB/year.

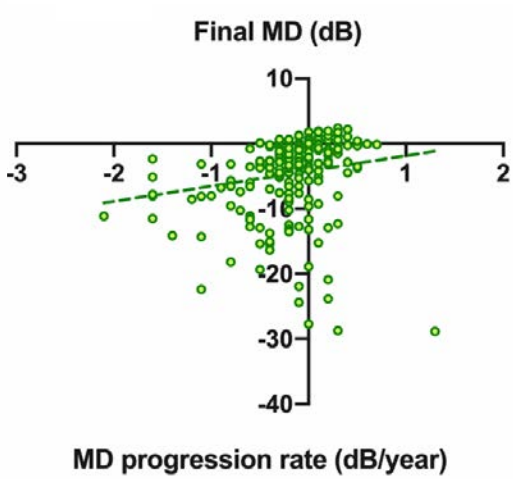
In general, ocular comorbidities that may have affected the visual field were relatively similar across both groups including age-related macular degeneration (4.4% in AGC vs 2.9% in COGS) and diabetic retinopathy (1.1% in AGC vs 3.8% in COGS). 32.9% of AGC patients had undergone cataract surgery vs 21.4% in COGS.

We also evaluated the visual field loss at the end of the study [Figure 3-2]. We defined early glaucoma as a visual field defect corresponding to a MD of -6 dB or better, moderate glaucoma as an MD between -6 and -12 dB, severe glaucoma as an MD between -12 and -20 dB and end-stage glaucoma as an MD of -20 dB or worse. COGS had a greater proportion of patients with early glaucoma (56.4% in AGC vs 72.9% in COGS) while AGC had a greater proportion of patients with moderate glaucoma (26.5% in AGC vs 13.8% in COGS). Interestingly, there was a similar percentage of patients with severe glaucoma in both groups (11% in AGC vs 10% in COGS). The proportion of patients with end-stage glaucoma in AGC was approximately double that seen in COGS (6.1% vs 3.3%). The proportion of patients in each group who did not have glaucomatous visual field loss at entry was 16% in AGC and 19.5% in COGS. At the end point of the study, these proportions were 10.2% in AGC and 18.1% in COGS. There was a significant correlation between the visual field loss observed at the end of the study and the rate of MD progression across both groups although the correlation was weaker for COGS patients (Spearman's correlation coefficient r = 0.60 for AGC vs 0.33 for COGS; $p<0.0001$in both groups). No significant correlation was seen between the initial MD and rate of MD progression (Spearman's correlation coefficient r = -0.07 for AGC; p=0.16 vs r = 0.03 for COGS; p-0.66) or the baseline severity between both groups (p=0.15). Figure 3-2D shows the relationship between initial MD and rate of MD progression across both groups.

A



B



C

Final MD (dB)	Tertiary (AGC)	Community (COGS)
x ≥ -6	204/362 (56.4%)	153/210 (72.9%)
-12 ≤ x < -6	96/362 (26.5%)	29/210 (13.8%)
-20 ≤ x < -12	40/362 (11.0%)	21/210 (10%)
x < -20	22/362 (6.1%)	7/210 (3.3%)

D

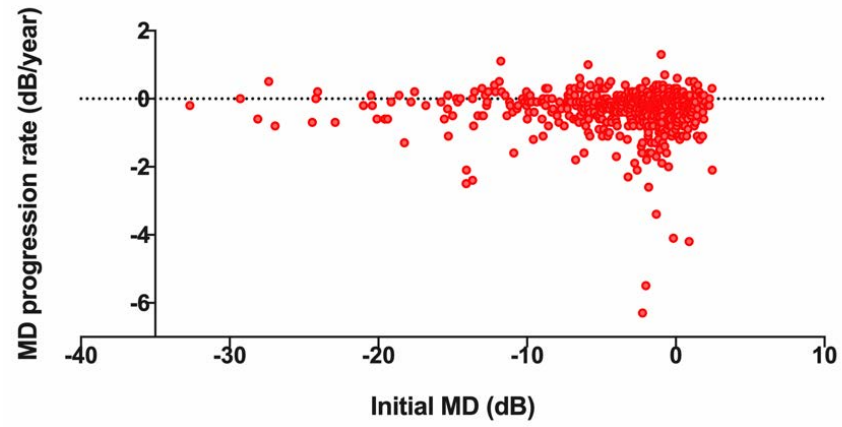


Figure 3-2: Visual field loss and MD progression rate. A: Relationship between visual field loss at end of study and rate of MD progression in AGC patients. Spearman's correlation coefficient r =0.60; p<0.0001. B: Relationship between visual field loss at end of study and rate of MD progression in COGS patients. Spearman's correlation coefficient r =0.33; p<0.0001. C: Distribution of final MD D: Relationship between initial MD and rate of MD progression.

The loss of sight year (LSY) analysis was performed in patients from whom data from both eyes was available [Figure 3-3]. This showed a median of 0 years (0-0) in both groups, suggesting that the majority of patients in either group were unlikely to become blind during the course of their lifetime. There were no rapid progressors in the COGS group and no patients in the COGS group were at risk of becoming blind within their lifetime. Fifteen patients were at risk in the AGC group. Weak correlation was seen between the presenting MD and LSY (Spearman's correlation coefficient r = -0.13; p=0.04).

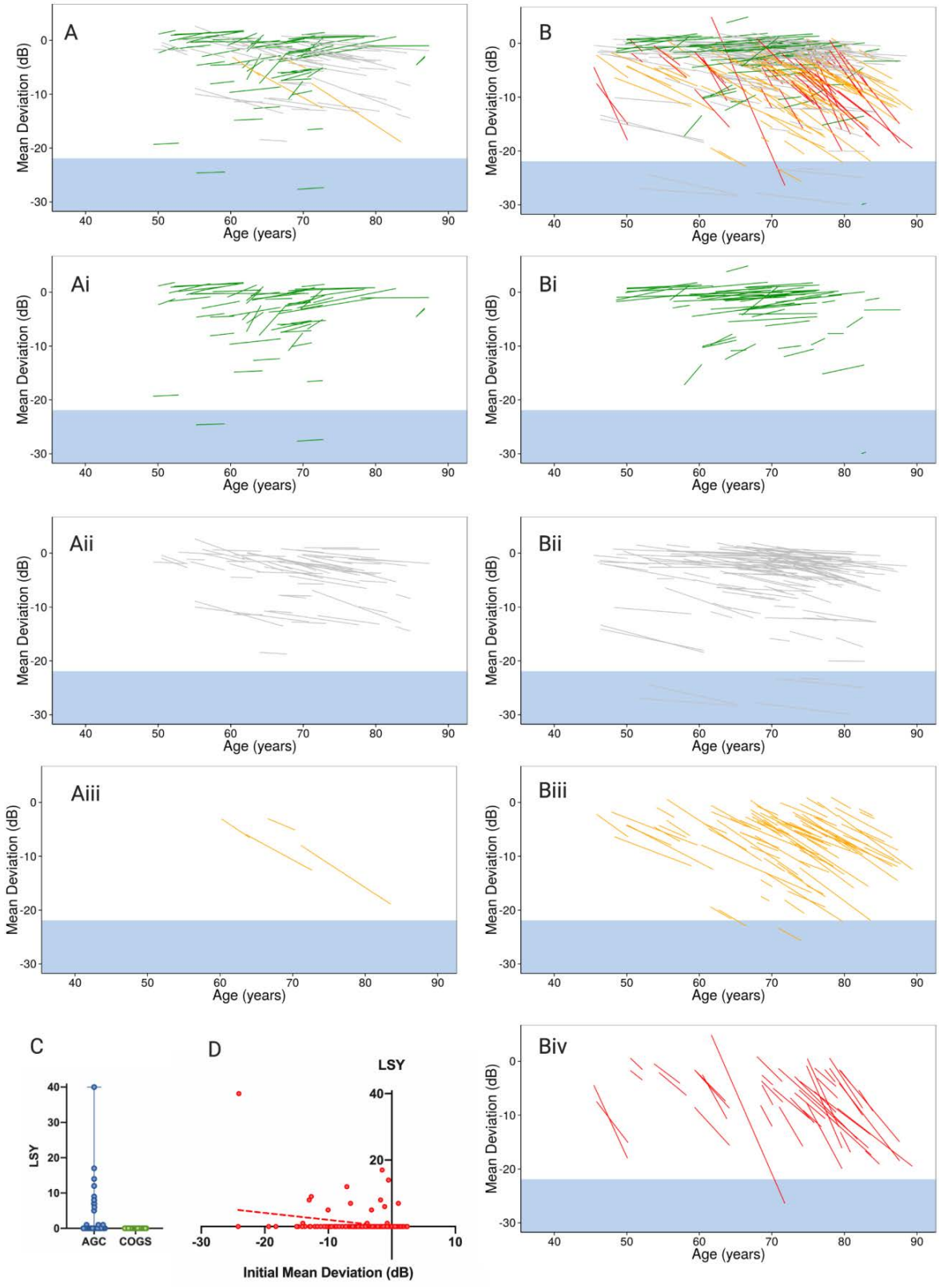


Figure 3-3: Loss of sight year (LSY) analysis A: Hedgehog plot for all AGC patients Ai:Stable AGC patients Aii: Slow AGC progressors Aiii: Moderate AGC progressors B: Hedgehog plot for all COGS patients Bi:Stable COGS patients Bii: Slow COGS progressors Biii: Moderate

COGS progressors C: LSY in AGC and COGS D: Correlation between initial MD and LSY Spearman's correlation coefficient r = -0.13; p=0.04)

3.4 DISCUSSION

Glaucoma patients have a detectable rate of progression across both community and hospital settins despite access to current best available treatment. COGS was established to help streamline the management of glaucoma in Cambridge, aiming to concentrate higher risk glaucoma patients in AGC and lower risk patients in community clinics. In the current study, there was a significantly greater rate of MD progression in the AGC compared to COGS. No patients were identified as at risk of becoming blind in their lifetime in the COGS group and all rapid progressors (progressing at greater than 3 dB/year) were followed up in AGC. COGS also followed up a greater proportion of slow progressors (between 0 to 1 dB/year) and 11 of 13 patients in the COGS group progressing at greater than 1 dB/year had other pathologies such as cataract, or coexisting neurological or retinal pathology. One patient from the COGS group progressing at greater than 1 dB/year also requested to remain under the COGS service rather transfer back to AGC.

Ongoing capacity pressures within AGC have led to an increase in the proportion of patients with more advanced glaucoma that are followed within the community scheme over time. This highlights the need for effective communication channels to identify patients requiring further hospital management reliably and efficiently. A recent internal audit conducted at the end of the period of analysis demonstrated that 41% of all patients (45% of moderate risk patients) monitored in COGS were deemed to be unstable at virtual review and required an AGC appointment. Upon review in hospital, the majority of those patients (72%) were correctly identified as unstable and required a change of treatment or closer AGC monitoring.

The widening scope of patients managed in COGS could be considered a strength of the scheme. Rather than exclude this higher risk cohort from community clinics, strategies

continue to be developed to manage these patients in the community. The planned transition to virtual amendment of treatment changes by the clinical reviewer with subsequent COGS follow up has the potential to reduce the AGC referral rate. Our risk stratification is based on empiric assessment in conjunction with local stakeholders and clinicians. Alternative stratification methods also include recent tools published by the Royal College of Ophthalmologists (RCOphth) and UK and Eire Glaucoma Society (UKEGS) (*Joint RCOphth and UKEGS Glaucoma Risk Stratification Tool (2020) Available at: Https://Www.Rcophth.Ac.Uk/Wp-Content/Uploads/2020/08/Glaucoma-Risk-Stratification-Tool-1.Pdf*, n.d.) and the UK Ophthalmology Alliance (UKOA)(*UKOA How to Stratify the Risk or Complexity for Glaucoma to Direct Patients to Appropriate Clinics (2020) Available at: Https://Uk-Oa.Co.Uk/Wp-Content/Uploads/2020/02/Glaucoma-Risk-and-Virtuals_PDF.Pdf*, n.d.) although it is likely that these guidelines will be tailored according to regional needs and available resources.

LSY analysis was used to help assess the safety of following patients predicted to be at low risk in primary care rather than hospital glaucoma clinics. However, it is important to remember that patients can also suffer a reduced quality of life with an increased risk of falls and other comorbidity due to visual loss before blindness and therefore LSY should not be used as a tool in isolation and the results should be interpreted with caution.

Streamlining and stratifying pathways to facilitate the management of an increasing glaucoma population is essential with community services continuing to grow in response to service need. However, a proportion of patients who have access to regular, high quality care also continue to deteriorate. It is therefore not surprising that patients followed in COGS still have a detectable rate of glaucoma progression.

The overall median rate of deterioration of -0.3 dB/year in AGC and -0.1 dB/year in COGS is comparable to previous reports of glaucoma progression in UK secondary care(Kirwan et al.,

2014), as is the proportion of patients progressing at a rate greater than 1 dB/year (14.2% in the AGC group). Our rates are lower than those reported from a large tertiary glaucoma service in Sweden (median -0.62 dB/year) (Heijl et al., 2013) , although that population has a higher proportion of patients with pseudoexfoliation glaucoma who are known to have a higher risk of progression (Leske et al., 2003; Moon et al., 2017). Another factor contributing to this difference between centres may be that our data was extracted from either eye whereas the Lund authors used data from the eye with the greater visual field defect.

Large multi-centre trials such as the Early Manifest Glaucoma Trial (Leske et al., 2003) and the United Kingdom Glaucoma Treatment Study (Garway-Heath et al., 2015) also found that a significant proportion of patients in the treatment arms progressed. Moreover, 30-40% or more of glaucoma patients in many populations show normal tension in IOP measurements (Kamal & Hitchings, 1998). In Japan, normal tension glaucoma (NTG) accounts for the majority of patients diagnosed with open-angle glaucoma (Cho & Kee, 2014). Although aggressively lowering the IOP by 30% has been shown to reduce the risk of progression for patients with NTG from 35% to 12 % over 5 years, this still means a large number of people will continue to lose vision despite best available current treatment.

The reasons why retinal ganglion cell loss and corresponding visual field deterioration continues despite best treatment are currently unknown, but contributing factors may include insufficient IOP lowering with conventional treatment, poor compliance with intended therapy, or progression despite optimised IOP lowering treatment. A variety of approaches are being undertaken to tackle these problems, from the refinement of medical, laser and surgical approaches to lower the intraocular pressure (Denis et al., 2019; Le et al., 2019; Samuelson et al., 2019; Sarrafpour et al., 2019; Sieck et al., 2018; Tanna & Johnson, 2018; Walters et al., 2019), understanding genetic predisposition and the development of personalised medicine (Craig et al., 2020; Qassim et al., 2020), to new sustained release drug-delivery devices (Lewis

et al., 2017) to minimise the effect of poor compliance and the development of neuroprotective strategies as an alternative or adjunct to IOP lowering therapies (Khatib & Martin, 2020).

Another consideration is the usefulness of OCT scanning in the assessment of glaucoma in the community setting. Abnormalities on OCT scanning of the optic nerve head in subjects over 50 years have been reported to have a false positive glaucoma detection rate of 30%.(Healey et al., 2010) In another study, focal abnormalities of the retinal nerve fibre layer on spectral domain OCT scanning had a false positive rate of 35% (Bussel et al., 2014). Furthermore, each OCT technology has different analysis software which is not interchangeable between machines. We therefore did not mandate OCT in the community setting at the time the current scheme was established, although this is currently being reassessed.

For the future, artificial intelligence techniques are playing a key role and their integration into clinical practice has the potential to significantly improve our early detection of at-risk patients and enhance our understanding of the underlying pathophysiology of glaucomatous visual loss (Thakur et al., 2020; Yousefi et al., 2018, 2020). More accurate endpoints to monitor disease progression and the effects of intervention will also be important (Khatib & Martin, 2020; Moraes et al., 2017). A number of functional outcome measures are being evaluated in the assessment of glaucoma patients in addition to visual field testing (Bayer & Erb, 2002; Beck et al., 1985; C. A. Johnson, 1993, 1995; J. A. Landers et al., 2003), from contrast sensitivity (Mayer et al., 2010; Mckendrick et al., 2007), electrophysiology (Wilsey & Fortune, 2016), task completion or simulation (Goh et al., 2018; Skalicky et al., 2016) to patient reported experience of visual loss (Crabb et al., 2013; Skalicky et al., 2019; Somner et al., 2012).

COGS appears an effective scheme to help manage lower risk glaucoma patients in the UK environment where accredited optometric support can be developed outside of the hospital setting, which increases the capacity within HES to manage higher risk patients. COGS

patients have a lower rate of visual field deterioration compared to patients seen in AGC. Effective communication between the community and tertiary schemes is essential to facilitate transfer of patients requiring further hospital management safely and efficiently.

The relatively high proportion of patients that continue to deteriorate across both groups despite conventional therapy and specialist care in a tertiary centre emphasises the importance of the continuing search for new diagnostic tools to facilitate targeted therapy and new therapeutic approaches and this will be the focus of the remainder of this body of work.

3.5 ACKNOWLEDGEMENTS FOR CHAPTER 3

Design and hypothesis

Keith Martin and Tasneem Khatib

Information governance approval

Tasneem Khatib

Data collection

Yusuf Mushtaq, Binita Panchasara, Nikou Nassehzadehtabriz, Hong Kai Lim, Maryam Mushtaq. Tasneem Khatib contributed to the data collection and also performed a quality control check of all the data collected.

Data analysis

Tasneem Khatib

Writing

Tasneem Khatib (prepared *first draft) and Keith Martin*

CHAPTER 4

DEVELOPING A NEW DIAGNOSTIC TOOL FOR GLAUCOMA: HAEMOGLOBIN VIDEO IMAGING

4.1 INTRODUCTION

Non-invasive, detailed measurement of the dynamics of human aqueous outflow is difficult to achieve with currently available clinical tools. Our knowledge of the anatomy and physiology of aqueous outflow is based on studies in *ex vivo* tissue (Ashton & Smith, 1953)(Huang, Camp, et al., 2017; Huang, Li, et al., 2017; Johnstone, 2004) as well as *in vivo* techniques that are either static,(Kagemann et al., 2012) invasive or involve a degree of manipulation of physiological parameters (Huang, Camp, et al., 2017). The widely used fluorescein disappearance test (Jones & Maurice, 1966; Yablonski et al., 1978) is at best an indirect estimate of aqueous outflow and the outflow pathway cannot be visualised using this technique.

The advent of minimally invasive glaucoma surgery (MIGS) procedures has led to renewed interest in the dynamics of aqueous outflow. The intraocular pressure (IOP) lowering effect of trabecular bypass devices is variable in different patients. (Craven et al., 2012; García-Feijoo et al., 2015; Minckler et al., 2008; Samuelson et al., 2011; Shah et al., 2018) The segmental and dynamic nature of aqueous outflow has previously been described (Huang, Camp, et al., 2017; Huang, Li, et al., 2017) and it has been suggested that targeting trabecular bypass stents to ocular quadrants with good aqueous outflow could improve the success rates of these procedures.

Here we describe a technique to visualise aqueous veins non-invasively using haemoglobin video imaging (Meyer, 2018) (HVI) which utilises the haemoglobin absorption spectrum to enhance the contrast between red blood cells and their surroundings. Erythrocytes are

displayed as darker objects against a brighter background of light reflected by sclera with a resolution down to the level of a single red blood cell. Aqueous is observed as an erythrocyte void, a clear column which displaces red blood cells as it flows into the episcleral venous circulation.

We describe characteristics of aqueous veins that are consistent with earlier reports and we have developed a quantification technique to measure the cross sectional area (CSA) of the aqueous column within episcleral veins. As an example of the type of clinical investigation possible with our technique, we performed a pilot study on 8 eyes of 7 patients who underwent selective laser trabeculoplasty (SLT) together with administration of pilocarpine and apraclonidine eye drops, as per our standard protocol, and correlated the change in CSA with IOP reduction and change in visual field mean deviation before and after intervention. We also propose a method that could be used to compare the flow rate from HVI images before and after intervention.

HVI can be incorporated into a routine clinic slit lamp examination to allow a detailed assessment of physiological and pathological aqueous outflow in real time. We suggest that HVI has the potential to be used as a tool to help target therapeutic interventions, to improve aqueous outflow and to further advance our understanding of aqueous outflow dysregulation in the pathogenesis of glaucoma.

4.2 RESULTS

The HVI technique demonstrates aqueous as an erythrocyte void at high contrast to haemoglobin in episcleral venous blood [Figure 4-1].

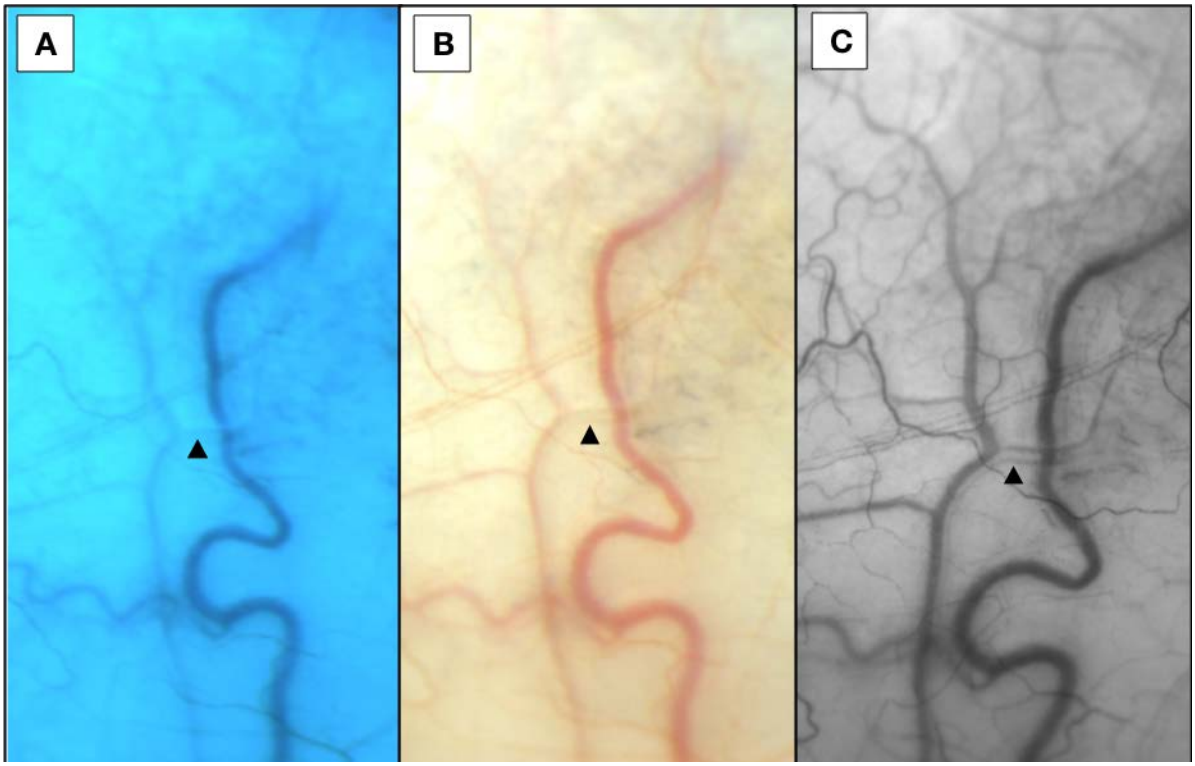


Figure 4-1: Aqueous vein (arrow) captured using conventional techniques (A and B) and haemoglobin video imaging (C).

In every vein observed, aqueous centralised within a laminar venous column, regardless of its point of entry into the episcleral circulation [Figure 4-2; Video clip 3]. A "∗" symbol briefly appears to denote the vessel(s) of interest in each video within the clip before disappearing to permit uninterrupted observation of flow dynamics. A corresponding header also identifies the main observation to be made from individual recordings.

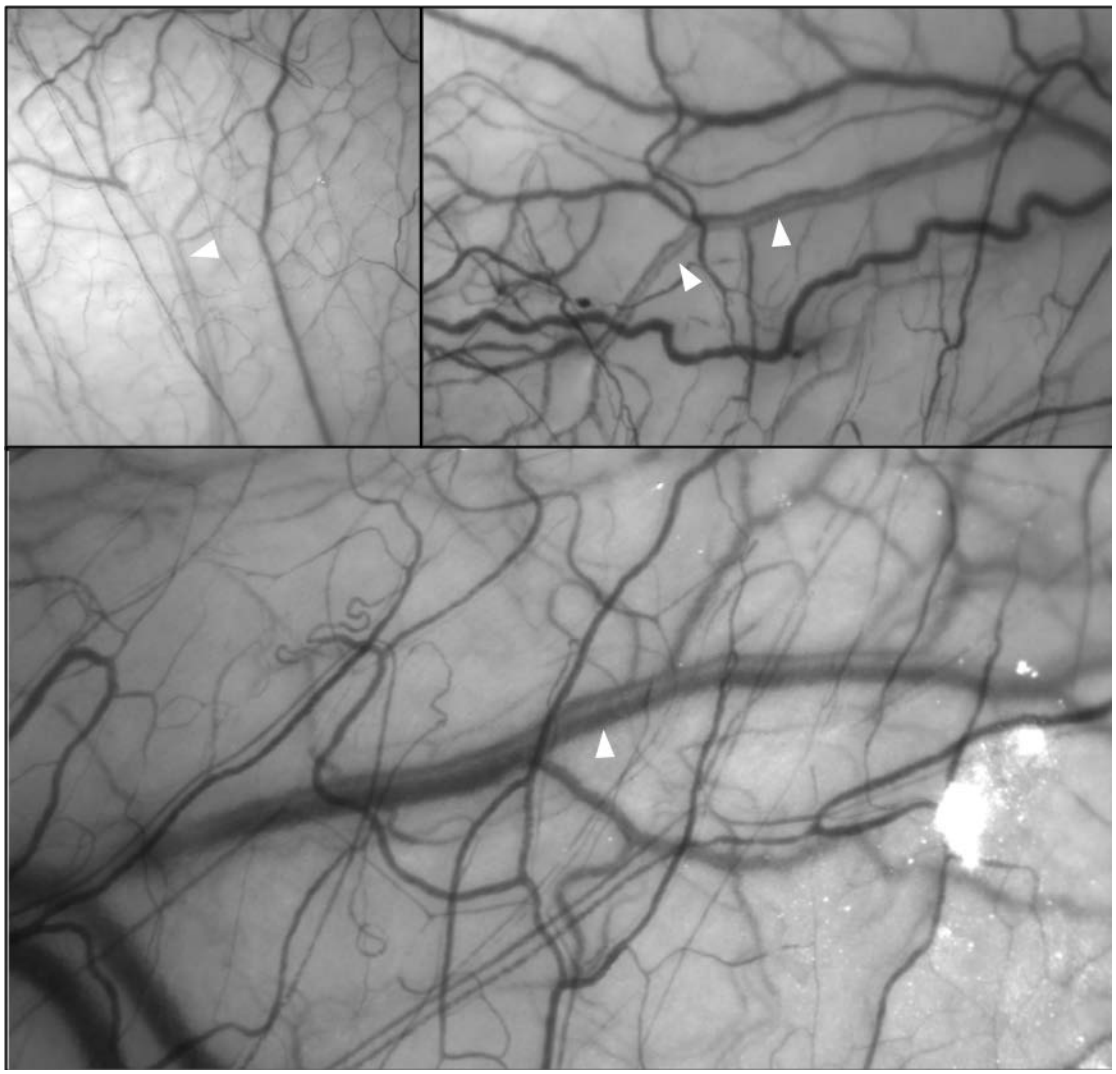


Figure 4-2: Examples of aqueous veins obtained using HVI (white arrows). Aqueous is seen as a centralised erythrocyte void.

The length and diameter of aqueous streams varied, but some continued beyond the conjunctival reflection. Fluctuations arose in the aqueous stream, corresponding with cardiac rhythm, eye movements and pressure on the globe [Figure 4-3, Video clip 4]. Compression of the aqueous vein resulted in the redirection of aqueous flow to other vessels that had previously been filled with blood [Figure 4-4, Video clip 4].

The cross-sectional area calculations arising from δ [Figure 4-5] were consistent and repeatable for each eye measured. Any variation between repeated measurements did not correlate with the size of δ.

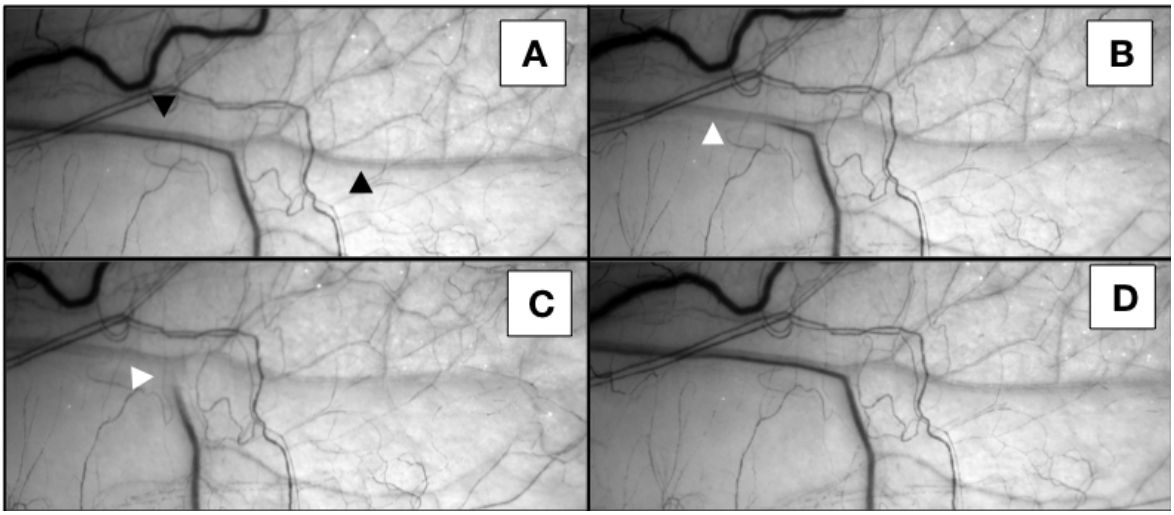


Figure 4-3: Displacement of aqueous following digital pressure on the inferior globe. A: Aqueous vein (black arrow) prior to digital manipulation. B-C: Aqueous is redirected into an episcleral blood filled vessel following digital pressure on the globe (white arrow). D: Immediate resumption of usual aqueous and blood flow following release of pressure.

There was a significant increase in the AQC immediately following administration of our SLT protocol [Figure 4-6A] and this correlated with the degree of IOP reduction observed [Figure 4-6B] as well as the improvement in mean deviation (MD) observed post intervention [Figure 4-6C]. Video clip 5 demonstrates individual aqueous veins from 4 glaucoma patients before and after intervention. Figure 4-7 uses example 1 (Video clip 5) to compute an autocorrelation analysis as described above in Chapter 2. There is an increase in the rate of decay following intervention indicating an increase in flow rate.

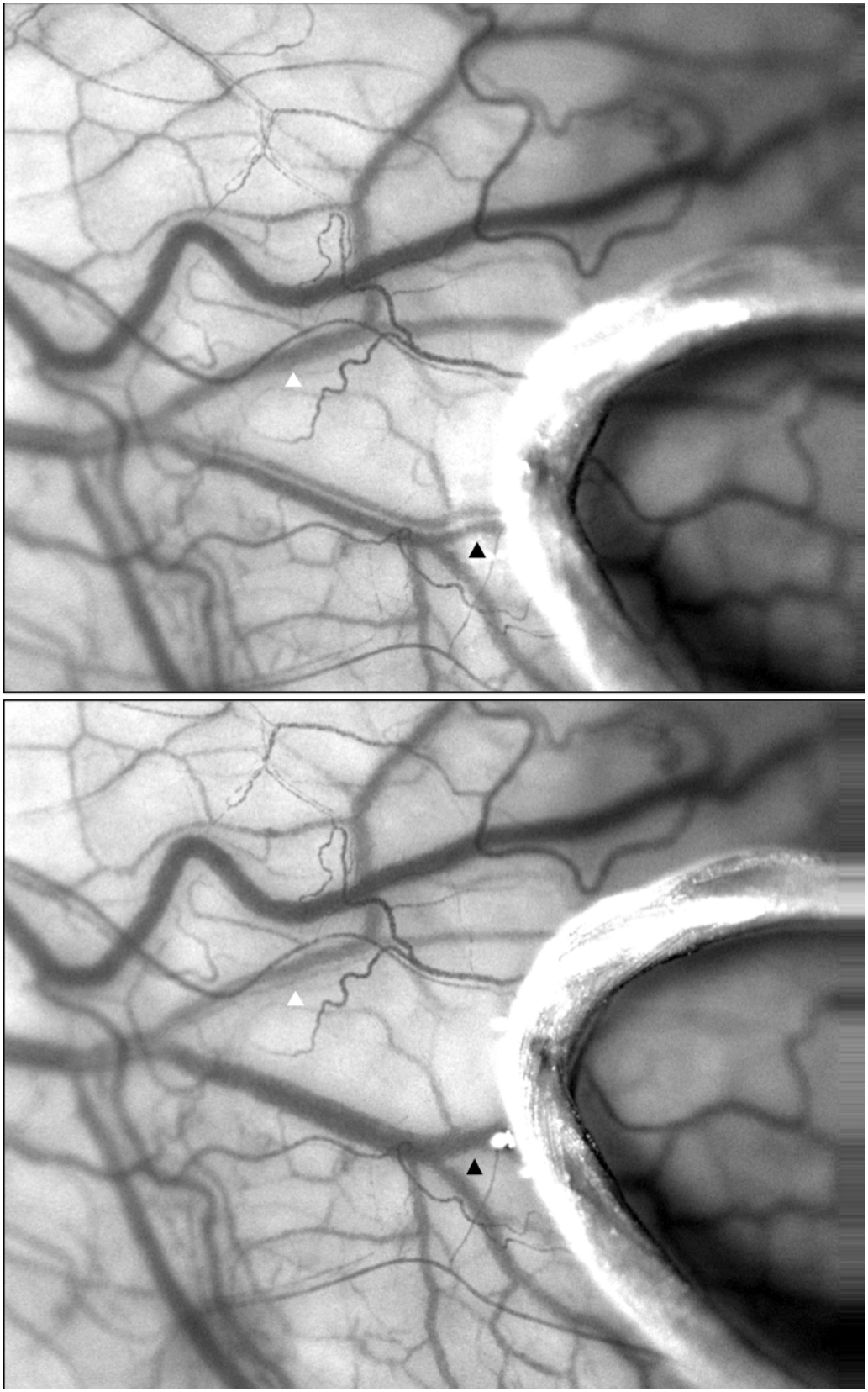


Figure 4-4: Compression of an aqueous vein (white arrow) using a 10/0 vicryl loop redirects aqueous to a nearby episcleral blood vessel (black arrow).

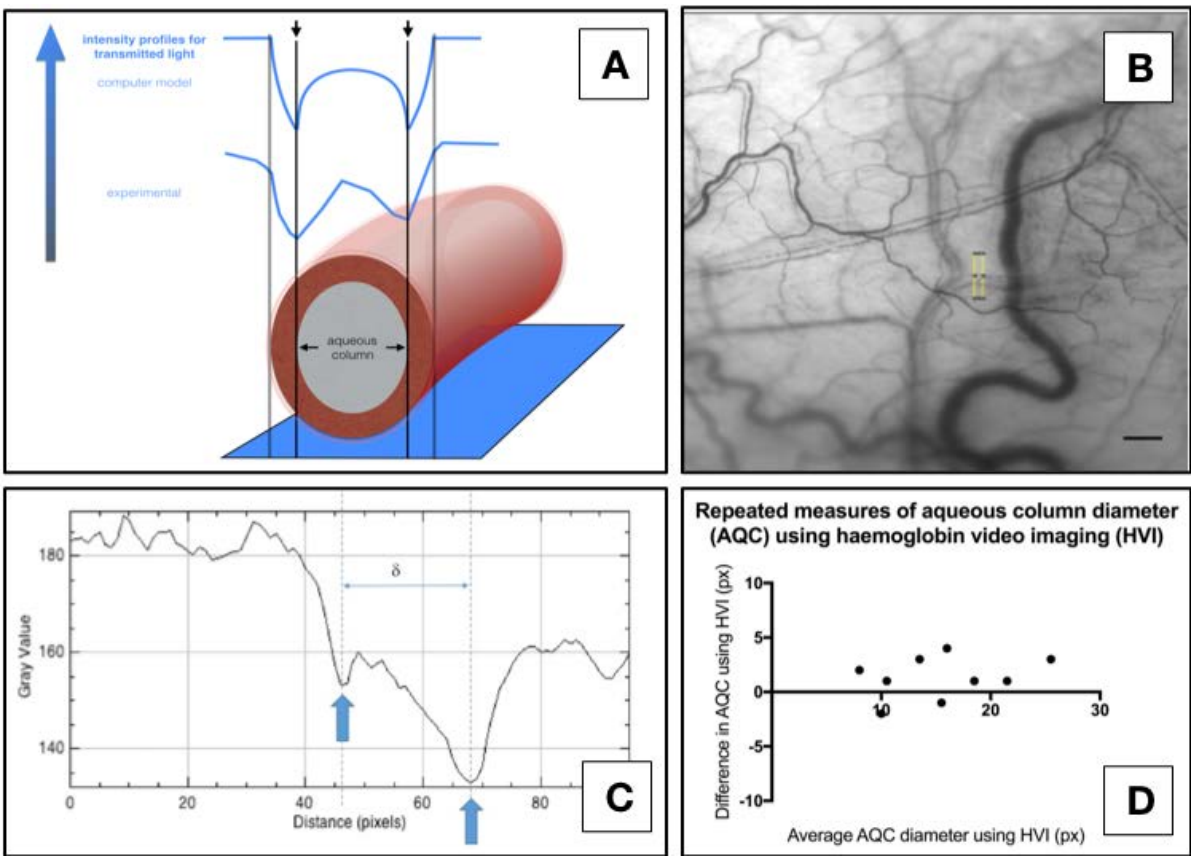


Figure 4-5: A: Schematic representation of the intensity profiles of transmitted light in an aqueous vein using HVI B-C: Aqueous vein transept with corresponding density profile and δ measurement. Scale bar = 0.5 mm. D: Bland-Altman plot of the difference in paired δ measurements using HVI against the mean δ measurement.

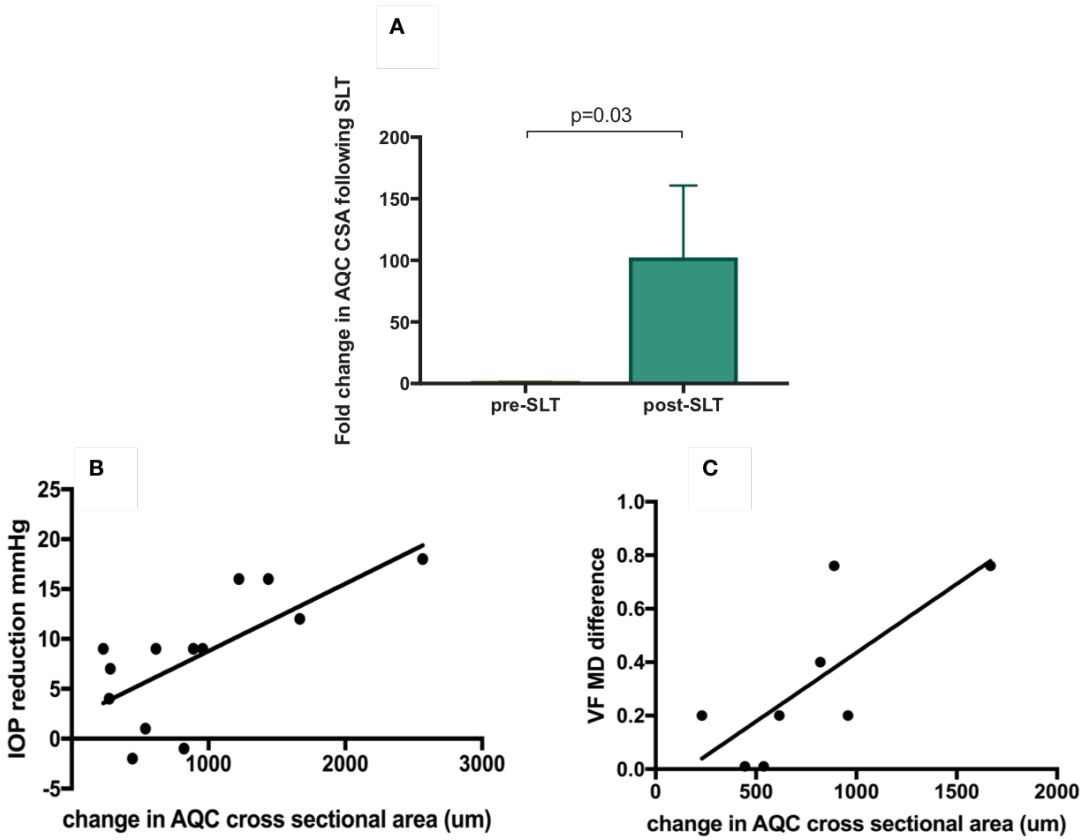


Figure 4-6: AQC as a tool for quantifying aqueous outflow. A: Fold change in AQC coss-sectional area following intervention (n=13; $p<0.05$; Students ratio paired t-test). B: Correlation between IOP reduction and AQC CSA following intervention (n=13; Pearson's correlation coefficient 0.7; p=0.007) C: Correlation between change in mean deviation and AQC CSA following intervention (n=8; Pearson's correlation coefficient 0.75; p=0.03)

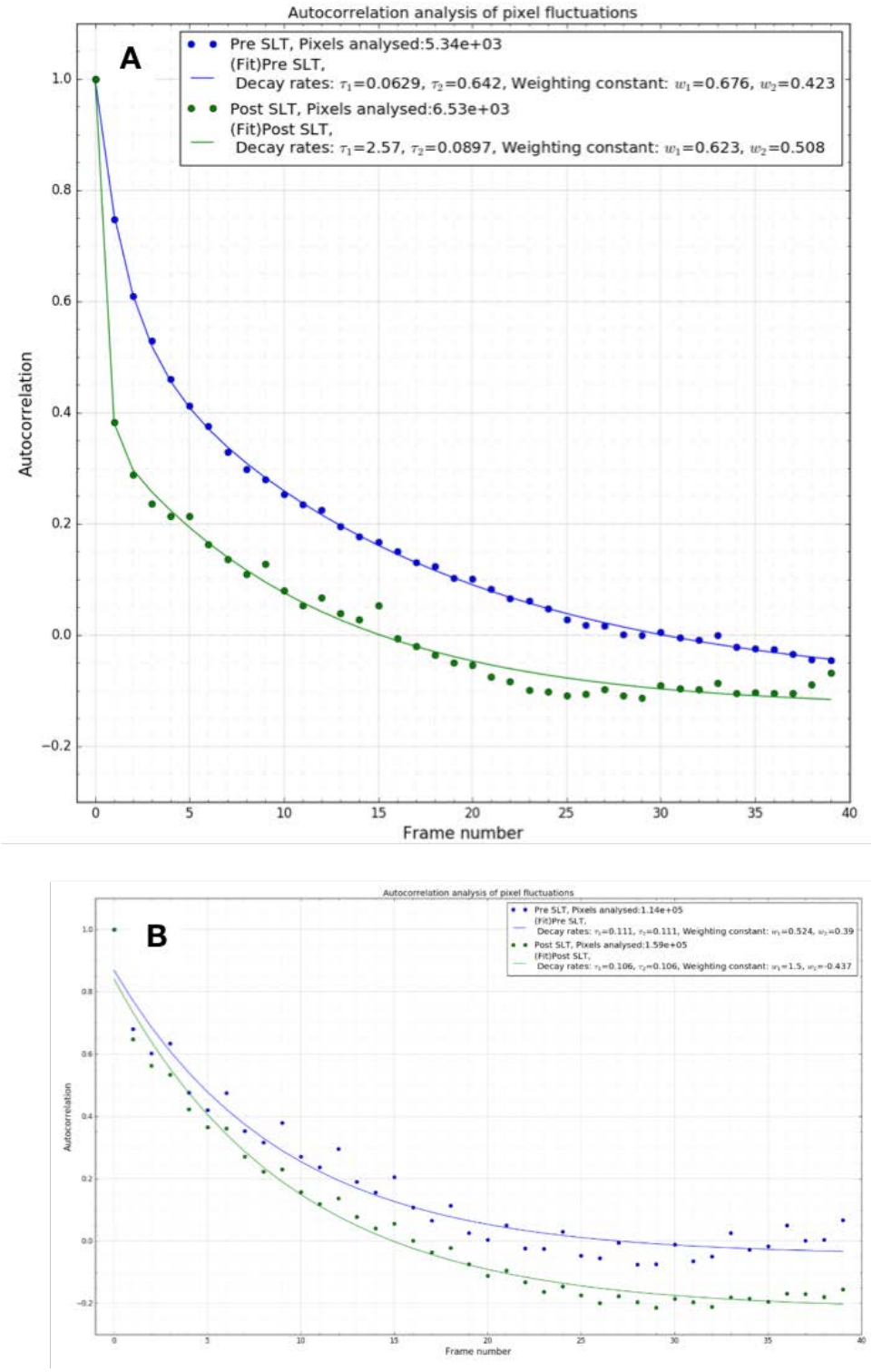


Figure 4-7: Flow rate using autocorrelation analysis before and after SLT: A: Faster rate of decay is seen post intervention indicating an increase in flow rate. B: Similar autocorrelation decay rates seen in non-aqueous vein or background areas of the HVI images.

4.3 DISCUSSION

We have used haemoglobin video imaging (HVI) to develop a method for the detailed observation and quantification of aqueous columns in episcleral venous blood. This technique can be performed non-invasively as part of a routine clinic assessment using a modified slit lamp and repeated multiple times facilitating longitudinal examination of individual patients over a period of time. We confirm previous observations on the characteristics of aqueous flow, including laminar flow, pulsatility and altered dynamics corresponding to transient fluctuations in pressure, including the redistribution of aqueous following occlusion of an aqueous vein. We also propose a technique to compare flow rates in an aqueous vein using HVI images. The method is based on principles used in photon correlation spectroscopy and laser doppler velocimetry where the velocity of fluids in channels is calculated by measuring fluctuations in the recorded intensity signal. When tracer particles cannot be added to maintain the physiological parameters and monitor aqueous flow non-invasively, flow velocity estimation becomes more complex. We do not aim to provide a velocity estimate, as an accurate measurement of the decay rate would require a faster sampling rate and thus a faster frame rate camera. However, the plots derived from autocorrelation analysis may be useful as simple metrics for comparing flow in videos.

The ability to visualise and quantify physiological aqueous flow provides us with the means to further explore the relationship between aqueous outflow and the diagnosis, monitoring and treatment of glaucoma patients. The correlation we have observed between well-established glaucoma parameters such as intraocular pressure and mean deviation reinforces the use of the aqueous cross-sectional area as a tool to quantify the outflow status of an eye.

Our measurements using the SLT protocol were taken serially on the same individual within an hour of each other immediately before and after intervention. This enabled a direct assessment of the effects of SLT (with simultaneous administration of apraclonidine and pilocarpine) on aqueous outflow, irrespective of the known variations in outflow in a given

individual during a 24 hour period. While we have been able to quantify a change in aqueous flow following intervention, the addition of pilocarpine and apraclonidine as part of our protocol may also have affected aqueous flow and we cannot fully attribute our observed changes to SLT alone.

Establishing the variation in outflow in a healthy population is also essential prior to considering the use of aqueous outflow facility to assess and monitor glaucoma patients alongside intraocular pressure and mean deviation.

The ability to perform a dynamic assessment at high resolution while visualising aqueous and blood in real time may help to further our understanding of the relationship between episcleral venous pressure and aqueous flow. Current tools to measure episcleral venous pressure are at best limited. Modelling the redistribution of aqueous in the presence of raised episcleral venous pressure and the turbulence at the interface between aqueous and blood using HVI may provide an estimate of the pressure in the venous circulation and should be a focus of future work in this area.

The HVI technique could be used more readily as described here during the management of those patients where MIGS implantation is being considered. A more precise targeting of the site of implantation, to correspond with the anatomy of an individual's aqueous vein distribution, may improve the reliability of these devices in lowering intraocular pressure. The quantification of the aqueous column could also be used to assess the relative effectiveness of various MIGS devices as we have demonstrated here for SLT. This may facilitate refinement and stratification of the choice of MIGS according to the subset of patients most likely to benefit from a particular device.

4.4 FUTURE DIRECTIONS

This work has since been adopted at Sydney Eye Hospital and through collaboration has been used to target iStent insertion into glaucoma patients. Post-operative successful re-

establishment of aqueous flow where none previously existed was demonstrated with some additional preliminary data demonstrating a reduction in aqueous flow in glaucoma patients (Lusthaus et al., 2020). Collaboration is also ongoing with the aqueous outflow laboratory at St Thomas' Hospital to validate HVI against other measures of outflow facility. I have been shortlisted for a competitive large project grant application to develop HVI further for widespread clinical use with support from Cambridge Enterprise, the commercialisation arm of the University of Cambridge (interview date after thesis submission deadline).

4.5 ACKNOWLEDGEMENTS FOR CHAPTER 4

Design and hypothesis of HVI for aqueous outflow

Keith Martin, Paul Meyer, Jed Lusthaus and Tasneem Khatib

Information governance approval

Keith Martin, Jed Lusthaus (original ethical approval) and Tasneem Khatib (formal amendment).

Data collection

Tasneem Khatib collected all the HVI data for the selective laser trabeculoplasty (SLT) experiment. Jed Lusthaus collected some of the observational work and taught Tasneem Khatib how to use HVI. Yusuf Mushtaq collected the IOP and visual field mean deviation data for the SLT patients under Tasneem Khatib's guidance.

MATLAB coding for HVI image registration

Tasneem Khatib under the guidance of Matthias Erhardt

Image registration

Tasneem Khatib

Design of the aqueous column cross sectional area calculation

Paul Meyer and Tasneem Khatib

Validation of aqueous column cross sectional area calculation

Tasneem Khatib

Data analysis

Aqueous column cross sectional area and correlation to IOP and visual field mean deviation.

Tasneem Khatib

Autocorrelation analysis

S*uggested by Tasneem Khatib, Implemented and performed by Ilya Manyakin*

Writing

Tasneem Khatib (prepared first draft) and Keith Martin

CHAPTER 5

GENE THERAPY AS A THERAPEUTIC TOOL FOR PRIMARY OPEN ANGLE GLAUCOMA

5.1 INTRODUCTION

Gene therapy approaches to treat monogenic disease are leading to a revolution in the treatment of previously debilitating neurological conditions such as Leber's Congenital Amaurosis (Russell et al., 2017), Spinal Muscular Atrophy (Mendell et al., 2017b) and Leber's Hereditary Optic Neuropathy (Vignal et al., 2018). However, the application of gene therapy to complex polygenic conditions, which make up the majority of neurodegenerative diseases, has been limited to date.

Disruption of axonal transport is a hallmark of neurodegenerative disease, and stimulating axonal transport with the enhancement of intrinsic neuronal growth mechanisms in the diseased central nervous system has been proposed as a promising strategy to improve neuronal repair.

Tropomyosin receptor kinase B (TrkB) promotion of axon growth has previously been described in regenerating corticospinal tract into subcortical lesions expressing BDNF mediated through the ERK signalling pathway (Hollis 2nd et al., 2009) and has been shown to be crucial for neuronal migration, neurite outgrowth, differentiation and connectivity (Gates et al., 2000; Pradhan et al., 2019). BDNF has also been implicated in axonal transport (Du et al., 2020) and a self-amplifying positive feedback mechanism mediated through cyclic AMP, protein kinase A and the PI3 kinase pathways to trigger further BDNF secretion, promote TrkB membrane insertion and stimulate anterograde axonal transport, thereby contributing to axonal development and the formation of neuronal polarity (P.-L. Cheng et al., 2011).

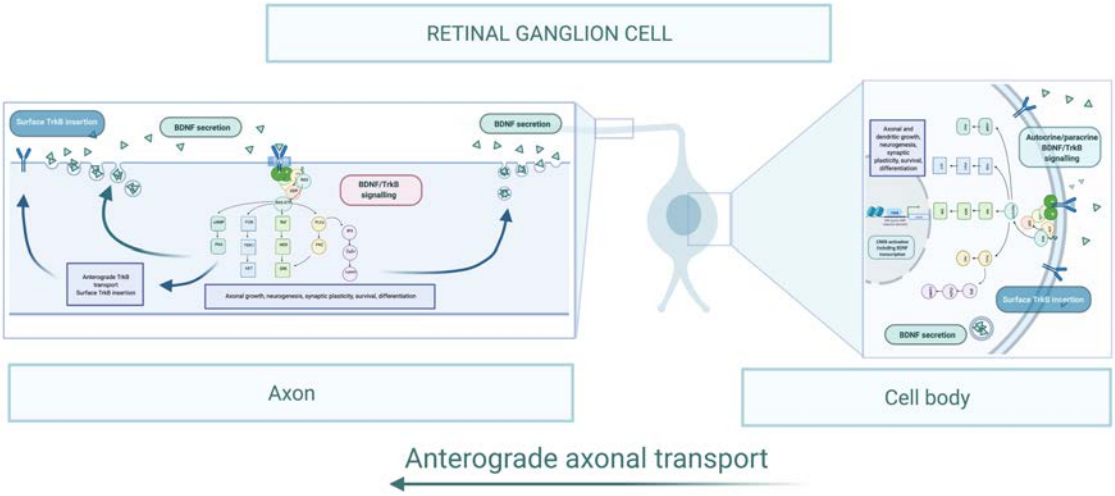


Figure 5-1: BDNF mediated autocrine self-amplifying positive feedback mechanism to stimulate anterograde axonal transport. Adapted from (P.-L. Cheng et al., 2011)

BDNF has also been shown to enhance TrkB receptor membrane stability and function by the recruitment of the receptor into lipid rafts of neuronal plasma membranes (Suzuki et al., 2004). However, the downregulation or dysfunction of TrkB expression in the disease state (Mazzaro et al., 2016) or in the presence of excess BDNF (A Di Polo et al., 1998) has been shown to compromise therapeutic efficacy.

Combination gene therapy, using multiple vectors administered in a single formulation, has been effective in targeting a diverse range of age-related pathologies in non-neuronal disease (Davidsohn et al., 2019). However, dual promoter techniques have previously shown selective expression (Emerman & Temin, 1984) and reduced efficiency (Y. Yang et al., 2016). The simultaneous administration of a ligand and its receptor by a single self-cleaving 2A peptide-based gene therapy vector under the control of one promoter aims to overcome this by ensuring relatively long-term expression of both proteins in target cells (A. Osborne, Khatib, et al., 2018).

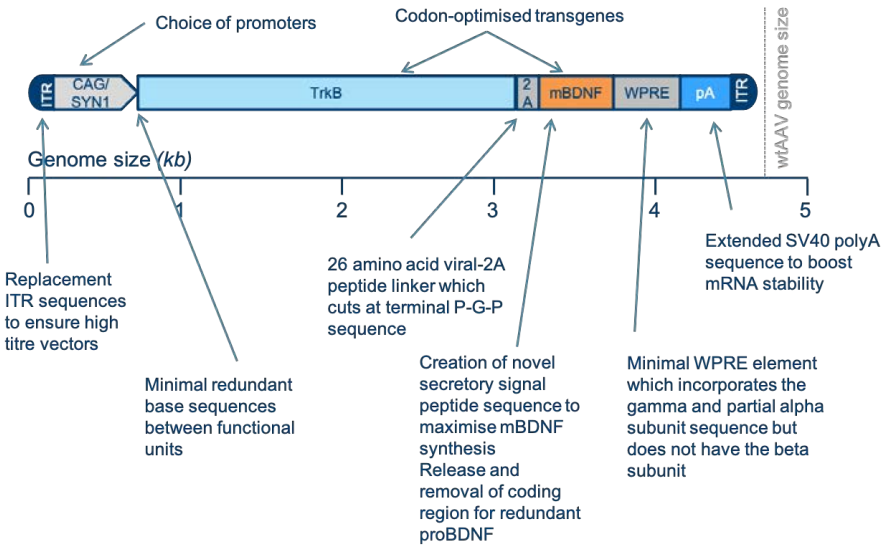


Figure 5-2: Development of the TrkB-2A-mBDNF construct. Adapted from (A. Osborne, Wang, et al., 2018)

We suggest this approach overcomes several problems relating to ligand deficiency and receptor downregulation in the diseased state or in the presence of excess ligand delivered therapeutically that may be relevant to multiple neurodegenerative diseases.

5.2 AIM

We hypothesised that combined BDNF and TrkB replacement would demonstrate superior efficacy compared to receptor or ligand alone and assessed this in two models of neurodegenerative disease known to be associated with reduced axonal transport (Bull et al., 2012; K. R. G. Martin et al., 2006; Pease et al., 2000) and in the presence of healthy endogenous receptors and ligand.

5.3 RESULTS

5.3.1 2A linker region does not interfere with TrkB receptor activation segment

Iterative Threading ASSEmbly Refinement (I-TASSER) was used to model the TrkB receptor administered via a single self-cleaving 2A peptide-based gene therapy vector under the control

of one promoter [Figure 5-3A] including the key tyrosine residues which are phosphorylated upon activation and the position of the 2A linker [Figure 5-3B]. The coding region for the TrkB receptor is linked to the coding region for mature BDNF (mBDNF) via the viral-2A peptide sequence. Intracellular processing of the transgene results in cutting of the viral-2A linker at the C-terminal proline-glycine and proline amino acids to generate the two proteins TrkB and mBDNF [Figure 5-3C]. While the N-terminal proline residue of the viral-2A peptide which is attached to the N-terminal of the BDNF signal peptide will eventually be lost in the intracellular vesicles, prior to cellular release, 20 amino acids of the viral-2A peptide remain attached to the C-terminal TrkB intracellular kinase portion. The beta-sheet layers (β1, β2, β3, β4 and β5) overlay the activation segment which is circled in white. The active site contains the central tyrosine residues (Y700, Y704 and Y705) which are phosphorylated upon dimerization in the presence of BDNF. The viral-2A peptide C-terminal extension [Figure 5-3B coloured red] is shown to overlay the kinase insert domain (KID) which lies at the foot of the helix complex (αD). The viral-2A peptide extension does not lie close to the activation segment, or interfere with the hinge region necessary for receptor conformational changes following phosphorylation and subsequent activation.

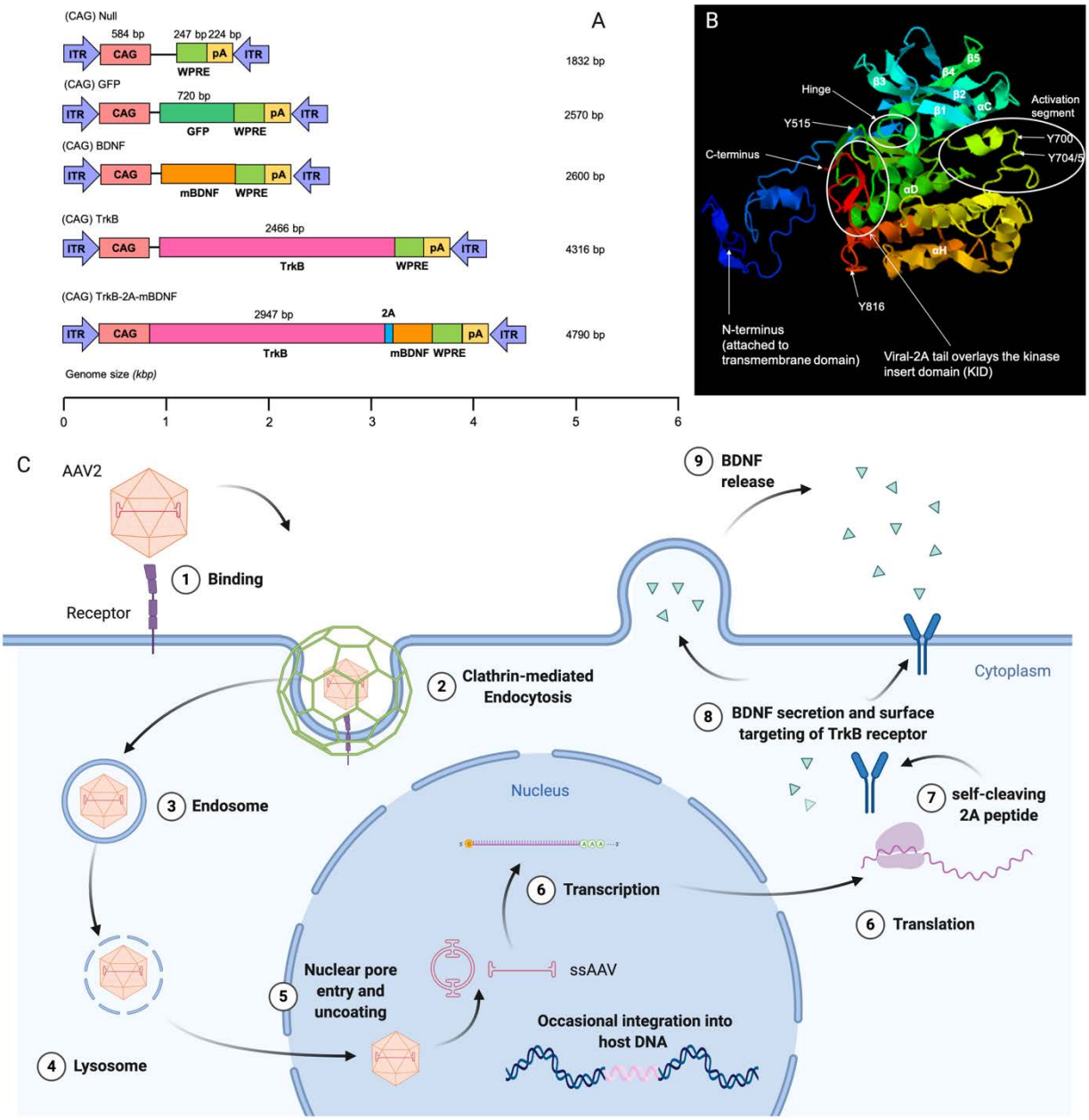


Figure 5-3: Simultaneous administration of a ligand and its receptor by a single self-cleaving 2A peptide-based gene therapy vector under the control of one promoter A: Plasmid maps (murine TrkB receptor) B: I-TASSER generated structure of TrkB receptor with residual 2A linker region C: Schematic demonstrating expression of TrkB and mature BDNF in target cell.

5.3.2 Transduction efficiency of the rodent retina

Intravitreal injection of the vector did not adversely affect RGC density [Figure 5-10A-C].

The vector transduced both mouse and rat retinal RGCs.

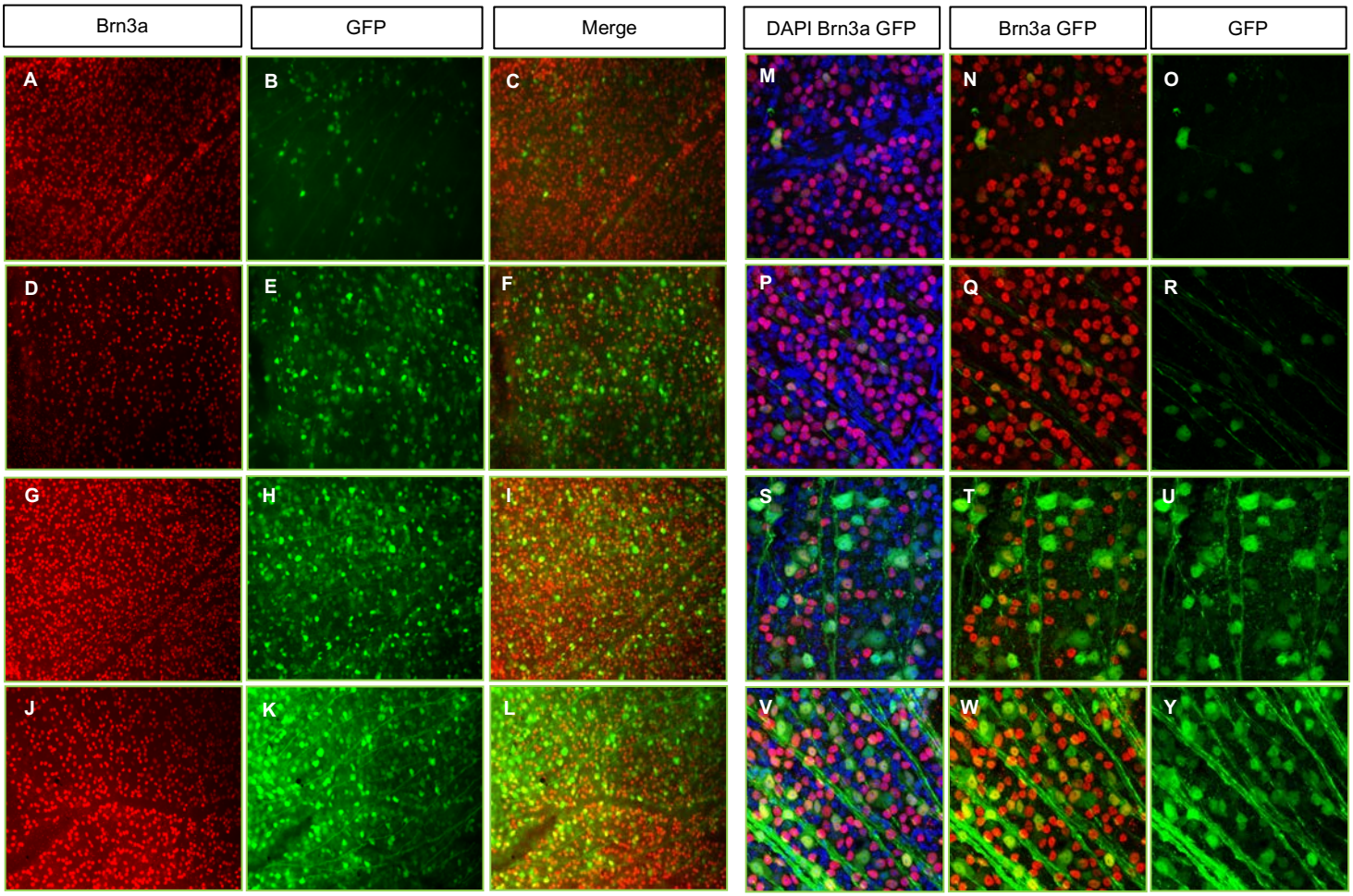


Figure 5-4: RGC transduction increases with viral titre. Immunolabelling of murine wholemount retinas with Brn3a as an RGC marker +- DAPI following intravitreal injection of AAV2-CAG-GFP at the following concentrations and volumes A-C;M-O: 1 x 10^{8} gp/eye, 2µl injection D-F;P-R: 1 x 10^{9} gp/eye, 2µl injection G-I;S-U: 1 x 10^{10} gp/eye, 2µl J-L;V-Y: 1 x 10^{10} gp/eye,1µl injection

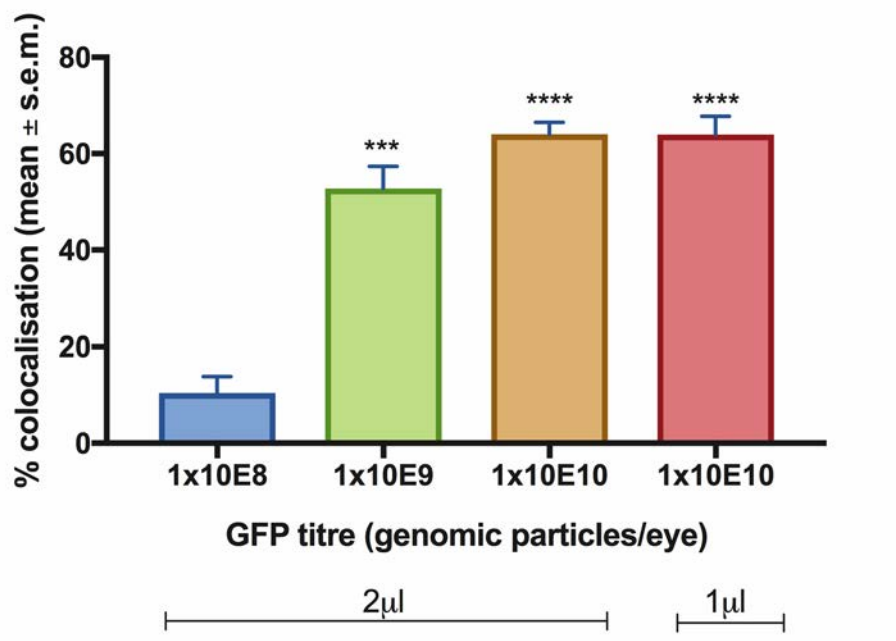


Figure 5-5: Mouse RGC transduction rate increased with viral titre; 10% at 1 x 10^{8}, 53% and 1 x 10^{9} and 64% at 1 x 10^{10} GC/eye. The volume injected did not appear to affect the transduction efficiency, with 64% of RGCs transduced at the highest titre using either 1 or 2 µl injection. Quantification performed using Volocity and Image J using 4 representative 20X images from each wholemount.

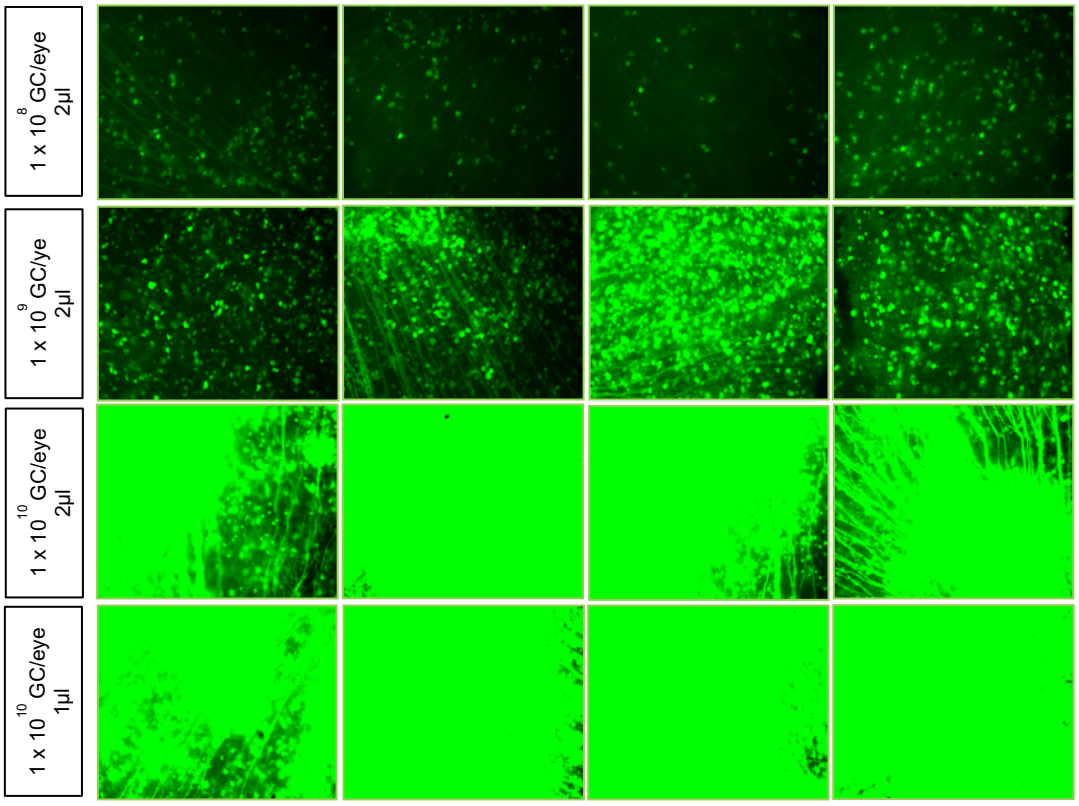


Figure 5-6: GFP intensity increases with viral titre. Images taken at X20 magnification, 190 ms exposure Top row: 1 x 10^{8} GC/eye, 2µl injection 2nd row: 1 x 10^{9} GC/eye , 2µl injection 3rd row: 1 x 10^{10} GC/eye, 2µl injection 4th row: 1 x 10^{10} GC/eye ,1µl injection

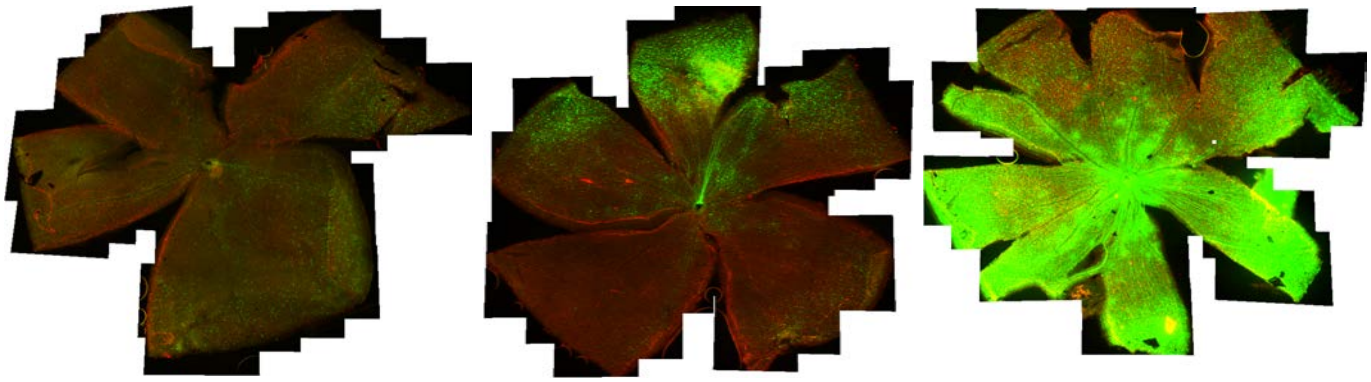


Figure 5-7: The spatial pattern of GFP expression is more extensive at the highest titre. GFP expression at lower titres tended to localise around the injection site. Immunolabelling of murine retinal wholemounts with Brn3a as an RGC marker. Reconstruction of wholemounts using 20 – 25 images at 10X magnification 3 weeks following intravitreal injection with AAV2-CAG-GFP. Left: 1 x 10^{8} GC/eye, 2µl injection Centre: 1 x 10^{9} GC/eye , 2µl injection Right: 1 x 10^{10} GC/eye,1µl injection

Other retinal cell types including bipolar, horizontal, Muller cells and amacrine cells are also transduced [Figure 5-8].

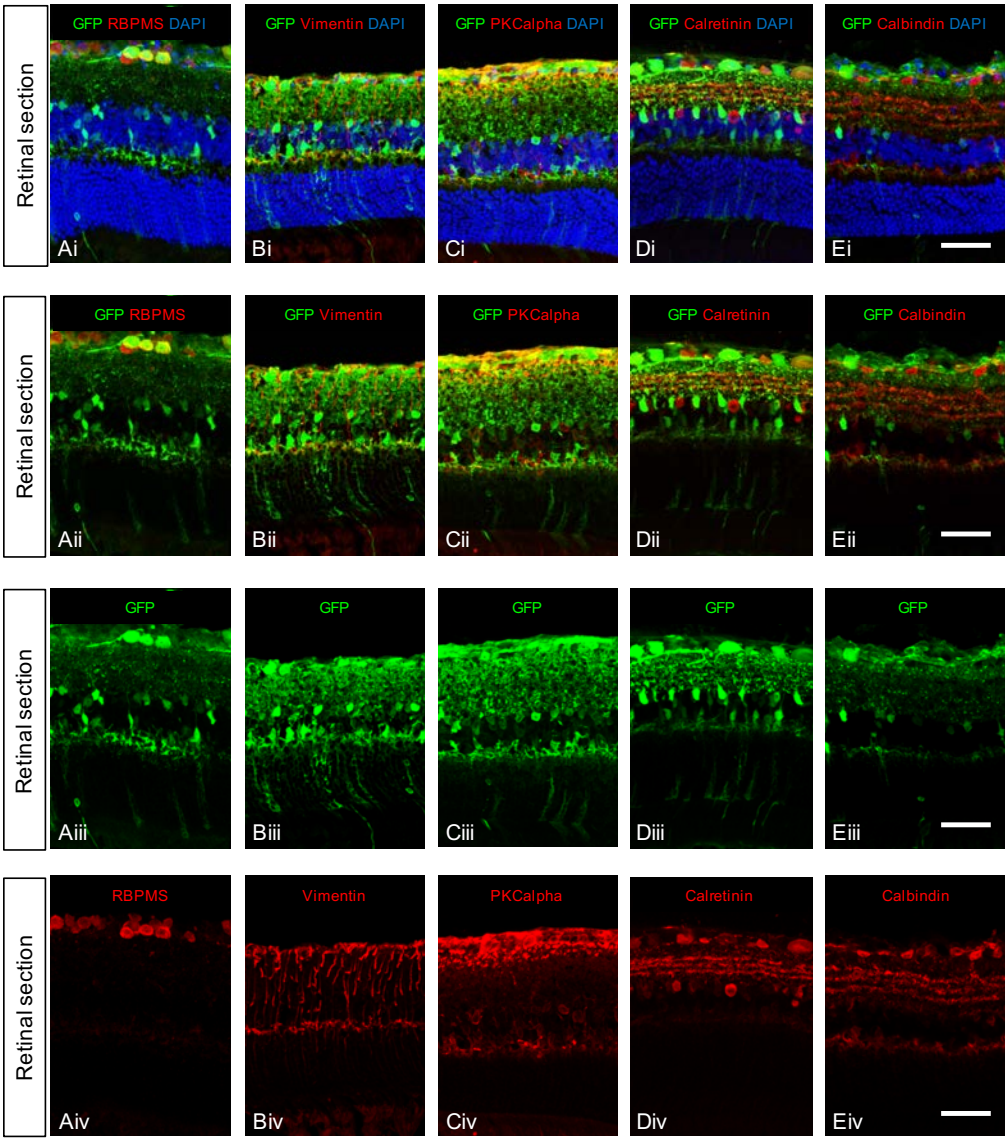


Figure 5-8: AAV2 GFP expression in retinal cells Ai-iv: Colocalisation with RBPMS (RGC) positive cells Bi-iv: Colocalisation with Vimentin (Muller) positive cells Ci-iv: Colocalisation with PKC α (bipolar) positive cells Di-iv: Colocalisation with Calretinin (amacrine, bipolar, horizontal) positive cells Ei-iv: Colocalisation with Calbindin (amacrine) positive cells. Scale bar 50 μm.

There was a significant increase in expression of BDNF and TrkB following retinal transduction with AAV2 TrkB-2A-mBDNF relative to AAV2 null [Figure 5-9].

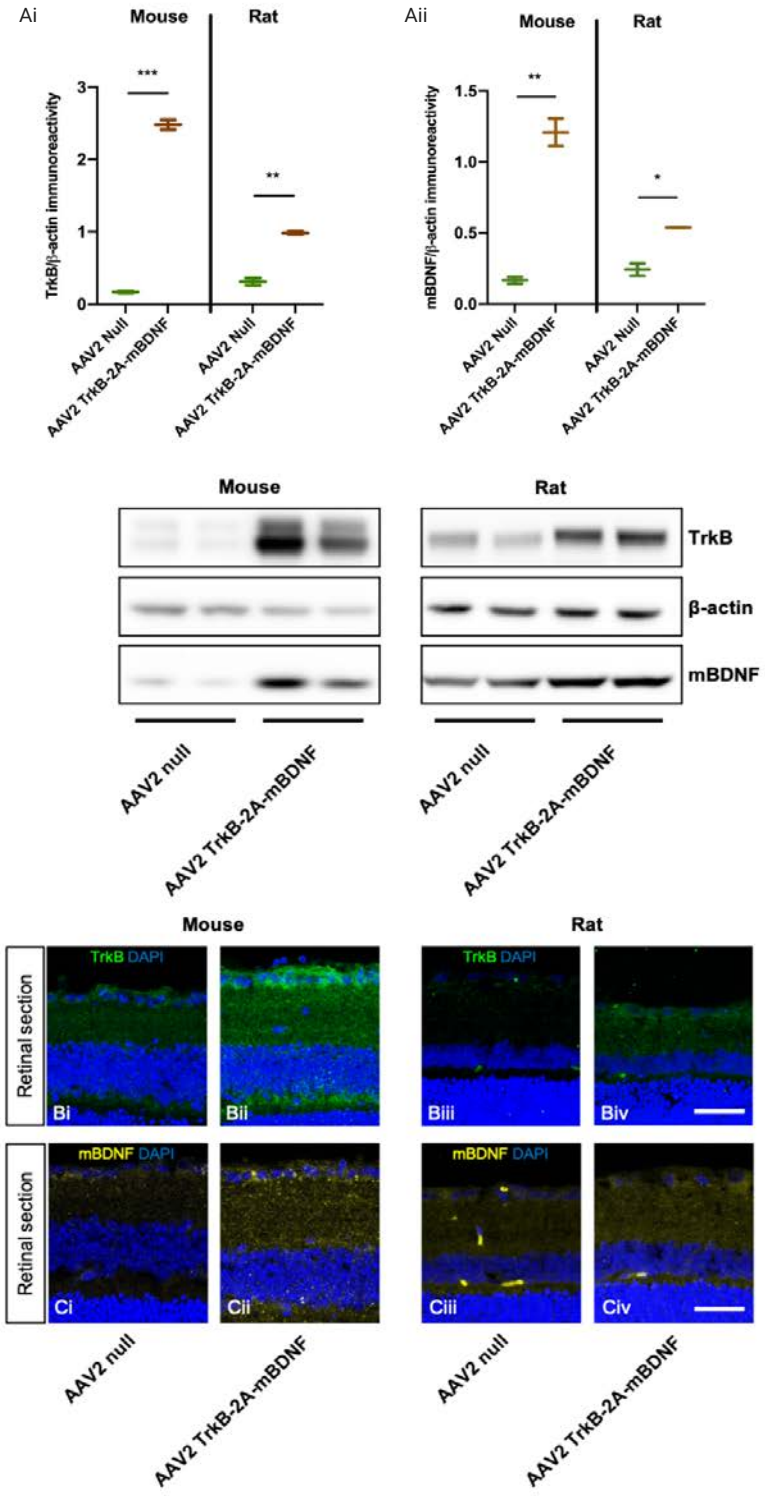


Figure 5-9: Increased expression of TrkB and BDNF following AAV2 TrkB-2A-mBDNF administration in the rodent retina Ai: TrkB overexpression in the mouse and rat retina

normalised to β-actin [mouse: AAV2 null 0.17±0.01 compared with AAV2 TrkB-2A-mBDNF 2.41±0.07 (n=2) p=0.0009; rat: AAV2 null 0.31±0.05 compared with AAV2 TrkB-2A-mBDNF 0.98±002 (n=2) p=0.007] Aii: mBDNF expression in the mouse and rat retina normalised to β-actin [mouse: AAV2 null 0.17±0.02 compared with AAV2 TrkB-2A-mBDNF 1.2±0.10 (n=2) p=0.009; rat: AAV2 null 0.24±0.04 compared with AAV2 TrkB-2A-mBDNF 0.54±0.001 (n=2) p=0.02] Bi-Bii: Overexpression of TrkB in mouse ganglion cell layer Biii-Biv: Overexpression of TrkB in rat ganglion cell layer Ci-Cii: Overexpression of mBDNF in mouse ganglion cell layer Ciii-Civ: Overexpression of mBDNF in rat ganglion cell layer. Box and whiskers plots: median displayed and whiskers 10-90 percentile with any outliers displayed as individual data points. Student t-test *p<0.05 ** p<0.01 *** p<0.001 Scale bar 50 μm.

5.3.3 Combined replacement is more effective than receptor or ligand replacement alone

Proximal optic nerve axonal transport [measured as shown in Figure 2E] increased following administration of AAV2-TrkB-2A-mBDNF in the uninjured optic nerve compared with naive levels [Figures 2G-L; 2Mi-ii; along the length of the nerve. The greatest effect was observed in the proximal 1 mm closest to the optic nerve head, where the site of obstruction to axoplasmic flow has previously been reported to occur in glaucoma (K. R. G. Martin et al., 2006; Pease et al., 2000). This enhancement of anterograde axonal transport was independent of any neuroprotective effect [Figure 2A-C] as there was no change in the density of Brn3a positive RGC bodies following intravitreal gene therapy administration. AAV2 injection did not affect retinal ganglion cell function as measured by the positive scotopic threshold response [Figure 2Fi-ii].

The effect of combined TrkB and mature BDNF administration in the single vector on axonal transport was superior to that seen with either AAV2 TrkB or AAV2 mBDNF alone [Figure 2Ni-ii] in the presence of healthy endogenous receptor or ligand afforded by the absence of injury.

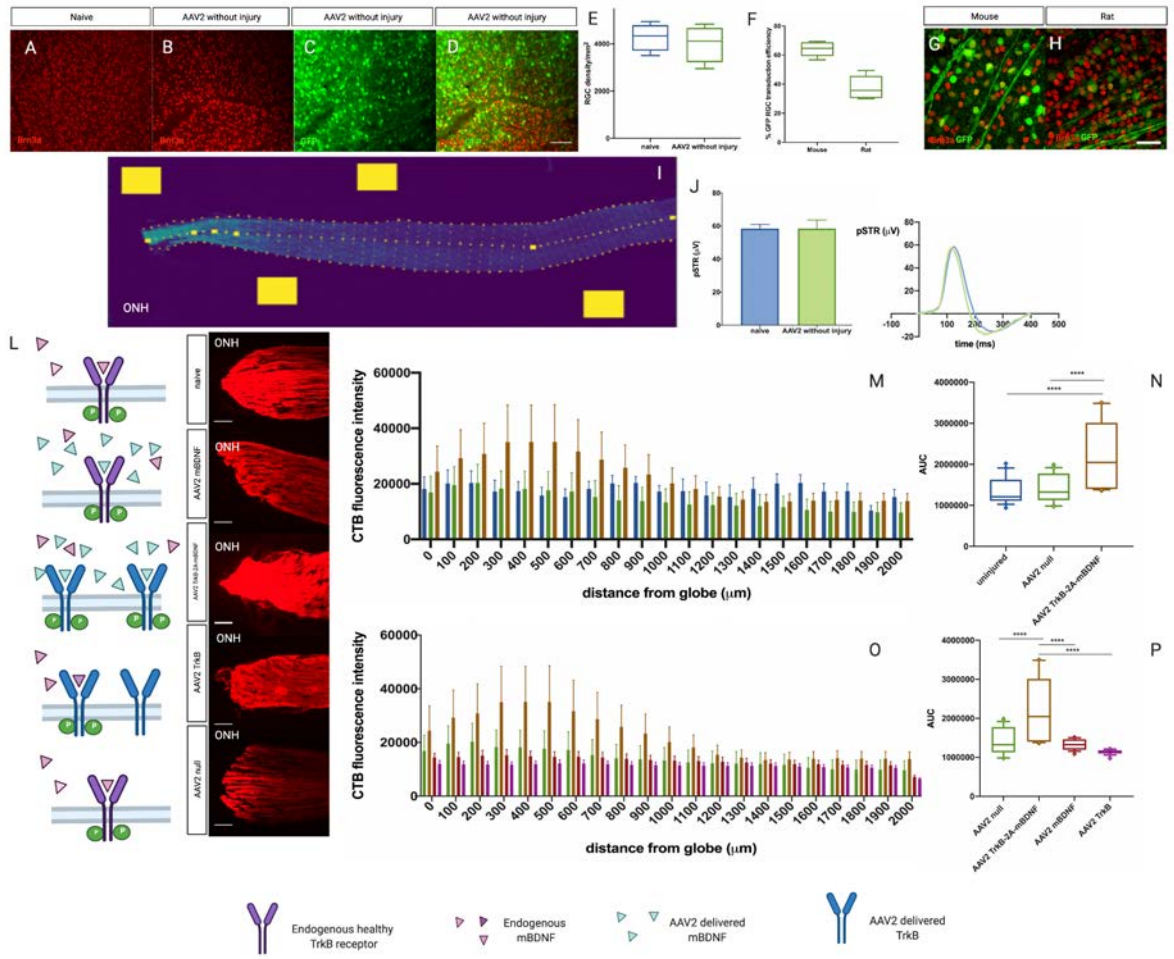


Figure 5-10: Combined ligand receptor replacement more effective than ligand or receptor alone A-C: AAV2 injection not associated with retinal ganglion cell loss [naive 4279±294 RGCs/mm^2 compared to AAV2 injection without injury 4004±391 RGCs/mm^2, p=0.59, (n=4)] Di-Diii: Transduction of Brn3a positive retinal ganglion cells in mouse and rat [mouse transduction efficiency 64.01±2.02 %; rat transduction efficiency 37.61±3.36% (n=6)] E: Semi-automated quantification of anterograde optic nerve axonal transport. Yellow boxes represent automated background fluorescence measurements taken and used to normalise readings. Fi-ii: AAV2 injection does not impair retinal ganglion cell function [naive 58.38±2.52 μV compared to AAV2 injection without injury 58.41±5.20 μV, p=0.99 (n=9)]. G-L: Schematic of AAV2 therapy with corresponding representative images of the proximal optic nerve with CTB Mi-ii: AAV2 TrkB-2A-mBDNF enhances anterograde axonal transport in the uninjured optic

nerve [uninjured 1356991±74285 (n=13), AAV2 null 1407781±76284 (n=4), AAV2 TrkB-2A-mBDNF 2224777±186617 (n=5)] Ni-ii: Combined ligand receptor replacement is more effective than ligand or receptor alone. [AAV2 TrkB-2A-mBDNF 2151629±191990 (n=5), AAV2 TrkB 1138337±13648 (n=4), AAV2 mBDNF 1327883±30372 (n=5)]. Data displayed as mean ± s.e.m. Box and whiskers plots: median displayed and whiskers 10-90 percentile with any outliers displayed as individual data points. Scale bar 100 μm. **** p<0.0001. Student t-test and ANOVA with Bonferroni correction.

5.3.4 Intervention is effective after the onset of pathology in a humanised tauopathy model

We explored whether this effect could be applied in the disease state, using the P301S humanised tauopathy model. Filamentous inclusions made of hyperphosphorylated tau are present in the central nervous system of 3- and 5-month old transgenic mice including RGCs (Gasparini et al., 2011). Figure 5-11Ai-ii shows a reduction in anterograde axonal transport in the optic nerves of 5 month old P301S mice compared to age-matched C57BL/6 mice. This reduction in transport was not associated with any reduction in retinal ganglion cell count [Figure 5-16].

There was a significant increase in proximal optic nerve axonal transport with AAV2 TrkB-2A-mBDNF in the tauopathy model administered after the onset of tau pathology relative to naive, AAV2 null and AAV2 GFP controls [Figure 5-11Bi-ii]. Administering the vector prior tau pathology onset had greater efficacy than when administered in the pathological state [Figure 5-11Ci-ii]. Representative images of CTB in the proximal optic nerve are shown in Figures 5-11E-J. Disruption in axonal transport occurred prior to observable functional loss, representing a possible early therapeutic target. There was no reduction in RGC function in the P301S tauopathy model up to the 5 month time point [Figure 5-11Ki-Mii].

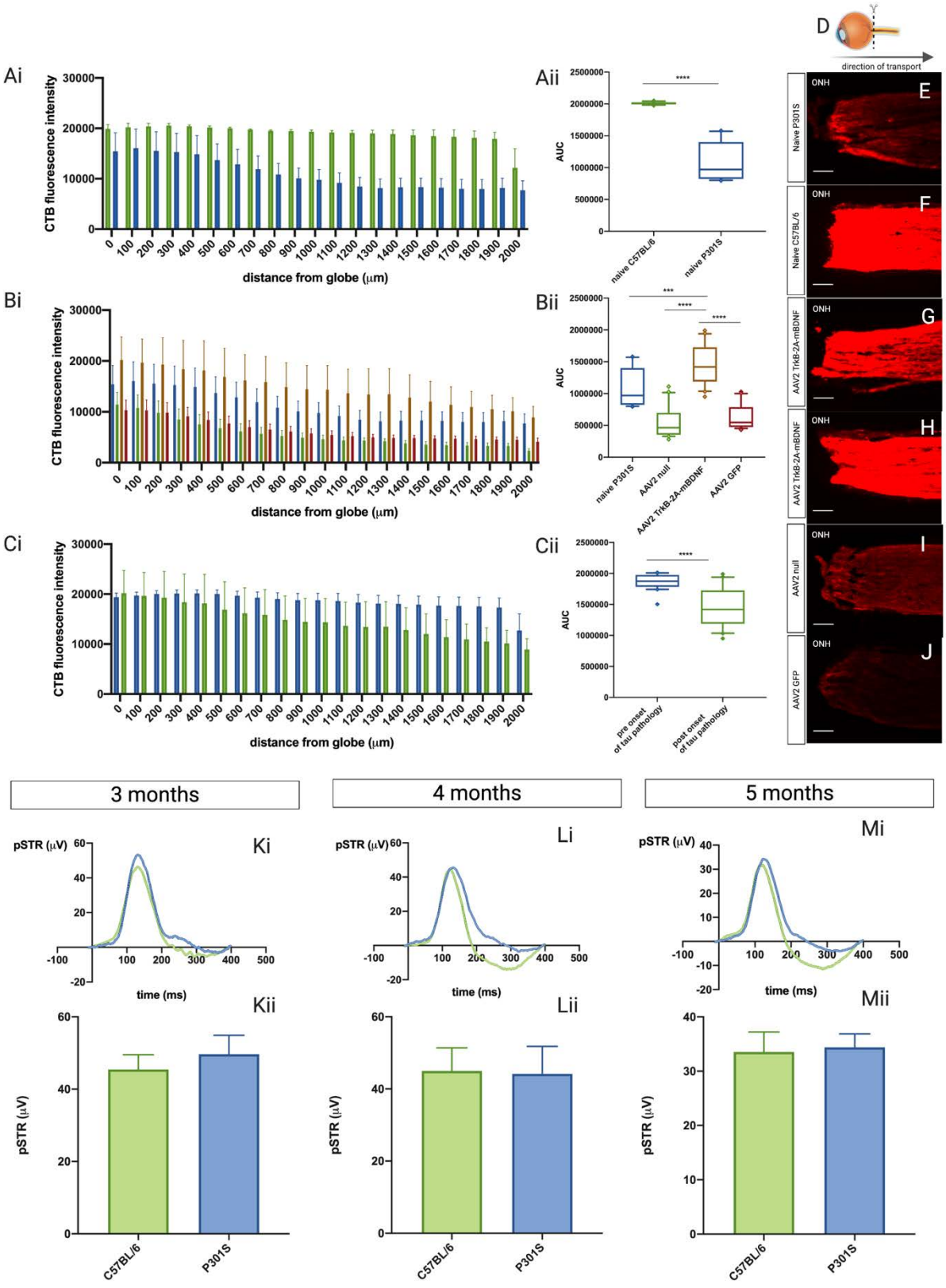


Figure 5-11: Intervention is effective after the onset of pathology in a humanised tauopathy model Ai-ii: Reduction in anterograde optic nerve axonal transport of CTB in P301S transgenic

mice [C57BL/6 2009762±4629 (n=3) compared to 5 month P301S 1085928±67416 (n=8)]. Bi-ii: AAV2 TrkB-2A-mBDNF enhances optic nerve axonal transport after the onset of tau pathology [AAV2 TrkB-2A-mBDNF 1454297±70125 (n=7), naive 1085928±67416 (n=8) AAV2 null 552603±54452 (n=4) AAV2 GFP 631690±44433 (n=5)]. Ci-ii: AAV2 TrkB-2A-mBDNF is more effective if administered prior to the onset of tau pathology [intervention pre-onset 1863778±27856 (n=5) post-onset 1454297±70125 (n=7)] D: Direction of axon transport E-J: Representative images of the proximal optic nerve with CTB G represents AAV2 TrkB-2A-mBDNF administered post onset of tau pathology; H represents AAV2 TrkB-2A-mBDNF administered prior to onset of tau pathology. Ki-Mii: Anterograde optic nerve axonal transport deficits precede retinal ganglion cell functional deficits in P301S transgenic mice Positive scotopic threshold response in 3 month (Ki-ii), 4 month (Li-ii) and 5 month (Mi-ii) P301S transgenic mice [Ki-ii: 3 month C57BL/6 45.4±4.10 μV (n=16) compared to P301S 49.7±5.25 μV (n=9); Li-ii: 4 month C57BL/6 45.0±6.40 μV (n=10) compared to P301S 44.1±7.66 μV (n=8); Mi-ii: 5 month C57Bl/6 33.5±3.69 μV (n=13) compared to P301S 34.3±2.47 μV (n=12)]. Data displayed as mean ± s.e.m. Box and whiskers plots: median displayed and whiskers 10-90 percentile with any outliers displayed as individual data points. Scale bar 100 μm. *** $p<0.001$ **** $p<0.0001$ Student t-test and ANOVA with Bonferroni correction.

5.3.5 AAV2 TrkB-2A-mBDNF enhances axonal transport in experimental glaucoma with functional recovery

Figure 5-14 shows anterograde optic nerve axonal transport in our experimental glaucoma model, which is known to cause RGC degeneration and disruption of axonal transport due to intraocular pressure (IOP) elevation (Levkovitch-Verbin et al., 2002; Marina et al., 2010; K. R. G. Martin et al., 2006; Pease et al., 2000; H. A. Quigley et al., 2000). Intravitreal injection of AAV2-TrkB-2A-mBDNF or with AAV2 null alone did not produce any changes in the IOP, as measured immediately prior to laser treatment [Figure 5-12A], or during the course of the

experiment when injected into the non-lasered eye [Figure 5-12B]. IOP elevation was similar for both AAV2 null and AAV2 TrkB-2A-mBDNF groups across all timepoints and returned to baseline levels 1 week following the second laser insult, remaining at baseline levels for the duration of the study [Figure 5-12A].

There was a reduction in the RGC specific positive scotopic threshold response (pSTR) in both groups at two days [Figure 5-13A,D] and 1 week [Figure 5-13B,Ei] following experimental IOP elevation, with functional recovery at 1 month in the AAV2 TrkB-2A-mBDNF treated group [Figure 5-13C,F].

Proximal optic nerve axonal transport decreased early post injury at 2 days [Figure 5-14A-B] and 1 week [Figure 5-14C-D] in the AAV2 null treated group and remained at baseline levels in the AAV2 TrkB-2A-mBDNF group. This reduction in transport and function was not associated with RGC loss [Figure 5-16].

The proximal transport started to recover at 1 month post injury [Figure 5-14E-F] but distal transport at the level of the superior colliculus remained depressed in the AAV2 null treated group [Figure 5-14I].

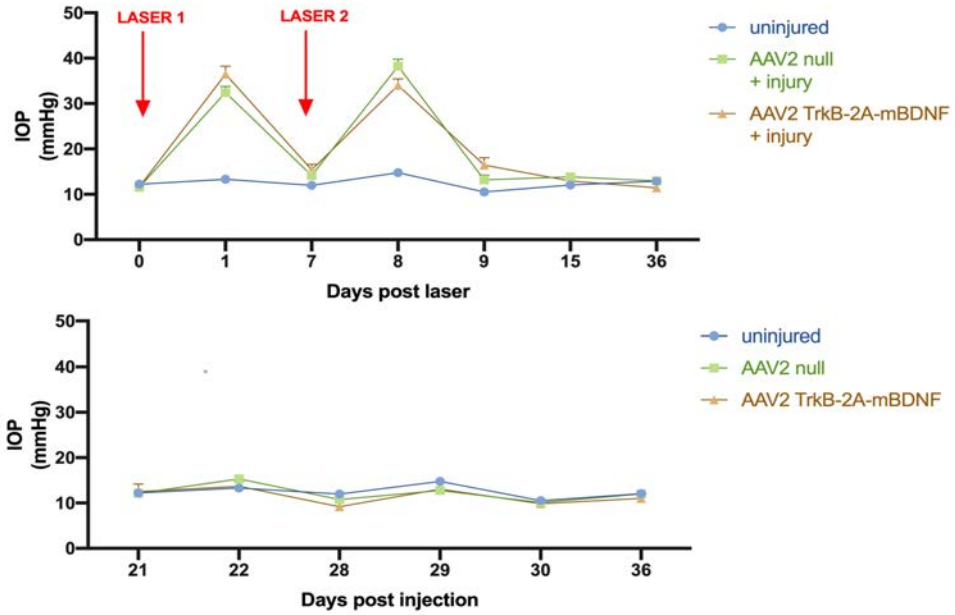


Figure 5-12: IOP profile A: Baseline IOP [uninjured 12.2±0.29mmHg; AAV2 null 11.5±0.28mmHg; AAV2 TrkB-2A-mBDNF 11.6±0.24mmHg]. IOP elevation [AAV2 null (D1 32.4±1.35mmHg, D7 14.1±0.76mmHg, D8 38.2±1.56mmHg, D9 13.2±1.06mmHg, D15 13.9±0.80mmHg, D36 12.9±0.70mmHg); AAV2 TrkB-2A-mBDNF (D1 36.5±1.73mmHg, D7 15.4±1.19mmHg, D8 34.0±1.44mmHg, D9 16.4±1.62mmHg, D15 13.0±0.0mmHg, D36 11.4±0.45mmHg)] B: AAV2 TrkB-2A-mBDNF does not affect IOP. Data displayed as mean ± S.E.M.

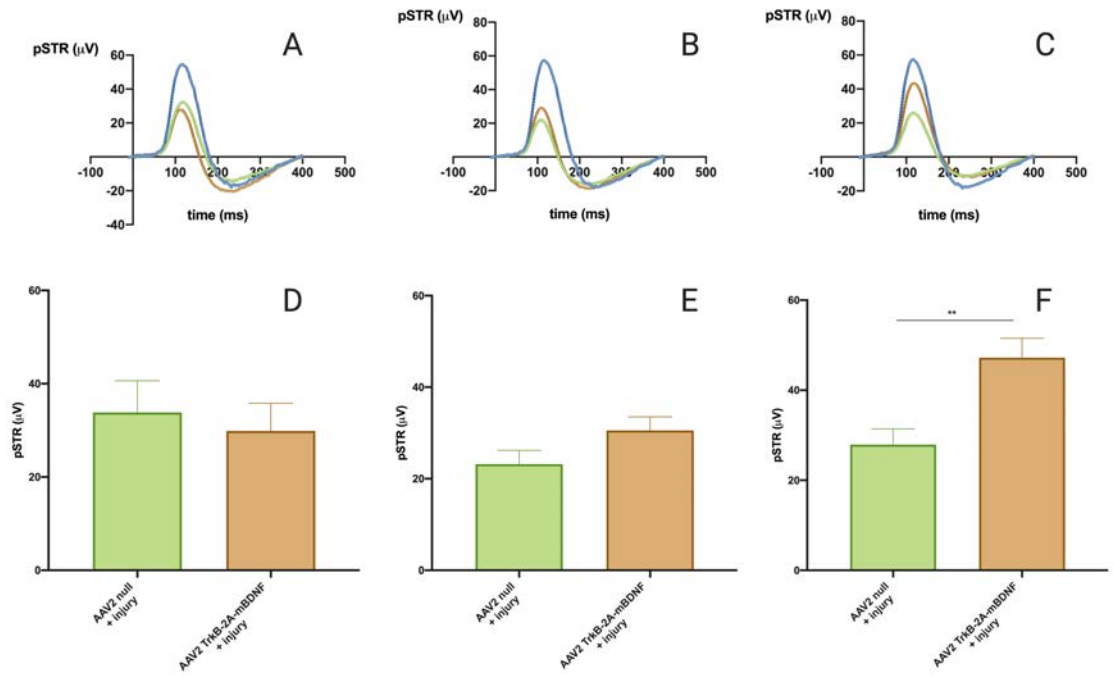


Figure 5-13: Functional deficits precede transport deficits and are restored with AAV2 TrkB-2A-mBDNF. pSTR D9 [A,D: AAV2 null + injury 33.8±6.81 μV, AAV2 TrkB-2A-mBDNF + injury 29.9±5.94 μV (n=9)], D14 [B,E: AAV2 null + injury 23.2±2.99 μV (n=24), AAV2 TrkB-2A-mBDNF + injury 30.4±3.00 μV (n=21)] and D35 [C,F: AAV2 null + injury 27.9±3.32 μV (n=23), AAV2 TrkB-2A-mBDNF + injury 47.2±4.34 μV, (n=20) p=0.002]. Data displayed as mean ± S.E.M. ** p<0.01. Student t-test.

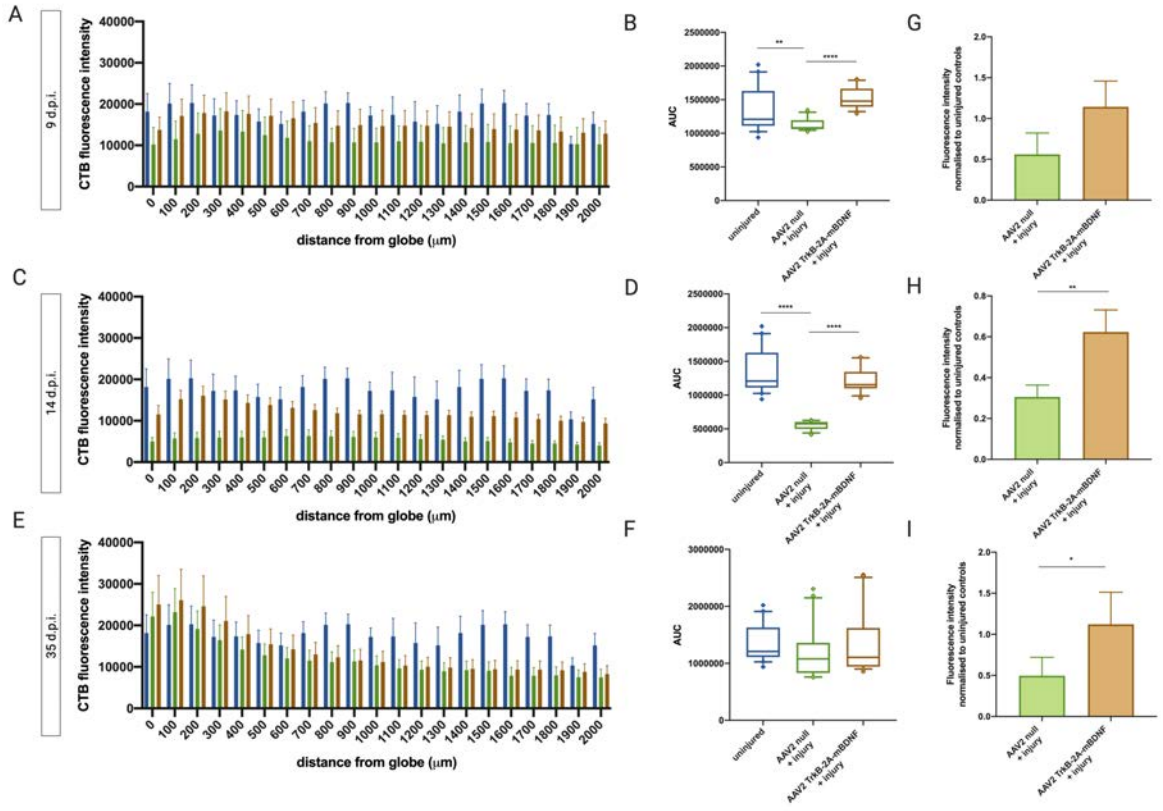


Figure 5-14: AAV2 TrkB-2A-mBDNF enhances anterograde optic nerve axonal transport in experimental glaucoma. Fi-Hii: Optic nerve axonal transport D9 [Fi-ii: uninjured 1356991±74285 (n=13), AAV2 null + injury 1123294±21687 (n=4) AAV2 TrkB-2A-mBDNF + injury 1517967±35554 (n=5)], D14 [Gi-ii: uninjured 1356991±74285 (n=13), AAV2 null + injury 549638±15124 (n=4) AAV2 TrkB-2A-mBDNF + injury 1214833±40492 (n=5) p<0.0001] D35 [Hi-ii: AAV2 null + injury 1192000±102085 (n=8), AAV2 TrkB-2A-mBDNF + injury 1349326±124332 (n=10)]. Ii-Kiii: Anterograde transport to the superior colliculus D9 [Ii: AAV2 null + injury 0.56±0.26 fold reduction from uninjured (n=4), AAV2 TrkB-2A-mBDNF + injury 1.14±0.31 fold increase from uninjured (n=5) p=0.39], D14 [Ji: AAV2 null + injury 0.30±0.11 fold reduction from uninjured (n=4), AAV2 TrkB-2A-mBDNF + injury 0.62±0.11 fold reduction from uninjured (n=5) p=0.009] D35 [Ki: AAV2 null + injury 0.50±0.22 fold reduction from uninjured (n=9), AAV2 TrkB-2A-mBDNF + injury 1.12±0.39 fold increase from uninjured (n=7) p=0.02] Data displayed as mean ± S.E.M. Box and whiskers plots: median displayed and

whiskers 10-90 percentile with outliers displayed as individual data points. *p<0.05 ** p<0.01 *** p<0.001 **** p<0.0001. Student t-test and ANOVA with Bonferroni correction.

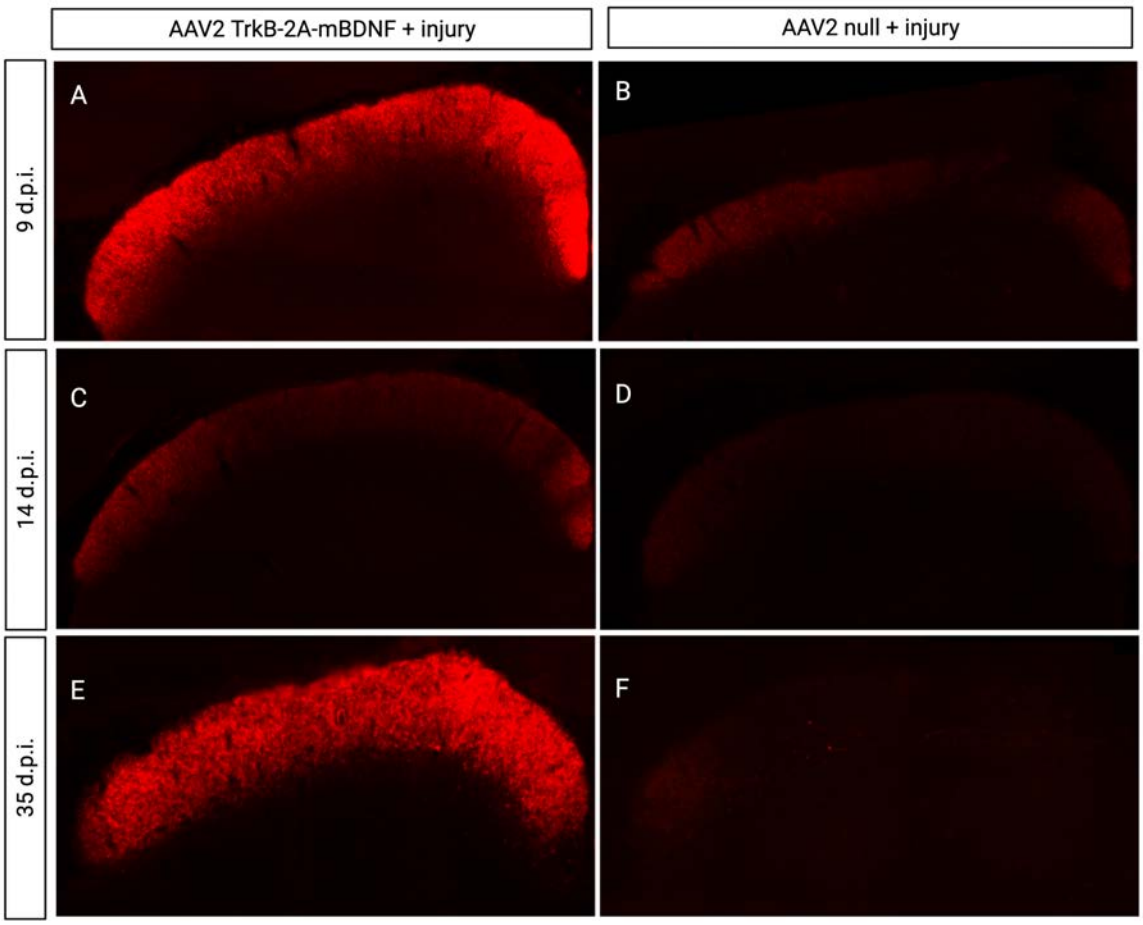


Figure 5-15: Anterograde transport of CTB in the superior colliculus. Representative images of D9 post injury [A: TrkB-2A-mBDNF + injury B: AAV2 null + injury], D14 [C: AAV2 TrkB-2A-mBDNF + injury D:AAV2 null + injury] D35 [E: AAV2 AAV2 TrkB-2A-mBDNF + injury F: AAV2 null + injury]

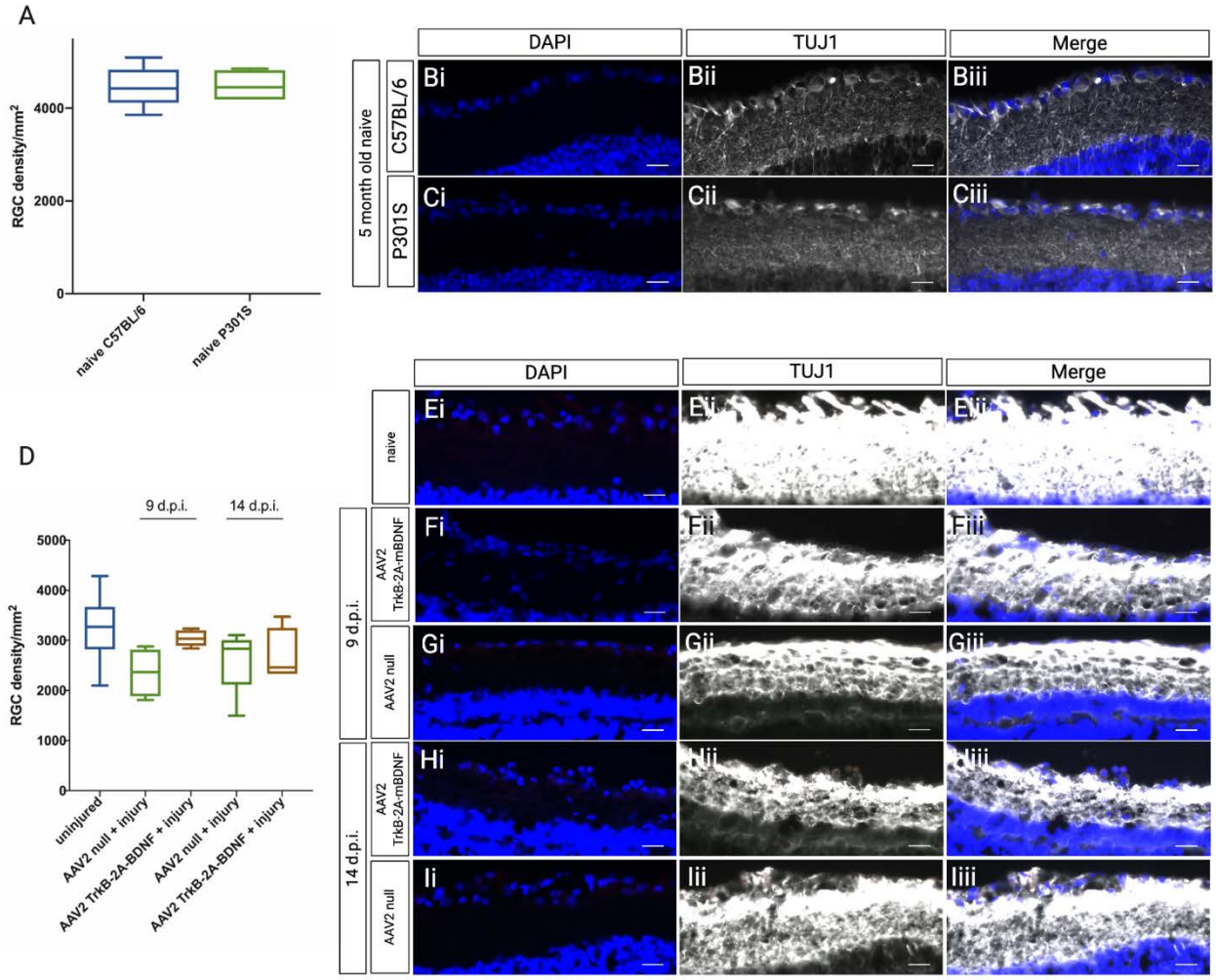


Figure 5-16: Reduction in optic nerve axonal transport or RGC function is not associated with RGC soma loss A: RGC density in 5 month old C57BL/6 and P301S transgenic mice [C57BL/6 4465±198.2 RGCs/mm^2 (n=5) compared with P301S 4490±136.1 RGCs/mm^2 (n=6) p=0.92] Bi-Ciii: Representative images of TUJ1 positive RGCs in 5 month old C57BL/6 and P301S transgenic mice D: RGC density following IOP elevation at 9 and 14 days post injury [uninjured 3220±232.6 RGCs/mm^2 (n=8), AAV2 null + 9 d.p.i 2356±241.3 RGCs/mm^2 (n=4) p=0.11, AAV2 TrkB-2A-mBDNF + 9 d.p.i 3044±72.1 RGCs/mm^2 (n=5) p=0.98, AAV2 null + 14 d.p.i. 2616±285.6 RGCs/mm^2 (n=5) p=0.33, AAV2 TrkB-2A-mBDNF 2682±271.1 RGCs/mm^2 (n=4)] p=0.51. Ei-Iiii: Representative images of TUJ1 positive RGCs in uninjured rats and following IOP elevation at 9 and 14 days post injury. Data displayed as mean ± s.e.m. Box and whiskers plots: median displayed and whiskers 10-90 percentile with any outliers

displayed as individual data points. Student t-test and ANOVA with Bonferroni correction. Scale bar 40 μm.

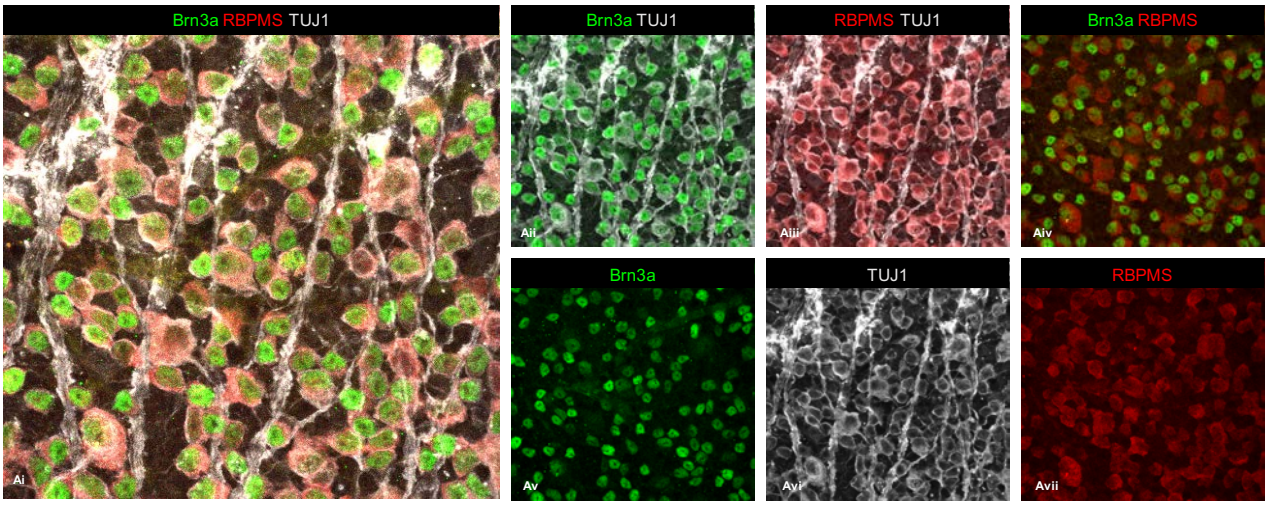


Figure 5-17: Colocalisation of RGC markers. Ai: Merged Brn3a, RBPMS, TUJ1 Aii: Merged Brn3a, TUJ1 Aiii Merged RBPMS, TUJ1 Aiv: Merged Brn3a, RBPMS Av: Brn3a alone Avi: TUJ1 alone Avii: RBPMS alone.

5.3.6 Translating from the visual pathway to memory: AAV5 TrkB-2A-mBDNF improves short term memory loss in a humanised dementia model.

The eye is widely considered to be an accessible experimental model of the central nervous system and there have been recent correlations in amyloid-related pathology in the brain and retina in Alzheimer's disease (Chiasseu et al., 2017; Hadoux et al., 2019). We therefore explored whether the improvement in optic nerve axonal transport seen in the P301S model using AAV2 TrkB-2A-mBDNF could be extrapolated to the brain, and specifically memory using the spontaneous object recognition test. We used the same P301S humanised transgenic tauopathy line used in the optic nerve experiments as our dementia model [Figure 5-18A;Bi]. Injection of AAV5 TrkB-2A-mBDNF into the perirhinal cortex was associated with promising evidence that there may be an improvement in short term memory at 8 weeks post

injection [Figure 5-18Bii]. Longer term memory deficit however persisted at the 8 week timepoint [Figure 5-18Biii].

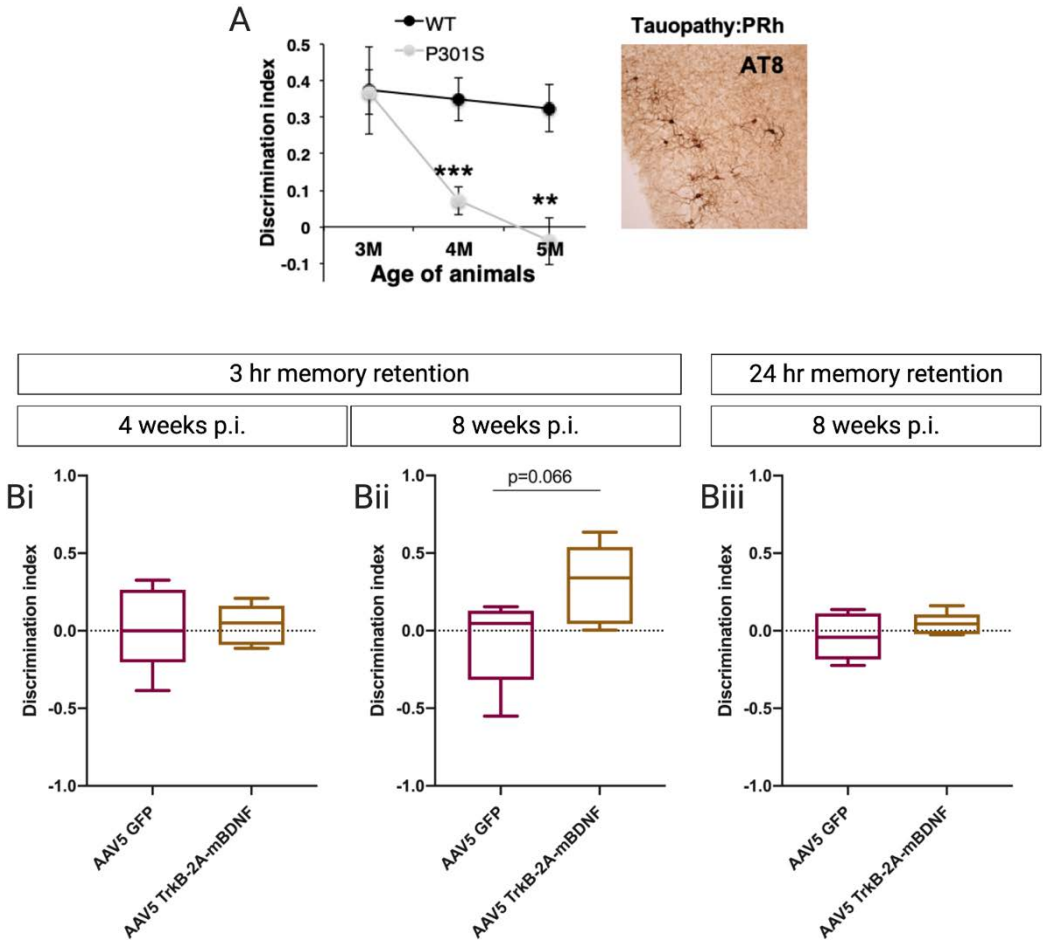


Figure 5-18: AAV5 TrkB-2A-mBDNF improves short term memory in a humanised tauopathy model of dementia. A: Memory deficit in the P301S tauopathy model *Reprinted with permission from Yang S et al. (2017)* (S. Yang et al., 2017). Bi: 3 hour memory retention at 4 weeks post injection [AAV5 GFP 0.02±0.12 discrimination index compared with AAV5 TrkB-2A-mBDNF 0.04±0.06 discrimination index; p=0.92 (n=5)] Bii: [AAV5 GFP -0.07±0.13 discrimination index compared with AAV5 TrkB-2A-mBDNF 0.30±0.16 discrimination index; p=0.066 (n=5)] Biii: [AAV5 GFP -0.03±0.07 discrimination index compared with AAV5 TrkB-

2A-mBDNF 0.04±0.03 discrimination index; p=0.32; (n=5)]. Data displayed as mean ± S.E.M. Box and whiskers plots: median displayed and whiskers 10-90 percentile with any outliers displayed as individual data points. Student t-test used as statistical test.

5.4 DISCUSSION

Here we offer evidence that combined overexpression of both BDNF and its receptor TrkB, by a single vector with one promoter is more effective in stimulating anterograde axonal transport than either receptor administration or ligand administration alone. The position of the viral-2A peptide extension on the TrkB receptor does not lie close to the activation segment and we have previously demonstrated that phosphorylation of the receptor is unaffected by the presence of the 2A linker with subsequent upregulation of downstream survival signalling pathways (A. Osborne, Khatib, et al., 2018; A. Osborne, Wang, et al., 2018).

We also report that simultaneous overexpression of BDNF and TrkB enhances axonal transport in two neurodegenerative disease models: a humanised tauopathy model of Alzheimer's disease and an experimental glaucoma model. We also show that deficits in axonal transport occur early in the tauopathy model prior to functional changes, representing a possible early therapeutic target. Functional recovery is also demonstrated in our experimental glaucoma model and we show there may be an improvement in short term memory deficit in a humanised dementia model.

This improvement in axonal transport is independent of any BDNF mediated neuroprotective increase in cell body or axon number, effects that have been previously reported (L. Cheng, Sapieha, Kittlerová, et al., 2002; A. Osborne, Khatib, et al., 2018), as it occurs without RGC loss in naive animals, early post injury and in the P301S tauopathy model of reduced axonal transport. Intervention is effective in our disease models and remains effective if administered after the onset of pathology suggesting a clinically relevant therapeutic window.

The underlying mechanisms through which the BDNF/TrkB pathway promotes axonal transport remain poorly understood. TrkB promotion of axon growth has been reported in regenerating corticospinal tract into subcortical lesions expressing BDNF mediated through the ERK signalling pathway (Hollis 2nd et al., 2009). BDNF has also been implicated in a self-amplifying positive feedback mechanism mediated through cyclic AMP, protein kinase A and the PI3 kinase pathways to trigger further BDNF secretion, promote TrkB membrane insertion and stimulate anterograde axonal transport (P.-L. Cheng et al., 2011). BDNF has also been shown to enhance TrkB receptor membrane stability and function by the recruitment of the receptor into lipid rafts of neuronal plasma membranes (Suzuki et al., 2004). Elevated levels of BDNF with TrkB activation of the PI3 kinase pathway and subsequent inactivation of glycogen synthase kinase-3β (GSK-3β) also modulate tau pathology and hyperphosphorylation (Elliott et al., 2005), and may reduce the progression of tau pathology with associated microtubule instability and axonal transport disruption (Bull et al., 2012; Mazzaro et al., 2016; Mercken et al., 1995). Similar effects have been suggested following exercise induced elevation of BDNF (Chrysostomou et al., 2014, 2016) and exercise-mediated reduction in central nervous system tau pathology in P301S mice (Ohia-Nwoko et al., 2014). Abnormalities in tau phosphorylation have also been implicated in the glaucomatous degenerative disease process in patients with intractable glaucoma not responsive to conventional therapies (Gupta et al., 2008). However, exogenous BDNF in the absence of TrkB overexpression has not been sufficient to promote axon outgrowth in the diseased state in P301S retinal explants (Gasparini et al., 2011). The demonstration of enhanced axonal transport above naive levels in adult wild-type Sprague Dawley rats lends support to previous findings that there may be a decline in axonal transport mechanisms with age including young adulthood (Milde et al., 2015) independent of injury and that mature neurons retain the capacity for enhancement and ability to support a higher transport rate. An evaluation of the impact of the therapy on retrograde axonal transport, which has also been implicated in glaucomatous pathology, together with a dynamic assessment of the transport of endogenous

proteins would address some of the limitations of this study.

The relationship between axonal transport and cellular function is complex, and, as we have demonstrated here, the disruption of function can occur both early and later in the disease process. We have demonstrated functional recovery where functional deficits occurred prior to axonal transport loss. Impaired inner retinal function has been shown to precede defects in anterograde active axonal transport of cholera toxin B following intraocular pressure elevation (Fahy et al., 2016; Pang et al., 2015), with a redistribution in the size and location of the axon initial segment postulated to alter action potential propagation following glaucomatous injury. Neuronal excitability has been reported as a response to IOP elevation (Risner et al., 2018) and visual stimulation and electrical activity has also been shown to influence axonal regeneration (Lim et al., 2016).

We observed recovery of the pSTR in our AAV2 TrkB-2A-mBDNF treated group following IOP elevation. This corresponds with functional recovery following IOP elevation previously described (Caprioli et al., 2016; Casson et al., 2014; Crowston et al., 2015) and supports the possibility of reversal of glaucomatous dysfunction of retinal ganglion cells and their connections, lending further support to the use of this treatment approach in the development of a clinical therapy for glaucoma. The construct is likely to have additional effects on neuronal connectivity and activity and our data would suggest that the effects observed cannot be attributed to transport alone. BDNF has also been shown to prevent dendritic retraction of RGCs (Binley et al., 2016), enhance synaptic activity (Kang & Schuman, 1995; Lohof et al., 1993) and autocrine BDNF/TrkB signalling on dendritic spines has been implicated in modulating structural and functional plasticity (Harward et al., 2016). The observation that the CTB intensity was reduced in the distal optic nerve but maintained in the superior colliculus following administration of AAV2 TrkB-2A-mBDNF in the experimental glaucoma model could be explained by improved neuronal connectivity or regeneration at the level of the colliculus. Transduction of non-target cells may also contribute and glial BDNF (A Di Polo et al., 1998)

and TrkB (Harada et al., 2011, 2015) signalling has previously been shown to play an important role in neural protection after traumatic optic nerve injury and can delay retinal degeneration. The improvement in short term memory in the humanised tauopathy dementia model is consistent with previous studies (Hopkins & Bucci, 2010; Schulz-Klaus et al., 2013; Seoane et al., 2011) and lends further support to the use of the eye and visual pathway as an accessible system to investigate CNS neurodegeneration. Whether the timing and pattern of delivery to the cortex can be optimised to affect longer term memory loss remains of interest. Structural comparison between the effect of BDNF and TrkB overexpression on cortical and retinal pathology should also be a focus of future work. It is therefore conceivable that overexpression of BDNF and TrkB could act through multiple mechanisms, by restoring neurotrophin support that has been lost through a disruption of axonal transport (K. R. Martin et al., 2003), boosting the ability of target cells to withstand pathological insults, and through the manipulating the underlying pathological processes that contribute to disruption of neuronal integrity and function.

We have previously discussed limitations associated with translation from pre-clinical to clinical studies for non-IOP lowering novel glaucoma therapies (Khatib & Martin, 2020). Refinements in clinical trial design together with optimisation of structural and functional endpoints are crucial in the assessment of future therapies. Allometric scaling and the pharmacokinetics of the human vitreous and the internal limiting membrane have also been suggested as potential barrier to viral transduction of the retina following intravitreal injection. We have demonstrated efficacy despite a reduction in transduction efficiency in the rat RGCs compared to mouse RGCs. It is of interest that the rAAV2/2-ND4 clinical trial for Leber's Hereditary Optic Neuropathy demonstrated efficacy following intravitreal injection in a younger LHON cohort who typically have a thicker internal limiting membrane and denser vitreous composition (Yu-Wai-Man et al., 2020). It remains to be seen whether the presence of vitreous syneresis or posterior vitreous detachment in the more elderly glaucoma patient population will lessen the structural barrier to viral transduction hence improving transgene expression.

The AAV8-RS1 gene therapy trial for X-linked retinoschisis also uses an intravitreal approach to administer a healthy copy of retinoschisin to target photoreceptors. Cukras *et al.* postulated that the retinal degeneration associated with the X-linked retinoschisis also compromises the structural integrity of the internal limiting membrane, facilitating retinal penetration following intravitreal administration of the viral vector (Cukras et al., 2018). Our intervention was administered prior to the induction of disease in the experimental glaucoma model. We feel these findings do have implication for clinical practice. The increasing role of artificial intelligence and functional imaging techniques have the potential to significantly improve our early detection of at-risk patients prior to the appearance of symptoms, together with progress in the molecular profiling of glaucoma patients and polygenic risk score stratification of disease progression. We have also shown that early intervention is more effective than late intervention in the tauopathy model of reduced axonal transport which also lends further support towards the role of early intervention.

In summary, we have demonstrated an enhancement of axonal transport in retinal ganglion cell axons in two disease models using AAV2 TrkB-2A-mBDNF and suggest that enhancements in the visual pathway can be translated to other regions in the CNS. We also show promising evidence that there may be an improvement in short term memory deficit using AAV5 TrkB-2A-mBDNF in a humanised tauopathy model of dementia. Given the recent correlation between Alzheimer's pathology in the brain and retina (Chiasseu et al., 2017; Hadoux et al., 2019), this approach shows promise as an overall strategy to target intrinsic neuronal mechanisms to improve neuronal repair, while overcoming several problems relating to ligand deficiency and receptor downregulation and dysfunction that may be relevant to multiple neurodegenerative diseases.

5.5 FUTURE DIRECTIONS: preliminary work

Understanding the underlying pathophysiology of the disruption to axonal transport in glaucoma may help us to explore why certain individuals are more sensitive to IOP elevation, and why certain individuals develop glaucomatous neurodegeneration with no demonstrable elevation in IOP (Mullany et al., 2021). The role of tau hyperphosphorylation in microtubule instability and impairment of optic nerve axonal transport after glaucomatous injury remains of interest and I have been able to complete some preliminary work towards this during the DM.

I have been able to demonstrate that tau hyperphosphorylation occurs following elevated IOP using a rat laser glaucoma model [Figure 5-19] at two known pathological epitopes, AT8 (Ser202/Thr205) and PHF-1 (Ser 396/Ser404). Total tau remains unchanged. These changes precede functional loss as determined by electrophysiology (RGC specific positive scotopic threshold response shown).

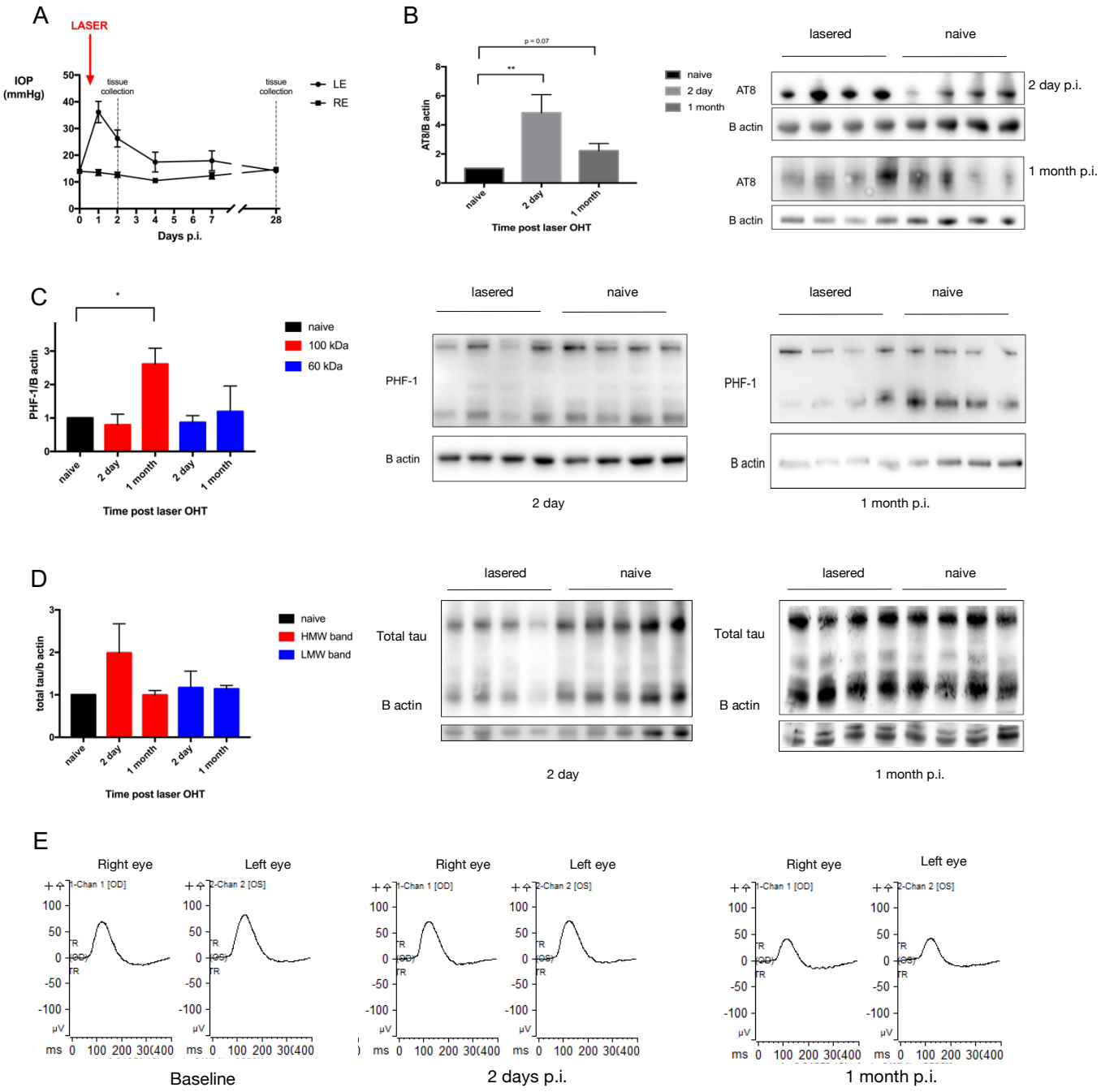


Figure 5-19: Changes in retinal tau and retinal ganglion cell function following laser induced ocular hypertension A: IOP profile following translimbal photocoagulation of the trabecular meshwork left eye B: Retinal tau phosphorylation at the AT8 (Ser202, Thr205) epitope following IOP elevation at 2 days and 1 month post-injury C: Retinal tau phosphorylation at the PHF-1 (Ser396/Ser404) epitope following IOP elevation at 2 days and 1 month post-injury D: Total retinal tau following IOP elevation at 2 days and 1 month post-injury. E: Retinal

ganglion cell function (positive scotopic threshold response) following laser induced ocular hypertension at 2 days and 1 month post-injury Data analysed using Student's t-test and displayed as fold change relative to control (mean ± S.E.M).

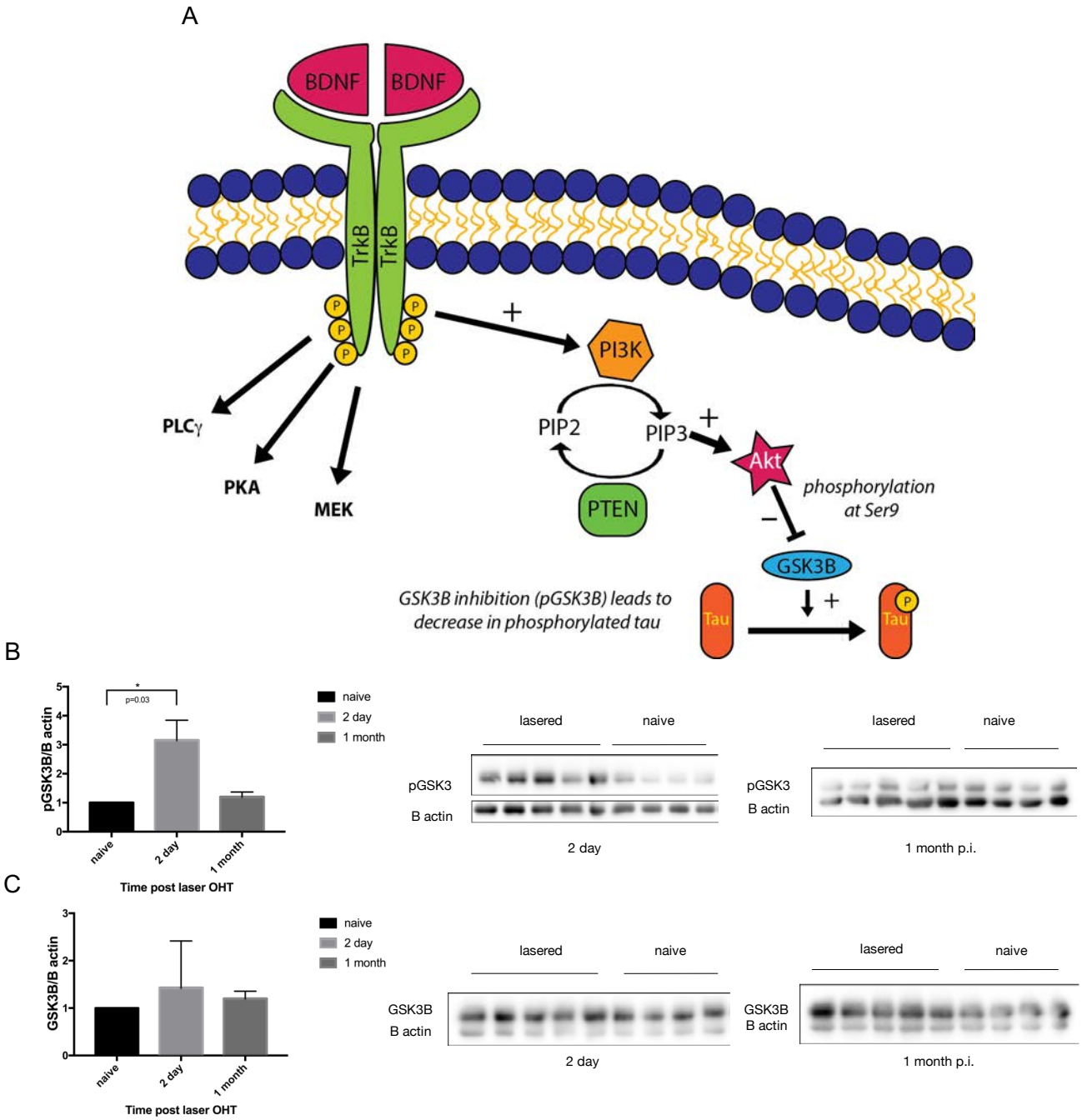


Figure 5-20: Regulation of retinal tau hyperphosphorylation following laser induced ocular hypertension A: Schematic demonstrating proposed mechanism of action of modulation of tau hyperphosphorylation via BDNF TrkB signalling pathway (adapted from Elliot et al. Brain-derived Neurotrophic Factor induces a rapid dephosphorylation of tau protein through a PI-3Kinase signalling mechanism Eur J Neuro 2005). B: GSK3B phosphorylation (inactivation) following IOP elevation at 2 days and 1 month post-injury C: Total GSK3B levels at 2 days and 1 month post injury. Data analysed using Student's t-test and displayed as fold change relative to control (mean ± S.E.M).

Regulation of phosphorylation via increased inactivation of the tau protein kinase GSK3B appears in the early response to injury but this negative regulation is lost more chronically [Figure 5-20]. Total levels of GSK3B remain unchanged relative to the naïve group. GSK3B is downstream of the BDNF TrkB signalling pathway [Figure 5-20A] and studies are ongoing explore this further by administering BDNF and TrkB via gene therapy delivery to retinal ganglion cells and the optic nerve following glaucomatous injury to assess the effect on retinal tau and GSK3B regulation.

Preliminary work appears to suggest that the improvement in optic nerve axonal transport following AAV2 TrkB-2A-mBDNF in tau transgenic mice appears to correlate with a reduction in pathological tau phosphorylation while total tau remains unchanged [Figure 5-21].

Structural correlation between retinal and cortical pathology to compare to the functional and behavioural changes described in Chapter 5 also remain of interest.

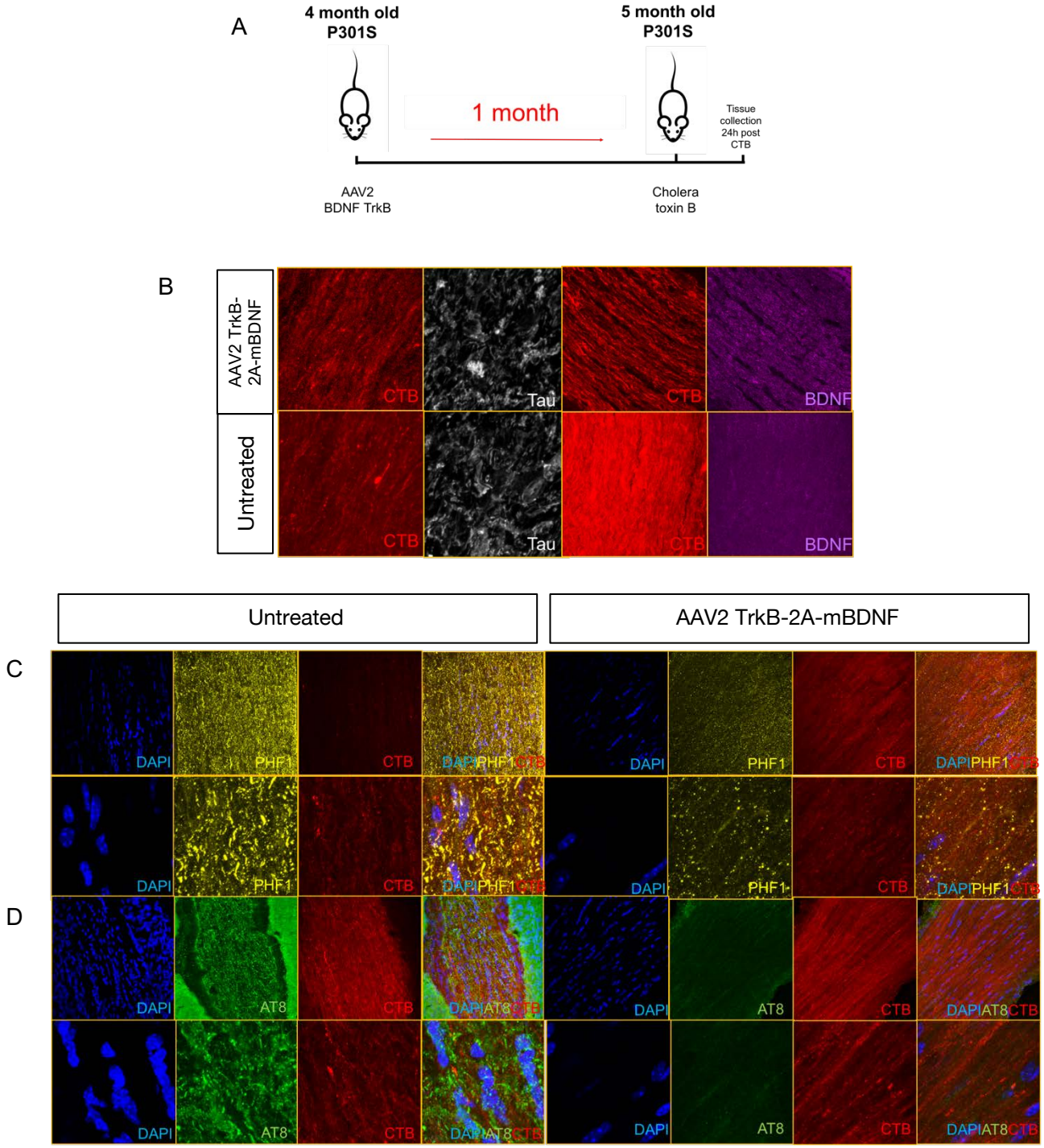


Figure 5-21: Retinal tau in the optic nerve of P301S mice homozygous for human mutant tau following administration of AAV2 TrkB-2A-BDNF A: Experimental timeline. B: BDNF expression in the optic nerve and total tau immunoreactivity C: PHF-1 immunoreactivity in the

optic nerve following AAV2 TrkB-2A-mBDNF D: AT8 immunoreactivity in the optic nerve following AAV2 TrkB-2A-mBDNF.

5.6 ACKNOWLEDGEMENTS FOR CHAPTER 5

Rights over use of the AAV2 and AAV5 TrkB-2A-mBDNF constructs are held by Astellas Pharmaceuticals Inc.

Hypothesis for the role of TrkB and BDNF in axonal transport

Tasneem Khatib and Keith Martin

Experimental design

Tasneem Khatib, Keith Martin, Andrew Osborne (specifically viral expression validation), Sujeong Yang (specifically memory loss in P301S mice), Peter Widdowson (specifically I-TASSER modelling of TrkB structure)

Ethical approval

Formal amendment to project licence completed by Tasneem Khatib and Keith Martin for the use of the P301S transgenic mouse line. Tasneem Khatib completed all the formal study plans required prior to undertaking the animal work

Animal work

Tasneem Khatib bred the animals (original P301S breeding pairs kind gift from Maria Spillantini) apart from the 10 P301S mice used in the dementia model experiments (Sujeong Yang). Tasneem Khatib performed all the animal procedures apart from the intravitreal injections for expression of the viral construct in naive wild type animals (Andrew Osborne) and the perirhinal cortex injections and behavioural analysis for the dementia model (Sujeong Yang). Andrew Osborne taught Tasneem Khatib the rat laser model of ocular hypertension and intravitreal injection technique. George Kong taught Tasneem Khatib the ERG technique.

Tissue collection

Tasneem Khatib collected all the tissue for processing apart from the eyes and retina for the for expression of the viral construct in naive wild type animals (Andrew Osborne). Andrew Osborne taught Tasneem Khatib how to collect the globes and retinal tissue. Craig Pearson

taught Tasneem Khatib how to collect the optic nerves. Barbara Haenzi taught Tasneem Khatib how to perfuse the animals and collect the brains. Robert Adalbert taught Tasneem Khatib how to isolate the superior colliculus.

Tissue processing

Rat glaucoma model

Tasneem Khatib performed all the eye and nerve tissue processing for the rat glaucoma model work. Andrew Osborne taught Tasneem Khatib microscopy, cryosectioning, immunohistochemistry and the western blot technique. The superior colliculus sectioning was outsourced professionally. Tasneem Khatib imaged and quantified the superior colliculus. Zara Ali imaged and quantified the axon transport in the nerves under Tasneem Khatib's guidance and protocol. The rat laser glaucoma model used in this experiment was previously developed by the Martin laboratory and collaborators.

Axon transport in naive animals

Robert Watt performed the cryosectioning of the nerves. Tasneem Khatib imaged and quantified the axon transport in the nerves.

Axon transport in the P301S model:

Tasneem Khatib and Wanyi Jia performed the cryosectioning, imaging and quantification of axon transport

AAV2 TrkB-2A-mBDNF construct expression.

Andrew Osborne performed the tissue processing for the viral construct expression and transduction of non RGC cell types

Data analysis

Tasneem Khatib performed all the data analysis apart from the AAV2 TrkB-2A-mBDNF construct expression (Andrew Osborne). Ilya Manyakin wrote the software for the semi-automated axon transport quantification.

Writing

Tasneem Khatib (prepared first draft), Keith Martin and Peter Widdowson.

CHAPTER 6

OPTIC NERVE REGENERATION IN EXPERIMENTAL GLAUCOMA

6.1 INTRODUCTION

A recent analysis of blindness and vision impairment trends over the past 30 years by the Vision Loss Expert Group for the Global Burden of Disease Study revealed that glaucoma remains the leading cause of irreversible blindness worldwide in an ageing population (Steinmetz et al., 2021). An estimated 1 in 8 patients will eventually become blind in at least one eye due to glaucoma progression, even with access to the best treatments currently available (Malihi et al., 2014; Peters et al., 2013). There is therefore a significant unmet clinical need to try to develop strategies to regenerate the optic nerve and regain function. Neuroregenerative strategies have specifically been included as a key target of the National Eye Institute Audacious Goals Initiative (Goldberg & Guido, 2016).

6.1.1 Mature retinal ganglion cells neurons lose ability to grow

One of the hallmarks of glaucomatous pathology is a characteristic degeneration of retinal ganglion cells (RGCs) and associated cupping of the optic nerve head. RGCs are able to extend axons during development via the progressive development of their growth cones along the visual pathway (Erskine & Herrera, 2014; Hevner, 2000; Jeffery, 2001; Kruger et al., 1998). However, over time they lose this ability to extend axons and grow (Goldberg et al., 2002). Recent work in aged mice indicates that the optic nerve does retain a record of youthful epigenetic information that can be accessed and manipulated to improve optic nerve function and promote regeneration (Lu et al., 2020).

6.1.2 Approaches to regenerate the optic nerve

Several approaches have demonstrated the potential for the mature optic nerve to regenerate following traumatic optic neuropathy, either by modulating the inhibitory extrinsic environment (Brown et al., 2012; Pearson et al., 2018) or stimulating the intrinsic ability of neurons to express axon-growth-promoting factors (Bray et al., 2019; Duan et al., 2015; Leibinger et al., 2016; Lim et al., 2016; Lorber et al., 2012; Lu et al., 2020; Mehta et al., 2016; Nieuwenhuis et al., 2020; K. K. Park et al., 2008; Sun et al., 2011). However the phenotype and mechanism of axonal degeneration in glaucoma is fundamentally distinct from other optic neuropathies including trauma (Beirowski et al., 2008; Crish et al., 2010; Fard et al., 2019; Fortune et al., 2016; Guo et al., 2005; K. R. G. Martin et al., 2006; Nuschke et al., 2015; Stowell et al., 2017; Vidal-Sanz et al., 2012; Vrabec & Levin, 2007). Little is known about the potential of using optic nerve regeneration strategies following glaucomatous injury.

6.1.3 Phosphatase and tensin homolog and the PI3 kinase pathway

Activation of cellular growth pathways through downstream signalling via the mTOR pathway is among the most robust and widely studied regeneration-promoting manipulations (de Lima et al., 2012; Lim et al., 2016; K. K. Park et al., 2008). Phosphatase and tensin homolog (PTEN) is a dual phosphatase with both protein and lipid phosphatase activities. It acts a negative regulator by dephosphorylating phosphatidylinositol-3, 4, 5-phosphate (PIP3) through its lipid phosphatase activity. In the absence of PTEN, PIP3 accumulates and inhibition of the mTOR pathway is relieved (C.-Y. Chen et al., 2018). PTEN is also crucial for development and null embryos die early during embryogenesis (Cristofano et al., 1998). Inducible tissue-specific PTEN deletion using the Cre-loxP system (Groszer et al., 2001) has therefore been widely adopted to explore its regenerative potential.

6.2 AIM

Here we assessed whether inducible PTEN deletion can promote retinal ganglion cell regeneration following glaucomatous injury.

6.3 RESULTS

We first validated our inducible PTEN deletion model [Figure 6-1] by testing AAV2-Cre-GFP activity using a Cre-reporter mouse which expresses tdTomato from the Rosa26 locus [Figure 6-1B-Biii]. We confirmed expression in PTEN$^{flx/flx}$ mice by the absence of PTEN in the GCL compared to wild-type mice and by examining GFP expression in the retina. Activation downstream of PI3K was confirmed by the colocalisation of phospho-S6 immunofluorescence with GFP expression [Figure 6-1G-Giii].

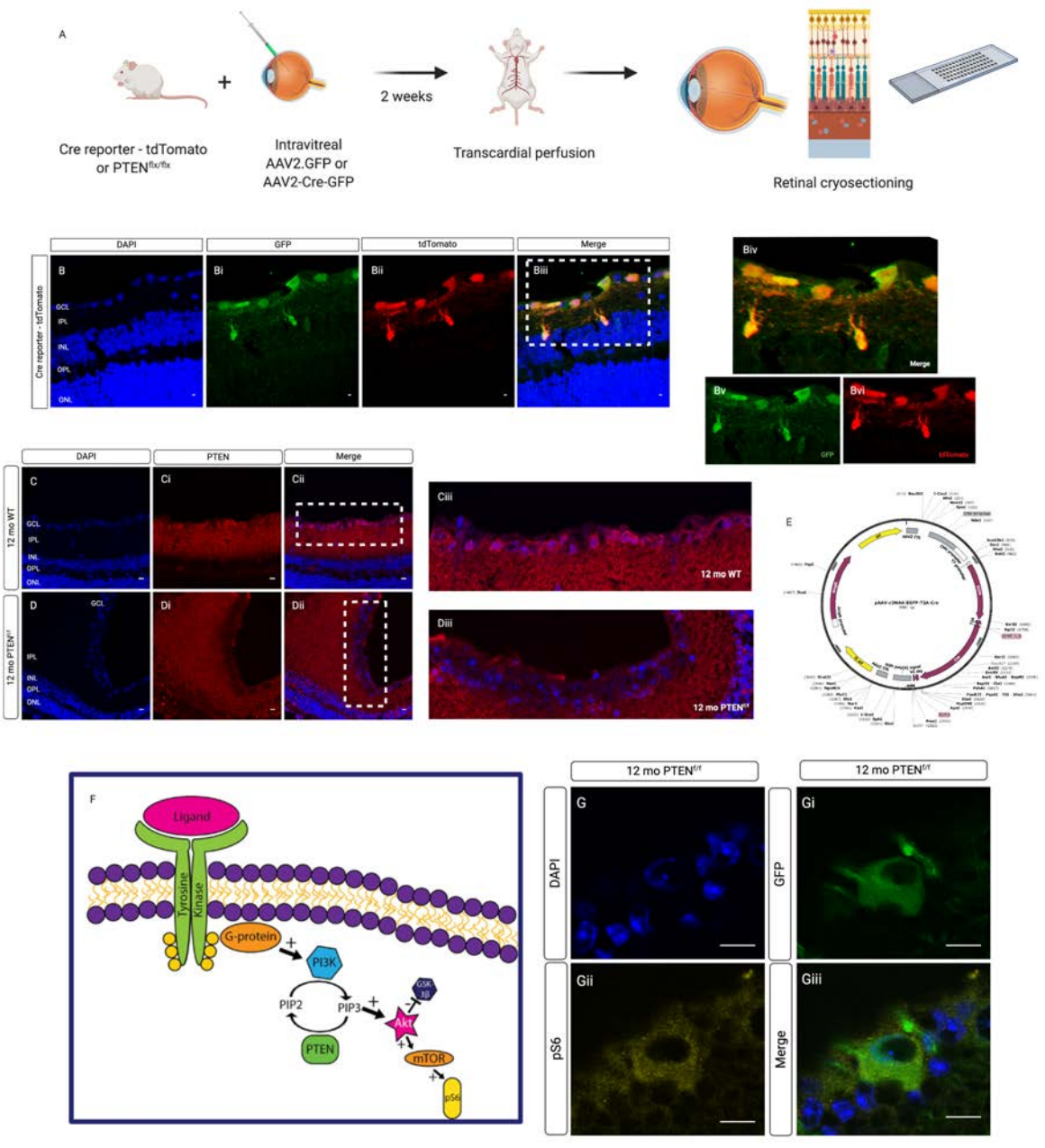


Figure 6-1: Validation of PTEN deletion A: Experimental timeline B-Bvi: Validation of AAV2-Cre-GFP virus in Cre-reporter strain C-Diii: Representative images of PTEN immunohistochemistry in [C-Ciii: wild type; D-Diii: $PTEN^{f/f}$] E: Plasmid map of AAV2-Cre-GFP F: Schematic illustrating the mTOR signalling pathway G-Giii: Validation of mTOR upregulation with colocalisation of pS6 in GFP positive cells in $PTEN^{f/f}$ mice. Scale bar 10 μm.

Figure 6-2 shows an age-related susceptibility to IOP elevation using the crosslinked hydrogel model of experimental glaucoma. There was a reduction in Brn3a and TUJ1 positive RGCs in the 12 month old mice but RGC numbers remained at control levels in the 3 month old mice.

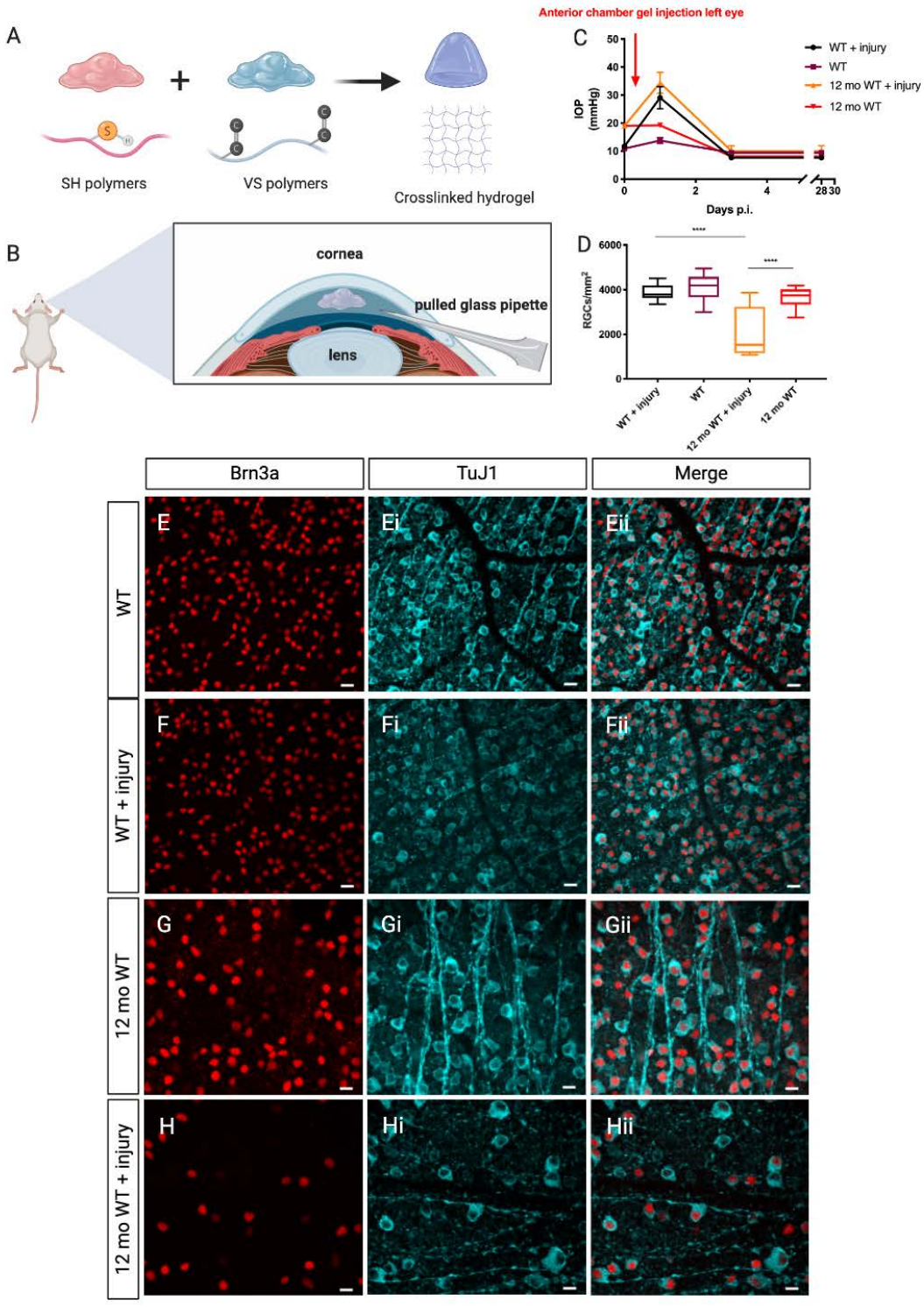


Figure 6-2: Validation of the intracameral gel model of IOP elevation A: Schematic illustrating crosslinking hydrogel (mixture of vinysulfonated hyaluronic acid and thiolated hyaluronic acid) B: Intracameral injection of crosslinking hydrogel C: IOP profile. D: Age related susceptibility to IOP elevation [wild type + injury 3889±119.1 RGC/mm^2; naive wild type 4109±177.1

RGC/mm^2; 12 mo wild type + injury 2086±321.4 RGC/mm^2; naive 12 mo wild type 3633±152.7 RGC/mm^2 (n=3] E-Hii: Representative images of RGC cell bodes and axons in E-Eii: naive wild type; F-Fii: wild type + injury; G-Gii: 12 mo wild type; H-Hii 12 mo wild type + injury]. Data displayed as mean ± S.E.M. Box and whiskers plots: median displayed and whiskers 10-90 percentile with outliers displayed as individual data points. **** p<0.0001. ANOVA with Bonferroni correction. Scale bar 10 μm.

There was a significant improvement in axonal transport in PTEN KO mice following IOP elevation compared to WT [Figure 6-3]. Axonal transport returned to baseline levels in the induced retinal PTEN KO mice. B tubulin positive cells in the GCL were not significantly reduced at 1 week post injury. Positive GAP43 immunohistochemistry was only observed in the optic nerve axons of PTEN KO mice following injury. GAP43 was not observed in axons in the absence of injury.

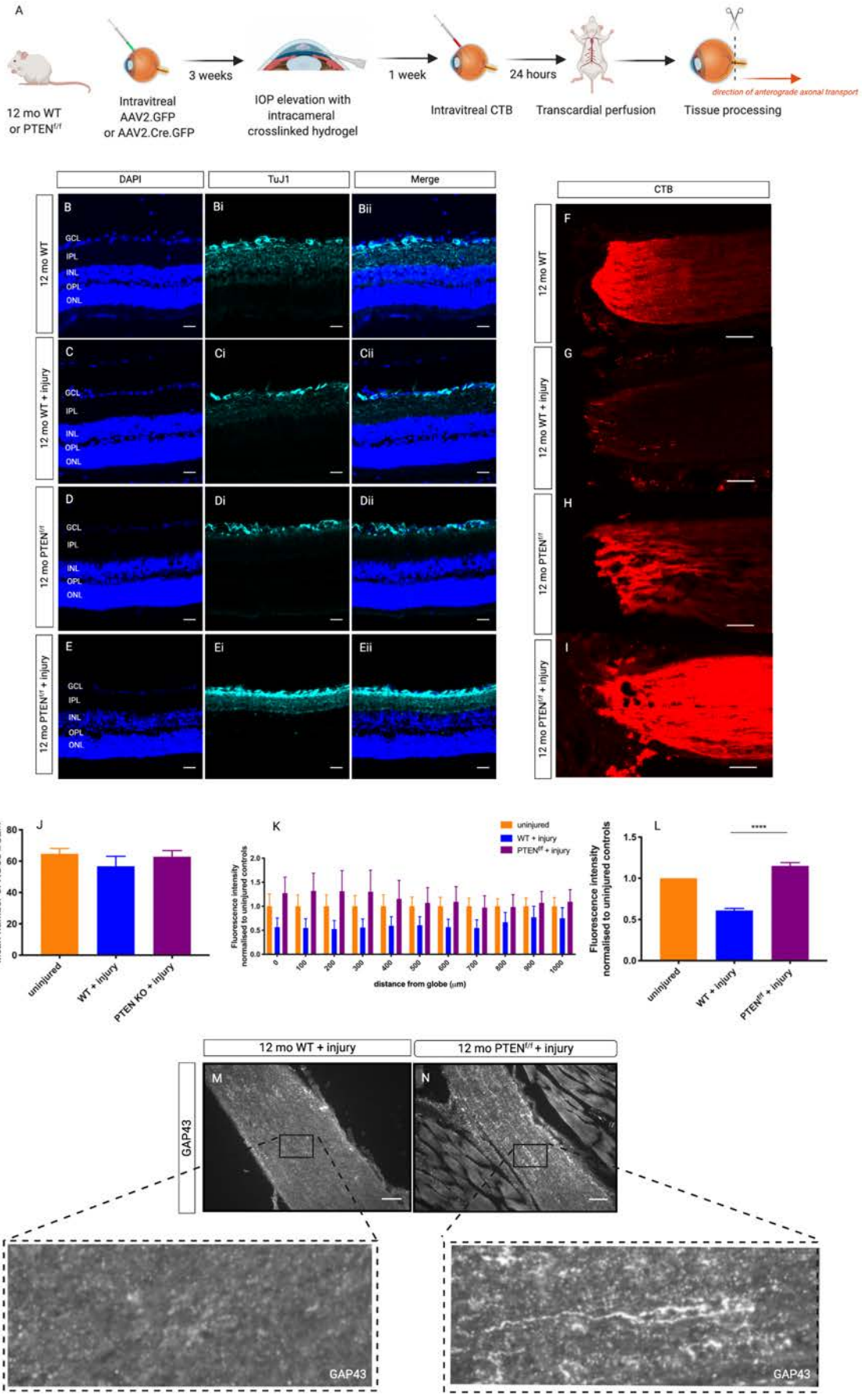

A
12 mo WT or PTEN$^{f/f}$
Intravitreal AAV2.GFP or AAV2.Cre.GFP
3 weeks
IOP elevation with intracameral crosslinked hydrogel
1 week
Intravitreal CTB
24 hours
Transcardial perfusion
Tissue processing
direction of anterograde axonal transport
DAPI
TuJ1
Merge
CTB
12 mo WT
12 mo WT + injury
12 mo PTEN$^{f/f}$
12 mo PTEN$^{f/f}$ + injury
GCL
IPL
INL
OPL
ONL
Mean number of RGCs ± SEM
uninjured
WT + injury
PTEN KO + injury
PTEN^{ff} + injury
Fluorescence intensity normalised to uninjured controls
distance from globe (μm)
****
GAP43

Figure 6-3: Effects of PTEN deletion on anterograde optic nerve axonal transport and optic nerve regeneration in experimental glaucoma. A: Experimental timeline B-Eii,J: Axonal transport deficits precede RGC cell loss. B-Eii: Representative images 1 week post injury [B-Bii: 12 month wild type; C-Cii: 12 month wild type + injury; D-Dii: 12 month $PTEN^{f/f}$; E-Eii 12 month $PTEN^{f/f}$ + injury] J: RGC number in uninjured 64.71±3.289 (n=19) vs 12 month wild type + injury 56.75±6.335 (n=6; p=0.70) vs 12 month $PTEN^{f/f}$ + injury 62.80±3.965 (n=10; p>0.99) RGCs. F-I,K-L: Optic nerve axonal transport 1 week post injury [F-I: Representative images of CTB anterograde transport K-L: CTB fluorescence intensity fold change from uninjured controls at K: 100μm intervals along the proximal nerve and L: Area under the curve fold change from uninjured controls [12 month wild type + injury 0.61±0.03 (n=6) vs 12 month $PTEN^{f/f}$ + injury + injury 1.15±0.04 (n=10) p<0.0001]. M: GAP43 immunohistochemistry in 12 month wild type + injury N: GAP43 immunohistochemistry in 12 month old $PTEN^{f/f}$ + injury. Data displayed as mean ± S.E.M. **** p<0.0001. Student t-test and ANOVA with Bonferroni correction. Scale bar B-Eii: 20 μm. Scale bar F-I; M-N: 50 μm

Next, we looked at the presence of GAP43 in the RGC cell body and synapses at the junction between the IPL and INL [Figure 6-4]. GAP43 was upregulated in the cell body and greater fluorescence was also seen at the IPL/INL junction following PTEN deletion. Furthermore, the GAP43 signal was stronger and more confluent at the IPL/INL border in the PTEN KO injury relative to PTEN KO alone, suggesting that GAP43 may either be locally upregulated in the dendrites or migrate to the synapses following injury. There seemed to be a small trend towards upregulation of GAP43 in the GCL following injury in the WT group, but this was not significant.

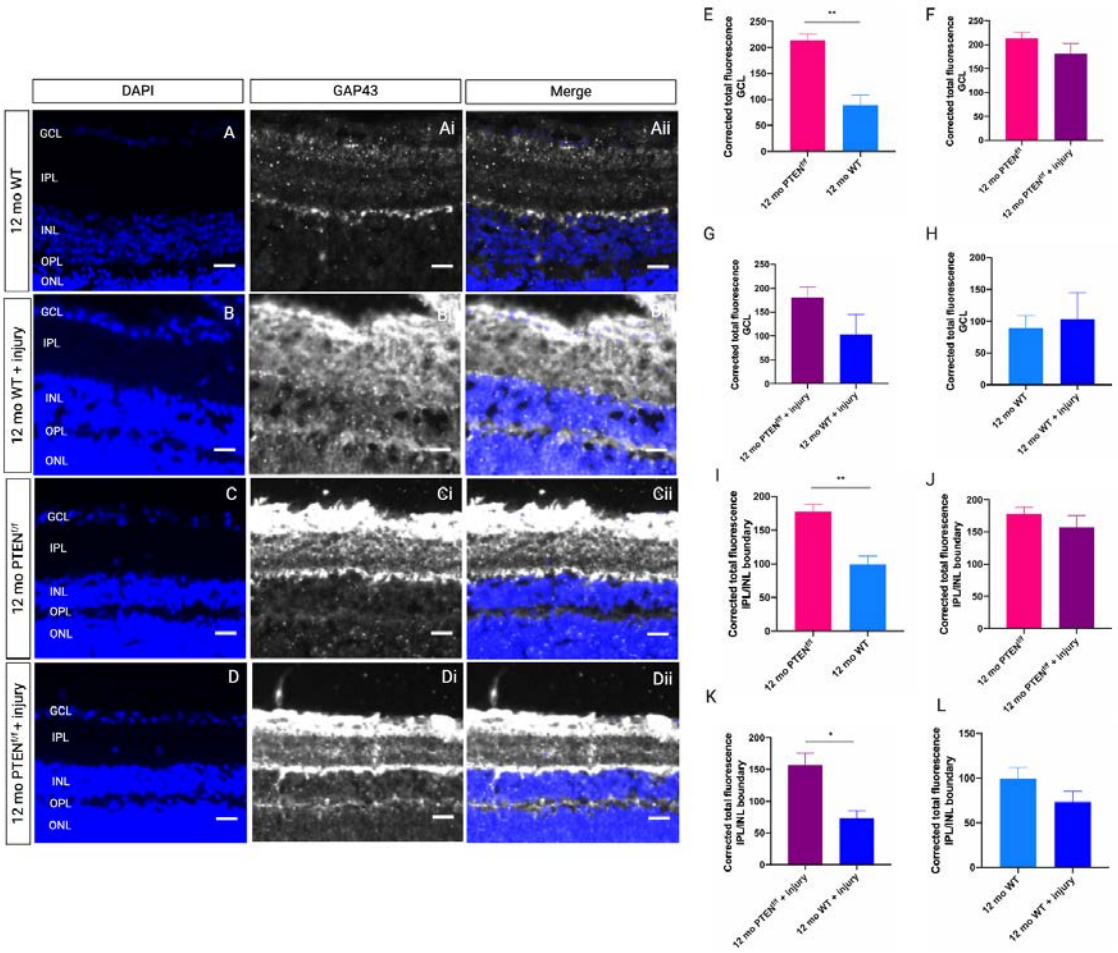


Figure 6-4: GAP43 levels in the RGC cell bodies and synapses A-Dii: Representative images 1 week post injury [A-Aii: 12 month wild type; B-Bii: 12 month wild type + injury; C-Cii: 12 month PTEN$^{f/f}$; D-Dii: 12 month PTEN$^{f/f}$ + injury] E-H: Corrected total fluorescence in the ganglion cell layer [E: 12 month PTEN$^{f/f}$ 213.6±11.82 (n=4) vs 12 month wild type 89.19±19.32 (n=4) p=0.0015 F: 12 month PTEN$^{f/f}$ 213.6±11.82 (n=4) vs 12 month PTEN$^{f/f}$ + injury 180.9±21.05 (n=5) p=0.25 G: 12 month PTEN$^{f/f}$ + injury 180.9±21.05 (n=5) vs 12 month wild type + injury 103.2±41.50 (n=3) p=0.11 H: 12 month wild type 89.19±19.32 (n=4) vs 12 month wild type + injury 103.2±41.50 (n=3) p=0.75]. I-L: Corrected total fluorescence in the inner plexiform layer/inner nuclear layer boundary. [I: 12 month PTEN$^{f/f}$ 177.6±11.2 (n=4) vs 12 month wild type 99.4±12.2 (n=4) p=0.003 J: 12 month PTEN$^{f/f}$ 177.6±11.2 (n=4) vs 12 month PTEN$^{f/f}$ + injury 156.9±18.4 (n=5) p=0.40 K: 12 month PTEN$^{f/f}$ + injury 156.9±18.4 (n=5) vs 12 month wild type + injury 73.5±11.8 (n=3) p=0.02 L: 12 month wild type 99.4±12.2 (n=4) vs 12

month wild type + injury 73.5±11.8 (n=3) p=0.20]. Data displayed as mean ± S.E.M. *p<0.05 ** p<0.01. Student t-test. Scale bar 20 μm.

We explored whether the regeneration effects observed could be explained by downstream mTOR activity as assessed by the level of pS6 in the RGC cell body [Figure 6-5]. Interestingly, while there was a significant increase in pS6 in the PTEN KO group, there was no difference in the absolute levels of pS6 following injury in either the PTEN KO group or the WT group. Axon regeneration only occurred in PTEN KO occurred after pS6 had been elevated prior to IOP elevation. There was a trend towards pS6 upregulation following injury in WT animals with no regeneration observed in the axon and possible GAP43 upregulation seen in the dendrites.

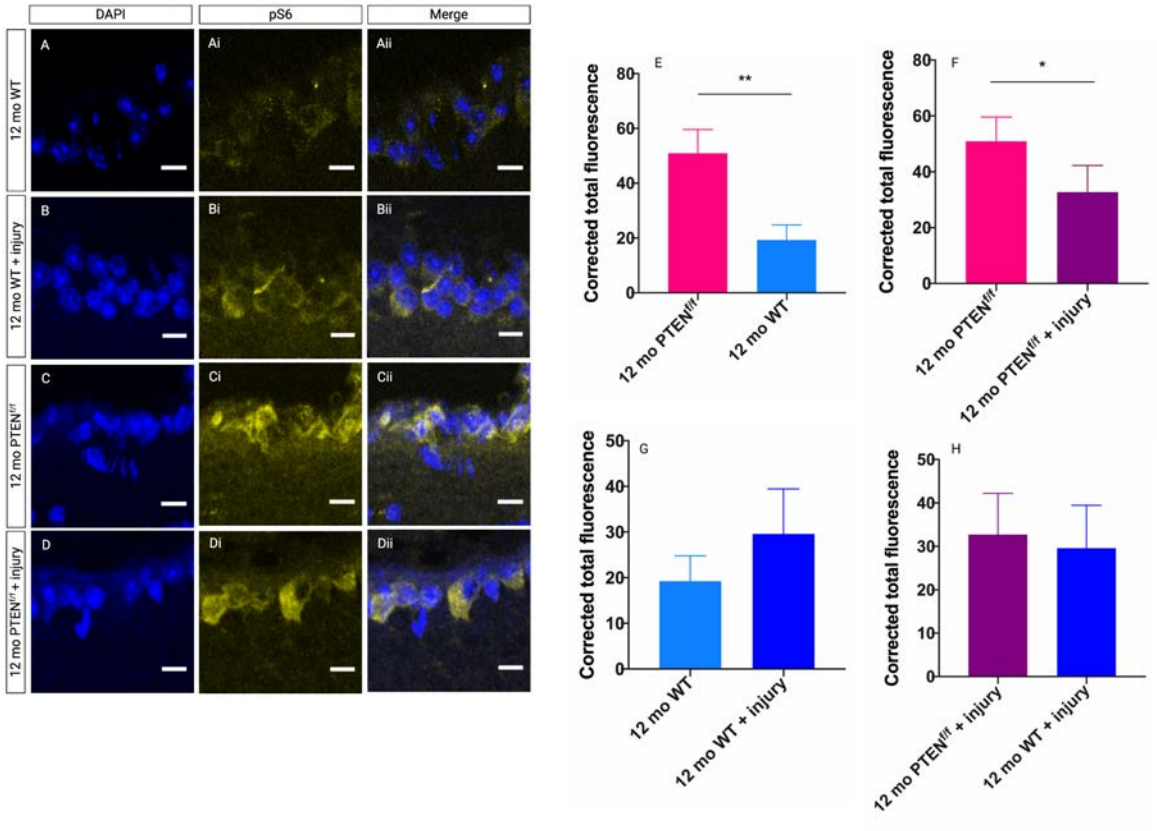


Figure 6-5: Phospho-S6 (pS6) ribosomal protein levels in the RGC layer A-Dii: Representative images 1 week post injury [A-Aii: 12 month wild type; B-Bii: 12 month wild type + injury; C-Cii: 12 month PTEN$^{f/f}$; D-Dii: 12 month PTEN$^{f/f}$ + injury] E-H: Corrected total fluorescence in the ganglion cell layer [E: 12 month PTEN$^{f/f}$ 50.9±8.6 (n=4) vs 12 month wild type 19.2±5.5 (n=4) p=0.007 F: 12 month PTEN$^{f/f}$ 50.9±8.6 (n=4) vs 12 month PTEN$^{f/f}$ + injury 32.7±9.5 (n=5) p= 0.01 G: 12 month PTEN$^{f/f}$ + injury 32.7±9.5 (n=5) vs 12 month wild type + injury 29.6±9.9 (n=3) p=0.82 H: 12 month wild type 19.2±5.5 (n=4) vs 12 month wild type + injury 29.6±9.9 (n=3) p=0.29]. Data displayed as mean ± S.E.M. *p<0.05 ** p<0.01. Student t-test. Scale bar 10 μm.

6.4 DISCUSSION

We have demonstrated that inducible PTEN deletion promotes regeneration of axons and dendrites in experimental glaucoma. There is a suggestion that this may be mediated in part through the mTOR pathway, but that for regeneration to occur the cells need to be primed with elevated mTOR activation prior to injury. It also remains possible that the effects of PTEN deletion mediated regeneration are through pathways independent of mTOR activation. We have previously demonstrated that other components of the PI3K pathway, specifically p110α and δ promote axon regeneration (Nieuwenhuis et al., 2020) which supports the involvement of the lipid phosphatase role of PTEN in regulating axon regeneration.

However, in unpublished work, we have also demonstrated that an alternate PTEN activity is involved in the process of axon regeneration. Simultaneously inhibiting endogenous PTEN expression and replacing with mutated forms of PTEN to either eliminate the lipid or both the protein and lipid phosphatase activity also stimulated axon regeneration following optic nerve crush. When PTEN gene expression is inhibited and replaced with PTEN that lacks the lipid phosphatase activity, axon regeneration was seen to be reduced by half, suggesting that 50%

of axon regeneration via PTEN gene silencing is mediated by lipid phosphatase activity. When both the lipid and protein phosphatase activity is eliminated, approximately 50% of regenerating axons were maintained. Further exploration of the alternative PTEN-related mechanisms contributing to regeneration remain of considerable interest with a view to pinpointing more specific targets to stimulate regeneration and refine strategies to reduce the risk of oncogenesis. However, PTEN deletion alone was not sufficient to promote full length regeneration and it is likely that a multifaceted approach targeting multiple mechanisms will be required (de Lima et al., 2012; Lim et al., 2016; K. K. Park et al., 2008)

Furthermore, anatomical regeneration is not implicitly associated with spontaneous recovery of function (Lim et al., 2016). When regeneration of RGC axons was observed in the dLGN or OPN nucleus, the mice did not recover function in the visual cliff tasks or the pupillary light reflex response respectively, although behaviour in some other vision-related tasks was improved. The authors hypothesised that functional recovery of the retino-geniculo-cortical pathway to restore spatial vision may be a greater challenge than restoration of sub-cortical visual function. Lack of axon myelination in regenerating fibres may also be an issue for recovery of some aspects of visual performance. Comparison of the genetic composition between regenerated and wild type neurons, supporting cells and connections is ongoing and will refine our understanding of the mechanisms required to reconnect circuits in disease and restore functionally useful vision once it has been lost.

6.5 ACKNOWLEDGEMENTS FOR CHAPTER 6

Experimental design

Tasneem Khatib and Keith Martin

Animal work

Tasneem Khatib performed all the animal procedures apart from validation of the AAV2-Cre-GFP virus (Rachel Evans). The hyaluronic acid gel polymers were a kind gift from Christopher Leung and their preparation was performed according to the protocol developed by Yu Yu.

Tissue collection

Tasneem Khatib collected all the tissue for processing apart from validation of the AAV2-Cre-GFP virus (Rachel Evans).

Tissue processing

Validation of PTEN deletion

Tasneem Khatib performed the immunohistochemistry and imaging to validate the PTEN deletion. Rachel Evans performed the immunohistochemistry and imaging to validate the AAV2-Cre-GFP virus.

Validation of the gel glaucoma model

Tasneem Khatib performed all the retinal tissue processing – tissue preparation, immunohistochemistry and imaging.

Axonal transport and regeneration

Tasneem Khatib performed the immunohistochemistry of the retinal ganglion cell bodies. Jared Ching imaged and quantified the RGCs. Tasneem Khatib and Rachel Evans cryosectioned the optic nerves. Zara Ali and Rachel Evans imaged and quantified the axonal transport according to a protocol developed by Tasneem Khatib. This protocol was based on previous work in the Martin laboratory performed by Natalie Bull. Michael Whitehead performed the phospho-S6 ribosomal protein immunohistochemistry and imaging. Michael Whitehead performed the GAP43 immunohistochemistry according to a protocol provided by Larry Benowitz. Tasneem Khatib performed the imaging of the retina and optic nerve axons.

Data analysis

Tasneem Khatib

Writing

Tasneem Khatib (prepared first draft), Keith Martin

CHAPTER 7

DISCUSSION

We have demonstrated the clinical need for ongoing development of new diagnostic and therapeutic tools for POAG, to facilitate targeted therapy and repair the neurodegenerative process and the potential for the optic nerve regeneration following glaucomatous injury.

7.1 NON-INVASIVE IMAGING

Non-invasive imaging permits longitudinal real time monitoring in a physiological and pathological state. HVI for the evaluation of aqueous outflow as we have described has the potential to aid glaucoma diagnosis and reduce the number of people presenting with advanced disease, facilitate targeted therapy and improve outcomes including patient quality of life, resource allocation and efficacy.

It also has the potential to facilitate future glaucoma drug and surgical device development by permitting direct functional comparison between promising candidates to take forward for future development. We have already been approached by several pharmaceutical companies who are keen to acquire the HVI system to that effect.

We also anticipate the ability to functionally assess and measure aqueous outflow in the physiological and pathological state without manipulation will further our understanding of aqueous outflow dysregulation in the pathogenesis of glaucoma and this may facilitate the generation of future novel therapies.

7.2 PRECLINICAL TO CLINICAL TRANSLATION

There are limitations associated with preclinical to clinical translation of new therapeutic interventions. Firstly, accurately modelling a variable and complex multifactorial disease process such as POAG, where the underlying pathology is not fully understood, is difficult. Available animal models replicate some aspects of the disease, but all have significant limitations. As an example, many glaucoma models involve induced elevation of IOP; such models may be helpful when assessing the site of injury, mechanisms of damage and gene expression changes, but do not model the increased susceptibility to glaucomatous damage that may be a contributing factor in many glaucoma patients. Factoring in this increased susceptibility is particularly relevant when distinguishing glaucomatous pathology from that seen in ocular hypertensive patients, where the IOP is elevated but who do not have detectable structural or functional deficit, or normotensive patients who display a characteristic glaucomatous phenotype.

The degree of induced IOP elevation has recently been shown to elicit differential and often opposing changes in the transcriptome profile of retinal ganglion cells, according to whether IOP elevation is mild (elevation between 1-4 mmHg) or moderate (elevation $\geq$ 4mmHg) (Y. H. Park et al., 2019). For example, activation of neuronal death pathways was seen following sustained 'mild' IOP elevation over a period of two weeks, whereas there was an increased activation of cell survival and neurite outgrowth pathways following 'moderate' IOP elevation. The authors postulated that this might indicate a selective impact on retinal ganglion cell somas or axons and dendrites according to the degree of IOP elevation, suggesting an additional level of complexity when selecting models of experimental glaucoma and selecting outcome measures to assess efficacy.

Chronic models of acquired or spontaneously developing glaucoma, such as the beagle or basset hound canine glaucoma model have a protracted time course, are expensive and at present telemetry is not advanced enough to monitor the level and time course of IOP elevation to quantify the level of exposure to injury. Advanced glaucoma in these models can

subsequently develop into a secondary angle closure with lens dislocation which also limits their usefulness in evaluating therapies for POAG.

Acute IOP elevation models (Crowston et al., 2014) are more reliable and reproducible, with the potential for repetitive injury and strain to modulate the degree of induced damage. The increased predictability also confers a reduction in the number of animals required to detect evidence of efficacy but has limitations in the degree of relevant information provided when modelling a chronic, progressive condition such as POAG. Acute studies also fail to take into account the fluctuations in IOP frequency and magnitude that are typical of the glaucomatous disease process.

7.3 OPTIMISING CLINICAL ENDPOINTS

There is also a need to optimise clinical trial endpoints. The failure to demonstrate efficacy in the oral memantine POAG neuroprotection trial highlighted the need to develop more relevant and appropriate clinical endpoints. Slow progression of POAG in patients recruited to clinical trials of neuroprotection has suggested that lengthy trials would be required with the individual variability that occurs when performing functional tests necessitating large group sizes to determine whether there is evidence of any therapeutic effect.

It is therefore of considerable interest that the UK Glaucoma Treatment Study (UKGTS) (Garway-Heath et al., 2015) which evaluated vision preservation in patients taking the prostaglandin analogue Latanoprost for POAG in a randomised, multicentre, placebo-controlled trial demonstrated statistically significant differences between treatment groups within one year with approximately 250 patients per group. It is conceivable that recruitment of patients progressing at a pre-defined rate prior to trial entry as well as enhancement of functional endpoints by clustering of measurements at the beginning and the end of studies could help to shorten neuroprotection trials and reduce the group sizes required still further.

De Moraes *et al.* proposed that decreasing the rate of visual field progression by 30% in a clinical trial of 12 to 18 month duration would yield clinically meaningful results and showed that a 30% decrease in rate of visual field progression had a significant effect on health-related quality of life (De Moraes, Liebmann, et al., 2017). It has also been suggested that the 10-2 visual field may be a more appropriate outcome measure as the 24-2 field can underestimate the degree of damage at the macular region involved in glaucomatous optic neuropathy(De Moraes, Hood, et al., 2017). The 10-2 visual field has also been shown to correlate with quality of life outcome measures (Blumberg et al., 2017) and may reduce the time required to detect glaucomatous progression (Wu, Medeiros, et al., 2019).

Wu *et al.* also indicate that lengthy and large trials are not essential, suggesting that the sample size required to assess the effect of any neuroprotective intervention depends on the baseline rate of progression, study duration, and quantification and outcome parameter(Wu, Crabb, et al., 2019). They suggest that the sample size could be lowered by assessing progression using the average mean deviation (MD) change rather than event-based guided progression analysis (GPA) analysis. Quigley suggested that selecting rapid progressors would limit the generalisability of any study, increase the time taken for recruitment and that selecting patients with low variability in previous tests would be most efficient, and stressed a greater role for futility trial designs to determine promising candidates to take to larger clinical trials(Harry A. Quigley, 2019).

UKGTS was also one of the first major clinical trials to use optical coherence tomography and structural parameters as a secondary outcome. Garway-Heath *et al.* showed that combining structural and functional outcome measures yielded higher sensitivity but did not improve overall discrimination. However, the study used time-domain OCT and the higher resolution provided by spectral-domain or swept-source OCT may help to refine endpoints further in a clinically meaningful way. The use of probability maps rather than summary measures when

analysing outcomes has also been suggested to improve sensitivity and earlier detection(Hood & Raza, 2011, 2014).

DARC Technology (Detection of Apoptosing Retinal Cells) is a technique currently being assessed in Phase II clinical trials which enables the direct visualisation of apoptosing retinal cells in real time following intravenous administration of ANX776 (annexin-5 labelled with a fluorescent dye DY-776). The proof-of-concept open-label Phase I study (ISRCTN10751859) demonstrated an increase in the 'DARC count' or total number of ANX776 spots in glaucoma patients relative to healthy controls, and the DARC count also corresponded with rates of structural or functional progression(Cordeiro et al., 2017).

The DARC count does not identify retinal ganglion cells specifically and the correlation of apoptosis detection through annexin V labelling with the 'health status' of a human retinal ganglion cell undergoing glaucomatous injury remains to be determined. However, DARC Technology does offer the potential to monitor retinal disease activity *in vivo* and longitudinally at the level of an individual cell and may prove to be a useful adjunct to clinical endpoints when assessing treatment efficacy.

7.4 COMPARTMENTALISED DEGENERATION

An understanding of the compartmentalised degenerative process will not only help to identify new targeted approaches for neuroprotection but also help to refine outcome measures and timings for therapeutic interventions in clinical trials. Ou *et al*. correlated structural and functional parameters of subsets of retinal ganglion cells following laser induced ocular hypertension using biolistic labelling and multielectrode array recordings of individual retinal ganglion cells(Ou et al., 2016). They found that α OFF-transient retinal ganglion cells were more susceptible to glaucomatous injury both structurally, with higher rates of cell death and reduction in dendrite area and synapse density, and functionally, with decreases in

spontaneous activity and receptive field size. Interestingly, while the function of the OFF-sustained and ON-sustained retinal ganglion cells were preserved, there was a decrease in excitatory post-synaptic sites of these cells, indicating that synapse loss occurs prior to any observable functional loss. They also reported an increased vulnerability of the presynaptic ribbon in the OFF sublamina of the inner plexiform layer, which suggests that retinal ganglion cells with dendrites stratifying in the OFF sublamina may be damaged earlier in the degenerative process. Whether the presynaptic changes occur prior to postsynaptic changes and are a secondary or primary event remains to be determined, including whether synapses that receive different bipolar cell type inputs are lost uniformly. Early dendrite pruning with synapse loss occurring prior to axon or soma loss has also been reported elsewhere using the microbead model of induced ocular hypertension (El-Danaf & Huberman, 2015) and the genetic DBA/2J model of chronic glaucoma (Williams et al., 2013), with dendritic atrophy also occurring prior to functional loss through visual field testing in primates (Weber & Harman, 2005). The authors did note preservation of the dendritic arbour in DBA/2J mice in eyes that had more significant ganglion cell loss and postulated that selective vulnerability of retinal ganglion cell types, along with possible functional recovery, may account for this finding.

Several factors are implicated in the loss of dendrites, synaptic pruning, remodelling and neuronal maintenance following glaucomatous injury including the transport, number and distribution of mitochondria, retrograde blockade of neurotrophic support to the cell body and synapses, complement cascade dysregulation, microglial activation and changes in neuronal activity. Whether the latter influences early structural remodelling or is a consequence remains under active debate. Impaired inner retinal function has been shown to precede defects in anterograde active axonal transport of cholera toxin B following intraocular pressure elevation (Fahy et al., 2016), with a redistribution in the size and location of the axon initial segment postulated to alter action potential propagation following glaucomatous injury. Visual stimulation and electrical activity has also been shown to influence axonal regeneration (Lim et al., 2016). Little is yet known about the relationship between retrograde transport blockade

or the transport of endogenous proteins and functional impairment.

The degree of IOP elevation appears to influence whether the retinal ganglion cell body or axon undergoes preferential degeneration (Y. H. Park et al., 2019). The mechanisms of degeneration are distinct and compartmentalised as are the functional requirements of retinal ganglion cells according to their distribution within the retina and between the myelinated, non-myelinated and laminar regions of the optic nerve. The Wlds allele, which slows Wallerian degeneration, has been shown to protect axons (Howell et al., 2007) but not retinal ganglion cell somata following experimental glaucoma (Beirowski et al., 2008).

7.5 FUNCTIONAL RECOVERY

Functional recovery has previously been demonstrated in glaucoma patients following intervention, suggesting the possibility of reversal of glaucomatous dysfunction of retinal ganglion cells and their connections. Caprioli *et al.* demonstrated evidence of persistent improvement in visual function in the longer-term (Caprioli et al., 2016). They assessed visual field progression before and up to 5 years following trabeculectomy in 74 eyes of 64 patients. Fifty-seven percent of eyes improved in 10 or more test locations compared with pre-operative values and the number of improved visual field loci correlated with the IOP lowering. Casson *et al.* demonstrated a glucose-mediated neuroenhancement of retinal function, where topical glucose was applied to pseudophakic glaucoma patients and significantly improved contrast sensitivity (Casson et al., 2014). Preclinical studies would indicate that ageing retinal ganglion cells recover more slowly (Y. X. G. Kong et al., 2012), and that exercise-mediated BDNF expression can enhance functional recovery of retinal ganglion cells following IOP elevation (Chrysostomou et al., 2014).

7.6 A NEW ERA OF TRANSLATIONAL MEDICINE: LESSONS LEARNED FROM OTHER GENE THERAPY TRIALS

Below we summarise how lessons learned from trials for other diseases may be used to further guide the development of neuroprotective gene therapies for glaucoma.

FDA approval for the first directly administered gene therapy product for any condition due to mutations in a specific gene was granted to Spark Therapeutics for Luxturna, (AAV2-hRPE65v2) a viral vector administered subretinally to augment function of the retinal pigment epithelial cells in Leber's Congenital Amaurosis (LCA). LCA is an inherited retinal condition caused by a loss of function mutation in the RPE65 gene. This leads to excessive build-up of all-trans retinal, disruption of the photochemical conversion of light into electrical impulses and severe visual impairment from childhood which was previously deemed untreatable. Russell *et al.* demonstrated significant functional improvement in children with LCA up to 1 year following Luxturna administration in Phase III clinical trials (NCT00999609) (Russell et al., 2017) and this effect has been reported to be maintained at 3 years. The primary efficacy endpoint was change in bilateral multiluminance mobility test (MLMT). The MLMT assesses the ability to navigate an obstacle course at varying light levels and was specifically designed for the trial to be a functional measure that would best capture the impact of treatment. A change of one light level in passing was considered clinically meaningful although it is not fully clear as yet how the MLMT score translates to real world outcomes. At one year, treated eyes were associated with a difference of 1.8 in the MLMT change score in treated eyes versus 0.2 in control eyes.

This trial was a landmark achievement which demonstrated the safety and efficacy of directly administered gene therapy for genetic conditions, particularly as early trials for patients with X-linked severe combined immunodeficiency induced leukaemia were associated with mortality in treated children. This subsequently halted the further development of gene therapy approaches for several years while risks were re-assessed and strategies were refined. Clinical trials using gene therapy to treat other debilitating genetic conditions such as spinal muscular atrophy (Mendell et al., 2017a), which has also recently been granted FDA approval,

and junctional epidermolysis bullosa (Hirsch et al., 2018) are also showing considerable promise with good safety profiles and functional improvement. Although evaluation is ongoing and the longer term impact remains uncertain, with other trials for LCA (NCT00643747) reporting a decline in the degree of visual improvement (Bainbridge et al., 2015) and the subsequent development of an optimised AAV5 viral vector and transgene expression cassette to improve retinal transduction and yield higher levels of RPE65 (Georgiadis et al., 2016), these advances all lend strong support to the use of directly administered gene therapies forming a core part of a clinician's toolkit when treating intractable illnesses in the foreseeable future.

There has been an economic burden associated with these significant scientific advances. The cost price for Luxturna is $850 000 for a single treatment (or $425 000 per eye). Following review by the Institute for Clinical and Economic Review and giving special weighting to the very rare nature of the disease, the price was considered to approach cost-effectiveness compared to current standard of care in a 'best-case' scenario, where a child aged 3 would receive a one off treatment that would last the duration of a lifetime. Spark Therapeutics have included refunds in the event of treatment failure and payment over several years as part of their overall strategy.

Concerns about current cost are understandable, but we would argue should not preclude continued development of gene therapies. An international gene therapy trial involving over 100 patients across 9 countries in the EU and North America is now underway for choroideremia, an X-linked retinal degeneration resulting in progressive blindness due to mutations in Rab-escort protein 1 (REP1). The results of the initial pilot study (NCT01461213) were reported in *Nature Medicine* where a significant improvement in visual acuity at 2 years following subretinal injection of AAV2.REP1 was seen in 14 choroideremia patients compared with controls (median 4.5 letter gain, versus 1.5 letter loss, p=0.04). 6 of the treated eyes gained more than one line of vision at 2 years (Xue et al., 2018). The timescale for

development of gene therapies continues to fall and the economics of providing gene therapies for common conditions such as POAG are likely to drive production costs down further over time.

Significant advances are also being made for optic neuropathies and clinical trials are currently being conducted to evaluate the efficacy of GS010, an AAV2 construct containing the human wild-type NADH dehydrogenase subunit 4 (ND4) gene to treat patients with Leber's Hereditary Optic Neuropathy due to the G11778A ND4 mitochondrial mutation (Vignal et al., 2018; Wan et al., 2016). Preliminary data from the Phase I/II trial showed promising results (NCT02064569) and provided the foundation for two Phase III clinical trials which are currently underway (NCT02652780, NCT02652767). Clinically meaningful functional improvement has recently been reported with 72 week data from the REVERSE Phase III clinical trial (NCT02652780) which demonstrates that 45.9% of treated eyes achieved a significant improvement of 0.3 LogCS or more compared to 24.9% improvement seen in sham treated eyes (p-0.0047) (Moster et al., 2019). Treated eyes were estimated to be more likely to achieve a visual acuity of 20/200 or more (p=0.0012) and this was also associated with relative preservation of structural parameters including the ganglion cell layer volume, papillomacular bundle thickness and total macular thickness. Transport of the administered vector to the fellow eye, reorganisation of the visual cortex or a placebo effect may go some way to towards understanding the basis of the improvement in visual acuity seen in the sham injected eyes (Yu-Wai-Man et al., 2020). A separate arm of the study, the REFLECT study (NCT03293524), evaluating the efficacy and safety of bilateral intravitreal injection of GS010 in LHON patients with the ND4 mutation, is currently recruiting and will also help to assess the sham-treated improvement and help guide future clinical trial design for gene therapies for POAG.

The most frequent treatment-emergent adverse effect (TEAE) seen in the initial Phase I/II clinical trial was intraocular inflammation, with 13 events reported in 11 out of 15 subjects. These were usually mild and treated topically but two patients required oral steroid

administration to treat the inflammation. The greatest percentage of those affected was seen at the highest vector doses: 33% (1 of 3 patients) at $9x10^9$ vector genomes/eye, 67% (2 of 3 patients) at 3×10^{10} vector genomes/eye, 83% (5 of 6 patients) at 9×10^{10} vector genomes/eye and 100% (3 of 3 patients) at 1.8×10^{11} vector genomes/eye. By week 96, no related TEAE required ongoing treatment and no structural or visual loss was reported as a result of vector administration or TEAE. A secondary analysis of the Phase I/II trial data calculated a composite ocular inflammation (OIS) score using the Standardization of Uveitis Nomenclature and correlated this with the viral titre and systemic immune response (Bouquet et al., 2019). The maximum OIS was seen in a patient with a previous history of idiopathic uveitis. The authors did not find an association between the OIS, humoral immune response, immune status of the patient or viral titre administered and overall concluded there were no intraocular inflammatory safety concerns that would preclude further clinical trials. However, in view of the transient intraocular inflammation that was reported after vector administration, it would appear that AAV vectors have a degree of immunogenicity. The authors recommended the systematic use of prophylactic steroids in future trials to decrease the inflammatory responses and also pointed to the need for ongoing animal studies to help elucidate the local immune response to gene therapy. The AAV8.RS1 Phase I/II three-dose-escalation trial (NCT02317887) for X-linked retinoschisis administers a healthy copy of retinoschisin to target photoreceptors and showed a dose-related intraocular inflammation that resolved with topical and oral steroids (Cukras et al., 2018). Systemic antibodies against AAV8 also increased in a dose-related fashion, but no antibodies against RS1 were observed.

It has been suggested that innate immune responses induced by the toll-like receptor (TLR) pathway can affect the adaptive immune responses to AAV gene transfer with TLR2, TLR9, and MyD88 being implicated in particular (Hösel et al., 2012; Martino et al., 2011; Rogers et al., 2015; Rogers & Herzog, 2014; Zhu et al., 2009). A number of refinements are ongoing to limit activation of the immune response while achieving efficient transgene transfer following AAV administration. These include single cell transcriptome based development of AAV

vectors and capsid modifications to alter the tropism and pattern of activity of viral efficacy (Bartel et al., 2011). This has been postulated to confer an increased ability to bypass structural barriers including the vitreous body while limiting the effect of neutralising antibodies.

Exosomal AAVs, where viral particles are carried inside small membrane vesicles, are another promising approach and have been shown to yield a higher retinal transduction efficiency and are more resistant to neutralising anti-AAV antibodies (Carvalho et al., 2015; György et al., 2016; Wassmer et al., 2017). This technology confers additional advantages over traditional AAV2 based approaches as the development of neutralising antibodies may preclude repeat injections in the event of treatment failure, reduced efficacy or the development of a separate disease process that may also be treated by gene therapy approaches. Scope therefore also exists to target multiple processes involved in glaucoma pathogenesis rather than taking a single 'one-size-fits-all' approach. It is unlikely that the immune response to viral vectors will be completely eliminated despite refinement. The degree of efficacy provided versus risk of inflammation should form part of the decision making prior to administering therapy.

It is also of interest that the rAAV2/2-ND4 trial enrolled patients from the age of 15 years onwards with diagnosed *ND4* LHON. The pharmacokinetics of the vitreous in younger patients may well be different from the often elderly population affected by POAG, and it remains to be seen whether the presence of vitreous syneresis or posterior vitreous detachment will lessen the structural barrier to viral transduction hence improving transgene expression. It is encouraging that efficacy has been demonstrated following intravitreal injection in the younger LHON cohort who typically have a thicker internal limiting membrane and denser vitreous composition. The AAV8-RS1 gene therapy trial for X-linked retinoschisis also uses an intravitreal approach to administer a healthy copy of retinoschisin to target photoreceptors. Cukras *et al.* postulated that the retinal degeneration associated with the X-linked retinoschisis also compromises the structural integrity of the internal limiting membrane, facilitating retinal

penetration following intravitreal administration of the viral vector(Cukras et al., 2018). Little is known about the structural integrity of the internal limiting membrane in glaucoma patients and how much of a barrier this will pose to viral transduction for future gene therapy trials.

7.7 TOWARDS PRECISION MEDICINE

Several neuroprotective approaches show significant promise but intrinsic regulatory mechanisms may determine their effectiveness in different individuals. In a similar vein, alternative compensatory pathways may limit the degree of efficacy which a neuroprotective approach can offer, reaching a plateau, without the modification of underlying pathophysiology. Scope therefore exists to continue to pinpoint specific mechanisms that are disrupted in POAG and the relative contribution of these in individuals to tailor treatment.

An effective treatment strategy may well require a multifaceted combinatorial approach to yield maximum therapeutic effect both to target pathological processes and compartmentalised degeneration. How we administer this combination approach is of interest and it is likely that neuroprotection strategies will serve as an adjunct to IOP-lowering therapies in the first instance.

Valuable lessons can be learned from the oncology community, where breast cancer molecular and genetic phenotyping are now used widely in clinical practice to tailor treatment to individuals (Cappelletti et al., 2017; Dai et al., 2016; Sioshansi et al., 2011). These molecular subtypes have phenotypic diversity with regard to multiple clinical outcomes, including response to chemotherapy, disease-free survival, and overall survival. It is therefore conceivable that continued progress in the molecular profiling of adult-onset POAG patients will improve our understanding of relative contributions of the various disease processes we know are implicated in POAG in individual patients and determine how they should be treated according to their underlying pathophysiology.

The UK Biobank holds large-scale genomic and detailed phenotypic and health-related data for 500,000 people and has already proved a powerful tool in linking genetic and epidemiological factors to disease risk and an understanding of the mechanisms that underlie those associations (Bycroft et al., 2018; Chua et al., 2019; Ollier et al., 2005). The project, which benefits greatly from the infrastructure of the NHS, has an open access approach so that researchers from around the world are able to use the dataset. To date there have been at least 8,294 approved registrations, and 796 formally registered projects, the results of which have been communicated in over 500 publications in peer-reviewed journals. Glaucoma parameters have also been included in the data collection process (M. P. Y. Chan et al., 2016) and we are starting to see the development of polygenic risk scores (X. R. Gao et al., 2019) to predict glaucoma progression and the need for intervention. The UK Biobank data, combined with other biobank centres and initiatives such as the 100,000 Genomes project has the potential to significantly enhance our understanding of the relative contributions of pathological mechanisms to a disease process and enable us to predict individual risk to target screening programmes, enhance our diagnostic capability and tailor treatment according to the pathological process.

In summary, refinements in trial design and the use of new modalities to define structural and functional endpoints may improve our assessment of disease activity and treatment efficacy. Advances in our understanding of compartmentalised glaucomatous degeneration and continued progress in the molecular profiling of glaucoma patients will enable us to predict individual risk and tailor treatment. New approaches to future glaucoma neuroprotection trials could improve the prospects for new glaucoma therapies. Functional recovery and the ongoing development of strategies to repair and regenerate the optic nerve hold promise. Furthermore, glaucoma treatment tailored according to an individual's unique risk profile may become increasingly common in the future.

APPENDIX 1 MATLAB CODE FOR HVI IMAGE REGISTRATION

```
fig0 = 'hvi-video-00000';
fixed = imread([fig0 '.pgm']);
basename = 'hvi-video-';
endname = '.pgm';
boundary = 20;
s_image = size(fixed);
I = boundary + 1: s_image(1) - boundary;
J = boundary + 1: s_image(2) - boundary;

imwrite(fixed(I, J), colormap (gray (256)), ['Reg_' fig0 '.png'])

for k=1:15

   fig2 = [basename num2str(k,'%05i')];

moving = imread ([fig2 '.pgm']);

% figure, imshowpair(moving, fixed, 'montage')
% title('Unregistered')

% figure, imshowpair(moving, fixed)
% title('Unregistered')

[optimizer,metric] = imregconfig('monomodal');

movingRegisteredDefault = imregister(moving, fixed, 'rigid', optimizer,
metric);

% figure, imshowpair(movingRegisteredDefault, fixed)
% title(['Registered: ' fig2])

imwrite(movingRegisteredDefault(I, J), colormap (gray(256)), ['Reg_' fig2
'.png'])

end


fig0 = 'Reg_hvi-video-00000.png';
fixed = imread(fig0);
basename = 'Reg_hvi-video-';
endname = '.png';
boundary = 0;
s_image = size(fixed);
I = boundary + 1: s_image(1) - boundary;
J = boundary + 1: s_image(2) - boundary;

imwrite(fixed(I, J), colormap (gray(256)), ['Aff_' fig0])

for k=1:15

   fig2 = [basename num2str(k,'%05i')];

moving = imread ([fig2 '.png']);

% figure, imshowpair(moving, fixed, 'montage')
% title('Unregistered')

% figure, imshowpair(moving, fixed)
% title('Unregistered')
```

```
[optimizer,metric] = imregconfig('monomodal');

movingRegisteredDefault = imregister(moving, fixed, 'affine', optimizer,
metric);

% figure, imshowpair(movingRegisteredDefault, fixed)
% title(['Registered: ' fig2])

imwrite(movingRegisteredDefault(I, J), colormap (gray(256)), ['Aff_' fig2
'.png'])

end
```

APPENDIX 2 PYTHON CODE FOR SEMI-AUTOMATED AXON TRANSPORT QUANTIFICATION

```
from PIL import Image
import numpy as np
import matplotlib.pyplot as plt
import cv2
import csv

def make_perpendicular(v):
	return np.asarray([-v[1],v[0]])

def normalize(v):
	sqr = np.sum(np.asarray(v))**2
	norm = np.sqrt(sqr)
	return np.asarray(v)/norm

def get_norm(v):
	return np.sqrt(np.sum([v[i]**2 for i in range(len(v))]))

def get_vector(v1,v2):
	return [v2[0]-v1[0],v2[1]-v1[1]]

def draw_big_point(x,y,img,side_length=5):
	img[y-side_length:y+side_length,x-side_length:x+side_length] =
128

def threshold_image(img, threshold=20):
	return (img > threshold) * 255


def make_line(p_start,p_stop):
	line = []
	step_vector = normalize(p_stop-p_start)

	current_point = p_start
	current_dist = get_norm(p_stop-p_start)
	next_point = p_start + step_vector
	next_dist = get_norm(p_stop-next_point)
	while next_dist < current_dist:
		line = line + [current_point]
		current_point = next_point
		current_dist = next_dist
		next_point = current_point + step_vector
		next_dist = get_norm(p_stop-next_point)
	return np.asarray(line,dtype=int)

def transform(line,translation=0, scaling=1):
	p_start = line[0]
	p_end = line[1]
	parallel = normalize(p_end-p_start)
	shifted = line + translation*parallel
	p_start = shifted[0]
	p_end = shifted[-1]
```

```
        vector = p_end - p_start
        p_end = p_start + vector*scaling

        return make_line(p_start,p_end)

def draw_perp(p_start,p_stop,pixel_distance=218,multiple=1):
        line = make_line(p_start=p_start,p_stop=p_stop)
        perp = normalize(make_perpendicular(p_stop-p_start))
        return np.asarray([l+multiple*pixel_distance*perp for l in
line],dtype=int)

def process(central_points,img):
        pass

def get_main_segment(img):
        blur = cv2.blur(img,(40,40))
        _,thresh = cv2.threshold(blur,20,255,cv2.THRESH_BINARY)
        _, markers = cv2.connectedComponents(thresh)
        unique, counts = np.unique(markers, return_counts=True)
        segments = [s for s in sorted(zip(unique,counts),key=lambda x:
x[1],reverse=True) if s[0] != 0]
        segmented = np.asarray(markers==(segments[0][0]),dtype=np.uint8)

        return segmented

def get_contour(segmented):
        segmented = np.asarray(segmented,dtype=np.uint8)
        im2, contours, hierarchy =
cv2.findContours(segmented,cv2.RETR_TREE,cv2.CHAIN_APPROX_SIMPLE)

        im = np.zeros(segmented.shape)
        cv2.drawContours(im, contours, -1, (0,255,0), 3)

        return im

def draw_line(img,p0,p1,value=128):
        line = make_line(p0,p1)
        for l in line:
                try:
                        img[l[1],l[0]] = value
                except:
                        pass
        return

def perpendicular_segment_positions(p_start,p_stop,spacing=218):
        parallel = normalize(p_stop-p_start)
        current_position = p_start
        current_dist = get_norm(p_stop-current_position)
        next_position = p_start + spacing*parallel
        next_dist = get_norm(p_stop-next_position)

        points = []
        while next_dist < current_dist:
                points = points + [current_position]
                current_position = next_position
                current_dist = next_dist
                next_position = current_position + spacing*parallel
                next_dist = get_norm(p_stop-next_position)
```

```
        return np.asarray(points,dtype=int)

def generate_perpendicular_line(p0,vector, segmented,img):
                line = [p0]
                lower = True
                while lower:
                        next_point = line[0]+vector
                        x = int(next_point[0])
                        y = int(next_point[1])
                        try:
                                if segmented[y][x] != 0:
                                        line = [next_point] + line
                                else:
                                        lower = False
                        except:
                                lower = False
                upper = True
                while upper:
                        next_point = line[-1] - vector
                        x = int(next_point[0])
                        y = int(next_point[1])

                        try:
                                if segmented[y][x] != 0:
                                        line = line + [next_point]
                                else:
                                        upper = False
                        except:
                                upper = False

                line = np.asarray(line,dtype=np.int)
                return np.asarray([line[0],line[-1]])


def get_pixel_values_on_line(img,p0,p1):
        line = make_line(p0,p1)
        positions = [l for l in line if l[1] >= 0 and l[1] <
img.shape[0] and l[0] >= 0 and l[0] < img.shape[1]]
        pixel_values = [ img[l[1],l[0]] for l in positions]
        return positions, pixel_values

class Renderer(object):

        def __init__(self,filepath, line_spacing, write_data,
write_path):

                if write_data==True and write_path is None:
                        print "Error - the write_data flag is True but
write_path is None, you need to specify a write_path if you want to
write the data out!"
                        raise ValueError("Write Path Not Specified")

                self.points = []
                self.fig, [self.ax1, self.ax2, self.ax3] =
plt.subplots(1,3,figsize=(24,8))

                im = Image.open(filepath)
                self.img = np.asarray(im)[:,:,0]
```

```
                #segment image - need to detect cell to be able to find
its edges
                self.segmented = get_main_segment(self.img)

                #downscale for ease of plotting lines
                self.img_modified= self.img/4.0

                self.line_spacing = line_spacing
                self.write_data = write_data
                self.write_path = write_path


                self.ax1.imshow(self.img,cmap="viridis")
                self.ax1.set_title("Raw image")
                self.annotated_plot =
self.ax2.imshow(self.img_modified,cmap="viridis")
                self.ax2.set_title("Marked
image".format(self.line_spacing))
                self.ax3.set_xlabel("Segment index")
                self.ax3.set_ylabel("Average pixel value")
                self.ax3.set_title("Average pixel value for a given
segment in image on the left.\n Index is at the top of the left image")

        def run(self,show_plot=True, write_data=False,write_path=None):

                self.img_modified= self.img/4.0


                #get the value of pixels on various segments in the image
                self.segments = []

                #draw vertical points defining centerline of cell as
large squares on self.img_modified - the "marked image"
                for p in self.points:

        draw_big_point(x=p[0],y=p[1],img=self.img_modified,side_length=3
0)

                #for every pair of vertical "backbone" points:
                for i in range(len(self.points)-1):

                        #get the vertical segment
                        vertical_p0 = self.points[i]
                        vertical_p1 = self.points[i+1]

                        #generate intermediate points
                        vertical_intermediates =
perpendicular_segment_positions(p_start=vertical_p0,p_stop=vertical_p1,
spacing=self.line_spacing)
                        #generate parallel and perpendicular vectors
                        parallel = normalize(vertical_p1- vertical_p0)
                        perpendicular =
normalize(make_perpendicular(vertical_p1- vertical_p0))

                        #use every intermediate point on "backbone"
segment
                        #generate perpendicular line
```

```
                        for p in vertical_intermediates:
                                #mark them - but slightly smaller points

        draw_big_point(x=p[0],y=p[1],img=self.img_modified,side_length=1
0)
                                #generate perpendicular line
                                seg =
generate_perpendicular_line(p,perpendicular,self.segmented,self.img)
                                start = seg[0]        #start of the
perpendicular segment
                                stop = seg[1]  #end of the perpendicular
segment

                                #draw the start and stop points

        draw_big_point(x=start[0],y=start[1],img=self.img_modified,side_
length=10)

        draw_big_point(x=stop[0],y=stop[1],img=self.img_modified,side_le
ngth=10)
                                #draw the line

        draw_line(p0=start,p1=stop,img=self.img_modified)

                                #get the positions and values of the
pixels under the line
                                positions,values =
get_pixel_values_on_line(self.img, p0=start, p1 = stop)
                                #add values to the segments list - this is
the only thing we care about
                                self.segments = self.segments +
[{"start_pixel":start,"stop_pixel":stop, "pixel_positions": positions,
"pixel_values":values}]


                segment_mean_pixel_value =
[np.sum(s["pixel_values"])/len(s["pixel_values"]) for s in
self.segments]
                if write_data:
                        with open(write_path, "w") as f:
                                writer = csv.writer(f, delimiter=',')
                                writer.writerow(['StartPixel',
"StopPixel","TotalPixels", "TotalPixelValue", "AveragePixelValue"])
                                for s in segments:
                                        start = s["start_pixel"]
                                        stop = s["stop_pixel"]
                                        pixel_total =
len(s["pixel_positions"])
                                        total_pixel_value =
np.sum(s["pixel_values"])
                                        avg_pixel_value =
total_pixel_value/float(pixel_total)

        writer.writerow([start,stop,pixel_total,total_pixel_value,avg_pi
xel_value])
```

```
                self.annotated_plot.set_data(self.img_modified)
                self.annotated_plot.autoscale()
                # self.ax2.imshow(self.img_modified,cmap="viridis")
                self.ax3.cla()
                self.ax3.set_xlabel("Segment index")
                self.ax3.set_ylabel("Average pixel value")
                self.ax3.set_title("Average pixel value for a given
segment in image on the left.\n Index is at the top of the left image")

                self.ax3.plot(segment_mean_pixel_value,"x-
",label="Average along line pixel intensity")
                self.fig.canvas.draw()
         # self.fig.canvas.flush_events()
                # plt.show()

def main():

        filename = "example_1.tif"
        points = np.asarray([
                [1481,148],
                [1689,1411],
                [1718,1827],
                [901,4561],
                [857,4873],
                [901,5274]
        ])

        write_path = "data.csv"
        # self,filepath, line_spacing, write_data, write_path
        renderer = Renderer(filename, 100, True, write_path)
        def onclick(event):
                CLICK_RADIUS = 30
                print renderer
                # print "Clicked point", event.button,event.x, event.y,
event.xdata, event.ydata
                pos = np.asarray([int(np.round(event.xdata)),
int(np.round(event.ydata))])
                print "POSITION", pos
                if event.button == 1:
                        renderer.points = renderer.points + [pos]
                        renderer.run()

                elif event.button == 3:
                        print "POINTS",[p for p in renderer.points]
                        print  "DISTANCES",[get_norm(p-pos) for p in
renderer.points]
                        print  "VALID",[get_norm(p-pos) <= CLICK_RADIUS
for p in renderer.points]

                        valid_points = [(i,get_norm(p-pos)) for i,p in
enumerate(renderer.points) if (get_norm(p-pos) <= CLICK_RADIUS) ==
True]
                        valid_points = sorted(valid_points, key=lambda
x:x[1])
                        valid_points = [v[0] for v in valid_points]
                        if len(valid_points) >= 1:
                                print renderer
```

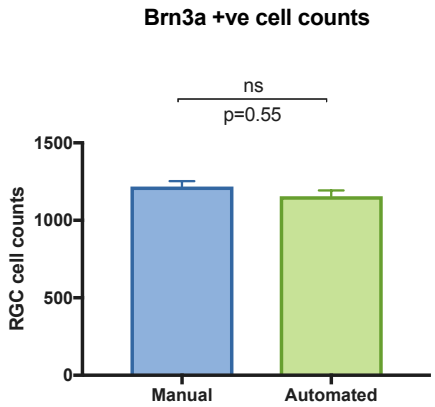
```
                                renderer.points = [renderer.points[j] for
j in xrange(len(renderer.points)) if j != valid_points[0]]
                                renderer.run()
                        else:
                                pass

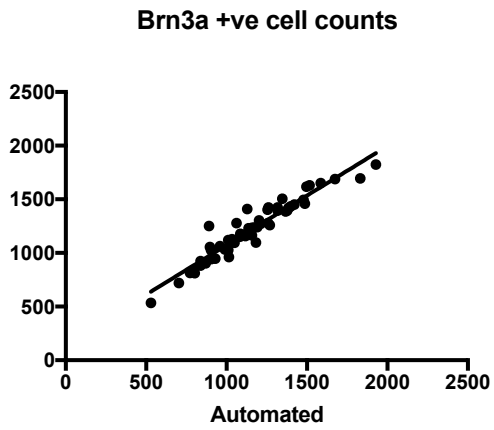

        cid = renderer.fig.canvas.mpl_connect('button_press_event',
onclick)

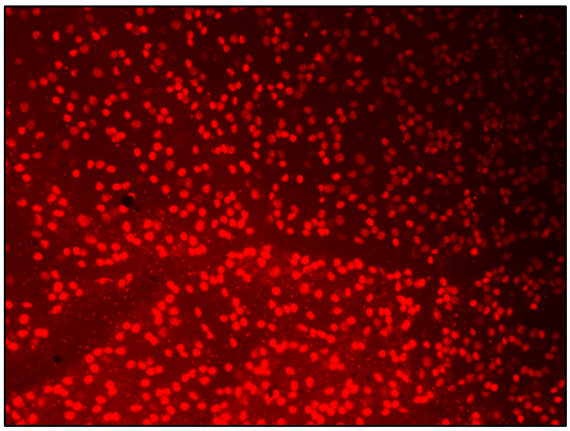
        plt.show()
        # run(points=points,filename=filename,line_spacing=100,
show_plot=True, write_data=False,write_path=write_path)

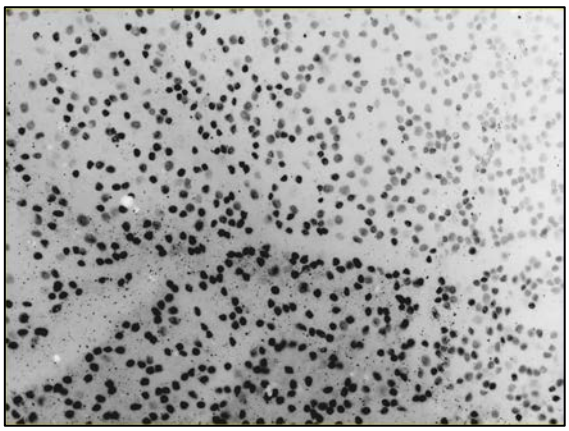
if __name__ == "__main__":
        main()
```

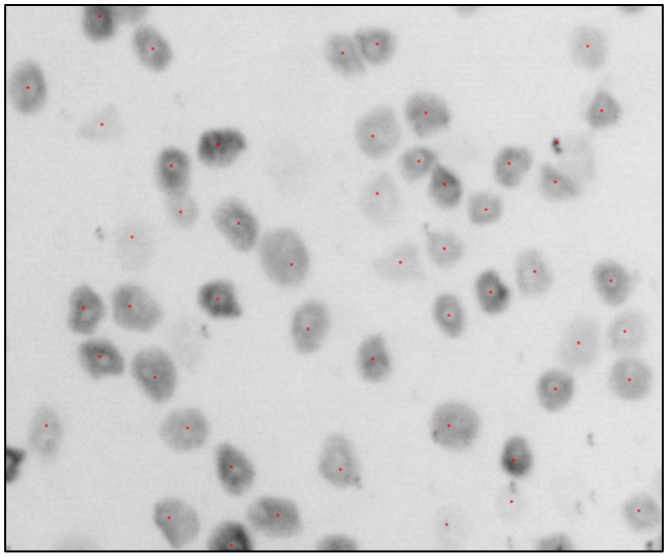
APPENDIX 3 MANUAL VALIDATION OF BRN3A RGC QUANTIFICATION AND GFP COLOCALISATION





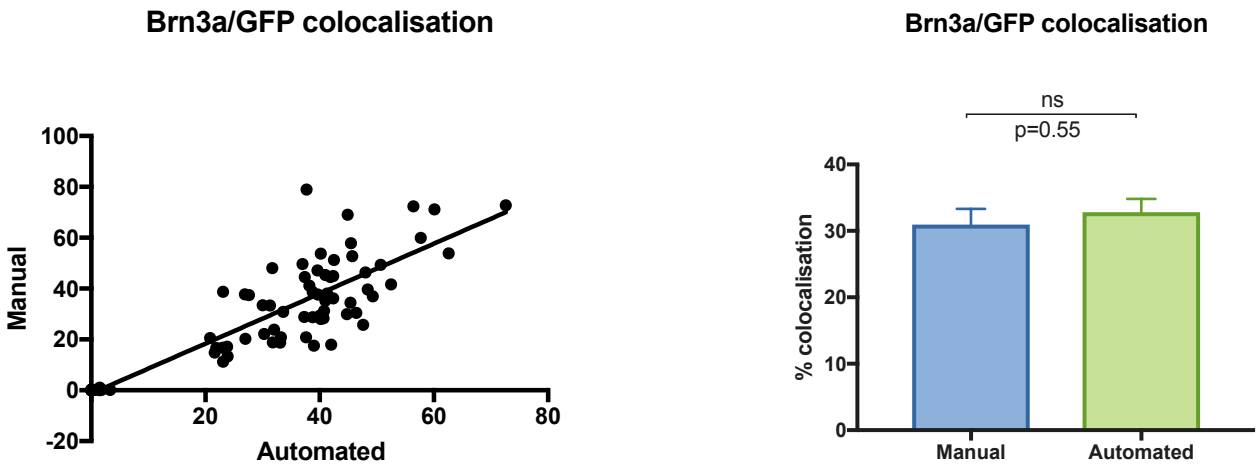






Brn3a: automated count

Appendix 3-1: Manual validation of the ITCN plugin for FIJI (Schneider et al., 2012) with optimised parameters for Brn3a positive retinal ganglion cells used in Chapter 6 and in (Conceição et al., 2019; Nieuwenhuis et al., 2020; A. Osborne, Khatib, et al., 2018).



Appendix 3-3: Manual validation of the GFP/Brn3a Volocity colocalisation used in Chapter 5.

REFERENCES

Akagi, T., Uji, A., Huang, A. S., Weinreb, R. N., Yamada, T., Miyata, M., Kameda, T., Ikeda, H. O., & Tsujikawa, A. (2018). Conjunctival and Intrascleral Vasculatures Assessed Using Anterior Segment Optical Coherence Tomography Angiography in Normal Eyes. *American Journal of Ophthalmology*, *196*, 1–9. https://doi.org/10.1016/j.ajo.2018.08.009

Allen, B., Ingram, E., Takao, M., Smith, M. J., Jakes, R., Virdee, K., Yoshida, H., Holzer, M., Craxton, M., Emson, P. C., Atzori, C., Migheli, A., Crowther, R. A., Ghetti, B., Spillantini, M. G., & Goedert, M. (2002). Abundant tau filaments and nonapoptotic neurodegeneration in transgenic mice expressing human P301S tau protein. *The Journal of Neuroscience : The Official Journal of the Society for Neuroscience*, *22*(21), 9340–9351. https://doi.org/10.1523/JNEUROSCI.22-21-09340.2002

Antón, A., Pazos, M., Martín, B., Navero, J. M., Ayala, M. E., Castany, M., Martínez, P., & Bardavío, J. (2013). Glaucoma Progression Detection: Agreement, Sensitivity, and Specificity of Expert Visual Field Evaluation, Event Analysis, and Trend Analysis. *European Journal of Ophthalmology*, *23*(2), 187–195. https://doi.org/10.5301/ejo.5000193

Artes, P. H., Nicolela, M. T., LeBlanc, R. P., & Chauhan, B. C. (2005). Visual Field Progression in Glaucoma: Total Versus Pattern Deviation Analyses. *Investigative Opthalmology & Visual Science*, *46*(12), 4600. https://doi.org/10.1167/iovs.05-0827

Artes, P. H., O'Leary, N., Nicolela, M. T., Chauhan, B. C., & Crabb, D. P. (2014). Visual Field Progression in Glaucoma: What Is the Specificity of the Guided

Progression Analysis? *Ophthalmology*, *121*(10), 2023–2027. https://doi.org/10.1016/J.OPHTHA.2014.04.015

ASHTON, N. (1952). Anatomical study of Schlemm's canal and aqueous veins by means of neoprene casts. II. Aqueous veins. *The British Journal of Ophthalmology*, *36*(5), 265–267; contd. https://doi.org/10.1136/bjo.36.5.265

Ashton, N., & Smith, R. (1953). Anatomical study of Schlemm's canal and aqueous veins by means of Neoprene casts: III. Arterial relations of Schlemm's canal. *British Journal of Ophthalmology*, *37*(10), 577–586. https://doi.org/10.1136/bjo.37.10.577

Bainbridge, J. W. B., Mehat, M. S., Sundaram, V., Robbie, S. J., Barker, S. E., Ripamonti, C., Georgiadis, A., Mowat, F. M., Beattie, S. G., Gardner, P. J., Feathers, K. L., Luong, V. A., Yzer, S., Balaggan, K., Viswanathan, A., de Ravel, T. J. L., Casteels, I., Holder, G. E., Tyler, N., … Ali, R. R. (2015). Long-Term Effect of Gene Therapy on Leber's Congenital Amaurosis. *New England Journal of Medicine*, *372*(20), 1887–1897. https://doi.org/10.1056/NEJMoa1414221

Bartel, M., Schaffer, D., & Büning, H. (2011). Enhancing the Clinical Potential of AAV Vectors by Capsid Engineering to Evade Pre-Existing Immunity. *Frontiers in Microbiology*, *2*, 204. https://doi.org/10.3389/fmicb.2011.00204

Bayer, A. U., & Erb, C. (2002). Short wavelength automated perimetry, frequency doubling technology perimetry, and pattern electroretinography for prediction of progressive glaucomatous standard visual field defects. *Ophthalmology*, *109*(5), 1009–1017. https://doi.org/10.1016/S0161-6420(02)01015-1

Beck, R. W., Bergstrom, T. J., & Lighter, P. R. (1985). A Clinical Comparison of Visual Field Testing With a New Automated Perimeter, the Humphrey Field Analyzer, and the Goldmann Perimeter. *Ophthalmology*, *92*(1), 77–82.

https://doi.org/10.1016/S0161-6420(85)34065-4

Beirowski, B., Babetto, E., Coleman, M. P., & Martin, K. R. (2008). The WldS gene delays axonal but not somatic degeneration in a rat glaucoma model. *European Journal of Neuroscience*, *28*(6), 1166–1179. https://doi.org/10.1111/j.1460-9568.2008.06426.x

Benowitz, L. I., Apostolides, P. J., Perrone-Bizzozero, N., Finklestein, S. P., & Zwiers, H. (1988). Anatomical distribution of the growth-associated protein GAP-43/B-50 in the adult rat brain. *The Journal of Neuroscience*, *8*(1), 339 LP – 352. https://doi.org/10.1523/JNEUROSCI.08-01-00339.1988

Bernier-Latmani, J., & Petrova, T. V. (2017). All TIEd up: mechanisms of Schlemm's canal maintenance. *The Journal of Clinical Investigation*, *127*(10), 3594–3597. https://doi.org/10.1172/JCI96840

Binley, K. E., Ng, W. S., Barde, Y.-A., Song, B., & Morgan, J. E. (2016). Brain-derived neurotrophic factor prevents dendritic retraction of adult mouse retinal ganglion cells. *The European Journal of Neuroscience*, *44*(3), 2028–2039. https://doi.org/10.1111/ejn.13295

Blumberg, D. M., De Moraes, C. G., Prager, A. J., Yu, Q., Al-Aswad, L., Cioffi, G. A., Liebmann, J. M., & Hood, D. C. (2017). Association Between Undetected 10-2 Visual Field Damage and Vision-Related Quality of Life in Patients With Glaucoma. *JAMA Ophthalmology*, *135*(7), 742–747. https://doi.org/10.1001/jamaophthalmol.2017.1396

Bonini, S., Lambiase, A., Rama, P., Sinigaglia, F., Allegretti, M., Chao, W., Mantelli, F., Bonini, S., Lambiase, A., Rama, P., Messmer, E., Aragona, P., Geerling, G., Mastropasqua, L., Mencucci, R., Dart, J., Leonardi, A., Montero, J., Rolando, M., … Torrao, L. (2018). Phase II Randomized, Double-Masked, Vehicle-Controlled

Trial of Recombinant Human Nerve Growth Factor for Neurotrophic Keratitis. *Ophthalmology*, *125*(9), 1332–1343. https://doi.org/10.1016/j.ophtha.2018.02.022

Bouquet, C., Vignal Clermont, C., Galy, A., Fitoussi, S., Blouin, L., Munk, M. R., Valero, S., Meunier, S., Katz, B., Sahel, J. A., & Thomasson, N. (2019). Immune Response and Intraocular Inflammation in Patients With Leber Hereditary Optic Neuropathy Treated With Intravitreal Injection of Recombinant Adeno-Associated Virus 2 Carrying the ND4 Gene: A Secondary Analysis of a Phase 1/2 Clinical TrialOutcomes i. *JAMA Ophthalmology*, *137*(4), 399–406. https://doi.org/10.1001/jamaophthalmol.2018.6902

Bray, E. R., Yungher, B. J., Levay, K., Ribeiro, M., Dvoryanchikov, G., Ayupe, A. C., Thakor, K., Marks, V., Randolph, M., Danzi, M. C., Schmidt, T. M., Chaudhari, N., Lemmon, V. P., Hattar, S., & Park, K. K. (2019). Thrombospondin-1 Mediates Axon Regeneration in Retinal Ganglion Cells. *Neuron*, *103*(4), 642-657.e7. https://doi.org/10.1016/j.neuron.2019.05.044

Brown, J. M., Xia, J., Zhuang, B., Cho, K.-S., Rogers, C. J., Gama, C. I., Rawat, M., Tully, S. E., Uetani, N., Mason, D. E., Tremblay, M. L., Peters, E. C., Habuchi, O., Chen, D. F., & Hsieh-Wilson, L. C. (2012). A sulfated carbohydrate epitope inhibits axon regeneration after injury. *Proceedings of the National Academy of Sciences*, *109*(13), 4768 LP – 4773. https://doi.org/10.1073/pnas.1121318109

Bryan, S. R., & Crabb, D. P. (2018). A New Graphical Tool for Assessing Visual Field Progression in Clinical Populations. *Translational Vision Science & Technology*, *7*(1), 22. https://doi.org/10.1167/tvst.7.1.22

Bull, N. D., Guidi, A., Goedert, M., Martin, K. R., & Spillantini, M. G. (2012). Reduced axonal transport and increased excitotoxic retinal ganglion cell degeneration in

mice transgenic for human mutant p301s tau. *PLoS ONE*, *7*(4), 2–9. https://doi.org/10.1371/journal.pone.0034724

Burke, J., & Schwartz, M. (1996). Preclinical evaluation of brimonidine. *Survey of Ophthalmology*, *41*, S9–S18. https://doi.org/http://dx.doi.org/10.1016/S0039-6257(96)82027-3

Bussel, I. I., Wollstein, G., & Schuman, J. S. (2014). OCT for glaucoma diagnosis, screening and detection of glaucoma progression. *British Journal of Ophthalmology*, *98*(Suppl 2), ii15 LP-ii19. https://doi.org/10.1136/bjophthalmol-2013-304326

Bycroft, C., Freeman, C., Petkova, D., Band, G., Elliott, L. T., Sharp, K., Motyer, A., Vukcevic, D., Delaneau, O., O'Connell, J., Cortes, A., Welsh, S., Young, A., Effingham, M., McVean, G., Leslie, S., Allen, N., Donnelly, P., & Marchini, J. (2018). The UK Biobank resource with deep phenotyping and genomic data. *Nature*, *562*(7726), 203–209. https://doi.org/10.1038/s41586-018-0579-z

Canadian Glaucoma Study Group. (2006). Canadian Glaucoma Study: 1. Study design, baseline characteristics, and preliminary analyses. *Canadian Journal of Ophthalmology*, *41*(5), 566–575. https://doi.org/10.1016/S0008-4182(06)80025-6

Cappelletti, V., Iorio, E., Miodini, P., Silvestri, M., Dugo, M., & Daidone, M. G. (2017). Metabolic Footprints and Molecular Subtypes in Breast Cancer. *Disease Markers*, *2017*, 1–19. https://doi.org/10.1155/2017/7687851

Caprioli, J. (2007). *The Importance of Rates in Glaucoma*. 191–192. https://doi.org/10.1016/j.ajo.2007.12.003

Caprioli, J., De Leon, J. M., Azarbod, P., Chen, A., Morales, E., Nouri-Mahdavi, K., Coleman, A., Yu, F., & Afifi, A. (2016). Trabeculectomy Can Improve Long-Term

Visual Function in Glaucoma. *Ophthalmology*, *123*(1), 117–128. https://doi.org/10.1016/j.ophtha.2015.09.027

Carvalho, L. S., György, B., Mu, D., Shah, S., Vandenberghe, L. H., & Maguire, C. A. (2015). 152. Retinal Tropism of Exosome-Associated AAV Vector Via Intravitreal Delivery. *Molecular Therapy*, *23*, S61. https://doi.org/10.1016/S1525-0016(16)33757-1

Casson, R. J., Han, G., Ebneter, A., Chidlow, G., Glihotra, J., Newland, H., & Wood, J. P. M. (2014). Glucose-induced temporary visual recovery in primary open-angle glaucoma: A double-blind, randomized study. *Ophthalmology*, *121*(6), 1203–1211. https://doi.org/10.1016/j.ophtha.2013.12.011

Chalk, D., & Smith, M. (2013). Guidelines on glaucoma and the demand for services. *British Journal of Healthcare Management*, *19*(10), 476–481. https://doi.org/10.12968/bjhc.2013.19.10.476

Chan, K. C., Yu, Y., Ng, S. H., Mak, H. K., Yip, Y. W. Y., van der Merwe, Y., Ren, T., Yung, J. S. Y., Biswas, S., Cao, X., Chau, Y., & Leung, C. K. S. (2019). Intracameral injection of a chemically cross-linked hydrogel to study chronic neurodegeneration in glaucoma. *Acta Biomaterialia*, *94*, 219–231. https://doi.org/10.1016/j.actbio.2019.06.005

Chan, M. P. Y., Grossi, C. M., Khawaja, A. P., Yip, J. L. Y., Khaw, K. T., Patel, P. J., Khaw, P. T., Morgan, J. E., Vernon, S. A., & Foster, P. J. (2016). Associations with intraocular pressure in a large cohort: Results from the UK Biobank. *Ophthalmology*, *123*(4), 771–782. https://doi.org/10.1016/j.ophtha.2015.11.031

Chen, A. C., Martin, A. J., Choy, B., Fernández-Peñas, P., Dalziell, R. A., McKenzie, C. A., Scolyer, R. A., Dhillon, H. M., Vardy, J. L., Kricker, A., St. George, G., Chinniah, N., Halliday, G. M., & Damian, D. L. (2015). A Phase 3 Randomized

Trial of Nicotinamide for Skin-Cancer Chemoprevention. *New England Journal of Medicine*, *373*(17), 1618–1626. https://doi.org/10.1056/NEJMoa1506197

Chen, C.-Y., Chen, J., He, L., & Stiles, B. L. (2018). PTEN: Tumor Suppressor and Metabolic Regulator. *Frontiers in Endocrinology*, *9*, 338. https://doi.org/10.3389/fendo.2018.00338

Cheng, L., Sapieha, P., Kittlerova, P., Hauswirth, W. W., & Di Polo, A. (2002). TrkB gene transfer protects retinal ganglion cells from axotomy-induced death in vivo. *The Journal of Neuroscience*, *22*(10), 3977–3986. https://doi.org/20026382

Cheng, L., Sapieha, P., Kittlerová, P., Hauswirth, W. W., & Di Polo, A. (2002). TrkB Gene Transfer Protects Retinal Ganglion Cells from Axotomy-Induced Death In Vivo. *The Journal of Neuroscience*, *22*(10), 3977–3986. https://doi.org/10.1523/JNEUROSCI.22-10-03977.2002

Cheng, P.-L., Song, A.-H., Wong, Y.-H., Wang, S., Zhang, X., & Poo, M.-M. (2011). Self-amplifying autocrine actions of BDNF in axon development. *Proceedings of the National Academy of Sciences of the United States of America*, *108*(45), 18430–18435. https://doi.org/10.1073/pnas.1115907108

Cheung, Z. H., So, K.-F., Lu, Q., Yip, H. K., Wu, W., Shan, J. J., Pang, P. K. T., & Chen, C.-F. (2002). Enhanced Survival and Regeneration of Axotomized Retinal Ganglion Cells by a Mixture of Herbal Extracts. *Journal of Neurotrauma*, *19*(3), 369–378. https://doi.org/10.1089/089771502753594936

Chew, E. Y., Clemons, T. E., Jaffe, G. J., Johnson, C. A., Farsiu, S., Lad, E. M., Guymer, R., Rosenfeld, P., Hubschman, J. P., Constable, I., Wiley, H., Singerman, L. J., Gillies, M., Comer, G., Blodi, B., Eliott, D., Yan, J., Bird, A., & Friedlander, M. (2019). Effect of Ciliary Neurotrophic Factor on Retinal Neurodegeneration in Patients with Macular Telangiectasia Type 2: A

Randomized Clinical Trial. *Ophthalmology*, *126*(4), 540–549. https://doi.org/10.1016/j.ophtha.2018.09.041

Chiasseu, M., Alarcon-Martinez, L., Belforte, N., Quintero, H., Dotigny, F., Destroismaisons, L., Vande Velde, C., Panayi, F., Louis, C., & Di Polo, A. (2017). Tau accumulation in the retina promotes early neuronal dysfunction and precedes brain pathology in a mouse model of Alzheimer's disease. *Molecular Neurodegeneration*, *12*(1), 58. https://doi.org/10.1186/s13024-017-0199-3

Cho, H., & Kee, C. (2014). Population-based glaucoma prevalence studies in Asians. *Survey of Ophthalmology*, *59*(4), 434–447. https://doi.org/10.1016/j.survophthal.2013.09.003

Chrysostomou, V., Galic, S., van Wijngaarden, P., Trounce, I. A., Steinberg, G. R., & Crowston, J. G. (2016). Exercise reverses age-related vulnerability of the retina to injury by preventing complement-mediated synapse elimination via a BDNF-dependent pathway. *Aging Cell*, *15*(6), 1082–1091. https://doi.org/10.1111/acel.12512

Chrysostomou, V., Kezic, J. M., Trounce, I. A., & Crowston, J. G. (2014). Forced exercise protects the aged optic nerve against intraocular pressure injury. *Neurobiology of Aging*, *35*(7), 1722–1725. https://doi.org/10.1016/j.neurobiolaging.2014.01.019

Chua, S. Y. L., Thomas, D., Allen, N., Lotery, A., Desai, P., Patel, P., Muthy, Z., Sudlow, C., Peto, T., Khaw, P. T., Foster, P. J., Zheng, Y., Aslam, T., Barman, S. A., Barrett, J. H., Bishop, P., Blows, P., Bunce, C., Carare, R. O., … Yip, J. (2019). Cohort profile: Design and methods in the eye and vision consortium of UK Biobank. *BMJ Open*, *9*(2), 1–13. https://doi.org/10.1136/bmjopen-2018-025077

Clemente-Tomás, R., Arciniegas-Perasso, C. A., Hervás-Hernandis, J. M., García-Ibor, F., Ruiz-del Río, N., & Duch-Samper, A. M. (2018). Hypertensive acute granulomatous anterior uveitis as a side effect of topical brimonidine. *Archivos de La Sociedad Española de Oftalmología (English Edition)*, *93*(10), 511–514. https://doi.org/https://doi.org/10.1016/j.oftale.2018.07.006

Comparison of glaucomatous progression between untreated patients with normal-tension glaucoma and patients with therapeutically reduced intraocular pressures. Collaborative Normal-Tension Glaucoma Study Group. (1998). *American Journal of Ophthalmology*, *126*(4), 487—497. http://europepmc.org/abstract/MED/9780093

Conceição, R., Evans, R. S., Pearson, C. S., Hänzi, B., Osborne, A., Deshpande, S. S., Martin, K. R., & Barber, A. C. (2019). Expression of Developmentally Important Axon Guidance Cues in the Adult Optic Chiasm. *Investigative Ophthalmology & Visual Science*, *60*(14), 4727–4739. https://doi.org/10.1167/iovs.19-26732

Cordeiro, M. F., Normando, E. M., Cardoso, M. J., Miodragovic, S., Jeylani, S., Davis, B. M., Guo, L., Ourselin, S., A'Hern, R., & Bloom, P. A. (2017). Real-time imaging of single neuronal cell apoptosis in patients with glaucoma. *Brain*, *140*(6), 1757–1767. https://doi.org/10.1093/brain/awx088

Crabb, D. P., Smith, N. D., Glen, F. C., Burton, R., & Garway-heath, D. F. (2013). How Does Glaucoma Look ? Patient Perception of Visual Field Loss. *OPHTHA*, *120*(6), 1120–1126. https://doi.org/10.1016/j.ophtha.2012.11.043

Craig, J. E., Han, X., Qassim, A., Hassall, M., Cooke Bailey, J. N., Kinzy, T. G., Khawaja, A. P., An, J., Marshall, H., Gharahkhani, P., Igo, R. P. J., Graham, S. L., Healey, P. R., Ong, J.-S., Zhou, T., Siggs, O., Law, M. H., Souzeau, E.,

Ridge, B., … MacGregor, S. (2020). Multitrait analysis of glaucoma identifies new risk loci and enables polygenic prediction of disease susceptibility and progression. *Nature Genetics*, *52*(2), 160–166. https://doi.org/10.1038/s41588-019-0556-y

Craven, E. R., Katz, L. J., Wells, J. M., & Giamporcaro, J. E. (2012). Cataract surgery with trabecular micro-bypass stent implantation in patients with mild-to-moderate open-angle glaucoma and cataract: Two-year follow-up. *Journal of Cataract & Refractive Surgery*, *38*(8), 1339–1345. https://doi.org/10.1016/J.JCRS.2012.03.025

Crish, S. D., Sappington, R. M., Inman, D. M., Horner, P. J., & Calkins, D. J. (2010). Distal axonopathy with structural persistence in glaucomatous neurodegeneration. *Proceedings of the National Academy of Sciences of the United States of America*, *107*(11), 5196–5201. https://doi.org/10.1073/pnas.0913141107

Cristofano, A. D., Pesce, B., Cordon-Cardo, C., & Pandolfi, P. P. (1998). Pten is essential for embryonic development and tumour suppression . *Nature Genetics*, *19*(4), 348–355. https://doi.org/10.1038/1235

Crowston, J. G., Kong, Y. X. G., Trounce, I. A., Dang, T. M., Fahy, E. T., Bui, B. V., Morrison, J. C., & Chrysostomou, V. (2014). An acute intraocular pressure challenge to assess retinal ganglion cell injury and recovery in the mouse. *Experimental Eye Research*, *141*, 3–8. https://doi.org/10.1016/j.exer.2015.03.006

Crowston, J. G., Kong, Y. X. G., Trounce, I. A., Dang, T. M., Fahy, E. T., Bui, B. V., Morrison, J. C., & Chrysostomou, V. (2015). An acute intraocular pressure challenge to assess retinal ganglion cell injury and recovery in the mouse.

Experimental Eye Research, *141*, 3–8. https://doi.org/10.1016/J.EXER.2015.03.006

Cukras, C., Wiley, H. E., Jeffrey, B. G., Sen, H. N., Turriff, A., Zeng, Y., Vijayasarathy, C., Marangoni, D., Ziccardi, L., Kjellstrom, S., Park, T. K., Hiriyanna, S., Wright, J. F., Colosi, P., Wu, Z., Bush, R. A., Wei, L. L., & Sieving, P. A. (2018). Retinal AAV8-RS1 Gene Therapy for X-Linked Retinoschisis: Initial Findings from a Phase I/IIa Trial by Intravitreal Delivery. *Molecular Therapy*, *26*(9), 2282–2294. https://doi.org/10.1016/j.ymthe.2018.05.025

Dai, X., Xiang, L., Li, T., & Bai, Z. (2016). Cancer hallmarks, biomarkers and breast cancer molecular subtypes. *Journal of Cancer*, *7*(10), 1281–1294. https://doi.org/10.7150/jca.13141

Davidsohn, N., Pezone, M., Vernet, A., Graveline, A., Oliver, D., Slomovic, S., Punthambaker, S., Sun, X., Liao, R., Bonventre, J. V, & Church, G. M. (2019). A single combination gene therapy treats multiple age-related diseases. *Proceedings of the National Academy of Sciences*, *116*(47), 23505–23511. https://doi.org/https://doi.org/10.1073/pnas.1910073116

de Lima, S., Koriyama, Y., Kurimoto, T., Oliveira, J. T., Yin, Y., Li, Y., Gilbert, H.-Y., Fagiolini, M., Martinez, A. M. B., & Benowitz, L. (2012). Full-length axon regeneration in the adult mouse optic nerve and partial recovery of simple visual behaviors. *Proceedings of the National Academy of Sciences*, *109*(23), 9149 LP – 9154. https://doi.org/10.1073/pnas.1119449109

De Moraes, C. G., Hood, D. C., Thenappan, A., Girkin, C. A., Medeiros, F. A., Weinreb, R. N., Zangwill, L. M., & Liebmann, J. M. (2017). 24-2 Visual Fields Miss Central Defects Shown on 10-2 Tests in Glaucoma Suspects, Ocular

Hypertensives, and Early Glaucoma. *Ophthalmology*, *124*(10), 1449–1456. https://doi.org/10.1016/j.ophtha.2017.04.021

De Moraes, C. G., Liebmann, J. M., & Levin, L. A. (2017). Detection and measurement of clinically meaningful visual field progression in clinical trials for glaucoma. *Progress in Retinal and Eye Research*, *56*, 107–147. https://doi.org/10.1016/j.preteyeres.2016.10.001

Denis, P., Hirneiß, C., Reddy, K. P., Kamarthy, A., Calvo, E., Hussain, Z., & Ahmed, I. I. K. (2019). A First-in-Human Study of the Efficacy and Safety of MINIject in Patients with Medically Uncontrolled Open-Angle Glaucoma (STAR-I). *Ophthalmology. Glaucoma*, *2*(5), 290–297. https://doi.org/10.1016/j.ogla.2019.06.001

Di Polo, A, Aigner, L. J., Dunn, R. J., Bray, G. M., & Aguayo, A. J. (1998). Prolonged delivery of brain-derived neurotrophic factor by adenovirus-infected Müller cells temporarily rescues injured retinal ganglion cells. *Proceedings of the National Academy of Sciences of the United States of America*, *95*(7), 3978–3983. https://doi.org/10.1073/pnas.95.7.3978

Di Polo, Adriana, Aigner, L. J., Dunn, R. J., Bray, G. M., & Aguayo, A. J. (1998). Prolonged delivery of brain-derived neurotrophic factor by adenovirus-infected Müller cells temporarily rescues injured retinal ganglion cells. *Proceedings of the National Academy of Sciences*, *95*(7), 3978 LP – 3983. https://doi.org/10.1073/pnas.95.7.3978

Dominici, M., Le Blanc, K., Mueller, I., Slaper-Cortenbach, I., Marini, F., Krause, D., Deans, R., Keating, a, Prockop, D., & Horwitz, E. (2006). Minimal criteria for defining multipotent mesenchymal stromal cells. The International Society for Cellular Therapy position statement. *Cytotherapy*, *8*(4), 315–317.

https://doi.org/10.1080/14653240600855905

Dong, C. J., Guo, Y., Agey, P., Wheeler, L., & Hare, W. A. (2008). Alpha2 adrenergic modulation of NMDA receptor function as a major mechanism of RGC protection in experimental glaucoma and retinal excitotoxicity. *Investigative Ophthalmology and Visual Science*, *49*(10), 4515–4522. https://doi.org/10.1167/iovs.08-2078

Du, R., Wang, X., & He, S. (2020). BDNF improves axon transportation and rescues visual function in a rodent model of acute elevation of intraocular pressure. *Science China Life Sciences*. https://doi.org/10.1007/s11427-019-1567-0

Duan, X., Qiao, M., Bei, F., Kim, I.-J., He, Z., & Sanes, J. R. (2015). Subtype-specific regeneration of retinal ganglion cells following axotomy: effects of osteopontin and mTOR signaling. *Neuron*, *85*(6), 1244–1256. https://doi.org/10.1016/j.neuron.2015.02.017

El-Danaf, R. N., & Huberman, A. D. (2015). Characteristic Patterns of Dendritic Remodeling in Early-Stage Glaucoma: Evidence from Genetically Identified Retinal Ganglion Cell Types. *Journal of Neuroscience*, *35*(6), 2329–2343. https://doi.org/10.1523/jneurosci.1419-14.2015

Elliott, E., Atlas, R., Lange, A., & Ginzburg, I. (2005). Brain-derived neurotrophic factor induces a rapid dephosphorylation of tau protein through a PI-3 Kinase signalling mechanism. *The European Journal of Neuroscience*, *22*(5), 1081–1089. https://doi.org/10.1111/j.1460-9568.2005.04290.x

Emerman, M., & Temin, H. M. (1984). Genes with promoters in retrovirus vectors can be independently suppressed by an epigenetic mechanism. *Cell*, *39*(3), 459–467. https://doi.org/10.1016/0092-8674(84)90453-7

Emre, E., Yüksel, N., Duruksu, G., Pirhan, D., Subaşi, C., Erman, G., & Karaöz, E. (2015). Neuroprotective effects of intravitreally transplanted adipose tissue and

bone marrow–derived mesenchymal stem cells in an experimental ocular hypertension model. *Cytotherapy*, *17*(5), 543–559. https://doi.org/10.1016/j.jcyt.2014.12.005

Erskine, L., & Herrera, E. (2014). Connecting the retina to the brain. *ASN Neuro*, *6*(6), 1759091414562107. https://doi.org/10.1177/1759091414562107

Fahy, E. T., Chrysostomou, V., Abbott, C. J., van Wijngaarden, P., & Crowston, J. G. (2016). Axonal transport along retinal ganglion cells is grossly intact during reduced function post-injury. *Experimental Eye Research*, *146*, 289–292. https://doi.org/10.1016/j.exer.2016.03.001

Fard, M. A., Moghimi, S., Sahraian, A., & Ritch, R. (2019). Optic nerve head cupping in glaucomatous and non-glaucomatous optic neuropathy. *British Journal of Ophthalmology*, *103*(3), 374 LP – 378. https://doi.org/10.1136/bjophthalmol-2018-312161

Feke, G. T., Bex, P. J., Taylor, C. P., Rhee, D. J., Turalba, A. V, Chen, T. C., Wand, M., & Pasquale, L. R. (2014). Effect of Brimonidine on Retinal Vascular Autoregulation and Short-term Visual Function in Normal Tension Glaucoma. *American Journal of Ophthalmology*, *158*(1), 105-112.e1. https://doi.org/10.1016/j.ajo.2014.03.015

Foot, B., & MacEwen, C. (2017). Surveillance of sight loss due to delay in ophthalmic treatment or review: frequency, cause and outcome. *Eye*, *31*(5), 771–775. https://doi.org/10.1038/eye.2017.1

Fortune, B., Reynaud, J., Hardin, C., Wang, L., Sigal, I. A., & Burgoyne, C. F. (2016). Experimental glaucoma causes optic nerve head neural rim tissue compression: A potentially important mechanism of axon injury. *Investigative Ophthalmology and Visual Science*, *57*(10), 4403–4411. https://doi.org/10.1167/iovs.16-20000

Foxton, R., Osborne, A., Martin, K. R., Ng, Y.-S., & Shima, D. T. (2016). Distal retinal ganglion cell axon transport loss and activation of p38 MAPK stress pathway following VEGF-A antagonism. *Cell Death & Disease*, *7*(5), e2212–e2212. https://doi.org/10.1038/cddis.2016.110

Friedman, D. S., Wilson, M. R., Liebmann, J. M., Fechtner, R. D., & Weinreb, R. N. (2004). An evidence-based assessment of risk factors for the progression of ocular hypertension and glaucoma. *American Journal of Ophthalmology*, *138*(3 SUPPL.). https://doi.org/10.1016/j.ajo.2004.04.058

Gao, H., Qiao, X., LB, C., & WuDunn, D. (2002). Upregulation of brain-derived neurotrophic factor expression by brimonidine in rat retinal ganglion cells. *Archives of Ophthalmology*, *120*(6), 797–803. http://dx.doi.org/10.1001/archopht.120.6.797

Gao, X. R., Huang, H., & Kim, H. (2019). Polygenic Risk Score Is Associated With Intraocular Pressure and Improves Glaucoma Prediction in the UK Biobank Cohort. *Translational Vision Science & Technology*, *8*(2), 10. https://doi.org/10.1167/tvst.8.2.10

García-Feijoo, J., Rau, M., Grisanti, S., Grisanti, S., Höh, H., Erb, C., Guguchkova, P., Ahmed, I., Grabner, G., Reitsamer, H., Shaarawy, T., & Ianchulev, T. (2015). Supraciliary Micro-stent Implantation for Open-Angle Glaucoma Failing Topical Therapy: 1-Year Results of a Multicenter Study. *American Journal of Ophthalmology*, *159*(6), 1075-1081.e1. https://doi.org/10.1016/j.ajo.2015.02.018

Garway-Heath, D. F., Crabb, D. P., Bunce, C., Lascaratos, G., Amalfitano, F., Anand, N., Azuara-Blanco, A., Bourne, R. R., Broadway, D. C., Cunliffe, I. A., Diamond, J. P., Fraser, S. G., Ho, T. A., Martin, K. R., McNaught, A. I., Negi, A., Patel, K., Russell, R. A., Shah, A., … Zeyen, T. G. (2015). Latanoprost for open-

angle glaucoma (UKGTS): A randomised, multicentre, placebo-controlled trial. *The Lancet*, *385*(9975), 1295–1304. https://doi.org/10.1016/S0140-6736(14)62111-5

Gasparini, L., Anthony Crowther, R., Martin, K. R., Berg, N., Coleman, M., Goedert, M., & Spillantini, M. G. (2011). Tau inclusions in retinal ganglion cells of human P301S tau transgenic mice: Effects on axonal viability. *Neurobiology of Aging*, *32*(3), 419–433. https://doi.org/10.1016/j.neurobiolaging.2009.03.002

Gates, M. A., Tai, C. C., & Macklis, J. D. (2000). Neocortical neurons lacking the protein-tyrosine kinase B receptor display abnormal differentiation and process elongation in vitro and in vivo. *Neuroscience*, *98*(3), 437–447. https://doi.org/https://doi.org/10.1016/S0306-4522(00)00106-8

Georgiadis, A., Duran, Y., Ribeiro, J., Abelleira-Hervas, L., Robbie, S. J., Sünkel-Laing, B., Fourali, S., Gonzalez-Cordero, A., Cristante, E., Michaelides, M., Bainbridge, J. W. B., Smith, A. J., & Ali, R. R. (2016). Development of an optimized AAV2/5 gene therapy vector for Leber congenital amaurosis owing to defects in RPE65. *Gene Therapy*, *23*, 857. https://doi.org/10.1038/gt.2016.66

Geyer, O., Almog, J., Lupu-Meiri, M., Lazar, M., & Oron, Y. (1995). Nitric oxide synthase inhibitors protect rat retina against ischemic injury. *FEBS Letters*, *374*(3), 399–402. https://doi.org/10.1016/0014-5793(95)01147-7

Goh, R. L. Z., Xiang, Y., Kong, G., Mcalinden, C., Liu, J., Crowston, J. G., & Skalicky, S. E. (2018). *Objective Assessment of Activity Limitation in Glaucoma with Smartphone Virtual Reality Goggles : A Pilot Study*. *7*(1), 10.

Goldberg, J. L., Espinosa, J. S., Xu, Y., Davidson, N., Kovacs, G. T. A., & Barres, B. A. (2002). Retinal Ganglion Cells Do Not Extend Axons by Default: Promotion by Neurotrophic Signaling and Electrical Activity. *Neuron*, *33*(5), 689–702.

https://doi.org/10.1016/S0896-6273(02)00602-5

Goldberg, J. L., & Guido, W. (2016). Report on the National Eye Institute Audacious Goals Initiative: Regenerating the Optic Nerve. *Investigative Ophthalmology & Visual Science*, *57*(3), 1271–1275. https://doi.org/10.1167/iovs.15-18500

Gordon, M. O., Kass, M. A., & Group, for the O. H. T. S. (1999). The Ocular Hypertension Treatment Study Design and Baseline Description of the Participants. *Arch Ophthalmol*, *117*(5), 573–583. https://doi.org/doi:10.1001/archopht.117.5.573

Goyal, R., & Raghu Ram, A. R. (2000). Brimonidine tartarate 0.2% (Alphagan) associated granulomatous anterior uveitis. *Eye*, *14*(6), 908–910. https://doi.org/10.1038/eye.2000.250

Gray, S. F., Spencer, I. C., Spry, P. G., Brookes, S. T., Baker, I. A., Peters, T. J., Sparrow, J. M., & Easty, D. L. (1997). The Bristol shared care glaucoma study – validity of measurements and patient satisfaction. *Journal of Public Health*, *19*(4), 431–436. https://doi.org/10.1093/oxfordjournals.pubmed.a024673

Gray, S. F., Spry, P. G. D., Brookes, S. T., Peters, T. J., Spencer, I. C., Baker, I. A., Sparrow, J. M., & Easty, D. L. (2000). The Bristol shared care glaucoma study: outcome at follow up at 2 years. *British Journal of Ophthalmology*, *84*(5), 456 LP – 463. https://doi.org/10.1136/bjo.84.5.456

Gregory-Ksander, M. S., Fei, F., Marshak-Rothstein, A., Ksander, B., & Krishnan, A. (2016). Soluble Fas ligand provides long-term protection in a chronic mouse model of glaucoma by inhibiting glial activation, inflammation, and apoptosis. *Investigative Ophthalmology & Visual Science*, *57*(12). http://dx.doi.org/

Groszer, M., Erickson, R., Scripture-Adams, D. D., Lesche, R., Trumpp, A., Zack, J. A., Kornblum, H. I., Liu, X., & Wu, H. (2001). Negative Regulation of Neural

Stem/Progenitor Cell Proliferation by the Pten Tumor Suppressor Gene in Vivo. *Science*, *294*(5549), 2186 LP – 2189. https://doi.org/10.1126/science.1065518

Guo, L., Moss, S. E., Alexander, R. A., Ali, R. R., Fitzke, F. W., & Cordeiro, M. F. (2005). Retinal ganglion cell apoptosis in glaucoma is related to intraocular pressure and IOP-induced effects on extracellular matrix. *Investigative Ophthalmology and Visual Science*, *46*(1), 175–182. https://doi.org/10.1167/iovs.04-0832

Gupta, N., Fong, J., Ang, L. C., & Yücel, Y. H. (2008). Retinal tau pathology in human glaucomas. *Canadian Journal of Ophthalmology*, *43*(1), 53–60. https://doi.org/10.3129/i07-185

György, B., Wassmer, S., Carvalho, L., Maguire, C., & Vandenberghe, L. H. (2016). 594. Exosome-Associated AAV Enhances Retinal Transduction Following Intravitreal Injection. *Molecular Therapy*, *24*, S235. https://doi.org/10.1016/S1525-0016(16)33402-5

Hadoux, X., Hui, F., Lim, J. K. H., Masters, C. L., Pébay, A., Chevalier, S., Ha, J., Loi, S., Fowler, C. J., Rowe, C., Villemagne, V. L., Taylor, E. N., Fluke, C., Soucy, J.-P., Lesage, F., Sylvestre, J.-P., Rosa-Neto, P., Mathotaarachchi, S., Gauthier, S., … van Wijngaarden, P. (2019). Non-invasive in vivo hyperspectral imaging of the retina for potential biomarker use in Alzheimer's disease. *Nature Communications*, *10*(1), 4227. https://doi.org/10.1038/s41467-019-12242-1

Hann, C. R., Bentley, M. D., Vercnocke, A., Ritman, E. L., & Fautsch, M. P. (2011). Imaging the aqueous humor outflow pathway in human eyes by three-dimensional micro-computed tomography (3D micro-CT). *Experimental Eye Research*, *92*(2), 104–111. https://doi.org/10.1016/j.exer.2010.12.010

Harada, C., Azuchi, Y., Noro, T., Guo, X., Kimura, A., Namekata, K., & Harada, T. (2015). TrkB Signaling in Retinal Glia Stimulates Neuroprotection after Optic Nerve Injury. *The American Journal of Pathology*, *185*(12), 3238–3247. https://doi.org/10.1016/j.ajpath.2015.08.005

Harada, C., Guo, X., Namekata, K., Kimura, A., Nakamura, K., Tanaka, K., Parada, L. F., & Harada, T. (2011). Glia- and neuron-specific functions of TrkB signalling during retinal degeneration and regeneration. *Nature Communications*, *2*, 189. https://doi.org/10.1038/ncomms1190

Hare, W. A., WoldeMussie, E., Lai, R. K., Ton, H., Ruiz, G., Chun, T., & Wheeler, L. (2004). Efficacy and Safety of Memantine Treatment for Reduction of Changes Associated with Experimental Glaucoma in Monkey, I: Functional Measures. *Investigative Opthalmology & Visual Science*, *45*(8), 2625. https://doi.org/10.1167/iovs.03-0566

Harward, S. C., Hedrick, N. G., Hall, C. E., Parra-Bueno, P., Milner, T. A., Pan, E., Laviv, T., Hempstead, B. L., Yasuda, R., & McNamara, J. O. (2016). Autocrine BDNF-TrkB signalling within a single dendritic spine. *Nature*, *538*(7623), 99–103. https://doi.org/10.1038/nature19766

Harwerth, R. S., Carter-Dawson, L., Shen, F., Smith Earl L., I. I. I., & Crawford, M. L. J. (1999). Ganglion Cell Losses Underlying Visual Field Defects from Experimental Glaucoma. *Investigative Ophthalmology & Visual Science*, *40*(10), 2242–2250. http://dx.doi.org/

Harwerth, R. S., & Quigley, H. A. (2006). *Visual Field Defects and Retinal Ganglion Cell Losses in Human Glaucoma Patients*. *124*(6), 853–859.

Healey, P. R., Lee, A. J., Aung, T., Wong, T. Y., & Mitchell, P. (2010). Diagnostic Accuracy of the Heidelberg Retina Tomograph for Glaucoma: A Population-

Based Assessment. *Ophthalmology*, *117*(9), 1667–1673. https://doi.org/https://doi.org/10.1016/j.ophtha.2010.07.001

Heijl, A., Buchholz, P., Norrgren, G., & Bengtsson, B. (2013). Rates of visual field progression in clinical glaucoma care. *Acta Ophthalmologica*, *91*(5), 406–412. https://doi.org/10.1111/j.1755-3768.2012.02492.x

Hernández, M., Urcola, J. H., & Vecino, E. (2008). Retinal ganglion cell neuroprotection in a rat model of glaucoma following brimonidine, latanoprost or combined treatments. *Experimental Eye Research*, *86*(5), 798–806. https://doi.org/10.1016/j.exer.2008.02.008

Hevner, R. F. (2000). Development of Connections in the Human Visual System During Fetal Mid-Gestation: A Dil-Tracing Study. *Journal of Neuropathology & Experimental Neurology*, *59*(5), 385–392. https://doi.org/10.1093/jnen/59.5.385

Hirsch, T., Rothoeft, T., Teig, N., Bauer, J. W., Rosa, L. De, Scaglione, D., Reichelt, J., Klausegger, A., Kneisz, D., Romano, O., Seconetti, A. S., Contin, R., Jurman, I., Carulli, S., Jacobsen, F., Luecke, T., Fischer, M., Kueckelhaus, M., Quaglino, D., … Luca, M. De. (2018). *Europe PMC Funders Group Regeneration of the entire human epidermis by transgenic stem cells*. *551*(7680), 327–332. https://doi.org/10.1038/nature24487.Regeneration

Hodapp, E., Parrish, R. I., & Anderson, D. (1993). St Louis: The CV Mosby Co. In *Clinical decisions in glaucoma.* (pp. 52–61). St Louis: The CV Mosby Co.

Hollis 2nd, E. R., Jamshidi, P., Löw, K., Blesch, A., & Tuszynski, M. H. (2009). Induction of corticospinal regeneration by lentiviral trkB-induced Erk activation. *Proceedings of the National Academy of Sciences of the United States of America*, *106*(17), 7215–7220. https://doi.org/10.1073/pnas.0810624106

Hood, D. C., & Raza, A. S. (2011). Method for comparing visual field defects to local

RNFL and RGC damage seen on frequency domain OCT in patients with glaucoma. *Biomedical Optics Express*, *2*(5), 1097–1105. https://doi.org/10.1364/BOE.2.001097

Hood, D. C., & Raza, A. S. (2014). On improving the use of OCT imaging for detecting glaucomatous damage. *The British Journal of Ophthalmology*, *98 Suppl 2*(Suppl 2), ii1–ii9. https://doi.org/10.1136/bjophthalmol-2014-305156

Hopkins, M. E., & Bucci, D. J. (2010). BDNF expression in perirhinal cortex is associated with exercise-induced improvement in object recognition memory. *Neurobiology of Learning and Memory*, *94*(2), 278–284. https://doi.org/10.1016/j.nlm.2010.06.006

Hösel, M., Broxtermann, M., Janicki, H., Esser, K., Arzberger, S., Hartmann, P., Gillen, S., Kleeff, J., Stabenow, D., Odenthal, M., Knolle, P., Hallek, M., Protzer, U., & Büning, H. (2012). Toll-like receptor 2–mediated innate immune response in human nonparenchymal liver cells toward adeno-associated viral vectors. *Hepatology*, *55*(1), 287–297. https://doi.org/10.1002/hep.24625

Howell, G. R., Libby, R. T., Jakobs, T. C., Smith, R. S., Phalan, F. C., Barter, J. W., Barbay, J. M., Marchant, J. K., Mahesh, N., Porciatti, V., Whitmore, A. V, Masland, R. H., & John, S. W. M. (2007). Axons of retinal ganglion cells are insulted in the optic nerve early in DBA/2J glaucoma. *The Journal of Cell Biology*, *179*(7), 1523 LP – 1537. https://doi.org/10.1083/jcb.200706181

Howell, G. R., MacNicoll, K. H., Braine, C. E., Soto, I., Macalinao, D. G., Sousa, G. L., & John, S. W. M. (2014). Combinatorial targeting of early pathways profoundly inhibits neurodegeneration in a mouse model of glaucoma. *Neurobiology of Disease*, *71*, 44–52. https://doi.org/10.1016/j.nbd.2014.07.016

Huang, A. S., Camp, A., Xu, B. Y., Penteado, R. C., & Weinreb, R. N. (2017).

Aqueous Angiography: Aqueous Humor Outflow Imaging in Live Human Subjects. *Ophthalmology*, *124*(8), 1249–1251. https://doi.org/10.1016/j.ophtha.2017.03.058

Huang, A. S., Li, M., Yang, D., Wang, H., Wang, N., & Weinreb, R. N. (2017). Aqueous Angiography in Living Nonhuman Primates Shows Segmental, Pulsatile, and Dynamic Angiographic Aqueous Humor Outflow. *Ophthalmology*, *124*(6), 793–803. https://doi.org/10.1016/j.ophtha.2017.01.030

Hui, F., Tang, J., Williams, P. A., McGuinness, M. B., Hadoux, X., Casson, R. J., Coote, M., Trounce, I. A., Martin, K. R., van Wijngaarden, P., & Crowston, J. G. (2020). Improvement in inner retinal function in glaucoma with nicotinamide (vitamin B3) supplementation: A crossover randomized clinical trial. *Clinical & Experimental Ophthalmology*, *48*(7), 903–914. https://doi.org/10.1111/ceo.13818

Jain, A., Zode, G., Kasetti, R. B., Ran, F. A., Yan, W., Sharma, T. P., Bugge, K., Searby, C. C., Fingert, J. H., Zhang, F., Clark, A. F., & Sheffield, V. C. (2017). CRISPR-Cas9–based treatment of myocilin-associated glaucoma. *Proceedings of the National Academy of Sciences*, *114*(42), 11199–11204. https://doi.org/10.1073/pnas.1706193114

Jeffery, G. (2001). Architecture of the Optic Chiasm and the Mechanisms That Sculpt Its Development. *Physiological Reviews*, *81*(4), 1393–1414. https://doi.org/10.1152/physrev.2001.81.4.1393

Johnson, C. A. (1993). Blue-on-Yellow Perimetry Can Predict the Development of Glaucomatous Visual Field Loss. *Archives of Ophthalmology*, *111*(5), 645. https://doi.org/10.1001/archopht.1993.01090050079034

Johnson, C. A. (1995). Short-Wavelength Automated Perimetry in Low-, Medium-,

and High-Risk Ocular Hypertensive Eyes. *Archives of Ophthalmology*, *113*(1), 70. https://doi.org/10.1001/archopht.1995.01100010072023

Johnson, T. V., Bull, N. D., Hunt, D. P., Marina, N., Tomarev, S. I., & Martin, K. R. (2010). Neuroprotective effects of intravitreal mesenchymal stem cell transplantation in experimental glaucoma. *Investigative Ophthalmology and Visual Science*, *51*(4), 2051–2059. https://doi.org/10.1167/iovs.09-4509

Johnson, T. V., Dekorver, N. W., Levasseur, V. A., Osborne, A., Tassoni, A., Lorber, B., Heller, J. P., Villasmil, R., Bull, N. D., Martin, K. R., & Tomarev, S. I. (2014). Identification of retinal ganglion cell neuroprotection conferred by platelet-derived growth factor through analysis of the mesenchymal stem cell secretome. *Brain*, *137*(2), 503–519. https://doi.org/10.1093/brain/awt292

Johnstone, M. A. (2004). The aqueous outflow system as a mechanical pump: Evidence from examination of tissue and aqueous movement in human and non-human primates. *Journal of Glaucoma*, *13*(5), 421–438. https://doi.org/10.1097/01.ijg.0000131757.63542.24

Joint RCOphth and UKEGS Glaucoma Risk Stratification Tool (2020) Available at: https://www.rcophth.ac.uk/wp-content/uploads/2020/08/Glaucoma-Risk-Stratification-Tool-1.pdf. (n.d.).

Jones, R. F., & Maurice, D. M. (1966). New methods of measuring the rate of aqueous flow in man with fluorescein. *Experimental Eye Research*, *5*(3), 208–220. https://doi.org/10.1016/S0014-4835(66)80009-X

Kagemann, L., Wollstein, G., Ishikawa, H., Nadler, Z., Sigal, I. A., Folio, L. S., & Schuman, J. S. (2012). Visualization of the conventional outflow pathway in the living human eye. *Ophthalmology*, *119*(8), 1563–1568. https://doi.org/10.1016/j.ophtha.2012.02.032

Kagemann, L., Wollstein, G., Ishikawa, H., Sigal, I. A., Folio, L. S., Xu, J., Gong, H., & Schuman, J. S. (2011a). 3D visualization of aqueous humor outflow structures in-situ in humans. *Experimental Eye Research*, *93*(3), 308–315. https://doi.org/10.1016/j.exer.2011.03.019

Kagemann, L., Wollstein, G., Ishikawa, H., Sigal, I. A., Folio, L. S., Xu, J., Gong, H., & Schuman, J. S. (2011b). 3D visualization of aqueous humor outflow structures in-situ in humans. *Experimental Eye Research*, *93*(3), 308–315. https://doi.org/10.1016/j.exer.2011.03.019

Kamal, D., & Hitchings, R. (1998). Normal tension glaucoma--a practical approach. *The British Journal of Ophthalmology*, *82*(7), 835–840. https://www.ncbi.nlm.nih.gov/pubmed/9924383

Kang, H., & Schuman, E. M. (1995). Long-lasting neurotrophin-induced enhancement of synaptic transmission in the adult hippocampus. *Science*, *267*(5204), 1658–1662. https://doi.org/10.1126/science.7886457

Keenan, J., Shahid, H., Bourne, R. R., White, A. J., & Martin, K. R. (2015). Cambridge community Optometry Glaucoma Scheme. *Clinical & Experimental Ophthalmology*, *43*(3), 221–227. https://doi.org/10.1111/ceo.12398

Kent, A. R., Nussdorf, J. D., David, R., Tyson, F., Small, D., & Fellows, D. (2001). Vitreous concentration of topically applied brimonidine tartrate 0.2%. *Ophthalmology*, *108*(4), 784–787. https://doi.org/10.1016/S0161-6420(00)00654-0

Kerrigan–Baumrind, L. A., Quigley, H. A., E., P. M., Kerrigan, D. F., & Mitchell, R. S. (2000). The number of retinal ganglion cells in glaucoma eyes compared to threshold visual field data in the same eyes. *Investigative Ophthalmology and Visual Science*, *41*, 741–748.

Khatib, T. Z., & Martin, K. R. (2020). Neuroprotection in Glaucoma: Towards Clinical Trials and Precision Medicine. *Current Eye Research*, *45*(3), 327–338. https://doi.org/10.1080/02713683.2019.1663385

Kim, J. Y., You, Y. S., Kim, S. H., & Kwon, O. W. (2016). EPIRETINAL MEMBRANE FORMATION AFTER INTRAVITREAL AUTOLOGOUS STEM CELL IMPLANTATION IN A RETINITIS PIGMENTOSA PATIENT. *Retinal Cases & Brief Reports*. https://doi.org/10.1097/ICB.0000000000000327

Kim, S.-Y., Kwak, J.-S., Shin, J.-P., & Lee, S.-H. (1998). The Protection of the Retina from Ischemic Injury by the Free Radical Scavenger EGb 761 and Zinc in the Cat Retina. *Ophthalmologica*, *212*(4), 268–274. http://www.karger.com/DOI/10.1159/000027305

Kirwan, J. F., Hustler, A., Bobat, H., & Toms, L. (2014). *Portsmouth visual field database : an audit of glaucoma progression*. *28*(8), 974–979. https://doi.org/10.1038/eye.2013.294

Kong, Y. X., Crowston, J. G., Vingrys, A. J., Trounce, I. A., & Bui, B. V. (2009). Functional changes in the retina during and after acute intraocular pressure elevation in mice. *Investigative Ophthalmology and Visual Science*, *50*(12), 5732–5740. https://doi.org/10.1167/iovs.09-3814

Kong, Y. X. G., van Bergen, N., Bui, B. V., Chrysostomou, V., Vingrys, A. J., Trounce, I. A., & Crowston, J. G. (2012). Impact of aging and diet restriction on retinal function during and after acute intraocular pressure injury. *Neurobiology of Aging*, *33*(6), 1126.e15-1126.e25. https://doi.org/10.1016/J.NEUROBIOLAGING.2011.11.026

Kotecha, A., Brookes, J., & Foster, P. J. (2017). A technician-delivered 'virtual clinic' for triaging low-risk glaucoma referrals. *Eye*, *31*(6), 899–905.

https://doi.org/10.1038/eye.2017.9

Kouassi Nzoughet, J., Chao de la Barca, J. M., Guehlouz, K., Leruez, S., Coulbault, L., Allouche, S., Bocca, C., Muller, J., Amati-Bonneau, P., Gohier, P., Bonneau, D., Simard, G., Milea, D., Lenaers, G., Procaccio, V., & Reynier, P. (2019). Nicotinamide Deficiency in Primary Open-Angle GlaucomaNicotinamide Deficiency in Glaucoma. *Investigative Ophthalmology & Visual Science*, *60*(7), 2509–2514. https://doi.org/10.1167/iovs.19-27099

Kruger, K., Tam, A. S., Lu, C., & Sretavan, D. W. (1998). Retinal Ganglion Cell Axon Progression from the Optic Chiasm to Initiate Optic Tract Development Requires Cell Autonomous Function of GAP-43. *The Journal of Neuroscience*, *18*(15), 5692 LP – 5705. https://doi.org/10.1523/JNEUROSCI.18-15-05692.1998

Krupin, T., Liebmann, J. M., Greenfield, D. S., Ritch, R., & Gardiner, S. (2011). A randomized trial of brimonidine versus timolol in preserving visual function: Results from the low-pressure glaucoma treatment study. *American Journal of Ophthalmology*, *151*(4), 671–681. https://doi.org/10.1016/j.ajo.2010.09.026

Kuriyan, A. E., Albini, T. A., Townsend, J. H., Rodriguez, M., Pandya, H. K., Leonard, R. E., Parrott, M. B., Rosenfeld, P. J., Flynn, H. W., & Goldberg, J. L. (2017). Vision Loss after Intravitreal Injection of Autologous “Stem Cells” for AMD. *New England Journal of Medicine*, *376*(11), 1047–1053. https://doi.org/10.1056/NEJMoa1609583

Kwon, Y. H., Fingert, J. H., Kuehn, M. H., & Alward, W. L. M. (2009). Primary Open-Angle Glaucoma. *New England Journal of Medicine*, *360*(11), 1113–1124. https://doi.org/10.1056/NEJMra0804630

Lack of Timely Monitoring of Patients with Glaucoma. Healthcare Safety Investigation 2019/001. United Kingdom: Healthcare Safety Investigation

Branch; 2020. (n.d.).

Lambiase, A., Rama, P., Bonini, S., Caprioglio, G., & Aloe, L. (1998). Topical Treatment with Nerve Growth Factor for Corneal Neurotrophic Ulcers. *New England Journal of Medicine*, *338*(17), 1174–1180. https://doi.org/10.1056/NEJM199804233381702

Landers, J. A., Goldberg, I., & Graham, S. L. (2003). Detection of early visual field loss in glaucoma using frequency-doubling perimetry and short-wavelength automated perimetry. *Archives of Ophthalmology*, *121*(12), 1705–1710. http://dx.doi.org/10.1001/archopht.121.12.1705

Landers, J., Martin, K., Sarkies, N., Bourne, R., & Watson, P. (2012). A twenty-year follow-up study of trabeculectomy: Risk factors and outcomes. *Ophthalmology*, *119*(4), 694–702. https://doi.org/10.1016/j.ophtha.2011.09.043

Le, J. T., Bicket, A. K., Wang, L., & Li, T. (2019). Ab interno trabecular bypass surgery with iStent for open-angle glaucoma. *The Cochrane Database of Systematic Reviews*, *3*(3), CD012743. https://doi.org/10.1002/14651858.CD012743.pub2

Lee, J. M., Caprioli, J., Nouri-Mahdavi, K., Afifi, A. A., Morales, E., Ramanathan, M., Yu, F., & Coleman, A. L. (2014). Baseline Prognostic Factors Predict Rapid Visual Field Deterioration in Glaucoma. *Investigative Ophthalmology & Visual Science*, *55*(4), 2228–2236. http://dx.doi.org/10.1167/iovs.13-12261

Leibinger, M., Andreadaki, A., Gobrecht, P., Levin, E., Diekmann, H., & Fischer, D. (2016). Boosting Central Nervous System Axon Regeneration by Circumventing Limitations of Natural Cytokine Signaling. *Molecular Therapy : The Journal of the American Society of Gene Therapy*, *24*(10), 1712–1725. https://doi.org/10.1038/mt.2016.102

Leon, S., Yin, Y., Nguyen, J., Irwin, N., & Benowitz, L. I. (2000). Lens Injury Stimulates Axon Regeneration in the Mature Rat Optic Nerve. *The Journal of Neuroscience*, *20*(12), 4615 LP – 4626. https://doi.org/10.1523/JNEUROSCI.20-12-04615.2000

Leske, M. C., Heijl, A., Hussein, M., Bengtsson, B., Hyman, L., Komaroff, E., & Group, for the E. M. G. T. (2003). Factors for Glaucoma Progression and the Effect of Treatment: The Early Manifest Glaucoma Trial. *Archives of Ophthalmology*, *121*(1), 48–56. https://doi.org/10.1001/archopht.121.1.48

Leske, M. C., Heijl, A., Hyman, L., & Bengtsson, B. (1999). Early manifest glaucoma trial: Design and baseline data. *Ophthalmology*, *106*(11), 2144–2153. https://doi.org/10.1016/S0161-6420(99)90497-9

Leske, M. C., Heijl, A., Hyman, L., Bengtsson, B., Dong, L., & Yang, Z. (2007). Predictors of Long-term Progression in the Early Manifest Glaucoma Trial. *Ophthalmology*, *114*(11), 1965–1972. https://doi.org/10.1016/j.ophtha.2007.03.016

Levkovitch-Verbin, H., Quigley, H. A., Martin, K. R. G., Valenta, D., Baumrind, L. A., & Pease, M. E. (2002). Translimbal laser photocoagulation to the trabecular meshwork as a model of glaucoma in rats. *Investigative Ophthalmology & Visual Science*, *43*(2), 402–410.

Lewis, R. A., Christie, W. C., Day, D. G., Craven, E. R., Walters, T., Bejanian, M., Lee, S. S., Goodkin, M. L., Zhang, J., Whitcup, S. M., Robinson, M. R., Aung, T., Beck, A. D., Christie, W. C., Coote, M., Crane, C. J., Craven, E. R., Crichton, A., Day, D. G., … Walters, T. R. (2017). Bimatoprost Sustained-Release Implants for Glaucoma Therapy: 6-Month Results From a Phase I/II Clinical Trial. *American Journal of Ophthalmology*, *175*, 137–147.

https://doi.org/https://doi.org/10.1016/j.ajo.2016.11.020

Lim, J.-H. A., Stafford, B. K., Nguyen, P. L., Lien, B. V, Wang, C., Zukor, K., He, Z., & Huberman, A. D. (2016). Neural activity promotes long-distance, target-specific regeneration of adult retinal axons. *Nature Neuroscience*, *19*(July), 1–14. https://doi.org/10.1038/nn.4340

Loewen, R. T., Waxman, S., Wang, C., Atta, S., Chen, S., Watkins, S. C., Watson, A. M., & Loewen, N. A. (2020). 3D-Reconstruction of the human conventional outflow system by ribbon scanning confocal microscopy. *PLOS ONE*, *15*(5), e0232833. https://doi.org/10.1371/journal.pone.0232833

Lohof, A. M., Ip, N. Y., & Poo, M. (1993). Potentiation of developing neuromuscular synapses by the neurotrophins NT-3 and BDNF. *Nature*, *363*(6427), 350–353. https://doi.org/10.1038/363350a0

Lorber, B., Guidi, A., Fawcett, J. W., & Martin, K. R. (2012). Activated retinal glia mediated axon regeneration in experimental glaucoma. *Neurobiology of Disease*, *45*(1), 243–252. https://doi.org/10.1016/j.nbd.2011.08.008

Lu, Y., Brommer, B., Tian, X., Krishnan, A., Meer, M., Wang, C., Vera, D. L., Zeng, Q., Yu, D., Bonkowski, M. S., Yang, J.-H., Zhou, S., Hoffmann, E. M., Karg, M. M., Schultz, M. B., Kane, A. E., Davidsohn, N., Korobkina, E., Chwalek, K., … Sinclair, D. A. (2020). Reprogramming to recover youthful epigenetic information and restore vision. *Nature*, *588*(7836), 124–129. https://doi.org/10.1038/s41586-020-2975-4

Lund, R. D. (1965). Uncrossed Visual Pathways of Hooded and Albino Rats. *Science*, *149*(3691), 1506–1507. https://doi.org/10.1126/science.149.3691.1506

Lusthaus, J. A., Khatib, T. Z., Meyer, P. A. R., McCluskey, P., & Martin, K. R. (2021). Aqueous outflow imaging techniques and what they tell us about intraocular

pressure regulation. *Eye (London, England)*, *35*(1), 216–235. https://doi.org/10.1038/s41433-020-01136-y

Lusthaus, J. A., Meyer, P. A. R., Khatib, T. Z., & Martin, K. R. (2020). The Effects of Trabecular Bypass Surgery on Conventional Aqueous Outflow, Visualized by Hemoglobin Video Imaging. *Journal of Glaucoma*, *29*(8), 656–665. https://doi.org/10.1097/IJG.0000000000001561

Malihi, M., Moura Filho, E. R., Hodge, D. O., & Sit, A. J. (2014). Long-Term Trends in Glaucoma-Related Blindness in Olmsted County, Minnesota. *Ophthalmology*, *121*(1), 134–141. https://doi.org/10.1016/j.ophtha.2013.09.003.Long-Term

Mandalos, A., Bourne, R., French, K., Newsom, W., & Chang, L. (2012). Shared care of patients with ocular hypertension in the Community and Hospital Allied Network Glaucoma Evaluation Scheme (CHANGES). *Eye*, *26*(4), 564–567. https://doi.org/10.1038/eye.2011.350

Marina, N., Bull, N. D., & Martin, K. R. (2010). A semiautomated targeted sampling method to assess optic nerve axonal loss in a rat model of glaucoma. *Nature Protocols*, *5*, 1642. https://doi.org/10.1038/nprot.2010.128

Martin, K. R. G., Quigley, H. A., Valenta, D., Kielczewski, J., & Pease, M. E. (2006). Optic nerve dynein motor protein distribution changes with intraocular pressure elevation in a rat model of glaucoma. *Experimental Eye Research*, *83*(2), 255–262. https://doi.org/10.1016/j.exer.2005.11.025

Martin, K. R. G., Quigley, H. A., Zack, D. J., Levkovitch-Verbin, H., Kielczewski, J., Valenta, D., Baumrind, L., Pease, M. E., Klein, R. L., & Hauswirth, W. W. (2003). Gene Therapy with Brain-Derived Neurotrophic Factor As a Protection: Retinal Ganglion Cells in a Rat Glaucoma Model. *Investigative Ophthalmology and Visual Science*, *44*, 4357–4365.

Martin, K. R., Quigley, H. A., Zack, D. J., Levkovitch-Verbin, H., Kielczewski, J., Valenta, D., Baumrind, L., Pease, M. E., Klein, R. L., & Hauswirth, W. W. (2003). Gene therapy with brain-derived neurotrophic factor as a protection: retinal ganglion cells in a rat glaucoma model. *Invest Ophthalmol Vis Sci*, *44*(10), 4357–4365. https://doi.org/10.1167/iovs.02-1332

Martino, A. T., Suzuki, M., Markusic, D. M., Zolotukhin, I., Ryals, R. C., Moghimi, B., Ertl, H. C. J., Muruve, D. A., Lee, B., & Herzog, R. W. (2011). The genome of self-complementary adeno-associated viral vectors increases Toll-like receptor 9-dependent innate immune responses in the liver. *Blood*, *117*(24), 6459–6468. https://doi.org/10.1182/blood-2010-10-314518

Marvasti, A. H., Tatham, A. J., Zangwill, L. M., Girkin, C. A., Liebmann, J. M., Weinreb, R. N., & Medeiros, F. A. (2013). The relationship between visual field index and estimated number of retinal ganglion cells in glaucoma. *PloS One*, *8*(10), e76590–e76590. https://doi.org/10.1371/journal.pone.0076590

Mayer, J., Wizov, S. S., & Spaeth, G. L. (2010). *Importance of Visual Acuity and Contrast Sensitivity in Patients With Glaucoma*. *128*(12), 1576–1582.

Mazzaro, N., Barini, E., Spillantini, M. G., Goedert, M., Medini, P., & Gasparini, L. (2016). Tau-Driven Neuronal and Neurotrophic Dysfunction in a Mouse Model of Early Tauopathy. *Journal of Neuroscience*, *36*(7), 2086–2100. https://doi.org/10.1523/JNEUROSCI.0774-15.2016

Mckendrick, A. M., Sampson, G. P., Walland, M. J., & Badcock, D. R. (2007). *Contrast Sensitivity Changes Due to Glaucoma and Normal Aging : Low-Spatial-Frequency Losses in Both Magnocellular and Parvocellular Pathways*. *48*, 2115–2122. https://doi.org/10.1167/iovs.06-1208

McNaught, A. I., Crabb, D. P., Fitzke, F. W., & Hitchings, R. A. (1996). Visual field

progression: Comparison of Humphrey Statpac and pointwise linear regression analysis. *Graefe's Archive for Clinical and Experimental Ophthalmology*, *234*(7), 411–418. https://doi.org/10.1007/BF02539406

Mehta, S. T., Luo, X., Park, K. K., Bixby, J. L., & Lemmon, V. P. (2016). Hyperactivated Stat3 boosts axon regeneration in the CNS. *Experimental Neurology*, *280*, 115–120. https://doi.org/10.1016/j.expneurol.2016.03.004

Mendell, J. R., Al-Zaidy, S., Shell, R., Arnold, W. D., Rodino-Klapac, L. R., Prior, T. W., Lowes, L., Alfano, L., Berry, K., Church, K., Kissel, J. T., Nagendran, S., L'Italien, J., Sproule, D. M., Wells, C., Cardenas, J. A., Heitzer, M. D., Kaspar, A., Corcoran, S., … Kaspar, B. K. (2017a). Single-Dose Gene-Replacement Therapy for Spinal Muscular Atrophy. *New England Journal of Medicine*, *377*(18), 1713–1722. https://doi.org/10.1056/NEJMoa1706198

Mendell, J. R., Al-Zaidy, S., Shell, R., Arnold, W. D., Rodino-Klapac, L. R., Prior, T. W., Lowes, L., Alfano, L., Berry, K., Church, K., Kissel, J. T., Nagendran, S., L'Italien, J., Sproule, D. M., Wells, C., Cardenas, J. A., Heitzer, M. D., Kaspar, A., Corcoran, S., … Kaspar, B. K. (2017b). Single-Dose Gene-Replacement Therapy for Spinal Muscular Atrophy. *New England Journal of Medicine*, *377*(18), 1713–1722. https://doi.org/10.1056/NEJMoa1706198

Mercken, M., Fischer, I., Kosik, K. S., & Nixon, R. A. (1995). Three distinct axonal transport rates for tau, tubulin, and other microtubule-associated proteins: evidence for dynamic interactions of tau with microtubules in vivo. *The Journal of Neuroscience : The Official Journal of the Society for Neuroscience*, *15*(12), 8259–8267. http://www.ncbi.nlm.nih.gov/pubmed/8613759

Meyer, P. A. R. (2018). Re-orchestration of blood flow by micro-circulations. *Eye (Basingstoke)*, *32*(2), 222–229. https://doi.org/10.1038/eye.2017.315

Milde, S., Adalbert, R., Elaman, M. H., & Coleman, M. P. (2015). Axonal transport declines with age in two distinct phases separated by a period of relative stability. *Neurobiology of Aging*, *36*(2), 971–981. https://doi.org/10.1016/j.neurobiolaging.2014.09.018

Minckler, D., Mosaed, S., Dustin, L., Francis, B., Apte, D., Bandel, R. E., Shetty, R., Barnett, E. M., C., B., D., B., T., C., D., R., R.L., C., K., D., D., M., J., C., F., C., N., D., R., F., … R., W. (2008). Trabectome (trabeculectomy - internal approach): Additional experience and extended follow-up. *Transactions of the American Ophthalmological Society*, *106*, 149–159. http://www.aosonline.org/xactions/2008/1545-6110_v106_p149.pdf%5Cnhttp://ovidsp.ovid.com/ovidweb.cgi?T=JS&PAGE=reference&D=emed11&NEWS=N&AN=358448094

Moon, Y., Sung, K. R., Kim, J. M., Shim, S. H., Yoo, C., & Park, J. H. (2017). Risk Factors Associated With Glaucomatous Progression in Pseudoexfoliation Patients. *Journal of Glaucoma*, *26*(12), 1107–1113. https://doi.org/10.1097/IJG.0000000000000791

Moraes, C. G. De, Liebmann, J. M., & Levin, L. A. (2017). Detection and measurement of clinically meaningful visual field progression in clinical trials for glaucoma. *Progress in Retinal and Eye Research*, *56*, 107–147. https://doi.org/10.1016/j.preteyeres.2016.10.001.Detection

Moster, M. L., Sadun, A., Klopstock, T., Vignal-Clermont, C., Newman, N. J., Carelli, V., Yu-Wai-Man, P., Sahel, J.-A., & Katz, B. (2019). rAAV2/2-ND4 for the Treatment of LHON: 72-week Data from the REVERSE Phase III Clinical Trial (Plen02.002). *Neurology*, *92*(15 Supplement), Plen02.002. http://n.neurology.org/content/92/15_Supplement/Plen02.002.abstract

Mozaffarieh, M., Grieshaber, M. C., Orgül, S., & Flammer, J. (2016). The Potential Value of Natural Antioxidative Treatment in Glaucoma. *Survey of Ophthalmology*, *53*(5), 479–505. https://doi.org/10.1016/j.survophthal.2008.06.006

Mullany, S., Xiao, L., Qassim, A., Marshall, H., Gharahkhani, P., MacGregor, S., Hassall, M. M., Siggs, O. M., Souzeau, E., & Craig, J. E. (2021). Normal-tension glaucoma is associated with cognitive impairment. *British Journal of Ophthalmology*, bjophthalmol-2020-317461. https://doi.org/10.1136/bjophthalmol-2020-317461

Musch, D. C., Lichter, P. R., Guire, K. E., & Standardi, C. L. (1999). The collaborative initial glaucoma treatment study: Study design, methods, and baseline characteristics of enrolled patients. *Ophthalmology*, *106*(4), 653–662. https://doi.org/10.1016/S0161-6420(99)90147-1

Nieuwenhuis, B., Barber, A. C., Evans, R. S., Pearson, C. S., Fuchs, J., MacQueen, A. R., van Erp, S., Haenzi, B., Hulshof, L. A., Osborne, A., Conceicao, R., Khatib, T. Z., Deshpande, S. S., Cave, J., Ffrench-Constant, C., Smith, P. D., Okkenhaug, K., Eickholt, B. J., Martin, K. R., … Eva, R. (2020). PI 3-kinase delta enhances axonal PIP3 to support axon regeneration in the adult CNS. *EMBO Molecular Medicine*, *12*(8), e11674. https://doi.org/https://doi.org/10.15252/emmm.201911674

Nouri-Mahdavi, K., Nassiri, N., Giangiacomo, A., & Caprioli, J. (2011). Detection of visual field progression in glaucoma with standard achromatic perimetry: A review and practical implications. *Graefe's Archive for Clinical and Experimental Ophthalmology*, *249*(11), 1593–1616. https://doi.org/10.1007/s00417-011-1787-5

Nuschke, A. C., Farrell, S. R., Levesque, J. M., & Chauhan, B. C. (2015). Assessment of retinal ganglion cell damage in glaucomatous optic neuropathy: Axon transport, injury and soma loss. *Experimental Eye Research*, *141*, 111–124. https://doi.org/10.1016/j.exer.2015.06.006

Ohia-Nwoko, O., Montazari, S., Lau, Y.-S., & Eriksen, J. L. (2014). Long-term treadmill exercise attenuates tau pathology in P301S tau transgenic mice. *Molecular Neurodegeneration*, *9*, 54. https://doi.org/10.1186/1750-1326-9-54

Ollier, W., Sprosen, T., & Peakman, T. (2005). UK Biobank: from concept to reality. *Pharmacogenomics*, *6*(6), 639–646. https://doi.org/10.2217/14622416.6.6.639

Osborne, A., Khatib, T. Z., Songra, L., Barber, A. C., Hall, K., Kong, G. Y. X., Widdowson, P. S., & Martin, K. R. (2018). Neuroprotection of retinal ganglion cells by a novel gene therapy construct that achieves sustained enhancement of brain-derived neurotrophic factor/tropomyosin-related kinase receptor-B signaling. *Cell Death and Disease*, *9*(10). https://doi.org/10.1038/s41419-018-1041-8

Osborne, A., Sanderson, J., & Martin, K. R. (2018). Neuroprotective Effects of Human Mesenchymal Stem Cells and Platelet-Derived Growth Factor on Human Retinal Ganglion Cells. *Stem Cells*, *36*(1), 65–78. https://doi.org/10.1002/stem.2722

Osborne, A., Wang, A. X. Z., Tassoni, A., Widdowson, P. S., & Martin, K. R. (2018). Design of a Novel Gene Therapy Construct to Achieve Sustained Brain-Derived Neurotrophic Factor Signaling in Neurons. *Human Gene Therapy*, *29*(7), 828–841. https://doi.org/10.1089/hum.2017.069

Osborne, N. N., Lascaratos, G., Bron, A. J., Chidlow, G., & Wood, J. P. M. (2006). A hypothesis to suggest that light is a risk factor in glaucoma and the

mitochondrial optic neuropathies. *The British Journal of Ophthalmology*, *90*(2), 237–241. https://doi.org/10.1136/bjo.2005.082230

Ou, Y., Jo, R. E., Ullian, E. M., Wong, R. O. L., & Della Santina, L. (2016). Selective Vulnerability of Specific Retinal Ganglion Cell Types and Synapses after Transient Ocular Hypertension. *Journal of Neuroscience*, *36*(35), 9240–9252. https://doi.org/10.1523/jneurosci.0940-16.2016

Pang, J.-J., Frankfort, B. J., Gross, R. L., & Wu, S. M. (2015). Elevated intraocular pressure decreases response sensitivity of inner retinal neurons in experimental glaucoma mice. *Proceedings of the National Academy of Sciences*, *112*(8), 2593–2598. https://doi.org/10.1073/pnas.1419921112

Parc, C. E., Johnson, D. H., Oliver, J. E., Hattenhauer, M. G., & Hodge, D. O. (2001). The long-term outcome of glaucoma filtration surgery. *American Journal of Ophthalmology*, *132*(1), 27–35. https://doi.org/10.1016/S0002-9394(01)00923-0

Park, K. K., Liu, K., Hu, Y., Smith, P. D., Wang, C., Cai, B., Xu, B., Connolly, L., Kramvis, I., Sahin, M., & He, Z. (2008). Promoting axon regeneration in the adult CNS by modulation of the PTEN/mTOR pathway. *Science (New York, N.Y.)*, *322*(5903), 963–966. https://doi.org/10.1126/science.1161566

Park, Y. H., Snook, J. D., Ostrin, E. J., Kim, S., Chen, R., & Frankfort, B. J. (2019). Transcriptomic profiles of retinal ganglion cells are defined by the magnitude of intraocular pressure elevation in adult mice. *Scientific Reports*, *9*(1), 1–12. https://doi.org/10.1038/s41598-019-39141-1

Pearson, C. S., Mencio, C. P., Barber, A. C., Martin, K. R., & Geller, H. M. (2018). Identification of a critical sulfation in chondroitin that inhibits axonal regeneration. *ELife*, *7*, e37139. https://doi.org/10.7554/eLife.37139

Pease, M. E., Mckinnon, S. J., Quigley, H. A., Baumrind, L. A. K., & Zack, D. J.

(2000). *Obstructed Axonal Transport of BDNF and Its Receptor TrkB in Experimental Glaucoma AND*. *41*(3), 764–774.

Pease, M. E., Zack, D. J., Berlinicke, C., Bloom, K., Cone, F., Wang, Y., Klein, R. L., Hauswirth, W. W., & Quigley, H. A. (2009). Effect of CNTF on retinal ganglion cell survival in experimental glaucoma. *Investigative Ophthalmology & Visual Science*, *50*(5), 2194–2200. https://doi.org/10.1167/iovs.08-3013

Peters, D., Bengtsson, B., & Heijl, A. (2013). Lifetime risk of blindness in open-angle glaucoma. *American Journal of Ophthalmology*, *156*(4), 724–730. https://doi.org/10.1016/j.ajo.2013.05.027

Pradhan, J., Noakes, P. G., & Bellingham, M. C. (2019). The Role of Altered BDNF/TrkB Signaling in Amyotrophic Lateral Sclerosis . In *Frontiers in Cellular Neuroscience* (Vol. 13, p. 368). https://www.frontiersin.org/article/10.3389/fncel.2019.00368

Qassim, A., Souzeau, E., Siggs, O. M., Hassall, M. M., Han, X., Griffiths, H. L., Frost, N. A., Vallabh, N. A., Kirwan, J. F., Menon, G., Cree, A. J., Galanopoulos, A., Agar, A., Healey, P. R., Graham, S. L., Landers, J., Casson, R. J., Gharahkhani, P., Willoughby, C. E., … Craig, J. E. (2020). An Intraocular Pressure Polygenic Risk Score Stratifies Multiple Primary Open-Angle Glaucoma Parameters Including Treatment Intensity. *Ophthalmology*, *127*(7), 901–907. https://doi.org/10.1016/j.ophtha.2019.12.025

Quigley, H. A., McKinnon, S. J., Zack, D. J., Pease, M. E., Kerrigan-Baumrind, L. A., Kerrigan, D. F., & Mitchell, R. S. (2000). Retrograde axonal transport of BDNF in retinal ganglion cells is blocked by acute IOP elevation in rats. *Investigative Ophthalmology and Visual Science*, *41*(11), 3460–3466.

Quigley, Harry A. (2019). Glaucoma Neuroprotection Trials Are Practical Using

Visual Field Outcomes. *Ophthalmology Glaucoma*, *2*(2), 69–71. https://doi.org/10.1016/j.ogla.2019.01.009

Rhee, J., & Shih, K. C. (2021). Use of Gene Therapy in Retinal Ganglion Cell Neuroprotection: Current Concepts and Future Directions. In *Biomolecules* (Vol. 11, Issue 4). https://doi.org/10.3390/biom11040581

Risner, M. L., Pasini, S., Cooper, M. L., Lambert, W. S., & Calkins, D. J. (2018). Axogenic mechanism enhances retinal ganglion cell excitability during early progression in glaucoma. *Proceedings of the National Academy of Sciences*, *115*(10), E2393–E2402. https://doi.org/10.1073/pnas.1714888115

Rogers, G. L., & Herzog, R. W. (2014). TLR9 and Dendritic Cells Are Required for CD8⁺ T Cell Responses to the AAV Capsid. *Blood*, *124*(21), 552 LP – 552. http://www.bloodjournal.org/content/124/21/552.abstract

Rogers, G. L., Suzuki, M., Zolotukhin, I., Markusic, D. M., Morel, L. M., Lee, B., Ertl, H. C. J., & Herzog, R. W. (2015). Unique Roles of TLR9- and MyD88-Dependent and -Independent Pathways in Adaptive Immune Responses to AAV-Mediated Gene Transfer. *Journal of Innate Immunity*, *7*(3), 302–314. https://doi.org/10.1159/000369273

Romberg, C., Yang, S., Melani, R., Andrews, M. R., Horner, A. E., Spillantini, M. G., Bussey, T. J., Fawcett, J. W., Pizzorusso, T., & Saksida, L. M. (2013). Depletion of perineuronal nets enhances recognition memory and long-term depression in the perirhinal cortex. *The Journal of Neuroscience : The Official Journal of the Society for Neuroscience*, *33*(16), 7057–7065. https://doi.org/10.1523/JNEUROSCI.6267-11.2013

Rosenthal, R., & Fromm, M. (2011). Endothelin antagonism as an active principle for glaucoma therapy. *British Journal of Pharmacology*, *162*(4), 806–816.

https://doi.org/10.1111/j.1476-5381.2010.01103.x

Royal College of Ophthalmologists (2016). Commissioning Guide: Glaucoma Available at: https://www.rcophth.ac.uk/wp-content/uploads/2016/06/Glaucoma-Commissioning-Guide-Long-June-2016-Final.pdf. (n.d.).

Russell, S., Bennett, J., Wellman, J. A., Chung, D. C., Yu, Z.-F., Tillman, A., Wittes, J., Pappas, J., Elci, O., McCague, S., Cross, D., Marshall, K. A., Walshire, J., Kehoe, T. L., Reichert, H., Davis, M., Raffini, L., George, L. A., Hudson, F. P., … Maguire, A. M. (2017). Efficacy and safety of voretigene neparvovec (AAV2-hRPE65v2) in patients with RPE65-mediated inherited retinal dystrophy: a randomised, controlled, open-label, phase 3 trial. *The Lancet*, *390*(10097), 849–860. https://doi.org/10.1016/S0140-6736(17)31868-8

Russo, R., Cavaliere, F., Berliocchi, L., Nucci, C., Gliozzi, M., Mazzei, C., Tassorelli, C., Corasaniti, M. T., Rotiroti, D., Bagetta, G., & Morrone, L. A. (2008). Modulation of pro-survival and death-associated pathways under retinal ischemia/reperfusion: effects of NMDA receptor blockade. *Journal of Neurochemistry*, *107*(5), 1347–1357. https://doi.org/10.1111/j.1471-4159.2008.05694.x

Samuelson, T. W., Chang, D. F., Marquis, R., Flowers, B., Lim, K. S., Ahmed, I. I. K., Jampel, H. D., Aung, T., Crandall, A. S., & Singh, K. (2019). A Schlemm Canal Microstent for Intraocular Pressure Reduction in Primary Open-Angle Glaucoma and Cataract: The HORIZON Study. *Ophthalmology*, *126*(1), 29–37. https://doi.org/10.1016/j.ophtha.2018.05.012

Samuelson, T. W., Katz, L. J., Wells, J. M., Duh, Y.-J., & Giamporcaro, J. E. (2011). Randomized Evaluation of the Trabecular Micro-Bypass Stent with Phacoemulsification in Patients with Glaucoma and Cataract. *Ophthalmology*,

118(3), 459–467. https://doi.org/10.1016/j.ophtha.2010.07.007

Sarrafpour, S., Saleh, D., Ayoub, S., & Radcliffe, N. M. (2019). Micropulse Transscleral Cyclophotocoagulation: A Look at Long-Term Effectiveness and Outcomes. *Ophthalmology Glaucoma*, *2*(3), 167–171. https://doi.org/https://doi.org/10.1016/j.ogla.2019.02.002

Schneider, C. A., Rasband, W. S., & Eliceiri, K. W. (2012). NIH Image to ImageJ: 25 years of image analysis. *Nature Methods*, *9*(7), 671–675. https://doi.org/10.1038/nmeth.2089

Schulz-Klaus, B., Lessmann, V., & Endres, T. (2013). BDNF-dependent consolidation of fear memories in the perirhinal cortex. *Frontiers in Behavioral Neuroscience*, *7*, 205. https://doi.org/10.3389/fnbeh.2013.00205

Seoane, A., Tinsley, C. J., & Brown, M. W. (2011). Interfering with perirhinal brain-derived neurotrophic factor expression impairs recognition memory in rats. *Hippocampus*, *21*(2), 121–126. https://doi.org/10.1002/hipo.20763

Shah, M., Campos-Möller, X., Werner, L., Mamalis, N., & Ahmed, I. I. K. (2018). Midterm failure of combined phacoemulsification with trabecular microbypass stenting: Clinicopathological analysis. In *Journal of Cataract & Refractive Surgery* (Vol. 44, Issue 5). https://doi.org/10.1016/j.jcrs.2018.03.030

Sheridan, C. L., & Shrout, L. L. (1966). Differences in the effectiveness of optic uncrossed fiber systems in albino and hooded rats. *Psychonomic Science*, *4*(1), 177–178. https://doi.org/10.3758/BF03342237

Sieck, E. G., Epstein, R. S., Kennedy, J. B., SooHoo, J. R., Pantcheva, M. B., Patnaik, J. L., Wagner, B. D., Lynch, A. M., Kahook, M. Y., & Seibold, L. K. (2018). Outcomes of Kahook Dual Blade Goniotomy with and without Phacoemulsification Cataract Extraction. In *Ophthalmology Glaucoma* (Vol. 1,

Issue 1, pp. 75–81). https://doi.org/10.1016/j.ogla.2018.06.006

Sioshansi, S., Huber, K. E., & Wazer, D. E. (2011). The Implications of Breast Cancer Molecular Phenotype for Radiation Oncology. *Frontiers in Oncology*, *1*(June), 1–9. https://doi.org/10.3389/fonc.2011.00012

Skalicky, S. E., Lamoureux, E. L., Crabb, D. P., & Ramulu, P. Y. (2019). Patient-reported Outcomes, Functional Assessment, and Utility Values in Glaucoma. *Journal of Glaucoma*, *28*(2), 89–96. https://doi.org/10.1097/IJG.0000000000001155

Skalicky, S. E., Mcalinden, C., Khatib, T., Anthony, L. M., Yue, S., Martin, K. R., Goldberg, I., & Mccluskey, P. (2016). *Activity Limitation in Glaucoma : Objective Assessment by the Cambridge Glaucoma Visual Function Test*. *57*, 6158–6166. https://doi.org/10.1167/iovs.16-19458

Somner, J. E. A., Sii, F., Bourne, R. R., Cross, V., Burr, J. M., & Shah, P. (2012). Moving from PROMs to POEMs for glaucoma care: a qualitative scoping exercise. *Investigative Ophthalmology & Visual Science*, *53*(9), 5940–5947. https://doi.org/10.1167/iovs.12-10223

Steinmetz, J. D., Bourne, R. R. A., Briant, P. S., Flaxman, S. R., Taylor, H. R. B., Jonas, J. B., Abdoli, A. A., Abrha, W. A., Abualhasan, A., Abu-Gharbieh, E. G., Adal, T. G., Afshin, A., Ahmadieh, H., Alemayehu, W., Alemzadeh, S. A. S., Alfaar, A. S., Alipour, V., Androudi, S., Arabloo, J., … Vos, T. (2021). Causes of blindness and vision impairment in 2020 and trends over 30 years, and prevalence of avoidable blindness in relation to VISION 2020: the Right to Sight: an analysis for the Global Burden of Disease Study. *The Lancet Global Health*, *9*(2), e144–e160. https://doi.org/10.1016/S2214-109X(20)30489-7

Stowell, C., Burgoyne, C. F., Ethier, C. R., Downs, C., Ellisman, M. H., Fisher, S.,

Fortune, B., Fruttiger, M., Jakobs, T., Lewis, G., Masland, R. H., Mitchell, C. H., Morrison, J., Sharma, S. C., Sigal, I., Sofroniew, M., Wang, L., Wiggs, J., & Wu, S. (2017). Biomechanical aspects of axonal damage in glaucoma: A brief review. *Experimental Eye Research*, *157*, 13–19. https://doi.org/10.1016/j.exer.2017.02.005

Sun, F., Park, K. K., Belin, S., Wang, D., Lu, T., Chen, G., Zhang, K., Yeung, C., Feng, G., Yankner, B. A., & He, Z. (2011). Sustained axon regeneration induced by co-deletion of PTEN and SOCS3. *Nature*, *480*(7377), 372–375. https://doi.org/10.1038/nature10594

Suzuki, S., Numakawa, T., Shimazu, K., Koshimizu, H., Hara, T., Hatanaka, H., Mei, L., Lu, B., & Kojima, M. (2004). BDNF-induced recruitment of TrkB receptor into neuronal lipid rafts: Roles in synaptic modulation. *Journal of Cell Biology*, *167*(6), 1205–1215. https://doi.org/10.1083/jcb.200404106

Tanna, A. P., & Johnson, M. (2018). Rho Kinase Inhibitors as a Novel Treatment for Glaucoma and Ocular Hypertension. *Ophthalmology*, *125*(11), 1741–1756. https://doi.org/10.1016/j.ophtha.2018.04.040

Tassoni, A., Gutteridge, A., Barber, A. C., Osborne, A., & Martin, K. R. (2015). *Molecular Mechanisms Mediating Retinal Reactive Stem Cell Transplantation*. 3006–3016. https://doi.org/10.1002/stem.2095

Thakur, A., Goldbaum, M., & Yousefi, S. (2020). Predicting Glaucoma before Onset Using Deep Learning. *Ophthalmology Glaucoma*, *3*(4), 262–268. https://doi.org/https://doi.org/10.1016/j.ogla.2020.04.012

The advanced glaucoma intervention study (AGIS): 1. Study design and methods and baseline characteristics of study patients. (1994). *Controlled Clinical Trials*, *15*(4), 299–325. https://doi.org/10.1016/0197-2456(94)90046-9

The College of Optometrists Learning Outcomes for the Professional Certificate in Glaucoma Available at: https://www.college-optometrists.org/uploads/assets/0e49d21f-7691-4e1c-ad46f8b4ac29268e/Learning-outcomes-Professional-Certificate-in-Glaucoma.pdf. (n.d.).

Thomson, B. R., Heinen, S., Jeansson, M., Ghosh, A. K., Fatima, A., Sung, H.-K., Onay, T., Chen, H., Yamaguchi, S., Economides, A. N., Flenniken, A., Gale, N. W., Hong, Y.-K., Fawzi, A., Liu, X., Kume, T., & Quaggin, S. E. (2014). A lymphatic defect causes ocular hypertension and glaucoma in mice. *The Journal of Clinical Investigation*, *124*(10), 4320–4324. https://doi.org/10.1172/JCI77162

Tomokazu Souma, 1, 2 Stuart W. Tompson, 3 Benjamin R. Thomson, 1, 2 Owen M. Siggs, 4 Krishnakumar Kizhatil, 5 Shinji Yamaguchi, 1, 2 Liang Feng, 6 Vachiranee Limviphuvadh, 7 Kristina N. Whisenhunt, 3 Sebastian Maurer-Stroh, 7, 8 Tammy L. Yanovitch, 9 Luba, 18, L., M., S., J. J., E., S., T., Z., A.W., H., B., K., K.P., B., D.A., M., K.F., A., J.B., R., S.-H., L., S., R., K.-N., T.-V., X., L., S., J. J., J.L., W., F., P., J.E., C., … Young, T. L. (2016). Angiopoietin receptor TEK mutations underlie primary congenital glaucoma with variable expressivity. *Journal of Clinical Investigation*, *126*(7), 2575–2587. https://doi.org/10.1172/JCI85830

Tzameret, A., Sher, I., Belkin, M., Treves, A. J., Meir, A., Nagler, A., Levkovitch-Verbin, H., Barshack, I., Rosner, M., & Rotenstreich, Y. (2014). Transplantation of human bone marrow mesenchymal stem cells as a thin subretinal layer ameliorates retinal degeneration in a rat model of retinal dystrophy. *Experimental Eye Research*, *118*, 135–144. https://doi.org/10.1016/j.exer.2013.10.023

UKOA How to stratify the risk or complexity for glaucoma to direct patients to appropriate clinics (2020) Available at: https://uk-oa.co.uk/wp-content/uploads/2020/02/Glaucoma-Risk-and-Virtuals_PDF.pdf. (n.d.).

Vernon, S. A., & Adair, A. (2010). Shared care in glaucoma: a national study of secondary care lead schemes in England. *Eye (London, England)*, *24*(2), 265–269. https://doi.org/10.1038/eye.2009.118

Vidal-Sanz, M., Salinas-Navarro, M., Nadal-Nicolás, F. M., Alarcón-Martínez, L., Valiente-Soriano, F. J., Miralles de Imperial, J., Avilés-Trigueros, M., Agudo-Barriuso, M., & Villegas-Pérez, M. P. (2012). Understanding glaucomatous damage: Anatomical and functional data from ocular hypertensive rodent retinas. *Progress in Retinal and Eye Research*, *31*(1), 1–27. https://doi.org/10.1016/j.preteyeres.2011.08.001

Vignal, C., Uretsky, S., Fitoussi, S., Galy, A., Blouin, L., Girmens, J.-F., Bidot, S., Thomasson, N., Bouquet, C., Valero, S., Meunier, S., Combal, J.-P., Gilly, B., Katz, B., & Sahel, J.-A. (2018). Safety of rAAV2/2- ND4 Gene Therapy for Leber Hereditary Optic Neuropathy. *Ophthalmology*, *125*(6), 945–947. https://doi.org/10.1016/j.ophtha.2017.12.036

Viswanathan, A. C., Crabb, D. P., McNaught, A. I., Westcott, M. C., Kamal, D., Garway-Heath, D. F., Fitzke, F. W., & Hitchings, R. A. (2003). Interobserver agreement on visual field progression in glaucoma: A comparison of methods. *British Journal of Ophthalmology*, *87*(6), 726–730. https://doi.org/10.1136/bjo.87.6.726

Vorwerk, C. K., Lipton, S. A., Zurakowski, D., Hyman, B. T., Sabel, B. A., & Dreyer, E. B. (1996). Chronic low-dose glutamate is toxic to retinal ganglion cells: Toxicity blocked by memantine. *Investigative Ophthalmology and Visual*

Science, *37*(8), 1618–1624.

Vrabec, J. P., & Levin, L. A. (2007). The neurobiology of cell death in glaucoma. *Eye (Basingstoke)*, *21*, S11–S14. https://doi.org/10.1038/sj.eye.6702880

Walters, T. R., Ahmed, I. I. K., Lewis, R. A., Usner, D. W., Lopez, J., Kopczynski, C. C., & Heah, T. (2019). Once-daily Netarsudil/Latanoprost Fixed-Dose Combination for Elevated Intraocular Pressure, the Randomized Phase 3 MERCURY-2 Study. *Ophthalmology Glaucoma*. https://doi.org/10.1016/j.ogla.2019.03.007

Wan, X., Pei, H., Zhao, M., Yang, S., Hu, W., He, H., Ma, S., Zhang, G., Dong, X., Chen, C., Wang, D., & Li, B. (2016). Efficacy and Safety of rAAV2-ND4 Treatment for Leber's Hereditary Optic Neuropathy. *Scientific Reports*, *6*, 21587. https://doi.org/10.1038/srep21587

Wassmer, S. J., Carvalho, L. S., György, B., Vandenberghe, L. H., & Maguire, C. A. (2017). Exosome-associated AAV2 vector mediates robust gene delivery into the murine retina upon intravitreal injection. *Scientific Reports*, *7*, 45329. https://doi.org/10.1038/srep45329

Weber, A. J., & Harman, C. D. (2005). Structure-function relations of parasol cells in the normal and glaucomatous primate retina. *Investigative Ophthalmology & Visual Science*, *46*(9), 3197–3207. https://doi.org/10.1167/iovs.04-0834

Weinreb, R. N., Leung, C. K. S., Crowston, J. G., Medeiros, F. A., Friedman, D. S., Wiggs, J. L., & Martin, K. R. (2016). Primary open-angle glaucoma. *Nature Reviews Disease Primers*, *2*(1), 16067. https://doi.org/10.1038/nrdp.2016.67

Wheeler, L. A., Lai, R., & WoldeMussie, E. (n.d.). *From the Lab to the Clinic: Activation of an Alpha-2 Agonist Pathway is Neuroprotective in Models of Retinal and Optic Nerve Injury*. *9*(Suppl. 1), 17.

https://doi.org/10.5301/EJO.2008.3854

Williams, P. A., Harder, J. M., Cardozo, B. H., Foxworth, N. E., & John, S. W. M. (2018). Nicotinamide treatment robustly protects from inherited mouse glaucoma. *Communicative and Integrative Biology*, *11*(1). https://doi.org/10.1080/19420889.2017.1356956

Williams, P. A., Harder, J. M., Foxworth, N. E., Cochran, K. E., Philip, V. M., Porciatti, V., Smithies, O., & John, S. W. M. (2017). Vitamin B3 modulates mitochondrial vulnerability and prevents glaucoma in aged mice. *Science*, *760*(February), 756–760. https://doi.org/10.1120/science.aal0092

Williams, P. A., Harder, J. M., John, S. W. M., & Harbor, B. (2018). *Nicotinamide Treatment in Glaucoma*. *0000000000*(12), 1161–1168. https://doi.org/10.1097/IJG.0000000000000767.Glaucoma

Williams, P. A., Howell, G. R., Barbay, J. M., Braine, C. E., Sousa, G. L., John, S. W. M., & Morgan, J. E. (2013). Retinal ganglion cell dendritic atrophy in DBA/2J glaucoma. *PLoS ONE*, *8*(8), 1–10. https://doi.org/10.1371/journal.pone.0072282

Wilsey, L. J., & Fortune, B. (2016). Electroretinography in glaucoma. *Current Opinion in Ophthalmology*, *27*(2), 118–124. https://doi.org/10.1097/ICU.0000000000000241.Electroretinography

Woldemussie, E., Ruiz, G., Wijono, M., & Wheeler, L. A. (2001). Neuroprotection of Retinal Ganglion Cells by Brimonidine in Rats with Laser-Induced Chronic Ocular Hypertension. *Investigative Ophthalmology & Visual Science*, *42*(12), 2849–2855.

Wu, Z., Crabb, D. P., Chauhan, B. C., Crowston, J. G., & Medeiros, F. A. (2019). Improving the Feasibility of Glaucoma Clinical Trials Using Trend-Based Visual Field Progression End Points. *Ophthalmology Glaucoma*, *2*(2), 72–77.

https://doi.org/10.1016/j.ogla.2019.01.004

Wu, Z., Medeiros, F. A., Weinreb, R. N., Girkin, C. A., & Zangwill, L. M. (2019). Comparing 10-2 and 24-2 Visual Fields for Detecting Progressive Central Visual Loss in Glaucoma Eyes with Early Central Abnormalities. *Ophthalmology Glaucoma*, *2*(2), 95–102. https://doi.org/https://doi.org/10.1016/j.ogla.2019.01.003

Xue, K., Jolly, J. K., Barnard, A. R., Rudenko, A., Salvetti, A. P., Patrício, M. I., Edwards, T. L., Groppe, M., Orlans, H. O., Tolmachova, T., Black, G. C., Webster, A. R., Lotery, A. J., Holder, G. E., Downes, S. M., Seabra, M. C., & MacLaren, R. E. (2018). Beneficial effects on vision in patients undergoing retinal gene therapy for choroideremia. *Nature Medicine*, *24*(10), 1507–1512. https://doi.org/10.1038/s41591-018-0185-5

Yablonski, M. E., Zimmerman, T. J., Waltman, S. R., & Becker, B. (1978). A fluorophotometric study of the effect of topical timolol on aqueous humor dynamics. *Experimental Eye Research*, *27*(2), 135–142. https://doi.org/10.1016/0014-4835(78)90083-0

Yang, S., Cacquevel, M., Saksida, L. M., Bussey, T. J., Schneider, B. L., Aebischer, P., Melani, R., Pizzorusso, T., Fawcett, J. W., & Spillantini, M. G. (2015). Perineuronal net digestion with chondroitinase restores memory in mice with tau pathology. *Experimental Neurology*, *265*, 48–58. https://doi.org/10.1016/j.expneurol.2014.11.013

Yang, S., Hilton, S., Alves, J. N., Saksida, L. M., Bussey, T., Matthews, R. T., Kitagawa, H., Spillantini, M. G., Kwok, J. C. F., & Fawcett, J. W. (2017). Antibody recognizing 4-sulfated chondroitin sulfate proteoglycans restores memory in tauopathy-induced neurodegeneration. *Neurobiology of Aging*, *59*,

197–209. https://doi.org/10.1016/j.neurobiolaging.2017.08.002

Yang, Y., Wang, L., Bell, P., McMenamin, D., He, Z., White, J., Yu, H., Xu, C., Morizono, H., Musunuru, K., Batshaw, M. L., & Wilson, J. M. (2016). A dual AAV system enables the Cas9-mediated correction of a metabolic liver disease in newborn mice. *Nature Biotechnology*, *34*(3), 334–338. https://doi.org/10.1038/nbt.3469

Yousefi, S., Elze, T., Pasquale, L. R., Saeedi, O., Wang, M., Shen, L. Q., Wellik, S. R., De Moraes, C. G., Myers, J. S., & Boland, M. V. (2020). Monitoring Glaucomatous Functional Loss Using an Artificial Intelligence–Enabled Dashboard. *Ophthalmology*. https://doi.org/https://doi.org/10.1016/j.ophtha.2020.03.008

Yousefi, S., Kiwaki, T., Zheng, Y., Sugiura, H., Asaoka, R., Murata, H., Lemij, H., & Yamanishi, K. (2018). Detection of Longitudinal Visual Field Progression in Glaucoma Using Machine Learning. *American Journal of Ophthalmology*, *193*, 71–79. https://doi.org/10.1016/j.ajo.2018.06.007

Yu-Wai-Man, P., Newman, N. J., Carelli, V., Moster, M. L., Biousse, V., Sadun, A. A., Klopstock, T., Vignal-Clermont, C., Sergott, R. C., Rudolph, G., La Morgia, C., Karanjia, R., Taiel, M., Blouin, L., Burguière, P., Smits, G., Chevalier, C., Masonson, H., Salermo, Y., … Sahel, J.-A. (2020). Bilateral visual improvement with unilateral gene therapy injection for Leber hereditary optic neuropathy. *Science Translational Medicine*, *12*(573), eaaz7423. https://doi.org/10.1126/scitranslmed.aaz7423

Yu, S., Tanabe, T., Dezawa, M., Ishikawa, H., & Yoshimura, N. (2006). Effects of bone marrow stromal cell injection in an experimental glaucoma model. *Biochemical and Biophysical Research Communications*, *344*(4), 1071–1079.

https://doi.org/10.1016/j.bbrc.2006.03.231

Zhang, Y. (2008). I-TASSER server for protein 3D structure prediction. *BMC Bioinformatics*, *9*(1), 40. https://doi.org/10.1186/1471-2105-9-40

Zhang, Y. (2009). I-TASSER: fully automated protein structure prediction in CASP8. *Proteins*, *77 Suppl 9*(Suppl 9), 100–113. https://doi.org/10.1002/prot.22588

Zhu, J., Huang, X., & Yang, Y. (2009). The TLR9-MyD88 pathway is critical for adaptive immune responses to adeno-associated virus gene therapy vectors in mice. *The Journal of Clinical Investigation*, *119*(8), 2388–2398. https://doi.org/10.1172/JCI37607